Universitat Autònoma de Barcelona

The applicability of in vitro models of the intestinal barrier for the risk assessment of engineered nanomaterials used as food additives

Alba Garcia Rodriguez

Universitat Autònoma de Barcelona

Facultat de Biociències

Departament de Genètica i de Microbiologia

Grup de Mutagènesi

The applicability of *in vitro* models of the intestinal barrier for the risk assessment of engineered nanomaterials used as food additives

DOCTORAL DISSERTATION

Alba Garcia Rodriguez

2018

Universitat Autònoma de Barcelona

Facultat de Biociències

Departament de Genètica i de Microbiologia

Grup de Mutagènesi

The applicability of *in vitro* models of the intestinal barrier for the risk assessment of engineered nanomaterials used as food additives

Dissertation respectfully submitted by

Alba Garcia Rodriguez

To Universitat Autònoma de Barcelona in partial fulfillment of the requirements for the degree of Doctor of Philosophy, as per the Doctorate Program in Genetics

Under the direction of Dr. Ricard Marcos Dauder and Dr. Constanza Cortés Crignola

Dr. Ricard Marcos Dauder **Dr. Constanza Cortés Crignola** **Alba Garcia Rodriguez**

AGRADECIMIENTOS

En primer lugar me gustaría agradecer a mis directores de Tesis la oportunidad que me dieron al dejarme realizar el doctorado en el grupo de Mutagénesis Ambiental del Departamento de Genética y Microbiología. En especial al Dr. Ricard Marcos, por alentarme con el presente proyecto y por involucrarme en tantas colaboraciones y proyectos, de los cuales he aprendido y disfrutado mucho. A la Dra. Constanza, por su gran ayuda y dedicación en la recta final de esta Tesis.

Mi más sincero agradecimiento al personal técnico del laboratorio por vuestra profesionalidad, dedicatória y paciencia que tanto os caracteriza. Glòria, Lourdes y Cristian sabéis de sobras que este laboratorio sería una “jaula de grillos” sin vosotros. A todos mis compañeros de laboratorio por su calidad humana y profesional, ha sido un gustazo trabajar codo con codo con todos vosotros. En especial a “UAB FEM POWER” y esas “MUTAS” que han hecho de estos tres años una de mis mayores aventuras, y de la cual sólo tengo momentos de risas inolvidables. Nunca me olvidaré de la gran ayuda que me brindó mi gran AMIGA Laura Vila Vecilla cuando empecé con todo esto de la “nanotoxicología”. Orgullosa de que seas mujer, científica y loca.

No quisiera olvidarme de todas esas amistades que han estado a mi lado en este agitado camino y que han creído en mis aptitudes en aquellos momentos que yo menos lo hacía. Desde las amigas de la infancia en Tossa "the little town of *la Costa Brava*", pasando por las de la Universidad en Girona y los del Máster en la UAB, como a mis numerosos "compis" de piso y en especial a la que ha aguantado la montaña rusa que he tenido como estado de ánimo. A TODOS VOSOTR@S MILLONES DE GRACIAS.

Por último y más importante, un enorme e infinito GRACIAS a mi querida familia. A mis padres (María y Rafa) y hermana (María petita), que desde su humildad y constancia me han ayudado SIEMPRE en todo aquello que ha estado a su alcance. No os imagináis qué orgullo de família Garcia-Rodriguez.

Gracias también a la Universitat Autònoma de Barcelona por la concesión de la beca PIF, la beca de mobilidad para estancias cortas, y a los proyectos del Ministerio de Economia y Competitividad (SAF2015-63519-R) y de la Comisión Europea FP7 NANoREG (Grant Agreement NMP4-LA-2013-310584).

A mi madre, por se la mujer más valiente que conozco.

The most dangerous in our language is

"we've always done it this way"

Rear Admiral Grace Hopper

ABSTRACT

Nano-technological approaches are allowing the development of deliberately engineered nanomaterials (ENMs), presenting promising new applications for many industrial fields. Especially, ENMs possess unique properties and novel uses in food or food packaging materials such as the enhancement of texture, colour, flavour, nutrient stability and food packaging safety.

Despite their innovative properties, there is an increasing concern about the possibility that human exposure to TiO_2NPs may lead to significant adverse health effects. The International Agency for Research on Cancer (IARC) classified TiO_2 as a human carcinogen group 2B because there was enough evidence that nano-TiO_2 may cause lung cancer by inhalation. Although oral exposure was also debated by IARC, the final report was inconclusive due to non-existing standardized procedures for nano-TiO_2 risk assessment. Due to the potential adverse effects of this ENMs and the lack of information regarding toxicological aspects over the oral exposure, in this Thesis we have carried out *in vitro* studies on the biological effects of TiO_2NPs.

For the aforementioned purpose, we set up and characterized, for the first time in our laboratory, an epithelial *in vitro* model that closely mimics the human small intestine. Thus, in our first study, we defined the best culture conditions for the already-described model, Caco-2/HT29/Raji-B. From our integrity and permeability findings, we confirmed that the best Caco-2/HT29 cell ratio is 90:10, respectively, as TEER values, paracellular LY permeability and the mucus shed formed correlated well with other studies. We also were able to detect the induction of M-like cells by TEM. Moreover, in order to monitor the proper barrier formation, we proposed a set of genes related to the cell junctional complexes, brush border enzymes, mucus shed components and M-cell markers. Finally, we tested the goodness of our epithelial *in vitro* model by exposing it to both TiO_2NPs and SiO_2NPs for 24 h. Our confocal results evidenced the potential adverse effects of TiO_2NPs and SiO_2NPs on the intestinal epithelium, as NPs internalization and NPs-cell nucleus interaction were observed.

Because of the heightened interest in the identification, validation and standardization of the effects associated to exposures to new ENMs, our second study aimed to assess the effects of three different shapes of TiO_2NPs (spheres, rods and wires) on the Caco-2/HT29 barrier. Our results demonstrated that the three types of TiO_2NPs have the ability to impair the membrane's integrity, translocate through the mucus shed and internalize in the cells, reaching the nucleus. Taking into account our confocal images results, we hypothesize that due to their shapes, nano-wires are more

likely to cross paracellularly, while nano-spheres and nano-rods used intracellular passage to cross the intestinal epithelium. Despite previous evidence that relate the capability of TiO_2NPs to produce ROS, we have not detected oxidatively DNA damage. However, and in accordance with the confocal images showing a great amount of NPs-cell nucleus events, we detected a slight but significant general DNA damage in the barrier's cells.

Finally, the third study was performed under the framework of an international mention carried out in the Biomedical Engineering Department at the Binghamton University (Binghamton, NY, USA). Nutrient absorption is one of the main and most important functions of the small intestine. Thus, to understand and evaluate whether ENPs can trigger physiological potential pathologies, the activity of the intestinal alkaline phosphatase (IAP), aminopeptidase-N (APN) and Na^+/K^+ ATPase enzymes were measured after exposing the Caco-2/HT29-MTX barrier to TiO_2NPs and SiO_2NPs for 4 h. Moreover, and in order to further mimic the physiological conditions of a real digestion, the Caco-2/HT29-MTX barrier was exposed to both NPs previously digested and co-cultured with both *Escherichia coli* and *Lactobacillus rhamnosus,* as examples of commensal microbiota.

ABBREVIATION LIST

2D	Two dimensions
3D	Three dimensions
8-oxo-dG	8-hydroxy-2'-deoxyguanosine
AgNPs	Silver nanoparticles
ALPI	Intestinal alkaliline phospatase
ANOVA	Analysis of variance
AJ	Adherent junctions
APN	Aminopeptidase-N
ATCC	American Type Culture Collection
BEUC	European Consumer Organization
BSA	Bovine serum albumin
bw/day	Body weight
C-13NPs	Nanoparticles of (13)C graphite
Caco-2	Colorectal adenocarcinoma
CalTech	California Institute of Technology
cDNA	Complementary deoxyribonucleic acid
CLDN2	Claudin 2
CPI	Consumer Products Inventory
CT-	Negative control
DNA	Deoxyribonucleic acid
DMEM	Dubelco's Modified Eagle's High Glucose Medium
DLS	Dynamic Light Scattering
E171	Food grade titanium dioxide
EDTA	Ethylenediaminetetraacetic acid
EFSA	European Food Safety Administration
EHS	Environmental Health Information

ENMs	Engineered nanomaterials
ENPs	Engineered nanoparticles
FAO	Food and Agriculture Organization
FAE	Follicle associated epithelium
FAPydG	2,6-diamino-4-hydroxy-5-formamidopyrimidine
FBS	Fetal bovine serum
$FeTiO_3$	Ilmenite
FPG	Formamidopyrimidine-DNA glycosylase
GB	Gelbond®
GIT	Gastrointestinal tract
GP2	Glycoprotein 2
Group 2B	Probable human carcinogen
HBSS	Hanks' balanced salt solution
HEPES	4-(2-hydroxyethyl)-1-piperazineethanesulfonic acid
HT29	Human colorectal adenocarcinoma
IAP	Intestinal alkaline phosphatase
IARC	International Agency for Research on Cancer
IBD	Irritable bowel syndrome
IBD	Inflammatory bowel disease
IEC-6	*Rattus norvegicus* small intestine/epithelium
IL-8	Interleukine-8
$KBrO_3$	Potassium bromate
LGALS9	Galactin-9
LDV	Laser Droppler Velocimeter
LY	Lucifer yellow
M cells	Microfold cells
MICRO	Micrometer scaled
MMS	Methyl methanesulfonate

MUC 1	Cell surface associated Mucin 1
MUC5AC	Gel forming Mucin 5
Na^+/K^+ ATPase	Sodium pump enzyme
NANO	Nanometer scaled
NEAA	Non-essential amino acids
NIOSH	Institute for Occupational Safety and Health
NMs	Nanomaterials
NNI	National Nanotechnology Initiative
NPs	Nanoparticles
OCLN	Occludin
OECD	Organisation for Economic Co-operation and Development
PBS	Phosphate-buffered saline
PCR	Polymerase chain reaction
PET	Polyethylene Terephtalate Transwells®
PDI	Polydispersity Index
PTAFR	Platelet-activating factor receptor
QDs	Quantum dots
qPCR	Quantitative polymerase chain reaction
Raji-B	B lymphocyte cells
RNA	Ribonucleic acid
ROS	Reactive oxigen species
SI	Sucrase isomaltase
SEM	Scanning electron microscopy
SLC15A1	Solute carrier family 15
SpiB	Spi-B transcription factor
SYBR	N',N'-dimethyl-N-[4-[(E)-(3-methyl-1,3-benzothiazol-2-ylidene)methyl]-1-phenylquinolin-1-ium-2-yl]-N-propylpropane-1,3-diamine
SiO_2	Silica dioxide

SiO_2NPs	Silica dioxide nanoparticles
SiO_2NPs-R	Nano-rods of silica dioxide
SiO_2NPs-S	Nano-spheres of silica dioxide
SiO_2NPs-W	Nano-wires of silica dioxide
T84	Human colon cells (derived from metastatic site: lung)
t/year	Tons per year
TEER	Trans-epithelial electrical resistance
TEM	Transmission electron microscopy
TiO_2	Titanium dioxide
$TiO_2 \times xFeO \times yH_2O$	Leucoxene ore
TiO_2-B	Titanium dioxide polymorph
TiO_2NPs	Titanium dioxide nanoparticles
TiO_2NPs-R	Nano-rods of titanium dioxide
TiO_2NPs-S	Nano-spheres of titanium dioxide
TiO_2NPs-W	Nano-wires of titanium dioxide
TJ	Tight junctions
TLR4	Toll-like receptor 4
TR146	Human buccal mucosa cell (derived from a neck metastasis)
UEA-1	Ulex europaeus agglutinin 1
UV	Ultra violet light
WGA	Wheat germ agglutinin
ZnO	Zinc oxide
ZO-1	Zonula occludens

INDEX

1. INTRODUCTION

1. INTRODUCTION

1.1. Occurrence and contextualization

Human beings have always been environmentally exposed to airborne nano-sized particles since nanoparticles (NPs) result from many natural processes (e.g. volcanic eruptions, forest fires, and simple erosions by plants and animals like shed skin and hair). Moreover, since industrialization, vast quantities of NPs (also known as anthropogenic NPs) are generated daily, affecting air quality worldwide, basically due to human activities (e.g. engine-combustion, aerosols' chemical manufacturing, charcoal burning, combustion of fuel oil for power generation, etc) (Buzea et al., 2007). To understand the risk of this type of exposures, different epidemiological studies have been performed, reporting a large number of health problems, especially cardiopulmonary impairments and diseases related with the respiratory system (e.g. nose and throat irritation, bronchitis symptoms, asthma, emphysema, etc) (Taylor, 2002; Meyer and Smith, 2002; Hoek et al., 2002; Vemylen et al., 2005; Matsukawa et al., 2014). In addition, the increased application of *ad hoc* designed nanomaterials (NMs) in a wide range of nano-enabled consumer and medical products has resulted in their increased presence in the environment and, consequently, enhanced human exposure (Bekker et al., 2013; Hanus and Harris, 2013; Hincapié et al., 2015; Vance et al., 2015 Kreider et al., 2017). These are the so-called engineered nanomaterials (ENMs), characterized for being *the novo* synthesized with unique and desirable physicochemical properties.

Regarding the potential exposure routes of ENMs, it should be pointed out that other routes have also been affected besides inhalation and these can be encountered through ingestion, dermal contact, injection, etc (Szakal et al., 2014; Gulson et al., 2015; Grieger et al., 2016). New estimations suggest that the use of ENMs will continue to increase in an exponential way, as substantial economic and technical resources are being dedicated to the investigation of advanced ENMs with industrial applicability and commercial distribution (Figure 1). The scientific field in charge of ENMs design, production and manufacture is called *Nanotechnology.*

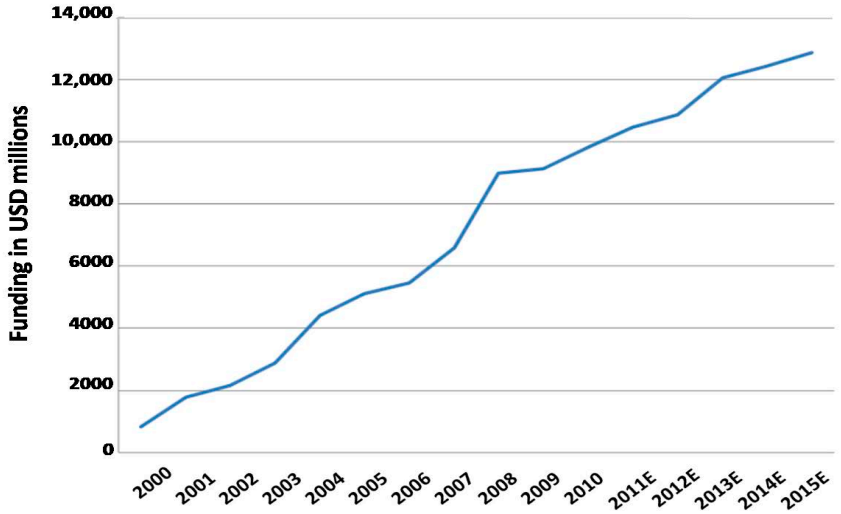

Figure 1. Total global funding of Nanotechnologies (Source: Cientifica Ldt., 2011).

1.2. Nanotechnology

1.2.1 Definition and origin

Generally, nanotechnology can be defined as the field dedicated to the design, synthesis, and application of materials and devices whose size and shape have been engineered at the nanoscale. It exploits unique chemical, physical, electrical, and mechanical properties that emerge when the matter is structured at the nanoscale, approximately from 1 to 100 nm (Figure 2). Thereby, unlike bulk materials, the behaviour of NMs vary with size, making them increasingly desirable for presenting numerous applications in areas ranging from molecular computing, energy storage, fuel cells and nanomedicine, among others. This is mainly due to their increased reactivity when compared to their micro-sized counterparts, since nanoscaled materials exhibit larger surface-to-volume ratio. This provides unsaturated and, thus, more reactive surface atoms (Oberdörster et al., 2005; Buzea et al., 2007; Stern and Mcneil, 2008) (Figure 2).

The ideas and concepts behind nanoscience and nanotechnology started with a talk entitled “There’s Plenty of Room at the Bottom” by physicist Richard Feynman at the American Physical Society meeting at California Institute of Technology (CalTech) in 1959. In his talk, Feynman postulated a process in which scientists would be able to manipulate and control individual atoms and molecules. Over the next decade, Professor Norio Taniguchi coined the term nanotechnology and it was not until 1981, when the development of the scanning tunnelling microscope allowed individual atoms to “be seen”, that modern nanotechnology began (NNI, 2000).

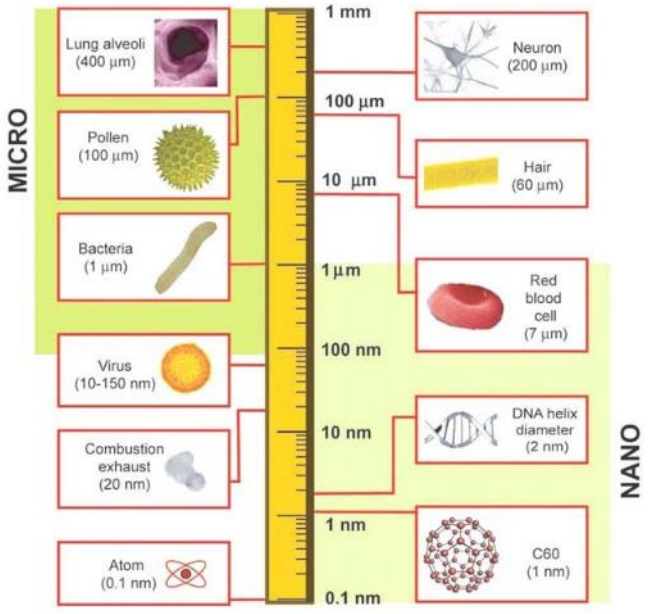

Figure 2. Logarithmical length scale showing differences between 'nano' and 'micro' sizes, compared to biological components (Source: Buzea et al., 2007).

Although the nanoscience and nanotechnology fields are quite new, nanoscaled materials have been used for centuries. Alternate-sized gold and silver particles created colours in the stained glass windows of medieval churches, hundreds of years ago. The artists did not realize that the process they used to create these works caused changes in the structure of the materials they were working with. Another example is the so-called Lycurgus cup, created by ancient Romans 2000 years ago, where different colours can appear depending on the direction of light's illumination due to metal nanoparticle optical scattering (Gartia et al., 2013).

1.2.2. Fundamental concepts in Nanoscience and Nanotechnology

The nanoscale range covers from the atomic level, over 0.2 nm, to 100 nm. In this range, NMs can behave significantly differently mainly by two primary factors: surface effects (causing smooth scaling properties due to the fraction of atoms at the surface), and quantum effects (showing discontinuous behaviour due to quantum confinement effects in materials with delocalized electrons) (Roduner, 2006).

Compared to micro-particles or bulk materials, the fraction of the surface atoms in NPs is increased. For instance, one carbon micro-particle with a diameter of 60 µm has a mass of 0.3 µg, and a surface area of 0.01 mm^2. The same mass of carbon nanoparticles consists of 1 billion NPs, where each particle has a diameter of 60 nm and a surface area of 11.3 mm^2 (Figure 3A). The surface area to volume or mass ratio

for a 60 nm diameter particle is 1000 times larger than a particle with a diameter of 60 µm. As the material in nanoparticulated form presents a much larger surface area for chemical reactions to take place, its reactivity is enhanced roughly 1000-fold (Oberdörster et al., 2005; Buzea et al., 2007).

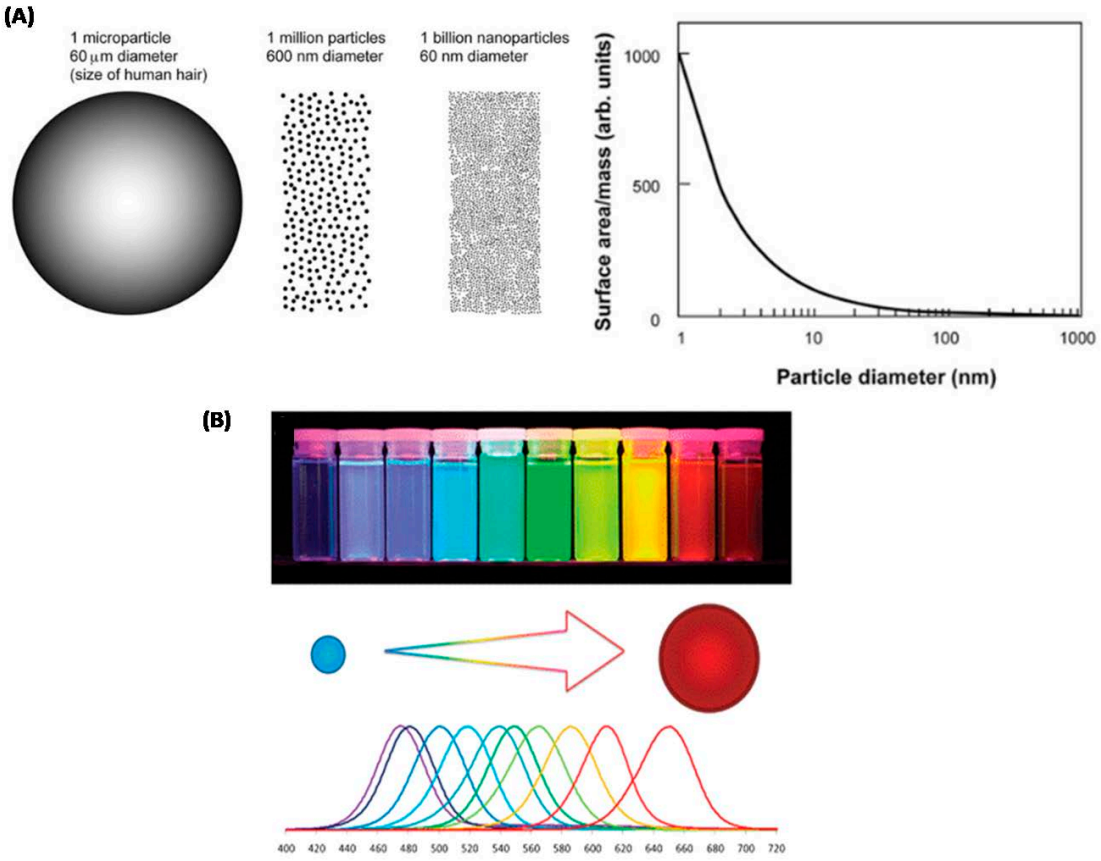

Figure 3. (A) Schematic illustration of differences between microparticles (µm) and nanoparticles (nm) having the same mass (left). Surface area normalized to mass versus particle diameter (right) (Source: Buzea et al., 2007). **(B)** Narrow size-tuneable light emission profile enables precise control over the probe colour via varying the nanoparticle size. (Source: Gao et al., 2005).

An example of a class of materials that clearly exploits quantum effects are the nano-structured quantum dots (QDs). Their electronic behaviour is similar to individual atoms or small molecules, thereby they are regarded as analogous to artificial atoms. Basically, the confinement of the electrons in all three spatial directions observed in QDs results in a quantized energy spectrum. More changes of quantum-confinement effects have been described, such as the appearance of magnetic moments in their nanoparticulated form which are not present in its bulk form, and changes in their ability to accept or donate electrical charge (or electron affinity) reflected in their catalytic ability (Tarucha, 2001; Björk et al., 2004; Buzea et al., 2007). Highly exploited as

fluorescent semiconductor NPs, QDs are suitable for advanced fluorescence imaging applications, such as multiplexed quantitative analysis of cellular phenotypes, real-time monitoring of intracellular processes, and *in vivo* molecular imaging (Figure 3B) (Gao et al., 2005; Zrazhevskiy et al., 2010).

1.2.3. The "*bottom-up*" and "*top-down*" approaches

The scientific community focused their research efforts on the development of novel production methods of NMs, to make their production more attractive for the industrial sector. Methods for large-scale synthesis of NMs are principally divided into two well-established approaches commonly used for industrial productions; *bottom-up* and *top-down*.

Top-down refers to processes in which a given bulk material is reduced in size to produce nanometer-scale particles, which are then systematically inserted into larger structures or mixed with other materials. Most of today's products involving fabricated nanostructures are produced using *top-down* conventional technologies. These processes are reported to be energy-intensive and waste-heavy, involving huge amounts of resources and having important adverse environmental impacts (Malanowski et al., 2007). Several techniques, illustrated in Table 1, have been described and currently carried out.

Concurrently, *bottom-up* approaches are characterized by building up larger structures atom by atom, molecule by molecule, or by self-assembly methods. To date, these methods are classified as aerosol-based processes or liquid-phase techniques (Hett, 2004; Malanowski et al., 2007; Charitidis et al., 2014) (Table 1). Undoubtedly, the existing technologies have allowed to specifically design NPs accordingly to their final desired applications.

1.2.4. Nanoparticles classification

Particle morphology has been used to categorize NPs (e.g. fullerenes, nanotubes, nanowires, nanodots, etc). However other classifications based on the type of application, origin (natural sources or anthropomorphic by-products) or synthesis method are also used. Nevertheless, NPs are generally classified based on their physical characteristics such as dimension, morphology, material composition, uniformity, and agglomeration (Chaudhry et al., 2006; Buzea et al., 2007; Bhatia, 2016). These aspects are discussed succinctly:

Table 1. Summary of *top-down* and *bottom-up* approaches to NM production (Source; Luther et al., 2004).

APPROACH	PROCESS	NM PRODUCED
TOP-DOWN	Mechanical milling	Mixtures of elemental or prealloyed powders, alloys and composites
	Etching (chemical)	Arrays of nano-scale shapes (e.g. Layers porous silicon and alumina)
	Electro-explosion (Thermical/chemical)	Metallic nanopowders, fullerenes, metallofullerenes, nanotubes
	Sputtering (kinetic)	Similar to vapour phase techniques
	Laser ablation (thermal)	Broad rang of NPs
BOTTOM-UP	Sol-gel	Colloidal NPs, oxide NPs, composite nanopowders
	Aerosol based process	Industrial production of NPs such as carbon black, titania pigment, fumed silica and titania, optical fibers, some metals, etc
	Chemical vapour deposition	Widely used to produce carbon nanotubes
	Atomic or molecular condensation	Metal-containing NPs
	Supercritical fluid synthesis	Various NPs
	Spinning	Thin polymer fibers
	Use of templates	Porous alumina, zeolites, di-block co-polymers, dendrimers, proteins and other molecules containing regular nano-sized pores or voids
	Self-assembly	Variety of organic and biological compounds, inorganic oxides, metals and semiconductors

a) Dimensionality

As NPs shape or morphology plays an important role in their toxicity, it could be useful to classify them based on their number of dimensions to further comprehend their potential behaviour.

- *One-dimensional NMs:* those materials with only one dimension in the nanometer scale are typically thin films or surface coatings, which can be grown in a controlled manner to be only one atom thick (so-called monolayer). They are very popular in electronics and engineering.
- *Two-dimensional NMs:* they present two dimensions in the nanometer scale. These include 2D nanostructured films, with nanostructures firmly attached to a substrate, or nanopore filters. Asbestos fibres would be an example of 2D NM.
- *Three-dimensional NMs:* materials that are nanoscaled in all three dimensions (3D). These NMs usually are free NPs with various morphologies (Figure 4) (Aitken et al., 2004; Buzea et al., 2007).

b) Morphology

The morphological aspects that have been taken into account to classify NMs have been: flatness, sphericity, and aspect ratio. High aspect ratio NPs include nanotubes and nanowires in various shapes such as helices, zig-zags, and belts. Small aspect

ratio morphologies include spherical, oval, cubic, prism, etc. forms (Figure 4) (Aitken et al., 2004; Buzea et al., 2007).

c) Composition

NPs can consist of a single constituent material or be a composite of several materials. As an example, NPs found in nature are often agglomerations of more than one type of materials, while pure single-composed NP powders are usually those synthesized by the methods mentioned in section *1.2.3* (Aitken et al., 2004; Buzea et al., 2007).

d) Uniformity and agglomeration

Based on their chemistry and electromagnetic properties, NPs can exist as dispersed aerosols, as suspensions/colloids, or in an agglomerated state. The agglomeration rate depends primarily on the number of particles (as concentration) and their mobility. When both of these parameters increase, particle size decreases. In an agglomerated state, NPs may behave as larger particles, depending on the size of the agglomerate (Figure 4) (Aitken et al., 2004; Buzea et al., 2007).

1.2.5. ENMs in consumer products.

Already in 2005, several studies reviewed, reported and listed the available information on the NMs industry sector. Estimations of NMs applicability were done by companies in the UK, Europe, and coming over the world. The companies selected were manufacturing and/or using NMs in their products. In this context, Chaudhry et al. (2006) defined a matrix approach to identify a vast array of applications for each type of NM, based on many of the common, then-known types of NMs.

The NMs' applications found in this study cover the use of NPs for drug delivery, ceramic applications, sensor and sensing devices, coating and pigments, and even lubrication. Thereby, the possible fields where the use of ENMs can be exploited comprise a vast numerous of industrial sectors and consumer applications such as advanced materials, display technologies, electronics, nutrition, cosmetics, and medical drug designing, among others (Table 2) (Aitken et al., 2004; Chaudhry et al., 2006; Piccinno et al., 2012). To report the marketing and distribution of the nano-enabled products in the commercial market, the Woodrow Wilson International Center for Scholars and the Project on Emerging Nanotechnologies created the Nanotechnology Consumer Products Inventory (CPI) in 2005, listing 54 products (Maynard and

Michelson, 2005). Five years after its creation, the CPI listed 1015 products from 409 companies in 24 countries. Updates of this inventory are generated annually (Table 3).

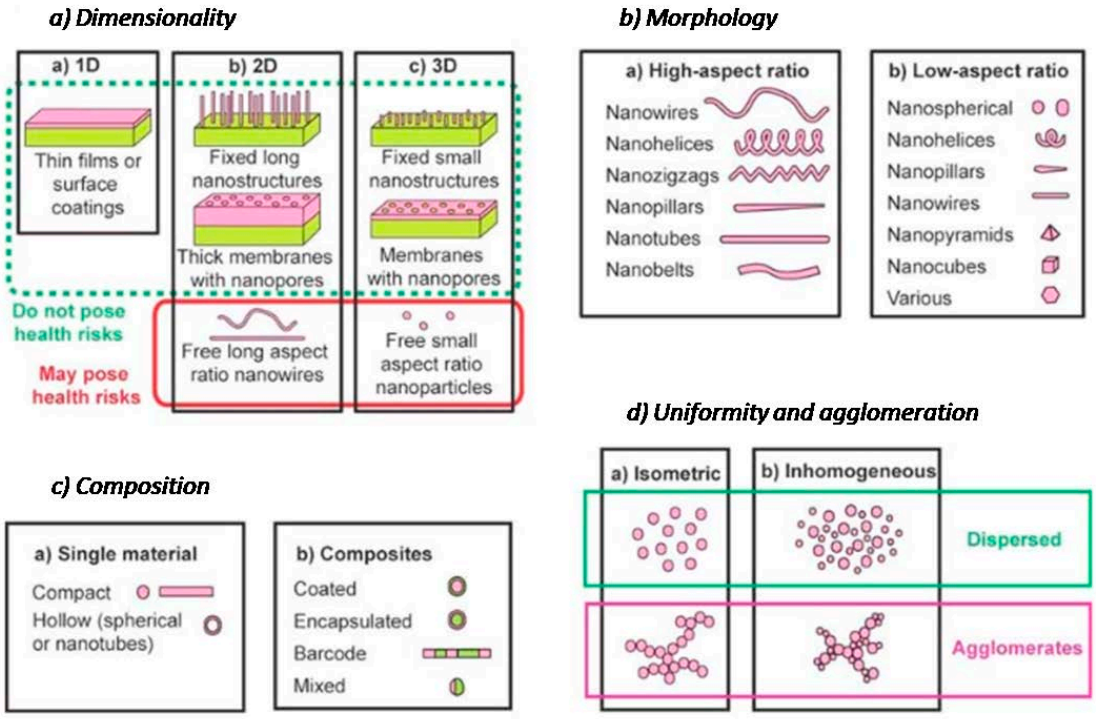

Figure 4. Nanomaterials classification from the point of view of nanostructure **a)** dimensions, **b)** morphology, **c)** composition and **d)** uniformity and agglomeration state. (Adapted from Buzea et al., 2007).

Moreover, due to the fast advance of nanoscience and nanotechnology and the resulting increased interest worldwide, parallel NMs-based products inventories and databases have been also developed by other groups. For example, in 2006, a German company launched a free-access internet database of nanotechnology products (Nano Products and Technologies, NPT), where 586 products were listed. In 2007, Japan's National Institute of Advanced Industrial Science and Technology created an inventory of "nanotechnology-claimed consumer products", where 541 product lines and 1241 products are listed to date (Michelson, 2013). Furthermore, two European organizations, the European Consumers Organization (BEUC) and the European Consumer Voice in Standardization (ANEC), joined efforts to develop another available inventory of "consumer products with nano-claims" (ECO, 2009).

Table 2. ENMs present in consumer products (Source: Piccinno and Gottschalk, 2012).

Nanomaterial	Product group	% of total use
Nano-TiO_2	Cosmetics (incl. sunscreens)	70–80
	Coatings & cleaning agents	<20
	Plastics	<20
	Paints	10–30
	Cement	1
	Others	<10
Nano-ZnO	Cosmetics (incl. sunscreens)	70
	Paints	30
CeO_x	Chemical mechanical planarization	45–80
	Fuel catalyst	1–50
	UV-coatings, paints	5–10
CNTs	Composites & polymer additives	20
	Materials	80
	Composites	50
	Batteries	50
Fullerenes	R&D	80
Nano-Ag	Paints, coatings & cleaning agents	10–30
	Textiles	30–50
	Consumer electronics & conductivity	10–20
	Cosmetics	20
	Medtech	20
	Anti-microbial coatings	80–100
Quantum dots	Light conversion for LED/OLED	90
	Lab use for imaging	10

In 2015, Vance and co-workers created eight new descriptors for consumer products to facilitate the use of the CPI database by a variety of regulatory communities such as industry, researchers, governmental and non-governmental organizations. The descriptive categories are: *i)* main NM composition or type; *ii)* NM shape and size; *iii)* NM coating or stabilizing agent; *iv)* NM location within the product; *v)* NM function in the product; *vi)* potential exposure pathways; *vii)* "how much we know" (mainly made to study the reliability of the manufacturer's claim that products contain NM); and *viii)* "researchers say" (based on nanotechnology experts survey) (Vance et al., 2015).

Interestingly, among the number of available products in the market, the Health and Fitness category comprised the largest list, with 505 products in 2014 (e.g. toothbrushes, lotions, sunscreens, cosmetics, etc.) (Figure 5). The following categories were Home and Garden (246 products), Automotive (152 products) and Cross-cutting (95 products), while Food and beverage reached the 6th position with 72 products listed by CPI in 2014 (Figure 5).

Table 3. Number of products in the CPI over time (Source: Vance et al., 2015).

Year	Total products	Products added	Products archived	Data collection notes
2005	54	54	0	Beginning of CPI as a static pdf document.
2006	356	302	0	Launch of the online CPI.
2007	580	278	0	Nanoscale silver emerged as most cited nanomaterial.
2008	803	223	0	Health and fitness products represented 60% of the inventory.
2009	1015	212	107	Added archiving function to the CPI.
2010	1015	0	0	No data collected.
2011	1015	0	0	No data collected.
2012	1438	426	0	Beginning of CPI 2.0 project, focus on adding new products.
2013	1628	190	288	Launch of crowdsourcing component. Extensive effort put into adding and archiving products.
2014	1814[a]	238[a]	223[a]	Extensive effort put into adding and archiving products.

[a]The CPI now has crowdsourcing capabilities, so these numbers are a snapshot in time and will not represent the CPI at the time of reading.

Out of the classical NMs that currently have commercial applications, nanoscale polymers and polymeric nanocomposite materials are the most manufactured and applied (e.g. from kilograms to tons of products a year). Several sources have estimated that the most produced ENM is titanium dioxide, with up to 10,000 tons (t) of worldwide production, followed by cerium dioxide, zinc oxide and carbo-nanotubes, with productions ranging from 100 to 1,000 t/year. Controversial data have been reported for nano-silica, since a range from less than 10,000 to more than 1,000,000 t/year is reported, depending on the source (Figure 6) (Aitken et al., 2004; Piccinno et al., 2012; Laux et al., 2017).

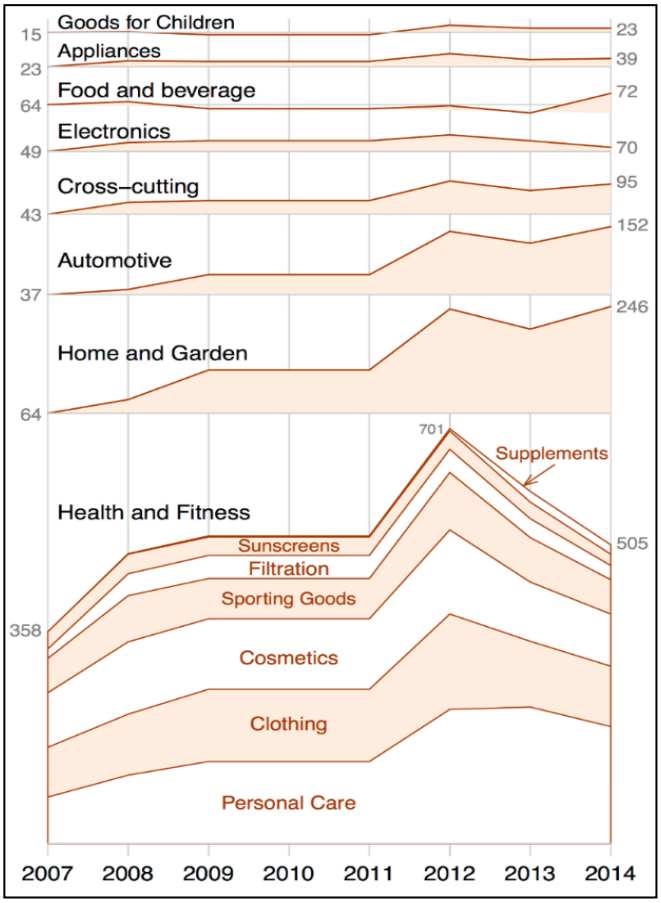

Figure 5. Number of available products over time, grouped under eight generally accepted consumer goods categories and Health and Fitness subcategories. (Source: Vance et al., 2015).

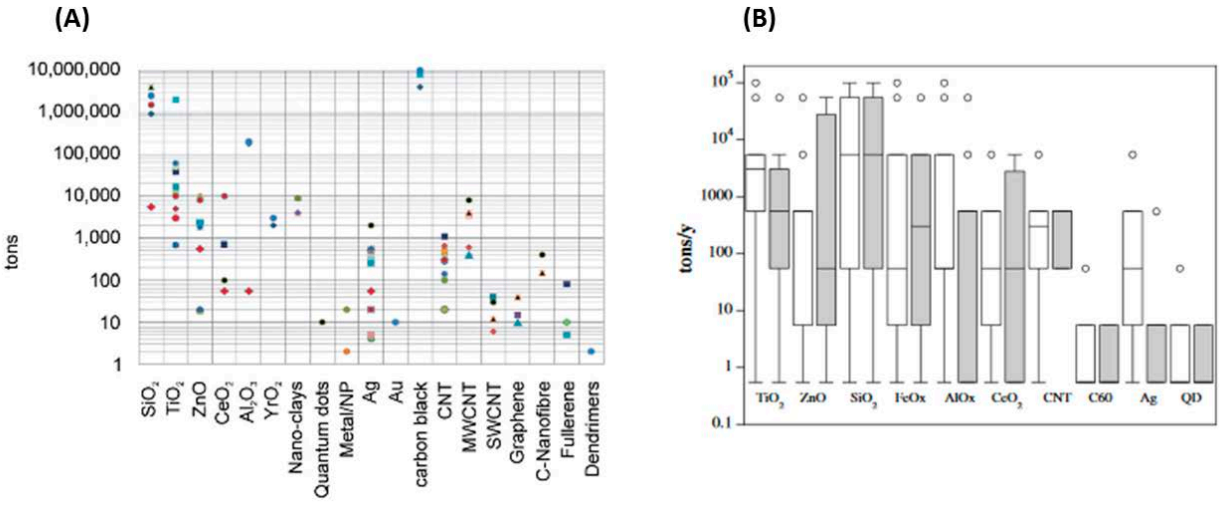

Figure 6. (A) Production of ENMs up to 2010. Different symbols represent estimations by different sources (Source: Laux et al., 2017). **(B)** Boxplots of the ENM production (in tons/year) showing the median and the 25/75 % quantiles. White boxes represent worldwide production and grey boxes European production (Source: Piccinno et al., 2012).

As shown in Figure 6, titanium dioxide (TiO_2), silicon dioxide (SiO_2), and zinc oxide (ZnO) are the most produced NMs worldwide. Although the global annual production of silver NPs (AgNPs) represents only 2% of that of TiO_2, AgNPs are the most popular NM in the CPI inventory, being present in 438 products (Vance et al., 2015) (Figure 7). Considering that AgNPs present important anti-microbial properties, this NM has become very used in a wide range of scientific and industrial areas. In this context, it has been published that 53% of EPA-registered biocides contain AgNPs (Nowack et al., 2011). In addition, AgNPs are found in water filters, algaecides and in antimicrobial additives that do not claim to contain NPs. Surprisingly, the constantly-updated CPI list contains a huge amount of products with unknown NM composition (Figure 7 (a)). In order to solve these gaps, further efforts are currently performed worldwide to address and regulate the production and stage handling/use of NMs by legislation and/or by recommendations and guidance (van der Meulen et al., 2014; Arts et al., 2014). Up to the last decade, there was no legislation entirely dedicated to the regulation of NMs in the EU or in any other country. In fact, only a few reports have been recently published aiming to summarize the existing legislation and to provide guidance for risk assessment, as well as other relevant documents related to NMs in different countries (Amenta et al., 2015).

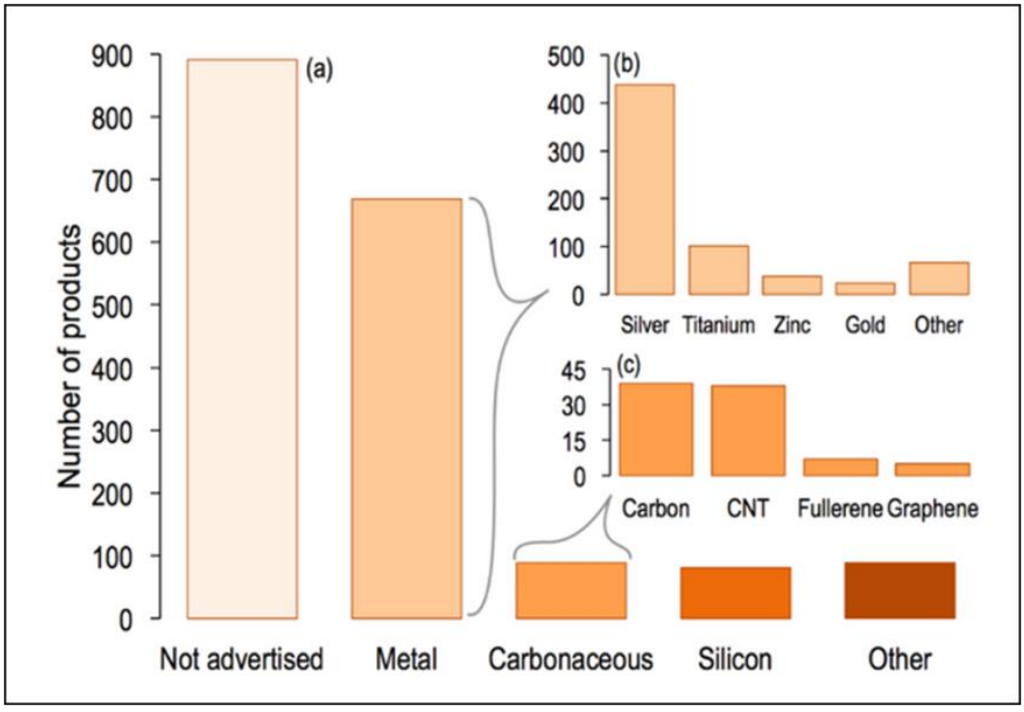

Figure 7. Composition of NMs included in the CPI list, grouped into five major categories: not advertised, metal, carbonaceous, silicon and others (Source: Vance et al., 2015).

A clear example of the little regulation of the nanoscience field is the information about the occupational exposure to NPs of workers. Very limited information has been found about exposures in the university/research sector or in nanotechnological companies. Three studies were carried out at workplaces that simulated laboratory work conditions. These studies covered a wide range of materials, including carbon black, various metal and metalloid oxides, silver, aluminium, fullerenes and nanotubes (single-walled and multiwalled), etc (Kaluza et al., 2009; Brouwer, 2010; Kuhlbusch et al., 2011). Surprisingly, all of them concluded that there are many information deficits requiring research activities and mentioned several deficiencies that make it difficult to compare results among studies, mainly i) the lack of a harmonized approach concerning the strategies and instrumental methods, parameters, dimensional ranges used, and the data analysis, ii) the absence of any indication of uncertainty and the instruments detection limits, and iii) the absence of precision regarding the contribution of other sources to the concentrations measured (Kuhlbusch et al., 2011). The urgent need of information to establish a framework on NMs regulatory approaches and guidance is well illustrated in Figure 8, which shows the time delay between the emergence of products containing NMs, the development of any associated environmental health information, and the subsequent lag in bringing this information to governmental institutions and regulatory agencies.

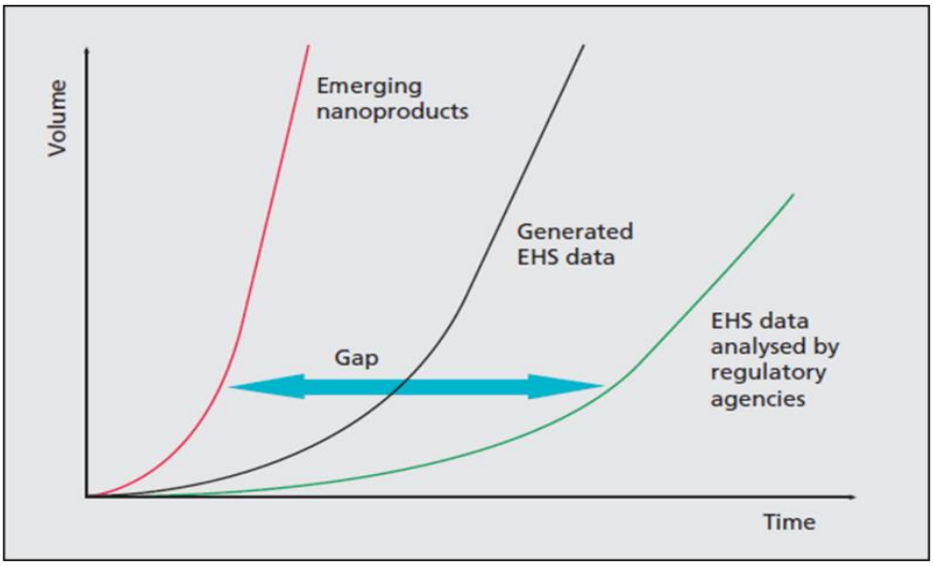

Figure 8. Reported gap among the emerging nanoproducts established in the market in comparison to the generation of health and safety data and their subsequent use by regulatory institutions.

1.2.6. Potential human exposure to ENMs and body entry routes

Human exposure to NPs can be described through different kinds of interaction. Firstly, occupational exposures mainly occur in workers (including engineers, scientist, and technicians) during the research, synthesis, and commercial production of NM-based products. This exposure mainly results from direct contact with raw materials while carrying out reactions. Moreover, packing and transport of the resulting NMs (big quantities of the NM powder) can also be a source of this type of exposure. Secondly, although not at the same amount as workers, consumers are also exposed to NMs during usage and application, potentially leading to harmful and toxic effects. Hence, potential interactions of NPs with target organs in the human body have been hypothesized, and they can occur through different routes of entry such as *i)* penetration through dermal absorption, *ii)* respiratory system intake via inhalation, and *iii)* digestive system intake via ingestion (Figure 9) (Tsuji et al., 2006; Debia et al., 2013; Sajid et al., 2015).

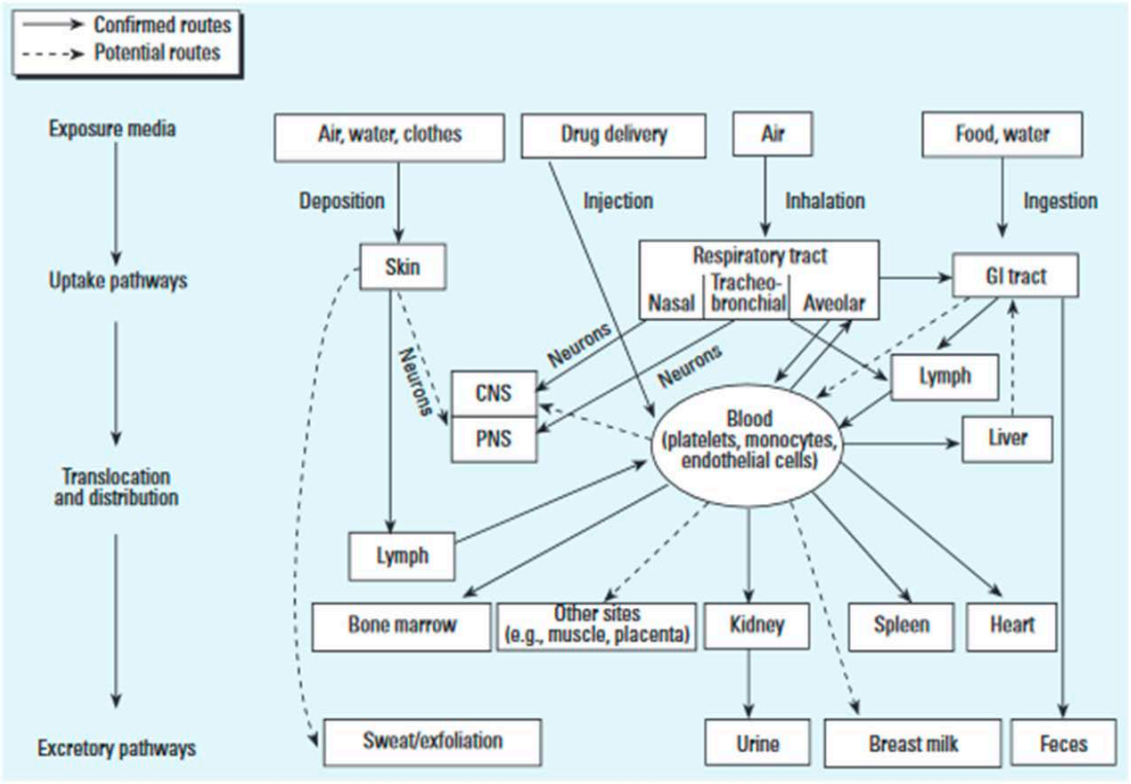

Figure 9. Body's entry and translocations routes of NMs. Many of these uptake and translocation routes have been demonstrated, while others are still hypothetical and need to be further investigated.

One of the most important points before predicting the putative toxicity of NPs is to present evidence and collect knowledge about the factors and properties that could play a major role in promoting their toxicity. The way these particles interact with the human body will decide their fate, effects and consequences. Uptake, clearance and distribution of NPs in the human body depend on several factors such as their nature (chemical composition and physical properties), as described in the section 1.2.4. Besides their intrinsic parameters, the biological barriers found will also play an important role. Thus, each NPs could behave differently depending on their morphological structure and biological components (e.g. number of epithelial layers, composition of the extracellular matrix, presence of mucus secretion, etc.).

a) Penetration through the skin

The exposure of human skin to NPs can occur in an intentional or unintentional manner. The first case could be due to the use of cosmetic products such as creams, lotions and sunscreens containing coated NPs of TiO_2 and ZnO. Unintentional exposure of NPs would occur through direct NPs manipulation during their manufacture or through vehicle emissions, natural gas/powdered equipment, welding fumes emissions, etc (Zimmer et al., 2002; Rundell, 2003; Oberdörster et al., 2005).

The skin is formed mainly of three epithelial layers: the epidermis, the dermis and the subcutaneous. Even though the *stratum corneum* (the outer portion of the epidermis) is 10 µm thick and keratinized of dead cells, some studies have shown that NPs are able to penetrate it (Tinkle et al., 2003; Toll et al., 2004; Sajid et al., 2015). Thus, there are different putative mechanisms of NPs penetration to the deeper layers of the skin: intercellular trans-epidermal mechanism, through broken or injured skin and/or diffusion through skin pores and hair cavities (Bennat and Müller-Goymann, 2000; Oberdörster et al., 2005; Teow et al., 2011). Disparity of hypotheses surrounds the putative toxic effects through this exposure route, as toxicity during epithelium or tissue accumulation for a long time, and the role of photo-activation in the reactivity of NPs (Tsuji et al.. 2006). Nevertheless, it must be highlighted that the amount of NPs able to penetrate the skin barrier is very low, as less than 1% of the total amount of sunscreen locates in the hair cavities (Lademann et al., 1999).

b) Intake by the respiratory system. Inhalation

Upon inhalation, NPs can penetrate deeper into the lungs and interact with the epithelium. Due to the lungs large surface area, conferred by gas-exchange surfaces

such as the alveoli, it is the primary entry interface for inhaled particles (Oberdörster et al., 2005). The behaviour of inhaled NPs differs significantly if they're gases or volatile liquids. NPs deposition on lungs depends on the aerodynamics of the particles, their physical-chemical characteristics, the respiratory tract anatomy, and the health status of the host (Hoet et al., 2007). Once deposited, these NPs could be able to cross the blood-air tissue barrier and translocate to the bloodstream, where they can spread and reach deeper organs (Oberdörster et al., 2005). NPs attached to the alveoli that linger for prolonged time periods may cause cell membrane damage, localized epithelial inflammation and, thus, the consequent lung impairment or malfunction (Miller et al., 2005; Mühlfeld et al., 2008). For example, compared to oral or dermal exposure which has little effects, CNTs' toxicity is more adverse in case of inhalation, causing severe inflammation (Foldvari and Bagonluri, 2008). Nevertheless, studies regarding the mechanisms of NPs translocation to other organs are still very rare and conflicting. While Oberdöster and coworkers found a fast translocation towards the liver of more than 50% of C-13NPs (26-nm size) in a rat model under inhalation exposures, Kreyling and colleges observed less than 1% of iridium NPs translocation (15-20 nm size) into the rats bloodstream which later reached several organs (Kreyling et al., 2011; Oberdörster et al., 2002).

c) Uptake by the digestive tract. Ingestion

According to Oberdöster et al. (2005), ingestion of NPs is one of the major exposure routes. NPs can directly be ingested, as they are employed in food, food additives or used in drugs, or they can be swallowed indirectly if they have been released from food packaging and have attached to the food. Once ingested, NPs can be absorbed through different mechanisms in the gastrointestinal tract, to subsequently enter the lymphatic tissue and translocate to the bloodstream (Teow et al., 2011). Many NPs characteristics are involved in controlling the absorption of NPs in the gastrointestinal tract, including the size, geometry, surface charge, ligand type, and the formed biocorona of particles (Hillyer and Albrecht, 2001). Moreover, perhaps the most significant aspect modulating NPs uptake is the extremely low pH of the stomach and the high ionic strength in the stomach and intestine, which can critically affect NPs properties (Bouwmeester et al., 2017).

The use of *ex-vivo* tissues and *in vitro* systems such as Caco-2 monolayers and Caco-2/HT29/Raji-B co-cultures, as well as *in vivo* models, has lead to a non-clear consensus to postulate specific uptake routes used by NPs to cross the intestinal

barrier. Nevertheless, several hypotheses have been postulated to explain how NPs can cross the intestinal epithelium. They include para-cellular transport, intracellular uptake, or through M cells, a well known mechanism involved in the active translocation/transport of macrophages and macromolecules to the inner regions of the epithelium (Corr et al., 2008; Schimpel et al., 2014; Bouwmeester et al., 2017; Farrell and Magnuson, 2017).

Gastrointestinal exposure to xenobiotics such as NPs can result in the alteration of food/nutrient metabolism and absorption, or even affect the gut flora composition. At this point, it should be remembered that changes in gastrointestinal permeability and intestinal epithelial inflammation or injuries may lead to chronic diseases such as Crohn's disease, the irritable bowel syndrome (IBS) or inflammatory bowel disease (IBD) (Guo et al., 2017; Bouwmeester et al., 2017).

The use of TiO_2NPs as food additives is well-known and, in addition, they are found in several consumer products such as toothpaste, chewing gum, and candies (Weir et al., 2012). This has prompted researchers to focus their efforts in the study of TiO_2NPs toxicity after ingestion, which results in oxidative stress damage to the digestive gland cell membrane (Valant et al., 2012). Also, it was found that Peyer's patches accumulate pigmented material from the gut lumen, including TiO_2, and that similar materials are present in inflammatory aggregates of Crohn's disease patients and in children suspected of having IBD (Shepherd et al., 1987; Hummel et al., 2014). The hypothesis associating the ingestion of TiO_2 with the pathogenesis of IBD and related disorders (Lomer et al., 2002) has recently been supported by experimental evidences. For example, administration of TiO_2NPs to rodents has shown to induce inflammation in the small intestine, exacerbate colitis, promote colitis-associated tumours, and induce colonic inflammation lesions (Nogueira et al., 2012; Ruiz et al., 2016; Urrutia-Ortega et al., 2016). Nevertheless, these murine studies used high doses of TiO_2NPs (10-100 mg/kg/day), which are far from the recently-published estimations of intake levels in the Dutch population, which are around 0.55 µg/kg/day in adults and up to 2.16 µg/kg/day in infants (Rompelberg et al.. 2016). Thus further work is needed to re-evaluate the potential toxicity of TiO_2NPs by using realistic and chronic doses.

1.3. Titanium dioxide NPs (TiO_2NPs)

Since the study of the potential health effects of TiO_2NPs constitutes one of the aims of our study, a detailed description of their characteristics and potential effects is required. Nanoscale titanium dioxide is one of the most commonly manufactured NPs,

since is a non-combustible, non-soluble and odourless white powder employed as a white pigment in paints and papers, as a photo-catalyst in solar cells and an optical coating in ceramics, among other applications. Moreover, TiO_2's bulk material was approved as a food additive by the Food and Drug Administration (USA) in 1966 (CFR, 2016). In the European Union, the European Food Safety Authority (EFSA) registered TiO_2 as E171, being "E numbers" codes for substances that can be used as food additives (EFSA, 2016). Thereby, the TiO_2 bulk form is commonly used as a whitening pigment in a wide variety of consumer products in the food industry and personal care products (FAO/WHO, 2010). Surprisingly, a significant amount of bulk TiO_2 found in food was identified as NM; in fact, a recent study found out that at least 36% of this TiO_2 is in its nano-form (Weir et al., 2012).

Estimations based on international and national reports postulated that a total of 165,050,000 metric tons of TiO_2 were produced worldwide from 1916 to 2011 (Figure 10). The United States was the leading producer until 2010, when it was surpassed by China, producing nearly 2,000,000 metric tons, a 35% share of the global market (Jovanovi, 2014). However, it is not known how much of this TiO_2 is used as a food additive or ends up in the environment each year.

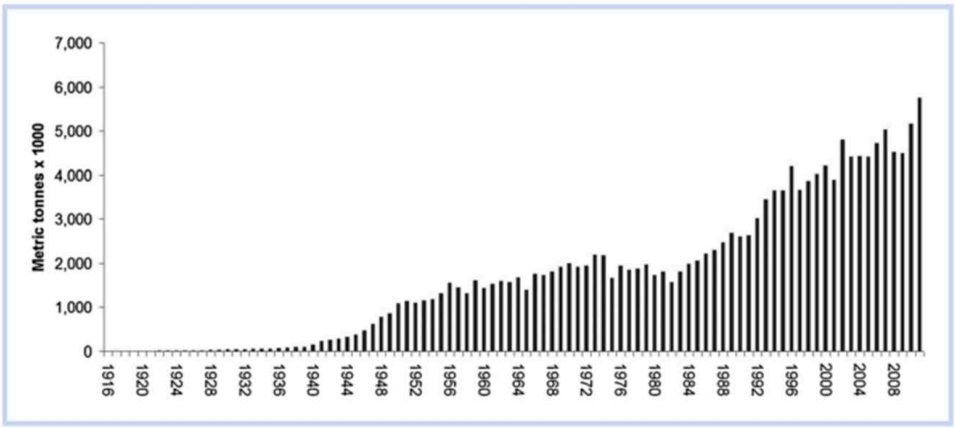

Figure 10. Historical worldwide production of titanium dioxide pigment (Source: Jovanovi, 2014).

1.3.1. Occurrence and industrial characteristics of TiO_2NPs

Titanium (Ti), the ninth most abundant elemet in the earth's crust, is widely distributed. Owing to its great affinity for oxygen and other elements, Ti does not exist in the metallic state in nature. The most common oxidation state of Ti is $^{+}4$, but $^{+}3$ and $^{+}2$ states also exist. TiO_2, also known as titanium (IV) oxide or Ti white, can naturally exist in three crystal structures: anatase (tetragonal), rutile (tetragonal), and brookite (orthorhombic). Anatase and rutile TiO_2 both have a tetragonal structure, but the TiO_6

octahedron structure of anatase TiO_2 is distorted or is larger than that of the rutile phase (Shi et al., 2013). Rutile TiO_2 is stable at most temperatures, while anatase is not at an equilibrium phase and is kinetically stabilized and have been described to be more chemically reactive (Warheit et al., 2007). Brookite TiO_2 is formed with the edge-sharing TiO_6 octahedron and has a larger cell volume. This form of TiO_2 is not often used in research. TiO_2 presents a very low dissociation constant in water and aqueous systems, thus, it is insoluble in water and organic solvents, as well as under other physiological conditions (Diebold, 2003).

In addition to the above-mentioned forms, Armstrong and co-workers were the firsts to synthesize nanowires of titanium dioxide polymorph (TiO_2-B). They synthesized it in high yield by a simple hydrothermal reaction between NaOH and TiO_2-anatase, followed by acid washing and subsequent heat treatment (Armstrong et al., 2004). Nowadays, TiO_2-B has a very small market as it is only used in the production of Ti nanowires. However high expectations and efforts are invested in its production as new applications are being proposed in the development of lithium-Ion batteries, as well as in enhanced photocatalytic and antibacterial applications (Pinilla et al., 2017; Xu et al., 2018). Nevertheless, rutile and anatase are currently the most important crystal structures of TiO_2 used in commercial products since they are the only ones that combine high refractive index and a high degree of transparency in the visible region of the spectrum (DuPont, 2007).

The main sources of industrial extraction of TiO_2 are mineral and ore-metal deposits. Although rutile and anatase mineral deposits may contain up to 95% of TiO_2, they are difficult to extract from primary rocks. Alternatively, they can be extracted from sand, where they are associated with other minerals. The majority of the TiO_2 pigment used in consumer products is extracted from ilmenite ore ($FeTiO_3$) or leucoxene ore (TiO_2 x $xFeO^x$ yH_2O), following sulphate or chloride processing (DuPont, 2007; Jovanovi, 2014).

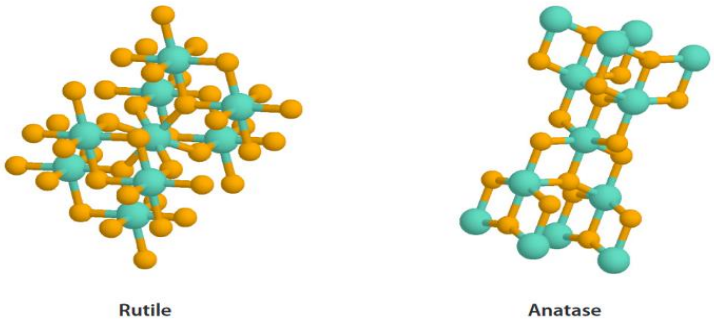

Figure 11. Rutile and anatase TiO_2 crystal structure (Source: NIOSH, 2011).

1.3.2. Human health effects of TiO_2NPs

The International Agency for Research on Cancer (IARC) reviewed the potential cancer risk of TiO_2 in 2010 (IARC, 2010). According to the reviewed information, TiO_2 was classified as a human carcinogen group 2B because there was enough evidence that TiO_2NPs may cause lung cancer by inhalation exposure. This category is used for chemicals that present limited evidence of carcinogenicity in humans and sufficient evidence of carcinogenicity in experimental animals (Jovanovi, 2014). The National Institute for Occupational Safety and Health (NIOSH) also concluded that TiO_2NPs were a potential occupational carcinogen, acting through a secondary genotoxicity mechanism primarily related to particle size and surface area (NIOSH, 2011). Although the role of oral exposure was debated by IARC, the final report was inconclusive about this exposure route due to the lack of standardized procedures for TiO_2NPs risk assessment (Jacobs et al., 2010).

Although several *in vitro* and *in vivo* studies have been carried out assessing TiO_2NPs toxicity in the past decade, they produced a vast amount of conflicting data. Regarding genotoxicity, a recent review including *in vitro* and *in vivo* data concluded that, although many studies detected positive responses, clear inconsistencies existed in the results. In this review, authors postulated that *in vitro* systems for assessing genotoxicity of TiO_2NPs generally produce more positive results than *in vivo* systems, whereas DNA and chromosome damage tests generate more positive results than the assays measuring gene mutation (Chen et al., 2014).

The most accepted hypothesis explaining the putative toxicity of TiO_2NPs involves the production of reactive oxygen species (ROS). Accordingly, evidence indicates that TiO_2NPs induce genotoxicity mainly by generating oxidative stress due to their relatively large surface area and greater reactivity than bulk TiO_2 particles (Jugan et al., 2012). Curiously, Jugan and colleagues reported that experiments performed under dark conditions decreased ROS accumulation, suggesting that TiO_2NPs generate ROS in the cells by a photo-catalytic mechanism (Figure 12). Other studies showed that nano-anatase produced more ROS and was more cytotoxic than nano-rutile, but only after UV irradiation or under sunlight (Sayes et al., 2006; De Matteis et Alm, 2016). Thus, photo-activation appears to be an important mechanism for increasing cytotoxicity of TiO_2NPs. In addition, the size, structure, and aggregation of TiO_2NPs could also play a pivotal role in ROS generation (Toyooka et al., 2012). Cells' differentiation status, as well as cell morphology, could attenuate or enhance the adverse effects of NPs in general and, in particular, of TiO_2NPs. For instance, Song et al. (2015) described how the cell-uptake ability of TiO_2NPs depends on the cell's

differentiation state, as undifferentiated Caco-2 cells swallowed native TiO_2NPs easily, compared to differentiated Caco-2 cells. As a consequence, TiO_2NPs did not generate ROS in differentiated Caco-2 cells, while significant amounts of ROS were detected in undifferentiated Caco-2 cells (Song *et al.*, 2015). The initial oxidative stress produced by TiO_2NPs exposure could also potentially affect DNA repair, cell cycle progression, cell proliferation, and apoptosis by affecting protein structure (Chen et al., 2014).

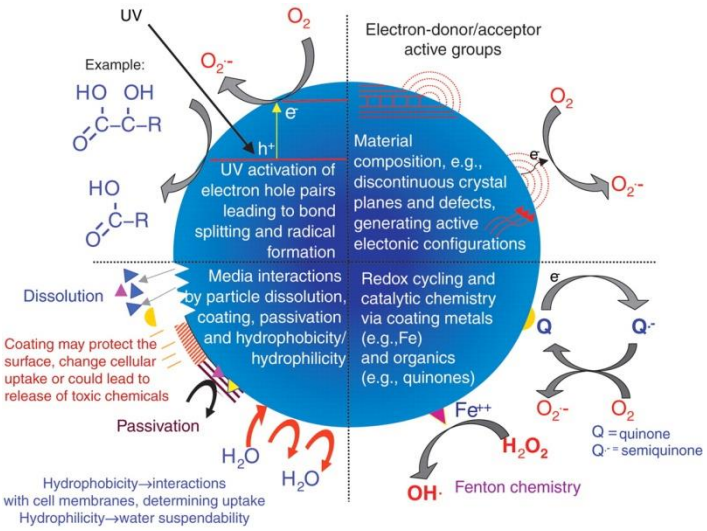

Figure 12. Possible mechanisms by which NPs interact with biological structures. The illustration points out the importance of material composition, electronic structure, bonded surface species, surface coatings and solubility, including interactions with other environmental factors such as UV activation (Source: Nel et al., 2006).

1.4. *In vitro* models for NPs risk assessment

The current risk assessment of NPs (and chemicals) mainly relies on *in vivo* studies using animal models (EFSA, 2011). While these *in vivo* studies provide unique information on the distribution of NPs in a whole organism, the number of animal studies should be reduced as much as possible for several reasons; *i)* the use of animals is ethically debatable, *ii)* animal models do not fully simulate the physiology of humans, *iii)* given the great number and variety of ENPs, it is categorically impossible and economically not feasible to test all of them through *in vivo* models (Hartung et al., 2013). According to this, *in vitro* models have been meticulously developed, gaining importance in the past decade to study the pharmacokinetics and toxicology of NPs in general and, specifically, the underlying mechanisms at molecular and cellular levels of TiO_2NPs effects.

The recently-described non-animal models can range from the utilization of *ex vivo* tissues to combined *in vitro* cell lines and further development of chip-based technologies, synthetic membrane system and *in silico* modelling. These approaches significantly influenced the development of human skin, intestine and lung barrier models that, as previously mentioned, are the main routes of NPs exposure (Figure 13). All these models evolved from the monolayer culture of the respective primary epithelial cells or cell lines to subsequent levels of systemic simulations. Skin models progressed from keratinocyte monolayers to full-thickness air-exposed skin cultures on-a-chip. Intestinal models progressed from monolayer Caco-2 cell line culture to systemic chip-based co-culture with liver and tumour cells. Also, lung models progressed from alveolar and bronchial epithelial barrier cultures to mechanically coupled alveolar models on-a-chip (Figure 13). However, only a single epidermis skin model has been validated at OECD level, fully replacing its respective animal models (OCDE, 2004; Gordon et al., 2015).

The increased interest of the food industry to introduce NMs in foods or in food packaging has triggered the potential ingestion by a large proportion of the population. Moreover, considering that oral exposure of NMs (as TiO_2NPs in candies and sweets) can overlap with the inhalation route because a considerable share of inhaled substances reaches the gastrointestinal tract (GIT) following clearance from the respiratory tract, further attention has to be paid to this entry route. For this purpose, and in order to increase the awareness of the behaviour and interaction of ENMs in the GIT, in the present Thesis we have developed and used two *in vitro* models that perfectly mimic the small intestinal epithelial barrier: the Caco-2/HT29 and the Caco-2/HT29/Raji-B co-culture. These system of co-culture has been previously described theoretically and developed in other laboratories, leading to diverse protocols and non-consensus approaches (Gullberg et al., 2000; des Rieux et al., 2007; Chen et al., 2010; Schimpel et al., 2014).

1.4.1. The Caco-2 cell monolayer

Various cell lines originating from different segments of the GIT are commonly used in chemical risk assessment (e.g. TR146, T84, IEC-6, Caco-2, HT29, etc.). Among the available cell-lines, intestinal Caco-2 cells have been the most commonly used (Lefebvre et al., 2015). Caco-2 cells were obtained from a colon adenocarcinoma of a 72 years-old Caucasian men. These intestinal cells gained popularity due to their capacity to undergo spontaneous cell differentiation, leading to the formation of a cell

monolayer (Figure 14A). This system accurately mimics the mature small intestine enterocytes, both at a morphological and a functional level (Pinto et al., 1983; Artursson, 1991). Basically, cultures of Caco-2 cells form a well-differentiated polarized monolayer of columnar absorptive cells expressing a brush border (also known as microvilli) where the typical small intestinal enzymes and transporters are expressed on their surface (Figure 14B) (Artursson, 1991; Hilgendorf et al., 2000). It has also been reported that Caco-2 cells are able to express all of the major amino acids-, electrolytes-, fatty acids-, sugars/carbohydrates-, iron-, and zinc-uptake, storage, transport, and carrier proteins, which make this model useful to study the potential alterations in nutrient absorption after putative toxicological or beneficial conditions (Hauri et al., 1985; Halleux and Schneider, 1991; Levy et al., 1995; Han and Wessling-Resnick, 2002; Kipp et al., 2003; Shen et al., 2008).

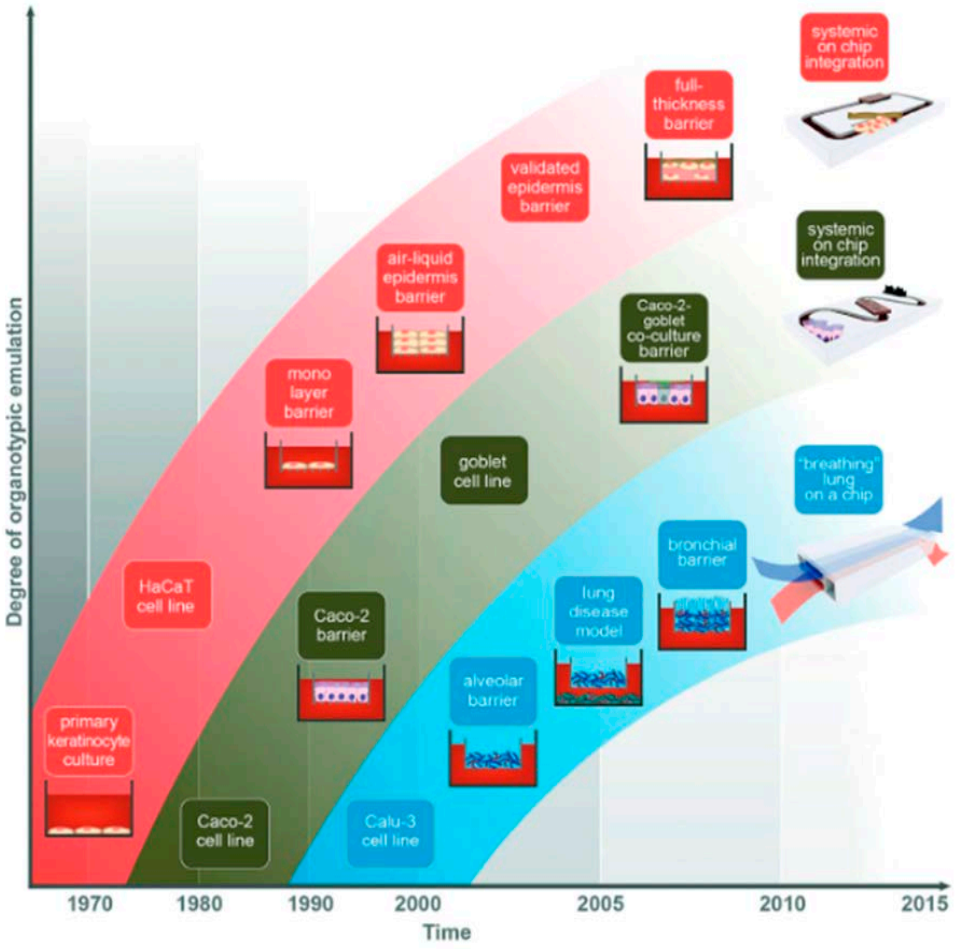

Figure 13. Development and evolution of *in vitro* models of human outer epithelia. *In vitro* models of skin (pink boxes), intestine (green boxes) and lung (blue boxes). (Source: Gordon et al., 2015).

The resulting monolayer of Caco-2 cells presents heavy integrity, mainly by the expression of junctional complexes mediating the communication between cells. The junctional complexes include diverse, well-defined structures such as gap junctions, desmosomes, adherent junctions (AJ), and the tight junctions (TJ). Specifically, TJ have been described to play an important role in polarized epithelial cells, providing a permeable barrier between two very different environments, and to enable vectorial transport across the cellular layer. These are the most apical structures of the junctional complex, and are basically composed by three different protein families: zonula occludens, occludins, and claudins (Figure 14B) (Denker and Nigam, 1998; Harhaj and Antonetti, 2004; Paris et al., 2008). Thus, as the transport of ENMs through the human epithelial barriers is one of the major endpoints to solve, the paracellular permeability and the role of the TJ components has been largely studied and exploited in the nanotoxicology field.

Worldwide, laboratories are using the same cell differentiation protocol for Caco-2 cells. Briefly, Caco-2 cells are seeded at the desired cell concentration onto polyethylene terephthalate transwells (PET) and are left differentiating for two or three weeks. This transwells/inserts present pores (with a diameter ranging from 0.4 to 3 μm) that allow the permeation of cell medium components and/or the studied compound (Figure 14C). Moreover, the transwells permit the cells to grow in a monolayer working as a support while separating the apical and the basolateral compartments (Artursson, 1991). Due to all the aforementioned characteristics, the use of Caco-2 cells monolayers as a standard permeability-screening assay for the prediction of drug intestinal absorption has been popular and widely used in many areas of nutrition, pharmacology and toxicology research. While some studies point out that permeability through Caco-2 monolayer system correlates well with *in vivo* absorption in humans (Shah et al., 2006), others postulate that the rate of paracellular transport in Caco-2 cells monolayer is typically more limited than in the human intestine. The total transport values for many conventional molecules through Caco-2 cells are similar to values obtained through human colon and rectum biopsies, but not for small intestine (Rubas et al., 1996; Chen et al., 2010). In addition, the permeability of Caco-2 monolayers to hydrophilic compounds that are generally transported by paracellular mechanisms is poor because of the relatively higher amount of tight junctions present in these cell monolayer (Walter et al.,1996; Artursson et al., 2001).

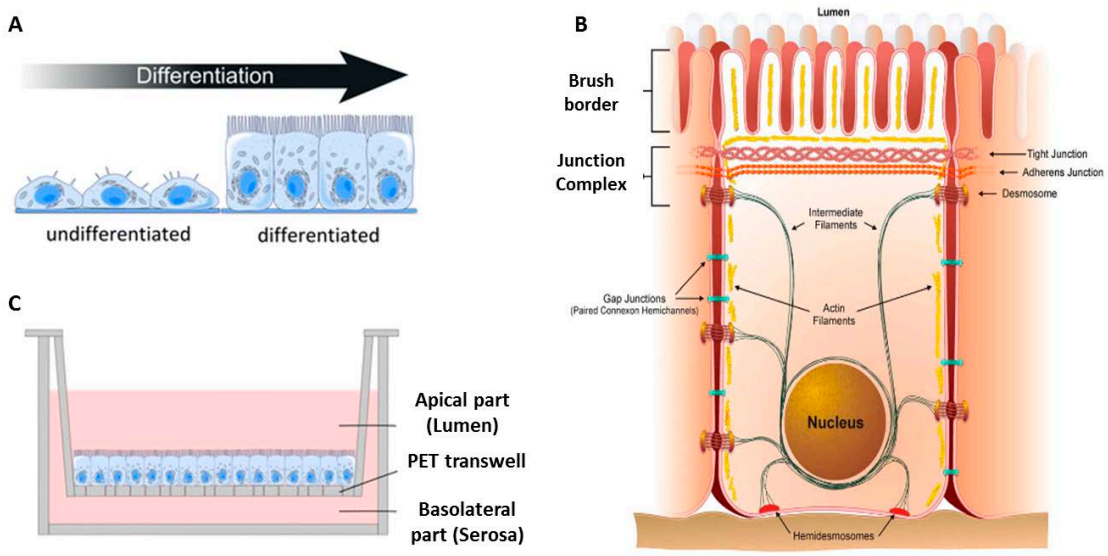

Figure 14. (A) Illustration of the Caco-2 cells' differentiation process. **(B)** Completely differentiated Caco-2 displaying its columnar shape, apical brush border and the junctional complexes. **(C)** Scheme of the *in vitro* Caco-2 monolayer and the devices used. (Adapted from Guttman and Finlay, 2009; Kucki et al., 2017)

Some disadvantages have appeared in the use of the Caco-2 model, as well as in other monocultures of epithelial cells, as they do not closely simulate the real conditions and/or composition of the normal epithelial layer, which presents several cell types (Hidalgo, 1996). For example, it is known that the intestinal epithelial cell layer is separated from the luminal space by a dense mucus layer. This mucus layer acts as a physical and chemical defence against food particles, chemicals, enzymes and host-secreted products such as bile acids, microbiota and microbial products (Johansson et al., 2008). As only goblet cells are mucus-secreting, a mucus layer will be lacking in the Caco-2 barrier model. In this context, it has been postulated that, since the HT29 cell-line produces both the membrane-bound MUC1 and the gel-forming MUC5 among others (Lesuffleur et al., 1993), it can be useful as a component of an *in vitro* model of the intestinal barrier. The presence of mucus in the *in vitro* intestinal model system is important for intestinal permeability estimation, as the mucus acts as a barrier against some compounds, particularly those that are lipophilic (Behrens et al., 2001).

1.4.2 Caco-2/HT29 as an *in vitro* model for intestinal exposure

HT29 is also a human colon adenocarcinoma cell line. It was isolated from a primary tumour of a 44 years old Caucasian female. Initially, this cell line was used to study different aspects of the biology of human cancer. However, these cells have attracted

attention due to their ability to express characteristics of mature intestinal cells, such as enterocyte-like cells and mucus-producing goblet cells (Verhoeckx et al., 2015). Under favourable culture conditions, HT29 cell differentiation is very similar to the observed in Caco-2 cells, but in HT29 the differentiation process into enterocyte-like cells is longer (30 days vs. 15-21 days in Caco-2), the levels of enzymatic activity is lower than in Caco-2, lactase is absent, and only 40-50% of HT29 cells express sucrose-isomaltase (SI) (Zweibaum et al., 2010). However, one of the main differences between this cell line and Caco-2 is that HT29 cells produce mucin at a relatively high level (Huet et al., 1987; Maoret et al., 1989). For this reason, a co-culture of these two cell lines will provide a model comprising the two most represented cell types in the normal small intestine epithelium: enterocyte and goblet cells (Figure 15).

Already in 1995, Wikman-Larhed and Artursson were the firsts in characterizing an *in vitro* co-culture model comprising Caco-2 cells and goblet-like HT29 cells (Wikman-Larhed and Artursson, 1995). One year later, Walter and colleagues established another *in vitro* model using HT29-MTX and absorptive Caco-2 cells in co-culture, although underestimations of absorption rates for active transport of drugs in the cell culture were found when compared to *in vivo* data (Walter et al., 1996). Both HT29-MTX and HT29 are clones adapted to high concentrations of methotrexate (MTX) and have been described as exclusively mucus-secreting differentiated cells that produce mucus at earlier stages of the differentiation. These co-culture components have been used posteriorly, but varying the ratio of Caco-2 (75%) and HT29-MTX (25%) cells, which completely covers the cell barrier with mucus. This model was used to study iron bioavailability, and the resulting data correlated well with human's *in vivo* data (Mahler et al., 2009). However, in vivo data seems to indicate that the amount of mucus-secreting goblet cells ranges from 10% in the small intestine to 24% in the distal colon (Forstner et al., 2004).

1.4.3. Caco-2/HT29/Raji-B model as a triple co-culture for the study of NPs translocation

Apart from enterocytes and goblet cells, epithelial microfold cells (M-cells) located in the follicle-associated epithelium (FAE) overlying the Peyer's patches (organized lymphoid follicles) also present a dominant role in the intestinal barrier permeability. Although they represent a minor population in the FAE, M cells have demonstrated to be responsible for the uptake of microorganisms and exogenous substances (Siebers and Finlay, 1996). They are highly specialized in phagocytosis and transcytosis of gut

luminal content across the epithelium. Under the M cells present in the basolateral membrane, there is an intraepithelial "pocket" where the luminal content samples are delivered (indicated with a red arrow in figure 16). This intraepithelial structure contains various populations of lymphocytes, macrophages and dendritic cells (Figure 16). Thus, M cells are thought to play a critical role in antigen-sampling and to be essential for mucosal immune responses (Iyono and Zegami, 2015).

***In vitro* model**	**Schematical Representation**	**Main Characteristics**
Differentiated Caco-2 cells (Monolayer)	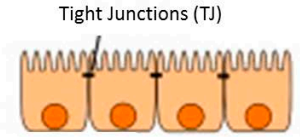	Simpler intestinal epithelium model: enterocytes mono-culture. It allows the study of both transport efficacy and safety of substances.
Caco-2 cells/HT29 co-culture (Barrier)	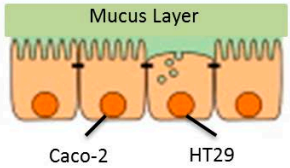	More complex intestinal epithelium model: enterocytes and goblet cells co-culture. It allows the study of both efficacy and safety of substances. Useful to study transport mechanisms and to evaluate the mucus layer impact.

Figure 15. Schematic comparison of Caco-2 mono-culture models from Caco-2/HT29 co-culture (Adapted from Ciappellano et al. 2016).

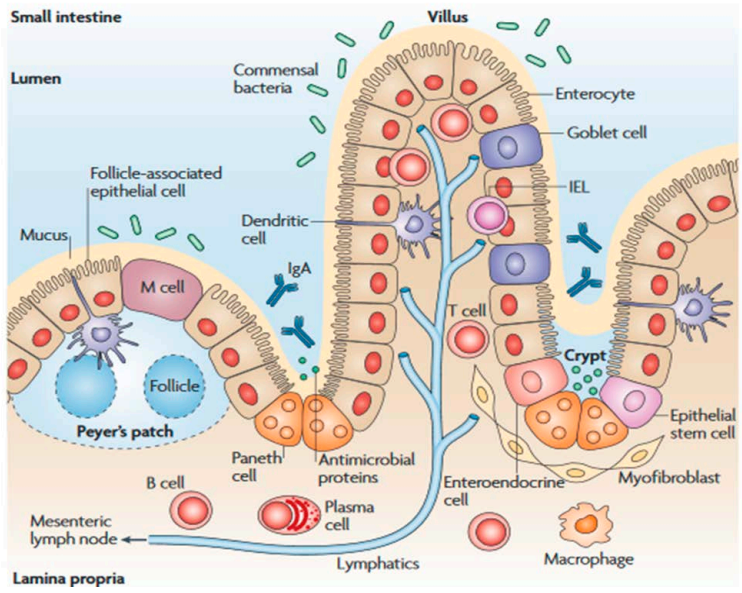

Figure 16. Anatomy of the intestinal immune system. A single layer of intestinal epithelial cells provides a physical barrier that separates the trillions of commensal bacteria in the intestinal lumen from the underlying lamina propria. The small intestine has regions of specialized epithelium termed follicle-associated epithelium where microfold (M) cells overlie the Peyer's patches (image adapted from Abreu, 2010).

Since approximately <5% of the cells within the FAE are M-cells, further efforts have been done to mimic this type of cells *in vitro* (Kernéis et al., 1997, 2000; Gullberg et al., 2000; Kanaya and Ohno, 2014). B-cells were found to be indispensable in M cells' development, given that the follicle-associated epithelium of Peyer's Patches lacks M-cell development in B-cell-deficient mice (Golovkina et al., 1999). According to this, Kernéis et al. constructed the first intestinal *in vitro* co-culture model based on Caco-2 cells on inverted inserts and mouse Peyer's patch lymphocytes which entered the epithelial monolayer and triggered M-cell differentiation. This incubation did not alter the membrane's polarity and the integrity of Caco-2 cells remained constant. However, villin and SI, two proteins that exhibit brush-border organization, disappeared from the apical side of the Caco-2 cells, and some enzymes were downregulated (Kernéis et al., 1997). Immediately, Gullberg and co-workers aimed to improve the system and developed a similar model based on a co-culture of Caco-2 cells on normally oriented inserts and human Raji-B lymphocytes instead of mouse cells. Raji cells exhibit B-cell markers, which are the major factor in the induction of M-cells (Gullberg et al., 2000; des Rieux et al., 2007). Thus, by co-culturing Caco-2 cells with Raji-B lymphocytes, Caco-2 cells lose their apical brush border organization,their typical columnar shape and, therefore, their digestive function as enterocytes. For this reason, the triple co-culture model Caco-2/HT29/Raji-B has become the most recent strategy to develop an *in vitro* model able to accurately reproduce the intestinal epithelium and to study intestinal absorption (Antunes et al., 2013).

Several efforts have been carried out to phenotype and describe the *in vitro* induced M-cells. As aforementioned, in comparison with polarized Caco-2 cells, M-cells lack microvilli on their apical surface, which can be observed by transmission electron microscope (TEM) or scanning electron microscope (SEM) (Kucharzik et al., 2000; Roberts et al., 2010; Schimpel et al., 2014). Furthermore, in agreement with their transcytotic capability, *in vitro* co-cultures expressing M-cells present a higher likelihood of transporting bacteria, viruses, NPs and even microparticles from the apical to the basolateral chamber of the system (Schulte et al., 2000; Gullberg et al., 2006; des Rieux et al., 2007; Lai and D'Souza, 2008; Roberts et al., 2010; Antunes et al., 2013). However, many discrepancies have appeared when the expression of specific molecular markers was investigated. For example, the use of lectin antigens such as *Ulex europaeus* agglutinin 1 (UEA-1) and *Wheat germ* agglutinin (WGA) was thought to specifically identify M cells (Giannasca et al., 1994; Schimpel et al., 2014). However, UEA-1 and WGA react not only with M-cells but also with goblet cells and the mucus layer covering the epithelium, suggesting that they are not specific markers for M-cells

(Giannasca et al., 1994; Ohno and Hase, 2010). Despite this, other molecules ranging from selectines to adherent membrane components have been investigated as likely and potential M cells markers (summarized in Table 4).

In spite of these gaps and discrepancies, the interest in *in vitro* model systems such as Caco-2/HT29/Raji-B co-culture is increasing due to their potential to improve the toxicokinetic analysis of ENMs with high-throughput, cost-effective, and good predictability potential analyses. An additional advantage is the possibility to use cell lines that are derived from humans.

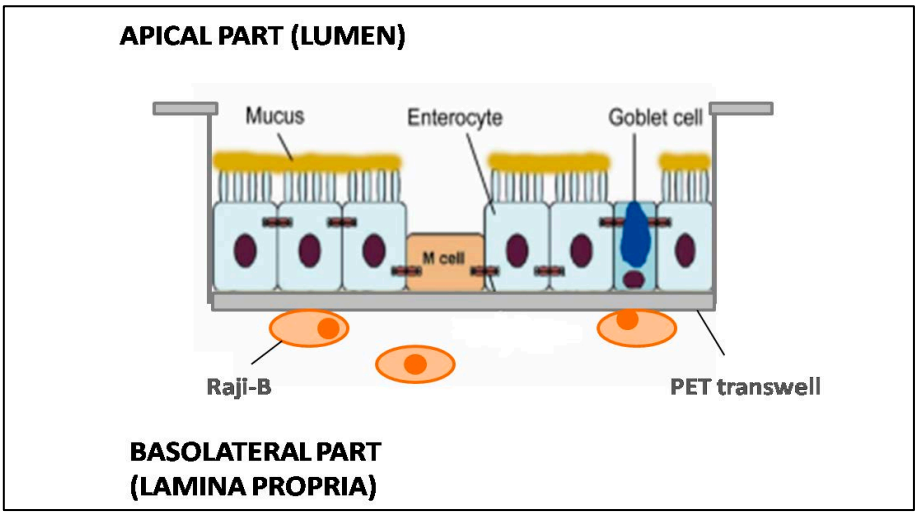

Figure 17. Schematic illustration of the *in vitro* triple co-culture model that approximates the most to the real small intestine physiological environment.

Different endpoints are utilized to evaluate the performance of intestinal system barrier function for the ENMs risk assessment. Some of these include the trans-epithelial electrical resistance (TEER), the permeability increase in epithelial cells, changes in gene expression of cell junction proteins (gap junctions, adherents junctions and tight junctions), brush border enzymes activity, immunotoxicity and genotoxicity. Also, the typical specific components of seeded cell lines used to evaluate the model's function are the apical and basal supernatant as well as cell lysates. These are used to monitor the bio-kinetics of the studied substance, signalling molecules and activation factors, as well as their concentrations and numerous other parameters.

Table 4. The most studied putative M cell markers.

Potential M-cells markers	Function and location	Study
Sialyl Lewis A	Identified as a ligand for selectines expressed in apical surfaces of human M cells in Peyer's Patches.	(Giannasca et al., 1999)
A5β1 integrin	Identified to play a role in the intestinal invasion by enteropathogens. Over-expressed in Caco-2 cultured with Peyers Patches lymphocytes	(Tyrer et al., 2002)
β1 integrin and CD9	Cell adhesion molecule abundantly expressed in Caco-2/Raji-B model and human FAE. Were identified improving NPs uptake.	(Gullberg et al., 2006)
Toll-like receptor 4 (TLR-4) and Platelet-activating factor receptor (PAFR)	Described as microbial pattern recognition receptor. Found *ex vivo* and *in vitro* on the apical surface of M cells.	(Tyrer et al., 2007)
Galectin-9 (Gal-9)	Mammalian lectin induced in Caco-2/Raji-B co-culture system	(Pielage et al., 2007)
Glycoprotein 2 (GP2)	Uptake receptor for a subset of commensal and pathogenic bacteria	(Ohno and Hase, 2010)

2. OBJECTIVES

2. OBJECTIVES

The use of ENPs, especially metal and metal-oxides NPs, has gained increasing popularity in the food industry throughout this decade due to their new, advantageous and innovative properties. Among their applications, NPs have been described as antioxidants, antimicrobials, photocatalysts, whiteners, etc. In this Thesis, we focused our attention on the role and behaviour of TiO_2NPs in the GIT. TiO_2NPs are the major industrially-produced NP worldwide (approximately 10.000 t/year), and they are used especially as pigment-enhancer and food additive in many consumer products ingested daily (candies, sweets, sugar, glazed bakery, puddings, etc.). In spite of their increasing use, no general consensus has been reached so far regarding the limit values in food, the marketplace regulatory aspects and the potential risk at the GIT level. For these reasons, the general objective of this Thesis was to evaluate the effects of TiO_2NPs in an *in vitro* model of the GIT in order to clarify the data disparity and gaps reported in the literature.

To achieve this goal, we planed the following specific objectives:

1. To set up, for the first time in our laboratory, the *in vitro* triple co-culture Caco-2/HT29/Raji-B system, which faithfully reproduces the real condition of a small intestine.
2. To characterize the goodness of this model at the physiological, morphological, and functional level.
3. To evaluate the behaviour and bio-interactions of three differently shaped TiO_2NPs (<25 nm nano-spheres, <100 nm nano-rods and <10 nm nano-wires) in the *in vitro* barrier model.

To cover the third objective, we also planned different sub-objectives:

   a. To evaluate the membrane's integrity and permeability after the exposure to the three TiO_2NPs.
   b. To analyze their potential translocation through the *in vitro* barrier.
   c. To analyze the putative cell internalization of TiO_2NPs.
   d. To analyze their potential genotoxicity by assessing general DNA damage and oxidatively DNA damage.
   e. To assess the barrier's functionality analysing the gene expression of several barrier components related to the digestive and permeability functions.

Since this Thesis has an International mention due to the three-month stay in the Biomedical Engineering Department at Binghamton University, in Binghamton (New York), a further main objective was planned:

4. To evaluate NPs' effects under different physiological states, measuring cellular enzymatic activity levels.

To achieve this goal, the following specific objectives were planed:

a. To set up two new protocols to evaluate the enzymatic activity of *i)* the brush border enzyme aminopeptidase-N (APN) and *ii)* the transmembrane enzyme Na^+/K^+ ATPase.
b. To evaluate the intestinal alkaline phosphatase (IAP), APN and Na^+/K^+ ATPase activity after exposing the *in vitro* barrier Caco-2/HT29-MTX to *i)* TiO_2NPs and SiO_2NPs, *ii) in vitro* digested TiO_2NPs and SiO_2NPs and *iii) in vitro* digested TiO_2NPs and SiO_2NPs co-cultured with *Escherichia coli* or *Lactobacillus rhamnosus*.

3. RESULTS

3. RESULTS

The results of this Thesis have been devided in three different studies and classified by chapters. On the one hand, the obtained results of the first chapter have been published in a peer-review journal. On the other hand, the obtained results of the second chapter are currently in the process of submission. Finally, the reults obtained from the three-month stay in the Biomedical Engineering Department at Binghamton University, in Binghamton (New York), have been placed in the third chapter.

Thus, the three articles/manuscripts ordered according with the objectives of this Thesis, are as follows:

3.1. Chapter 1 (Study 1): Exploring the usefulness of the complex *in vitro* intestinal epithelial model Caco-2/HT29/Raji-B in nanotoxicology.

3.2. Chapter 2 (Study 2): Effects of differently shaped TiO_2NPs (nano-spheres, nano-rods and nano-wires) on the complex *in vitro* model (Caco-2/HT29) of the intestinal barrier.

3.3. Chapter 3 (Study 3): Dysfunctional alterations of the small intestine brush border enzymes IAP, APN and Na^+/K^+ ATPase, caused by metal oxide nanoparticles.

3.1. Chapter 1 (Study 1)

Exploring the usefulness of the complex *in vitro* intestinal epithelial model Caco-2/HT29/Raji-B in nanotoxicology

Food and Chemical Toxicology, 113: 162-170 (2018)

Doi: 10.1016/j.fct.2018.01.042

This chapter is a verbatim reproduction from the following published paper (published version can be found in Annexes):

García-Rodríguez A, Vila L, Cortés C, Hernández A, Marcos R. Exploring the usefulness of the complex in vitro intestinal epithelial model Caco-2/HT29/Raji-B in nanotoxicology. Food Chem Toxicol. 2018. 113:162-170.

Exploring the usefulness of the complex *in vitro* intestinal epithelial model Caco-2/HT29/Raji-B in nanotoxicology

Alba García-Rodríguez[1], Laura Vila[1], Constanza Cortés[1], Alba Hernández[1,2,§] , Ricard Marcos[1,2,§]

[1]*Grup de Mutagènesi, Departament de Genètica i de Microbiologia, Facultat de Biociències, Universitat Autònoma de Barcelona, Bellaterra, Spain;*

[2]*CIBER Epidemiología y Salud Pública, ISCIII, Madrid, Spain.*

[§]Corresponding authors at: Grup de Mutagènesi, Departament de Genètica i de Microbiologia, Universitat Autònoma de Barcelona, Edifici C3, Campus de Bellaterra, 08193 Cerdanyola del Vallès (Barcelona), Spain.

E-mail: alba.hernandez@uab.es (A. Hernández)

ricard.marcos@uab.es (R. Marcos)

Running title: The Caco-2/HT29/Raji-B model in nanotoxicology

3.1.1. ABSTRACT

The use of *in vitro* barrier models is gaining relevance as an alternative to animal studies in risk assessment, pharmacokinetic, and toxicological studies in general. These models permit an easier evaluation of the underlying mechanisms taking place at the molecular and cellular levels on the barrier site. Here, we report several methodological modifications of the three-dimensional *in vitro* intestinal epithelial model Caco-2/HT29/Raji-B for its successful application in the Nanotoxicology field. In addition, new insights in the study of specific molecular markers and new confocal microscope approaches have also been incorporated. Due to the multiple variables and parameters playing a part when the model's complexity is increased, we have monitored the barrier's formation and cell differentiation over time. Finally, the practical usability of the proposed model was tested by evaluating the action of the food additives titanium dioxide and silica dioxide nanoparticles (TiO_2NPs and SiO_2NPs). The NPs-associated effects were evaluated by confocal microscopy. We have demonstrated the essential role of the mucus layer in the decrease of cellular uptake, avoiding potential NPs-cell nuclei interactions.

3.1.2. INTRODUCTION

Because of the apparent lack of predictivity observed in animal models (Leist et al., 2014), a variety of *in vitro* approaches are currently used to mimic different biological targets, including epithelial barriers. Until now, the described non-animal models aiming to simulate epithelial barriers include the utilization of *ex vivo* tissues, reconstructed combined *in vitro* cell lines, the use of synthetic membranes, and the use of *in silico* modelling approaches. In all the aforementioned cases, efforts have pursued rapid and economic methods able to evaluate the interactions between defined compounds and the biological barriers they must cross (Gordon et al., 2015).

The interest in the development of *in vitro* epithelial barriers is common to various industrial fields such as pharmaceutics, cosmetics, and food industries. In addition, different research fields like toxicology and biomedical engineering also need to focus their research on the processes taking part in these entry gates. Furthermore, different institutional organisms as the Center for Alternatives to Animal Testing or the European Food Safety Authority are demanding information on this direction to enforce the scientific regulatory laws towards more sustainable and efficient *in vitro* alternatives (Gordon et al., 2015).

The rapid emergence of new nanotechnology products demands to improve the existing methodologies to test the potentially harmful effects of nanocompounds.

Different nanoparticles (NPs) are increasingly used by the food industry in different consumer products (i.e. food packaging, food additives, colourants, antimicrobial agents, etc.) (Vance et al., 2015). In this way, the intestinal epithelium became the main entrance portal of such NPs. To evaluate their potential health effects, different *in vitro* intestinal barrier models have been proposed so far (Schimpel et al., 2014; Braakhuis et al., 2015; Guo et al., 2017). Among them, one of the most common examples of *in vitro* gut model, the intestinal Caco-2 monolayer, has been largely described and used in the past two decades. Derived from a human colorectal adenocarcinoma, Caco-2 cells have the capability to differentiate themselves forming a morphologically and functionally enterocyte-like monolayer (Pinto et al., 1983; Sambuy et al., 2005). Caco-2 monolayers disposed into inserts with distinct, differentiated apical and basolateral sides, have been widely used in the past for chemical transport and drug pharmacokinetics studies, because of its well-known correlation with human studies (Artursson et al., 2001; van Breemen and Li, 2005). Recently, the Caco-2 monolayer has also been used and adapted to test potential detrimental and bio-dynamics effects of metallic-based NPs such as titanium dioxide (TiO_2NPs), silica dioxide (SiO_2NPs) and silver (AgNPs) nanoparticles (Faust et al., 2014; Sakai-Kato et al., 2014; Imai et al., 2017).

However, there is a fine balance of endogenous and exogenous factors in the intestine, provided by the multiple types of cells existing in the mucosa niche. Accordingly, assays based on a single cell line do not properly represent the complex gut environment. Thus, improved and more complex intestinal *in vitro* barrier models have been proposed to accomplish a more realistic *in vitro* system. Different studies added the goblet cell clones HT29 or HT29-MTX to the barrier model, which are capable to secrete vacuoles full of mucin conferring an extracellular protective shed of mucus (Mahler et al., 2009; Araújo and Sarmento, 2013; Lozoya-Agullo et al., 2017). The presence of the mucus layer led to the protection against ROS and a decrease in IL-8 release when treating the Caco-2/HT29 model with AgNPs (Georgantzopoulou et al., 2016).

A further improvement of the system was the addition of cell types to generate advanced three-dimensional co-culture models. Some studies have paid special attention to the development of an *in vitro* follicle-associated epithelium (FAE), characterized by the presence of microfold cells (M cells) (Smith and Peacock, 1980). M cells are considered antigen-sampling cells, acting as a gateway for antigens from the gut lumen and promoting particle transcytosis (Kucharzik et al., 2000). Thus, by adding human Raji-B lymphocytes to the basolateral chamber of the insert, Caco-2 are

induced to differentiate into M-like cells (Gullberg et al., 2000; des Rieux et al., 2007). In this context, it is important to indicate that several reports suggested that NPs are capable to enter intestinal epithelium mainly via M-cells (Gullberg E. et al., 2000; des Rieux A. et al., 2005).

Despite the efforts put to improve the existing intestinal epithelium models that have led to the generation of a more complex and realistic bioengineered three-dimensional co-culture Caco-2/HT29/Raji-B, further efforts are required. The absence of integrated and common methodological strategies between laboratories supposes the lack of a defined model to be used when testing nanomaterials. In this context, this works aims to further adapt and standardize the three-dimensional bioengineered co-culture Caco-2/HT29/Raji-B described previously by different authors (Antunes et al., 2013; Araújo et al., 2013; Schimpel et al., 2014) for the study of nanomaterials-associated effects. We have focused our attention on enhancing cell culture conditions to improve their visualization by using confocal microscopy, and on incorporating new molecular endpoints to determine the cells' status. In addition, the interaction of TiO_2NP and SiO_2NPs with our model was evaluated by confocal microscopy to test the model's performance.

3.1.3. MATERIALS AND METHODS

Cell culture and the in vitro co-culture model

Dr Isabella Angelis (Istituto Superiore di Sanità, Italy), kindly provided the human colorectal adenocarcinoma cell line Caco-2. HT29, a human cell line derived from a colorectal adenocarcinoma, and Raji-B, a B-lymphocyte cell line derived from a human Burkitt's lymphoma, were both purchased from the American Type Culture Collection (ATCC, Manassas VA 20108, USA). All cell lines were maintained in Dulbecco's modified Eagle's High Glucose medium without Pyruvate (DMEM w/o Pyruvate, Life Technologies, USA) and supplemented with 10% fetal bovine serum (FBS), 1% non-essential amino acids (NEAA) (PAA Laboratories GmbH, Pasching, Austria), and 2.5 mg/mL plasmocin (Invivo Gen, San Diego, USA). Cells were placed in a humidified atmosphere of 5% CO_2 and 95% air at 37 ºC. Routinely, Caco-2 and HT29 cell lines were subcultured once a week with 1% trypsin-EDTA (PAA Laboratories GmbH, Pasching, Austria) in 75 cm^2 flasks at $7.5x10^5$ cells/flask and $4x10^5$ cells/flask, respectively. Raji-B cells were grown in suspension, and sub-cultured weekly by diluting the cells at $3x10^5$ cells/mL.

The co-cultures were grown in 12-well culture plates using 1.12 cm^2 Polyethylene Terephthalate Transwells® with a pore size of 1 or 3 µm (Millipore®) (Merck KGaA,

Darmstadt, Germany) as previously validated by Araújo and Sarmento (Araújo & Sarmento 2013). These transwells act as a support chamber to differentiate between the cells' apical and basolateral side, mimicking the intestinal epithelium lumen and mucosa, respectively. Briefly, $1.7x10^5$ Caco-2 and HT29 cells were mixed and seeded on the Transwells® apical compartment, following a 90:10, 80:20, and 70:30 ratio, respectively. For the M-like cell induction, at day 14 of co-culture differentiation, $5x10^5$ Raji-B cells were seeded in the basolateral compartment. Finally, Caco-2/HT29/Raji-B co-cultures were left to differentiate until day 21, when a fully-formed functional barrier is obtained. Culture medium was changed every two days.

Integrity evaluation of the in vitro co-culture model

In order to oversee the integrity of the cell barrier, the trans-epithelial electrical resistance (TEER) was measured with an epithelial Voltmeter (Millicell-ERS volt/ohm meter) (Millipore®) (Merck KGaA, Darmstadt, Germany). TEER values were checked during the differentiation process of the Caco-2 monolayer, Caco-2/Raji-B and Caco-2/HT29/Raji-B co-cultures at days 7, 14 and 21 after seeding the different Caco-2/HT29 ratios to establish the best proportion. TEER values were calculated according to the formula TEER = [Ω (cell inserts) – Ω (cell-free inserts)] x 1.12 cm^2. Only Caco-2/HT29/Raji-B co-cultures with TEER values higher than 250 $Ω/cm^2$ were used for further experiments.

Paracellular permeability of the in vitro co-culture model

To study the *in vitro* barrier permeability, the paracellular transport of Lucifer yellow (LY) (ThermoFisher Scientific, USA) was measured. Briefly, after 21 days of cellular differentiation and barrier formation, Transwells® membranes were washed twice with transport buffer (HBSS Ca^{2+}, Mg^{2+}, +10 mM HEPES, pH 7.4). Then, membranes were transferred to a new 12-well plate filled with 1.5 mL of transport buffer in the basolateral compartment. Lucifer yellow was also diluted in transport buffer and added to the apical compartment at a final concentration of 0.4 µg/mL. *In vitro* co-cultures were placed in the incubator during 2 h. Subsequently, triplicates of 100 µL of each basal compartment were transferred to a black 96-well plate to measure fluorescence leakage. A prompt fluorimetry plate reader (Victor III, Perkin Elmer, USA) was used to determine the amount of LY able to cross the barrier by using 405-535 nm as an excitation-emission spectrum.

Histochemical characterization of the in vitro mucus secretion

To locate mucus secretion and visualize mucus shedding, differentiated HT29 and Caco-2 monocultures and Caco-2/HT29 co-cultures at 90:10, 80:20 and 70:30 ratios were cultured for 21 days in 1.12 cm^2 Transwells® with a pore size of 3 µm. Next, Transwells® were washed twice with PBS (1x), fixed with 3% acetic acid for 5 min, and stained with Alcian Blue (pH 2.5) (abcam plc., USA) for 30 min. After washing the samples with running tap water for 1 minute, the obtained cell barriers were separated from their supports and 3-5 µm cross-sections were obtained with a microtome and fixed in microscope slides. A cross-section of a rat intestine was used as positive control of the staining assay. Sample images were obtained with an inverted light Axio Observer A1 microscope (Zeiss, Germany) complemented with an AxioCam MRm camera (Zeiss, Germany).

Morphological characterization of the M-like cell phenotype induction

To see the morphological changes associated with Caco-2 cells differentiation into M-like cells, we used transmission electron microscopy (TEM). Caco-2/HT29 co-cultures were seeded in Transwells® with two different pore sizes (1 or 3 µm). After 14 days of co-culture, Raji-B cells were seeded in the basolateral chamber and the Caco-2/HT29/Raji-B co-culture was maintained until day 21. Then, the cell barrier was fixed in 2% (w/v) paraformaldehyde (Hatfield, PA, USA) and 2.5% (v/v) glutaraldehyde (Merck, Darmstadt, Germany) in 0.1 M cacodylate buffer (Sigma-Aldrich, Steinheim, Germany) at pH 7.4. Cells were post-fixed with osmium, dehydrated in acetone, embedded in Epon, polymerized at 60 ºC, and cut with an ultramicrotome. Finally, ultrathin barrier's cross-sections placed in copper grids were contrasted with conventional uranyl acetate and Reynolds lead citrate solution and observed using a Jeol 1400 (Jeol LTD, Tokyo, Japan) transmission electron microscope equipped with a CCD GATAN ES1000 W Erlangshen camera.

Cell type detection and barrier characterization using confocal microscopy

Laser Confocal Microscopy was used to visualize and discriminate Caco-2 cells from HT29 cells in the same co-culture while observing a three-dimensional disposition of the *in vitro* barrier model and its components (i.e. nucleus, mucus layer, cell membranes). *In vitro* co-culture barriers, Caco-2 monolayers and HT29 mono-cultures, were seeded in Transwells® as previously stated. Briefly, *in vitro* cultures were stained after the differentiation period in the Transwells® during 15 minutes at room

temperature with *Cellmask*^{TM}, *Hoechst 33342,* and *WGA Alexa Fluor*^{TM} fluorochromes diluted in DMEM culture medium at concentrations of 1/500, 1/500, and 1/100, respectively. *Cellmask*^{TM} Deep Red plasma (Life Technologies, USA) was used to stain the cell membrane, having an excitation/emission spectrum of 633/785 nm. For the staining of the cell nucleus, we used *Hoechst 33342* (ThermoFisher Scientific, USA) with a maximum excitation/emission of ~405/425-475 nm. Finally, the *Wheat Germ Agglutinin, Alexa Fluor*^{TM} *633 Conjugate* (WGA) (ThermoFisher Scientific, USA) was used to stain the mucus layer (maximum excitation/emission of ~632/647). After the incubation with the fluorochromes, samples were washed twice with culture medium and separated from the Transwells®' supports by cutting the Transwells®' membrane with a scalpel. The cells' co-culture attached to the membrane was placed face down in a *Glass Bottom Microwell Dishes* (MatTek, USA) petri dish with 250 µL of culture medium to maintain cell integrity and homeostasis while acquiring images. A confocal Leica TCS SP5 complemented with an HC x PLAPO Lambda blue 63x x1.40 *oil* UV objective was used. Images were processed with Huygens essential 4.4.0p6 (Scientific Volume Imaging, Netherlands) and Imaris 7.2.1 (Bitplane, AG) software.

Gene expression studies of molecular markers from the in vitro co-culture model.

The total RNA from Caco-2/HT29/Raji-B co-cultures was extracted 7, 14 and 21 days after seeding using TRIzol® Reagent (Invitrogen, USA), following the manufacturer's instructions. To remove residual DNA contamination, the samples were then treated with RNase-free DNase I (DNA-free TM kit; Ambion, UK) and, subsequently, the First-strand cDNA Synthesis Kit (Roche, Basel, Switzerland) was used to obtain cDNA by using 100 ng of total RNA. The resulting cDNA was subjected to real-time PCR analysis on a LightCycler-480 to evaluate the relative expression of different genes. We selected the brush border genes *Sucrase-isomaltase* (*SI*) and *Alkaline phosphatase* (*ALPI*). As genes of tight-junctions components, we selected *Occludin* (*OCLN*), *Claudin* (*CLDN2*), and *Zona occludens* (*ZO1*) genes. In addition, the membrane receptors *Glycoprotein* (*GP2*), *Galactine-9* (*LGALS9*), and *Toll-like receptor 4* (*TLR-4*) genes and *Mucine 1* and *5* (*MUC1, MUCA5C*) genes were also selected. The expression of β-actin was used as housekeeping control. (*SI*: direct 5'-TGGTGGCACTGTTATCCGAC-3' and reverse 5'-GACCACCACGGACATGTAGG-3'; *ALPI*: direct 5'-GTCCATCCTGTACGGCAATG-3' and reverse 5'-ACATGCGCTACGAAGCTCTG-3'; *CLDN2*: direct 5'-TACTCACCACTGGTGCCTGA-3' and reverse 5'-GAGAGCTCCTTGTGGCAAGA-3'; *ZO-1*: direct 5'-GAGAGGTGTTCCGTGTTGTG-3'

and reverse 5'-GCTGCGAAGACCTCTGAATC-3'; *GP2*: direct 5'-CAGTGCAGCGAGGTTATGGA-3' and reverse 5'-ACAGGCAGTGTGGTTGGTGA-3': *LGALS9*: direct 5'-GATGGAGGGTACGTGGTGTG-3' and reverse 5'-AGCCATTGACGGAGATGGTG-3'; *MUC1*: direct 5'-CGACGTGGAGACACAGTTCA-3' and reverse 5'-GACAGACAGCCAAGGCAATG-3'; *MUCA5C*: direct 5'-GTGTGCCTGCGTCTACAACG-3' and reverse 5'-GTGTGCCTGCGTCTACAACG-3'; *SPIB*: direct 5'-AGACTTACCGTTGGACAGCC-3' and reverse 5'-AGCTTCTGGTAGGTCATGCG-3'; *PAFR*: direct 5' TAATGGCTACGTGCTGTGGG 3' and reverse 5' TGGCCTGAGCAGTCTTGATG 3'; *TLR4*: direct 5' TGCGTGGAGGTGGTTCCTA 3' and reverse 5' GGGCTAAACTCTGGATGGGG 3'; *β-actin*: direct 5'-GCATGGAGTCCTGTGGCATC-3' and reverse 5'-CCACACGGAGTACTTGCGCT- 3'). Each 20 µL of reaction volume contained 5 µL cDNA, 10 µL of 2x LightCycler 480 SYBR Green I Mater (Roche, Germany), 3 µL of distilled H_2O, and 1 µL of each primer (forward and reverse) at a final concentration of 10 µM. The cycling parameters were the following: an initial step of 95 ºC for 5 min, then 45 cycles of 95 ºC for 10 s, 62 ºC for 15 s and 72 ºC for 25 s. Cycle time (Ct) values were calculated with the LightCycler 480 software package and then normalized with β-actin Ct values.

Nanoparticles exposure

Titanium dioxide (TiO_2NPs, NM100) and silica dioxide (SiO_2NPs, NM203) nanoparticles were supplied by the Joint Research Center (Ispra, Italy) in the frame of the EU project NanoReg, and were dispersed according to the EU Nanogenotox protocol (Nanogenotox, 2011). The primary particle size of TiO_2NPs and SiO_2NPs were 110 and 24.7 nm, respectively. Briefly, 15.3 mg of TiO_2NPs and SiO_2NPs were pre-wetted in 0.5% absolute ethanol and dispersed in 0.05% bovine serum albumin (BSA) in MilliQ water. Each NP was sonicated in the dispersion medium for 16 min at 10% of amplitude to obtain a stock dispersion of 2.56 mg/mL. The NPs used were characterized in a previous work (Vila et al., 2017).

After the cell differentiation process and barrier maturation, Caco-2/HT29/Raji-B co-cultures were exposed to 150 µg/mL of TiO_2NPs and 150 µg/mL of SiO_2NPs for 24 h per separate. Briefly, after 21 days of co-cultures seeding, the apical culture medium was replaced by adding 150 µg/mL of the selected NPs diluted in DMEM culture medium. Fresh culture medium without NPs was placed in the basolateral chamber of

the insert. Finally, membranes were placed in the incubator at 37 ºC for 24 h for further confocal microscopy analysis.

Statistical analysis

All sample treatments were measured in triplicate in at least three separate experiments. Results are expressed as mean ± standard error. One-way ANOVA with Tukey's post hoc test, unpaired Student's *t*-test, or two-way ANOVA were performed as convenient using GraphPad Prism version 5.00 for Windows (GraphPad Software, San Diego California USA, www.graphpad.com). Differences were considered significant at $P<0.05$.

3.1.4. RESULTS

Functional and Morphological Evaluation of the Caco-2/HT29 barrier

To increase the Caco-2 monolayer's complexity, HT29 colon adenocarcinoma cells were added to the *in vitro* barrier. HT29 cells, also known as goblet cells, have the capability to produce mucine secretions, forming an extracellular mucus shed. Thus, to set the best suitable Caco-2/HT29 ratio of cells, different ratios of both cell clones were studied: 70:30, 80:20, 90:10 and 100:0 of Caco-2 and HT29, respectively.

Firstly, the barrier integrity was evaluated by measuring the TEER throughout the differentiation time. As expected, the TEER values of all cultured ratios, except for HT29 monocultures, increased progressively during the differentiation span (Figure 1.A). At the end of the 21 days of differentiation process, TEER values reached a plateau where Caco-2 monoculture presented the highest value (513.28±16 Ω/cm^2) followed by 90:10 (277.15±17.55 Ω/cm^2), 80:20 (207.91±69.35 Ω/cm^2) and 70:30 (142.01±10.93 Ω/cm^2), while HT29 monoculture barely showed resistance (26.28±7.06 Ω/cm^2). Following the functional characterization of the different co-cultures, the percentage of paracellular LY transported was also calculated (Figure 1.B). The LY assay is commonly used to complement the membrane integrity studies and to address paracellular permeability studies due to the capability of this compound to cross *in vitro* epithelial barriers by paracellular transport. As shown in figure 1.B, the amount of LY able to cross the co-culture barrier decreases while the of Caco-2 cells in the co-culture increases. LY results matched well with TEER values, since Caco-2 monoculture and 90:10 co-culture, the cultures with highest TEER values, present the lowest amount of paracellular LY passage. Accordingly, co-cultures with a ratio of 90% Caco-2 and 10%

HT29 were considered as the best combination, maintaining high barrier integrity and, consequently, was used for further experiments. It should be pointed out that when 3 μm pore-sized Transwells® were used, as important cell migration from the apical to the basolateral chamber was observed. To avoid this problem, further experiments were done using 1 μm pore-size Transwells®. This simple change avoids migration and the subsequent formation of a second barrier on the basolateral side of the filter (see Supplementary Figure S1).

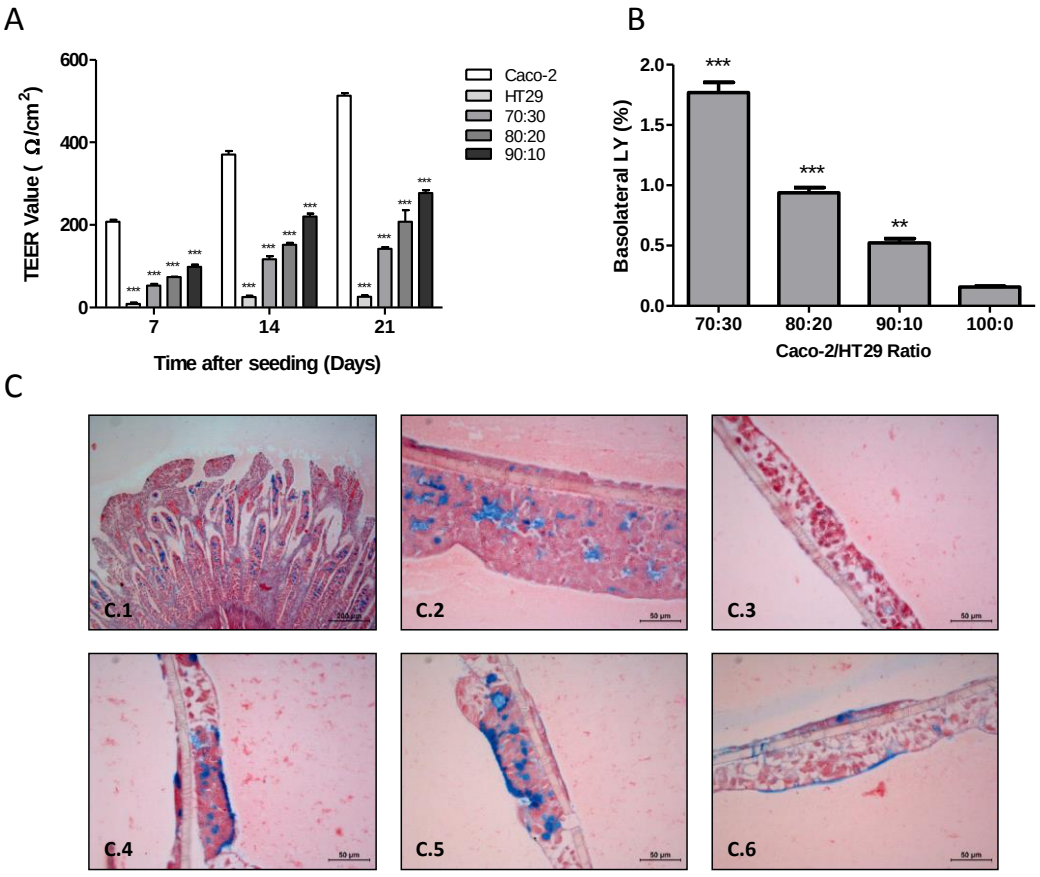

Figure 1. Several characteristics of Caco-2/HT29 co-cultures. (A) TEER values of different co-cultures ratios compared with the Caco-2 and HT29 monocultures. (B) Amount (%) of Lucifer Yellow detected in the basolateral chamber of different co-cultures ratios. (C) Transversal cuts and Alcian Blue staining of (C.1) rat intestine as a positive control, (C.2) HT29 monoculture, (C.3) Caco-2 monoculture, (C.4) Caco-2/HT29 co-culture in a ratio of 70:30, (C.5) 80:20, and (C.6) 90:10 %. Results are represented as mean ± SEM. One-way ANOVA with a Tukey's post-test was performed. ***P*<0.01, ****P*<0.001.

In addition, the secreted and scattered mucus along the barrier model was evaluated using the Alcian Blue staining. Also, the Caco-2/HT29 cell distribution over the Transwells® was checked. Alcian Blue is a histochemical staining dye that interacts

with the acidic mucosubstances and acetic mucins, allowing the qualitative visualization of the amount of mucus secreted. As observed in the images from Figure 1.C, our HT29 cell clone (C.2) grown in Transwells® for 21 days was able to produce mucus in a physiologically-relevant amount, similar to the positive control (rat intestine) (C.1). On the other hand, Caco-2 monolayers' mucus was barely noticeable. No differences were seen in mucus secretion and distribution between the different co-culture ratios evaluated. As observed in the supplied images, all Caco-2/HT29 ratios tend to form a mucus shed close to HT29-rich regions. One interesting observation detected with this assay is that the structure and morphology of the barrier and the barrier integrity are compromised when the proportion of HT29 cells increase. Since HT29 cells do not grow in a monolayer, they tend to form small piles whose width directly affects the barrier integrity (data not shown).

Induction of M cells-like cells and their characterization

To mimic as much as possible the real conditions of an intestinal epithelium, this *in vitro* epithelial barrier model was further modified. After 14 days of Caco-2 monolayers and Caco-2/HT29 co-culture, Raji-B lymphocytes were placed in the basolateral chamber of the Transwells®. It is already known that co-culturing Caco-2 with lymphocytes induce several morphological changes, such as stumpy and short microvilli and the loss of Caco-2 brush border, indicating the generation of M-like cells. Our TEM images evidence the correct induction of an M-like phenotype in Caco-2 monolayers (Figure 2; A.1 and A.3) and in Caco-2/HT29 co-culture barriers (Figure 2; A.2 and A.4). Both cell phenotypes can be clearly distinguished due to their different morphology and cell structure arrangement. As previously demonstrated by TEM studies, differentiated, enterocyte-like Caco-2 cells display a well-organized brush border, with tight junctions and a granulated cytoplasm that confers a dark contrast to the cells under the microscope (data not shown). Aside from the brush border rearrangement, our TEM images also show that M-like modified Caco-2 cells lose the columnar shape common on differentiated, enterocyte-like Caco-2 cells, and present a shinier cytoplasm due to their cytoskeleton reorganization. In addition, slight but significant differences (P<0.05) were found between differentiated Caco-2 cells (413.25±6.53 Ω/cm^2) and differentiated Caco-2/Raji-B (457.3±37.9 Ω/cm^2) co-cultures when the TEER was measured at 21 days (Figure 2.C).

Since our work also aimed to develop new tools to characterize and detect these M cell-like cells, we also analysed several molecular markers previously described as

putative indicators of M-like cells. The induction of M-like cells was additionally confirmed by detecting changes in gene expression of genes involved in pathogen recognition, membrane receptors, intracellular transport or cell adhesion, among others. After one week of co-culture of differentiated Caco-2 with Raji-B lymphocytes, a significant upregulation in the expression of *GP2* and *TLR4* genes (1.45±0.13 and 4.37±2.06 fold, respectively) was observed when compared with the control (mono-cultured differentiated Caco-2 cells) (Figure 2.B).

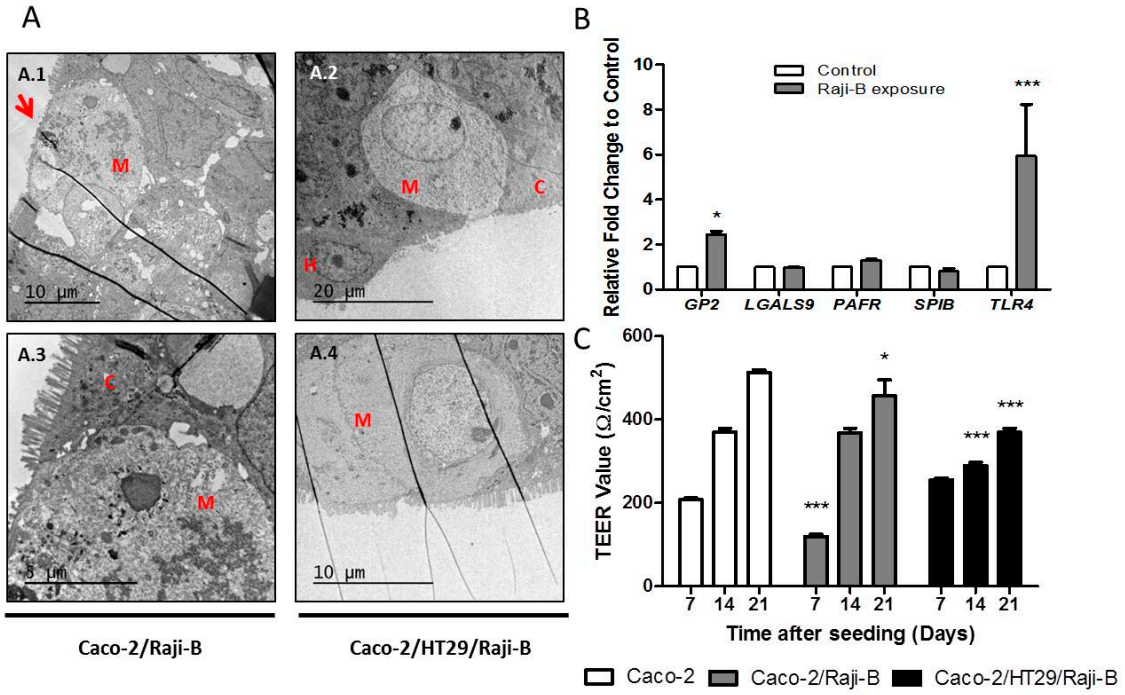

Figure 2. Caco-2 cells conversion into M-like cells. TEM images of Caco-2 cells monocultures (A.1 and A.3), and Caco-2/HT29 co-cultures (A.2 and A.4) exposed to Raji-B cells at day 14 of culture differentiation. Images shows M cells (M), Caco-2 cells (C), and HT29 cells (H). The red arrow indicates the little microvillis present in M cells. (B) Gene expression of Caco-2 cells in response to Raji-B exposure. Data represented as mean ± SEM, *denotes significant differences according to an unpaired Student's *t*-test. (C) TEER values of differentiated Caco-2, Caco-2/Raji-B and Caco-2/HT29/Raji-B co-cultures. Data represented as mean ± SEM. Two-way ANOVA with a Bonferroni's post-test was performed. *P<0.05, **P<0.01, and ***P<0.001.

Gene expression: complementary verification of a well-barrier formation using molecular markers

Considering the high complexity of the *in vitro* epithelial barrier model, further efforts to monitor the system must be carried out. Thus, we checked a set of genes that could act as molecular markers as complementary data to better understand the behaviour of

the Caco-2/HT29/Raji-B barrier and its proper development over the differentiation process. The selected genes play essential roles in several barrier functions such as barrier integrity (*ZO-1* and *CLDN2*), nutrient digestion and hydrolysis (*ALPI* and *SI*), protective mucus shed (*MUC1* and *MUC5AC*), and pathogen recognition and macromolecules transcytosis (*GP2* and *TLR4*). As Figure 3 shows, there is a progressive increase over the differentiation span in the expression of all genes except SI, which expression decreases at day 21. At the end of the co-culture differentiation, most of the genes significantly increased at least 2-fold compared to the first 7 days. Interestingly, *ALPI, ZO-1* and *MUC1* were highly upregulated (4.78±0.11, 3.32±0.17, and 4.52±0.27 fold, respectively). As expected, the gene expression of the M-like cells markers *GP2* (6.54±0.79 fold) and *TLR4* (6.78±1.87 fold) only increased after the second week, when the co-cultures were grown with Raji-B cells in the basolateral chamber.

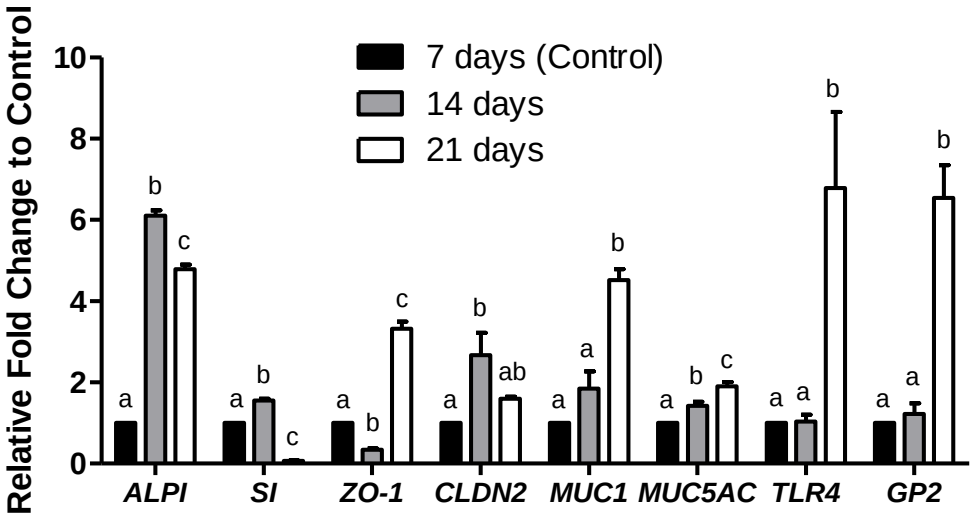

Figure 3. Study of the correct Caco-2/HT29 barrier formation using RT-qPCR. Gene expression in response to the barrier differentiation, through the culture time (7, 14 and 21 days). Data represented as mean ± SEM. Bars that do not share any letters are significantly different according to a one-way ANOVA with a Tukey's post-test (P<0.05).

Laser Scanning Confocal Microscope barrier characterization

To better understand the intestinal epithelial barrier and illustrate it as a complete system, we analysed the Caco-2/HT29/Raji-B co-culture under the confocal microscope. Thanks to the use of different immunostaining fluorochromes and their combinations, it was possible to identify various barrier structures and distinguish them

in an *in situ* staining (Figure 4). In this case, the fluorochromes used were Hoetch, CellMask (Figure 4; A.1, A.2 and A.3) and WGA (Figure 4; B.1, B.2 and B.3) to stain the nucleus membrane, cell membrane and the mucus secretion, respectively. Caco-2 (Figures A.1 and B.1) and HT29 (Figures A.2 and B.2) monocultures, and the Caco-2/HT29 (Figure 4; A.3 and B.3) co-culture were grown in Transwells® for 21 days and immediately stained with the aforementioned fluorochromes. Clearly, WGA tends to bind strongly to mucin residues produced by the HT29 cells, making the mucus shed easy to identify (Figure B.2). As Figure 4 displays, confocal images can cover a wide area of the barrier surface and, at the same time, transversal x/y-scans. In this case, we can specifically distinguish i) the apical from the basal side of the barrier (membrane polarization), ii) differences between both Caco-2 and HT29 cell types (i.e distribution, conformation, etc.), iii) the mucus shed cover, and iv) in more detail, the cell membrane, the cell nucleus, and the cell-to-cell interaction.

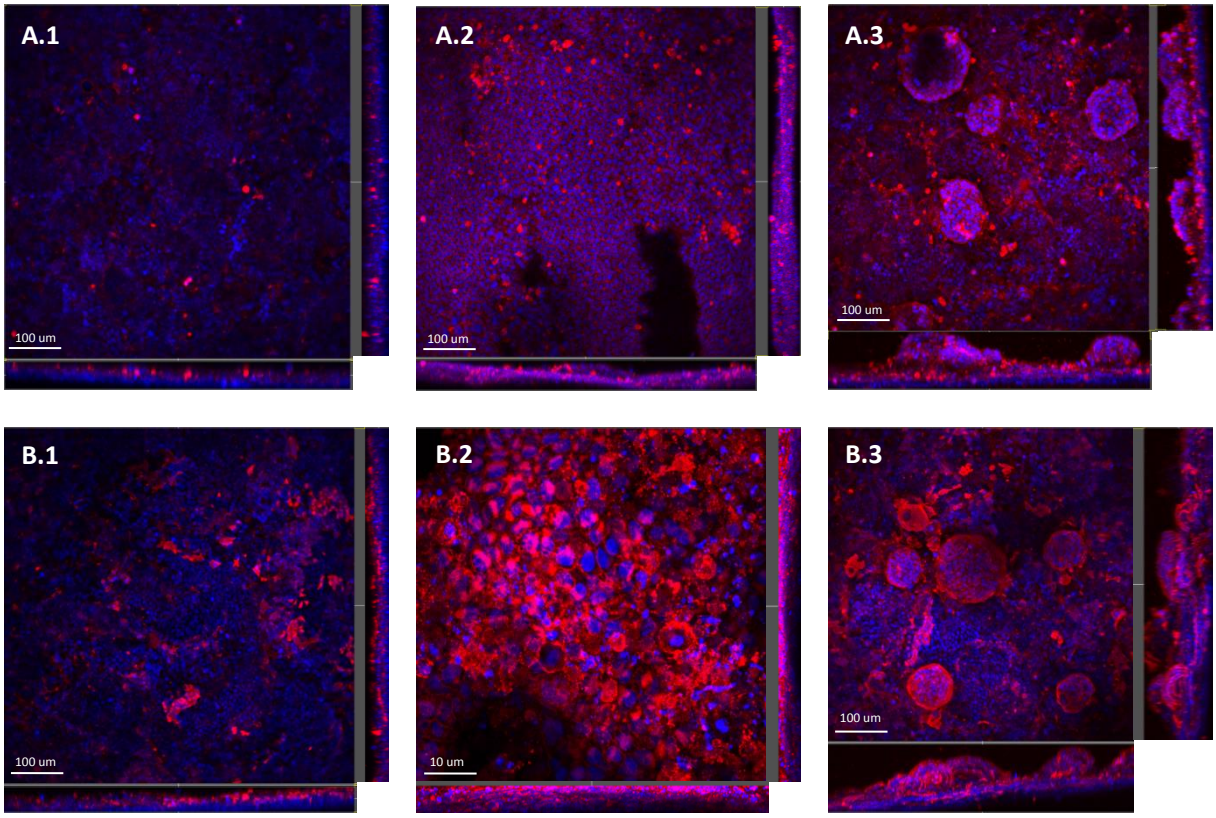

Figure 4. Evaluation of the barrier distribution using a laser scanning confocal microscope. Confocal images of Caco-2 monolayers (A.1 and B.1); 21 days HT29 mono-culture (A.2 and B.2); and the complete co-culture Caco-2/HT29/Raji-B (A.3 and B.3). Cell nuclei were stained with Hoechst (blue), cells membrane were stained with CellMask (A.1, A.2 and A.3), and mucus shed was stained with WGA (B.1, B.2 and B.3).

NPs identification in the Caco-2/HT29/Raji-B model

Regarding the exponential growth of research studies in the nanotoxicology field, several assays must be modified and improved to make them suitable for studying the biological effects of NPs exposure. The interaction (uptake and translocation) of nanomaterials with epithelial barriers is of particular relevance in nanotoxicological screening. To detect such interactions, we exposed our Caco-2/HT29/Raji-B co-culture model to TiO_2NPs and SiO_2NPs. A 24 h exposure to a concentration of 150 µg/mL of both nanomaterials [TiO_2NPs (<100 nm) and SiO_2NPs (25 nm)] was selected as in previous studies with Caco-2 monolayers (unpublished data) we have not seen any cell viability reduction up to 200 µg/mL. Figure S2 and Table S1 show some characteristics of the NPs used. Laser scanning confocal microscopy was used to locate the selected metallic NPs, which are considered appropriate for this study since they refract the polarized light, allowing their localization over the co-culture barrier using the confocal microscope (Figure 5). As the confocal images show, both NPs (green dots) are easily distinguished from the rest of the co-culture barrier components. At first sight, both NPs are found homogenously spread over the surface barrier and stratified across the barrier thickness (Figure 5; A.1 and B.1). Moreover, we were also able to go further on the barrier imaging and create accurate three-dimensional images using the Imaris® software. Accordingly, we were able to observe that both types of NPs were able to cross the mucus shed, the cell membrane and, finally, reach the cell nucleus (Figure 5; A.3 and B.3). These results support the suitability of this co-culture model to study the fate of NPs when they interact with the epithelial barriers.

3.1.5. DISCUSSION

The combination of Caco-2/HT29/Raji-B cells is an already-described *in vitro* epithelial barrier model that tries to simulate as much as possible the real environment of the human small intestine (Antunes et al., 2013). This complex model, as well as the more simple Caco-2 monolayer model, have been proposed as predictive tools to evaluate the permeability of different drugs (Ingels et al., 2004; Lozoya-Agullo et al., 2017). In this work, we have analyzed the suitability of little modifications in the protocols found in the literature to evaluate the interaction of nanomaterials with the intestinal barrier. Hence, we propose the use of the HT29 cell clone instead of the commonly used HT29-MTX, since clear pictures of mucus layer are obtained using this clone. Furthermore, we suggest a new ratio Caco-2/HT29 to optimize translocation resistance. In addition, the use of a wide set of gene markers showed its

appropriateness to evaluate the integrity of the model. We also demonstrated that confocal microscopy is a powerful tool to visualize many of the events taking place in these barriers. Finally, we have shown the usefulness of this well-structured barrier to study its interaction with nanomaterials.

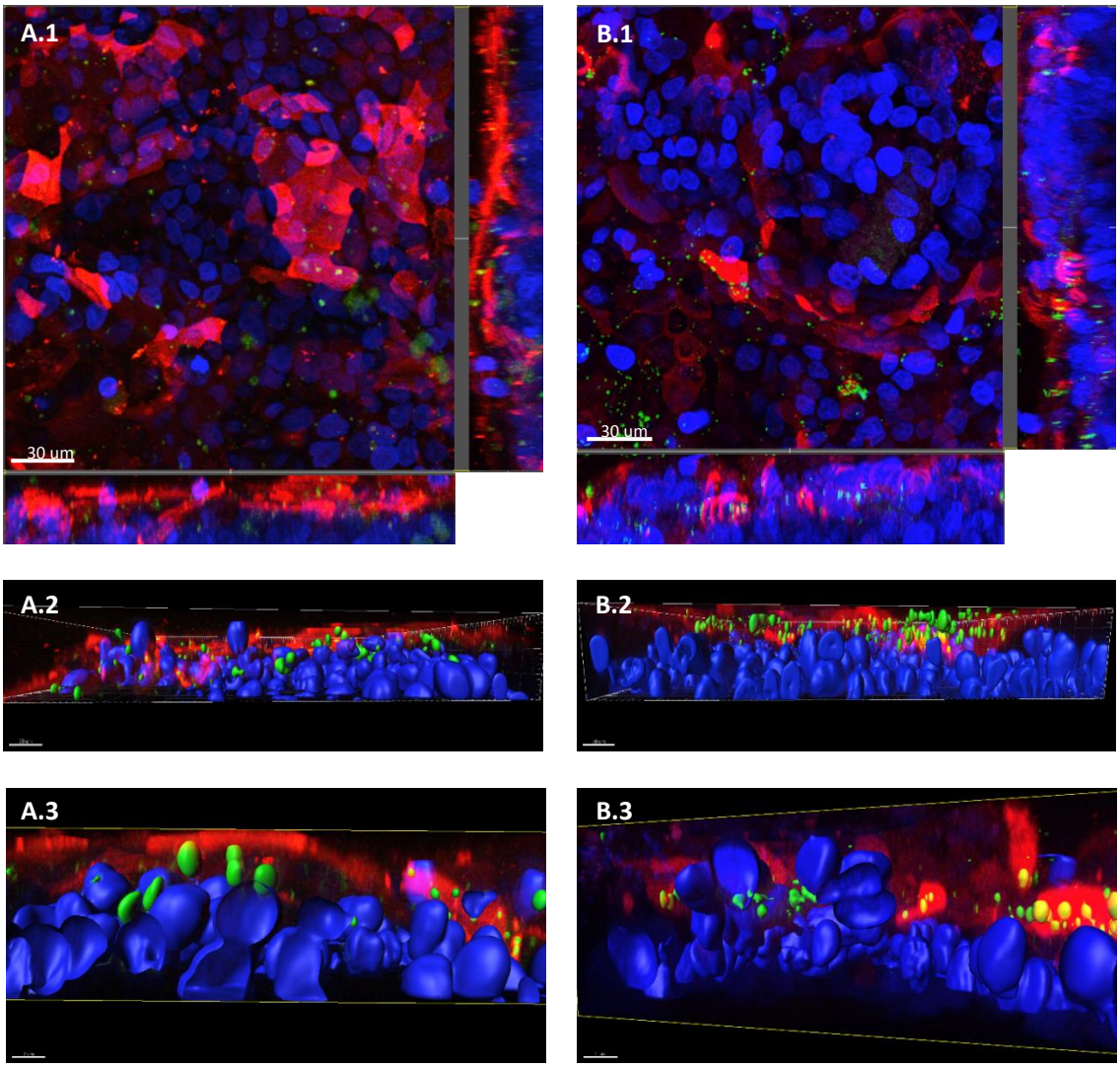

Figure 5. Confocal microscope images of the in vitro co-culture model Caco-2/HT29/Raji-B treated with SiO_2NPs (A) and TiO_2NPs (B) at 150 µg/mL for 24 h. Cells nucleus were stained with Hoecht (blue), mucus shed with WGA (red) and the NP refraction visualized in green. X, Y and Z-scans were done (A.1 and B.1). Three-dimensional images of the intestinal barrier model treated with SiO_2NPs (A.2 and A.3), and TiO_2NPs (B.2 and B.3). White arrows indicate the interaction between both, NPs and cell nuclei (A.3 and B.3).

Several differences were demonstrated when comparing the complex Caco-2/HT29/Raji-B barrier with the Caco-2 monolayer at a functional and morphological level. Firstly, we observed a significant reduction in the TEER values, confirming previous findings by other authors (Schimpel et al., 2014; Araújo et al., 2015). This can be explained by the presence of HT29 cells, which blocks the contact between enterocyte-like cells and, as a consequence, the formation of tight junctions. Moreover, we confirmed these results by measuring the paracellular transport of LY through the different co-culture barriers. As expected, the amount of LY found in the basolateral chamber increased concomitantly with the amount of HT29 cells. To choose the optimal ratio of HT29 cells to have a well-established mucus shed, the Alcian Blue staining protocol was performed in transversal cuts of the co-culture. We did not find differences in the mucus extension throughout the barrier with different proportions of HT29, unlike Schimpel et al. (2014). These differences can be attributed to the used cell clones, or to the fact that they did not use transversal cuts to visualize mucus distribution. Since the ratio 90:10 of Caco-2/HT29 produced the most well-established barrier according to TEER and LY values and without significant variations in mucus shed formation, we propose this ratio as the optimal one. Interestingly, with this staining we also observed cells crossing through the 3 μm pore-size membrane and, as a consequence, a second cell layer was formed facing the basolateral chamber. This double membrane represents an extra obstacle for the NPs crossing and is far from the real scenario, therefore, further experiments were carried out using 1 μm pore-size Transwells® (see Figure S1). Accordingly, the use of 1 μm pore-size Transwells® constitutes a further improvement of the method.

In the intestinal barrier, M-cells are located in the epithelia overlying mucosa-associated lymphoid tissues, where they work as the antigen-sampling cells of the mucosal immune system (Clark and Jepson, 2003). According to our goal of establishing a more realistic barrier structure, we promoted the transformation of Caco-2 cells into M-cells. Although M-like cell induction could be achieved by the proximity of B-lymphocytes to Caco-2 cells, no direct contact is required since soluble factors and mediators secreted by B-lymphocytes are enough for its formation (des Rieux et al., 2005). M-cells are characterized by an irregular brush border, few microvilli and decreased glycocalyx. Several methodologies have been proposed to demonstrate their induction besides morphological analyses, including the quantification of the enzymatic activity of proteins such as alkaline phosphatase (API) and sucrose isomaltase (SI) (Schimpel et al., 2014). Nevertheless, these molecules are not ubiquitously expressed among different species and do not present a high specificity

for M-like cells, making them a controversial differentiation marker (Ohno and Hase 2010). For instance, the WGA fluorochrome strongly stained the mucus layer produced by the HT29 cells, hampering M-like cell recognition in our model. To overcome these difficulties, we evaluate the expression of a set of genes related to M-like cells functions as possible biomarkers for M-cells differentiation. The cell surface markers *LGALS9, GP2, TLR4* and *PAFR,* and the transcription factor *Spi-B* were chosen because they have already been described as M-like cells' biommmarkers in previous works (Wang et al., 2015; Albac et al., 2016). In our case, the gene expression of *GP2* and *TLR4* was significantly upregulated after the addition of Raji-B cells to the basolateral chamber. Nevertheless, no changes were detected for *LGALS9, PAFR* and *Spi-B* markers. Our results agree with those reporting the expression of *TLR4* and *GP2*, as detected by immunolabelling (Tyrer et al., 2006; Albac et al., 2015). Both genes encode integral membrane proteins, playing fundamental roles in M-cells such as membrane receptors, transcytotic machinery, signal inductors in pathogen recognition, uptake, and activators of innate immunity pathways (Hase et al., 2009; Kanaya et al., 2014). According to our results, we propose the detection of expression changes in *TLR4* and G*P2* genes as an indicator of the functional M-cells presence in our *in vitro* model of the intestinal barrier.

Traditionally, TEM and SEM microscopy techniques have been the most used tools for M-like cells' detection (Schimpel et al., 2014; Araújo et al., 2016), despite the difficulty to find them due to their variable and poor rate of differentiation (Albac et al., 2015). We have been able to detect their presence in both Caco-2/Raji-B and Caco-2/HT29/Raji-B co-cultures thanks to morphological characteristics like their typically short and irregular microvilli structures, their loss of enterocyte-like shape and the cytoskeleton rearrangement. Therefore, we suggest that a simple preliminary study by gene expression of the molecular markers *TLR4* and *GP2*, in addition to the microscope imaging could be useful to show up a good procedure in the barrier seeding, culturing and cell differentiation.

The pristine *in vitro* Caco-2/HT29/Raji-B model must comprise the main functions of the human small intestine. One of its most important activities is the digestion and absorption of the uptaken nutrients, where several proteins and enzymes such as the intestinal alkaline phosphatase (ALPI) and sucrose isomaltase (SI), are involved (Nakano et al., 2009; Cheng et al., 2014). Additionally, the coordinated task of the tight junctions' (TJ) components (zonula occludens, occludin, claudins, etc) confers membrane integrity and stability, and the extracellular mucus shed grants an extra-protective layer to the barrier (Suzuki et al., 2013). In our model, *ALPI* and *SI* gene

expression steadily increased during the first 2 weeks; however, on day 21 of their differentiation, they experiment a significant reduction. This could be explained by the inclusion of Raji-B cells and the consequent formation of M-like cells, reducing the expression of brush border markers (Schimpel et al., 2014). We have also demonstrated that the gene expression of the TJ components *ZO-1* and *CLDN2*, and the mucus produced components *MUC1* and *MUC5AC*, are significantly increased during the barrier differentiation process but with different expression rates and plateaus. These outcomes were associated with our TEER values, Alcian Blue staining, and confocal images. Regarding the transcytotic capability of the barrier associated with the presence of M-like cells, the increase in the expression of the *GP2* and *TLR4* genes was only detected at the 21st day of barrier differentiation, right after the exposure to Raji-B cells during one week. Taken together, we propose all the aforementioned markers as indicators to demonstrate the integrity of the barrier given that the principal functions of the intestinal barrier are working properly.

Another aspect of this study to be pointed out is the usefulness of the laser scanning confocal microscopy to demonstrate the integrity of this *in vitro* intestinal model. We have observed a good signal when fluorochrome CellMasK™ was used, staining the plasma membranes of Caco-2 and HT29 cells uniformly. Likewise, the lectin-labelling fluorochrome WGA stained both cell types in a different manner. Our confocal images displayed the strong reaction of WGA to the mucin-secreting goblet cells HT29. Moreover, we were not able to distinguish any M-like cell specifically labelled by WGA, like Schimpel and co-workers (2014) described. Consequently, we propose the use of WGA only as mucus shed detector. Summarizing the goodness of this microscopic approach, this technique allows the observation of the multicellular barrier conformation and the disposition of its components, characterized by being thicker than the Caco-2 monolayer and for forming rounded protuberances. We hypothesize that these protuberances are mainly formed by HT29 cells, as mucus production is higher near this structures.

In the nanotoxicology field, very few studies have used the complex Caco-2/HT29 or the Caco-2/HT29/Raji-B models to quantitatively assess cell uptake rates and transport kinetics of nanomaterials. In fact, the few existing studies have only focused on the effects of drug delivery nano-carriers (Antunes et al., 2013; Lopes et al., 2016). Nonetheless, since metallic NPs are increasingly used as food additives in many consumer products (Yang et al., 2014; Vance et al., 2015), the interest to uncover their potential interactions with the gastrointestinal tract is raising. Similarly, nano-carrier drugs should also be screened with this complex, more realistic barrier model, to better

select potentially-interesting NPs for drug-delivery. Once our model was well established, we carried out a preliminary test to qualitatively assess its interaction with the metallic TiO_2NPs and SiO_2NPs, which are highly used as food additives. Assuming that NPs transport through an epithelial barrier can take place via paracellular or intracellular mechanisms, we aimed to check this process by confocal microscopy. Using this methodology, it is possible to distinguish between cell components and NPs, since metallic NPs have the ability to refract polarized light when visualized under a scanning laser microscope. To reduce possible agglomerations, NPs were dispersed and characterized as done in previous works (Vila et al., 2017) (see supplementary data). Our confocal images clearly demonstrated that, after the exposure, a significant amount of NPs remained in the apical side of the membrane, detained between microvilli and by the mucus matrix. In both cases, some NPs were detected actively crossing the barrier, mainly by cellular uptake. Finally, we were also able to detect several NPs-cell nucleus interactions, what would imply the potential risk of inducing DNA damage.

Summarizing, in addition to the data that reinforces the general usefulness of the proposed Caco-2/HT29 model, we defend its use as a powerful tool to evaluate the gastrointestinal barrier's interaction with nanomaterials, mainly those used in the food industry. The obtained data qualitatively shows that the protective function of the barrier is working well, as NPs are mostly located in the mucus shed. However, some NPs are able to enter the cell's cytoplasm, even reaching the cells' nucleus, suggesting a potential toxic/genotoxic hazard. Accordingly, further efforts should be done in order to understand the mechanisms of NPs' internalization and its effects at both cellular and barrier level.

Acknowledgements

A. Garcia-Rodriguez and L. Vila were funded by postgraduate fellowships from the Universitat Autònoma de Barcelona and the Generalitat de Catalunya, respectively.

Funding

This investigation has been partially supported by the Ministry of Economy and Competition (SAF2015-63519-R), and the EC FP7 NANoREG (Grant Agreement NMP4-LA-2013-310584).

Declaration of interest

The authors report no conflict of interest. The authors alone are responsible for the content and writing of the paper.

3.1.6. REFERENCES

Albac, S., Schmitz, A., Lopez-Alayon, C., d'Enfert, C., Sautour, M., Ducreux, A., Labruère-Chazal, C., Laue, M., Holland, G., Bonnin, A., Dalle, F., 2016. *Candida albicans* is able to use M cells as a portal of entry across the intestinal barrier *in vitro*. Cell Microbiol. 18, 195-210.

Antunes, F., Andrade, F., Araújo, F., Ferreira, D., Sarmento, B., 2013. Establishment of a triple co-culture *in vitro* cell models to study intestinal absorption of peptide drugs. Eur. J. Pharm. Biopharm. 83, 427-435.

Araújo, F., Pereira, C., Costa, J., Barrias, C., Granja, P.L., Sarmento, B., 2016. *In vitro* M-like cells genesis through a tissue-engineered triple-culture intestinal model. J. Biomed- Mater- Res. B. Appl- Biomater. 104, 782-788.

Araújo, F., Sarmento, B., 2013. Towards the characterization of an *in vitro* triple co-culture intestine cell model for permeability studies. Int. J. Pharm. 458, 128-134.

Artursson, P., Palm, K., Luthman, K.. 2001. Caco-2 monolayers in experimental and theoretical predictions of drug transport. Adv. Drug Deliv. Rev. 46, 27-43.

Braakhuis, H.M., Kloet, S.K., Kezic, S., Kuper, F., Park, M.V., Bellmann, S., van der Zande, M., Le Gac, S., Krystek, P., Peters, R.J., Rietjens, I.M., Bouwmeester, H., 2015. Progress and future of *in vitro* models to study translocation of nanoparticles. Arch. Toxicol. 89, 1469-1495.

Cheng, M.W., Chegeni, M., Kim, K.H., Zhang, G., Benmoussa, M., Quezada-Calvillo, R., Nichols, B.L., Hamaker, B.R., 2014. Different sucrose-isomaltase response of Caco-2 cells to glucose and maltose suggests dietary maltose sensing. J. Clin. Biochem. Nutr. 54, 55-60.

Clark, M.A., Jepson, M.A., 2003. Intestinal M cells and their role in bacterial infection**.** Int. J. Med. Microbiol. 293, 17-39.

des Rieux, A., Fievez, V., Théate, I., Mast, J., Préat, V., Schneider, Y.J., 2007. An *improved in vitro* model of human intestinal follicle-associated epithelium to study nanoparticle transport by M cells. Eur. J. Pharm. Sci. 30, 380-391.

Faust, J.J., Doudrick, K., Yang, Y., Westerhoff, P., Capco, D.G., 2014. Food grade titanium dioxide disrupts intestinal brush border microvilli *in vitro* independent of sedimentation. Cell Biol. Toxicol. 30, 169-188.

Georgantzopoulou, A., Serchi, T., Cambier, S., Leclercq, C.C., Renaut, J., Shao, J., Kruszewski, M., Lentzen, E., Grysan, P., Eswara, S., Audinot, J.N., Contal, S., Ziebel, J., Guignard, C., Hoffmann, L., Murk, A.J., Gutleb, A.C., 2016. Effects of silver nanoparticles and ions on a co-culture model for the gastrointestinal epithelium. Part. Fibre Toxicol. 13, 9.

Gordon, S., Daneshian, M., Bouwstra, J., Caloni, F., Constant, S., Davies, D.E., Dandekar, G., Guzman, C.A., Fabian, E., Haltner, E., Hartung, T., Hasiwa, N., Hayden, P., Kandarova, H., Khare, S., Krug, H.F., Kneuer, C., Leist, M., Lian, G., Marx, U., Metzger, M., Ott, K., Prieto, P., Roberts, M.S., Roggen, E.L., Tralau, T., van den Braak, C., Walles, H., Lehr, C.M.. 2015. Non-animal models of epithelial barriers (skin, intestine and lung) in research, industrial applications and regulatory toxicology. ALTEX 32, 327-778.

Gullberg, E., Leonard, M., Karlsson, J., Hopkins, A.M., Brayden, D., Baird, A.W., Artursson, P., 2000. Expression of specific markers and particle transport in a new human intestinal M-cell model. Biochem. Biophys. Res. Commun. 279, 808-813.

Guo, Z., Martucci, N.J., Moreno-Olivas, F., Tako, E., Mahler, G.J., 2017 Titanium dioxide nanoparticle ingestion alters nutrient absorption in an *in vitro* model of the small intestine. NanoImpact 5, 70-82.

Hase, K., Kawano, K., Nochi, T., Pontes, G.S., Fukuda, S., Ebisawa, M., Kadokura, K., Tobe, T., Fujimura, Y., Kawano, S., Yabashi, A., Waguri, S., Nakato, G., Kimura, S., Murakami, T., Iimura, M., Hamura, K., Fukuoka, S., Lowe, A.W., Itoh, K., Kiyono, H., Ohno, H., 2009. Uptake through glycoprotein 2 of FimH(+) bacteria by M cells initiates mucosal immune response. Nature 462, 226-230.

Imai, S., Morishita, Y., Hata, T., Kondoh, M., Yagi, K., Gao, J.Q., Nagano, K., Higashisaka, K., Yoshioka, Y., Tsutsumi, Y., 2017. Cellular internalization, transcellular transport, and cellular effects of silver nanoparticles in polarized Caco-2 cells following apical or basolateral exposure. Biochem. Biophys. Res. Commun. 484, 543-549.

Ingels, F., Beck, B., Oth, M., Augustijns, P., 2004. Effect of simulated intestinal fluid on drug permeability estimation across Caco-2 monolayers. Int J Pharm. 274, 221-232.

Kanaya, T., Ohno, H., 2014. The mechanisms of M-cell differentiation. Biosci. Microbiota Food Health 33, 91-97.

Kucharzik, T., Lügering, N., Rautenberg, K., Lügering, A., Schmidt, M.A., Stoll, R., Domschke, W., 2000. Role of M cells in intestinal barrier function. Ann. NY Acad. Sci. 915, 171-183.

Leist, M., Hasiwa, N., Rovida, C., Daneshian, M., Basketter, D., Kimber, I., Clewell, H., Gocht, T., Goldberg, A., Busquet, F., Rossi, A.M., Schwarz, M., Stephens, M., Taalman, R., Knudsen, T.B., McKim, J., Harris, G., Pamies, D., Hartung, T., 2014. Consensus report on the future of animal-free systemic toxicity testing. ALTEX 31, 341-356.

Lopes, M., Shrestha, N., Correia, A., Shahbazi, M.A., Sarmento, B., Hirvonen, J., Veiga, F., Seiça, R., Ribeiro, A., Santos, H.A., 2016. Dual chitosan/albumin-coated alginate/dextran sulfate nanoparticles for enhanced oral delivery of insulin. J. Control Release 232, 29-41.

Lozoya-Agullo, I., Araújo, F., González-Álvarez, I., Merino-Sanjuán, M., González-Álvarez, M., Bermejo, M., Sarmento, B., 2017. Usefulness of Caco-2/HT29-MTX and Caco-2/HT29-MTX/Raji B coculture models to predict intestinal and colonic permeability compared to Caco-2 monoculture. Mol. Pharm. 14, 1264-1270.

Mahler, G.J., Shuler, M.L., Glahn, R.P., 2009. Characterization of Caco-2 and HT29-MTX cocultures in an *in vitro* digestion/cell culture model used to predict iron bioavailability. J. Nutr. Biochem. 20, 494-502.

Nakano, T., Inoue, I., Alpers, D.H., Akiba, Y., Katayama, S., Shinozaki, R., Kaunitz, J.D., Ohshima, S., Akita, M., Takahashi, S., Koyama, I., Matsushita, M., Komoda, T., 2009. Role of lysophosphatidylcholine in brush-border intestinal alkaline phosphatase release and restoration. Am. J. Physiol. Gastrointest Liver Physiol. 297, G207-214.

Nanogenotox, http://www.nanogenotox.eu/files/PDF/Deliverables/nanogenotox% 20deliverable% 203_wp4_%20dispersion%20protocol.pdf (2011).

Ohno, H., Hase, K., 2010. Glycoprotein 2 (GP2): grabbing the FimH bacteria into M cells for mucosal immunity. Gut Microbes 1, 407-410.

Pinto, M., Robine, S., Appay, M-D., Kedinger, M., Triadou, N., Dussaulx, E., Lacroix, B., Simon, P., Haffen, K., Fogh, J., Zweibaum, A., Assam, P.F., Robineleon, S., Simonassmann, P., Robin, S., Zwwibaum, A., 1983. Enterocyte-like

differentiation and polarization of the human colon carcinoma cell line Caco-2 in culture. Biol. Cell. 47, 323-330.

Sambuy, Y., De Angelis, I., Ranaldi, G., Scarino, M.L., Stammati, A., Zucco, F., 2005. The Caco-2 cell line as a model of the intestinal barrier: influence of cell and culture-related factors on Caco-2 cell functional characteristics. Cell Biol. Toxicol. 21, 1-26.

Sakai-Kato, K., Hidaka, M., Un, K., Kawanishi, T., Okuda, H., 2014. Physicochemical properties and *in vitro* intestinal permeability properties and intestinal cell toxicity of silica particles, performed in simulated gastrointestinal fluids. Biochim. Biophys. Acta 1840, 1171-1180.

Schimpel, C., Teubl, B., Absenger, M., Meindl, C., Fröhlich, E., Leitinger, G., Zimmer, A., Roblegg, E., 2014. Development of an advanced intestinal *in vitro* triple culture permeability model to study transport of nanoparticles. Mol. Pharm. 11, 808-818.

Smith, M.W., Peacock, M.A., 1980. "M" cell distribution in follicle-associated epithelium of mouse Peyer's patch. Am. J. Anat. 159, 167-175.

Suzuki, T., 2013. Regulation of intestinal epithelial permeability by tight junctions. Cell. Mol. Life Sci. 70, 631-659.

Tyrer, P., Foxwell, A.R., Cripps, A.W., Apicella, M.A., Kyd, J.M., 2006. Microbial pattern recognition receptors mediate M-cell uptake of a gram-negative bacterium. Infect. Immun. 74, 625-631.

van Breemen, R.B., Li, Y., 2005. Caco-2 cell permeability assays to measure drug absorption. Expert Opin. Drug Metab. Toxicol. 1: 175-185.

Vance, M.E., Kuiken, T., Vejerano, E.P., McGinnis, S.P., Hochella, M.F. Jr., Rejeski, D., Hull, M.S., 2015. Nanotechnology in the real world: Redeveloping the nanomaterial consumer products inventory. Beilstein J. Nanotechnol. 6, 1769-1780.

Vila, L., Rubio, L., Annangi, B., García-Rodríguez, A., Marcos, R., Hernández, A., 2017. Frozen dispersions of nanomaterials are a useful operational procedure in nanotoxicology. Nanotoxicology 11, 31-40.

Wang, L., Luo, X., Zheng Zhou, L., Zhu, Y., Wu, X., 2015. Culture supernatants of lymphocytes from different lymphoid tissues induce transdifferentiation of Caco2 cells into M-like cells. Xi Bao Yu Fen Zi Mian Yi Xue Za Zhi. 31, 1311-1315.

Yang, Y., Doudrick, K., Bi, X., Hristovski, K., Herckes, P., Westerhoff, P., Kaegi, R., 2014. Characterization of food-grade titanium dioxide: the presence of nanosized particles: Environ. Sci. Technol. 48, 6391-6400.

3.2. Chapter 2 (Study 2)

Effects of differently shaped TiO_2NPs (nano-spheres, nano-rods and nano-wires) on the complex *in vitro* model (Caco-2/HT29) of the intestinal barrier

Submitted paper

Effects of differently shaped TiO_2NPs (nano-spheres, nano-rods and nano-wires) on the complex *in vitro* model (Caco-2/HT29) of the intestinal barrier

Alba García-Rodríguez[1], Laura Vila[1], Constanza Cortés[1], Alba Hernández[1,2,§] , Ricard Marcos[1,2,§]

[1]*Grup de Mutagènesi, Departament de Genètica i de Microbiologia, Facultat de Biociències, Universitat Autònoma de Barcelona, Bellaterra, Spain;*

[2]*CIBER Epidemiología y Salud Pública, ISCIII, Madrid, Spain.*

[§]Corresponding authors at: Grup de Mutagènesi, Departament de Genètica i de Microbiologia, Universitat Autònoma de Barcelona, Edifici Cn, Campus de Bellaterra, 08193 Cerdanyola del Vallès (Barcelona), Spain.

E-mail: alba.hernandez@uab.es (A. Hernández)

ricard.marcos@uab.es (R. Marcos)

Running title: TiO_2NPs (spheres, rods, nano-wires) and Caco-2/HT29 barrier

3.2.1. ABSTRACT

Background: The biological effects of nanoparticles depend on several characteristics such as size and shape that must be taken into account in any type of assessment. The increased use of titanium dioxide nanoparticles (TiO_2NPs) for industrial applications, and specifically as a food additive, demands a deep assessment of their potential risk for humans, including their abilities to cross biological barriers.

Methods: We have investigated the interaction of three differently shaped TiO_2NPs (nano-spheres, nano-rods and nano-wires) in a complex *in vitro* model of the intestinal barrier, where the co-culture of Caco-2/HT29 cells confers inherent intestinal epithelium characteristics to the model (i.e. mucus secretion, brush border, tight junctions, etc.).

Results: Adverse effects in the intestinal epithelium were detected by studying the barrier's integrity (TEER), permeability (LY) and changes in the gene expression of selected specific markers. Using Laser Scanning Confocal Microscopy, we detected a different behaviour in the bio-adhesion and bio-distribution of each of the TiO_2NPs. Moreover, we were able to specifically localize each type of TiO_2NPs inside the cells. Interestingly, general DNA damage, but not oxidative DNA damage effects, were detected by using the FPG version of the comet assay.

Conclusions: Results indicate different interactions and cellular responses related to differently shaped TiO_2NPs.

3.2.2. BACKGROUND

The food industry has used titanium dioxide (TiO_2) for a long time since it was approved by the Food and Drug Administration (USA) in 1966 as a human food additive [1](CFR, 2016). The European Food Safety Authority (EFSA) designated the "E number" E171 to TiO_2, granting it as a substance that can be used as a food additive [2](EFSA, 2016). In addition, recent evidence indicates that the use of nano-sized titanium dioxide (TiO_2NPs) in consumer and industrial products has exponentially increased due to their highly valuable refractive, photocatalytic and pigmenting properties [3,4](Chen and Mao 2007; Horei et al., 2016). Even though TiO_2 was classified by the International Agency for Research on Cancer (IARC) as a possible carcinogen to humans on group 2B in 2010, to date, the Nanotechnology Consumer Products Inventory has documented around 100 consumer products containing TiNPs and TiO_2NPs [5](Vance et al., 2015). Estimations based on the consumption of TiO_2-containing food lead to the conclusion that, in the US, children and adults may be

ingesting around 1-2 and 0.2-0.7 mg/kg bw/day of TiO_2, respectively [6](Weir et al., 2012). This points out the relevance of ingestion as the main entryway of TiO_2 and TiO_2NPs in human exposures.

Nanotechnology allows to design and synthesize personalized TiO_2NPs with the desired physicochemical characteristics (e.g. shape, phase, and structure) in order to improve, increase, and diversify NPs' applicability. Therefore, as the range of nanoparticle types and applications increases, the potential toxicities of these novel materials and the properties driving such toxic responses must be fully understood. To date, research with microorganisms has evidenced that the biocidal activity and cytotoxic effects of NPs are structure-, shape-, and size-dependent [7-9](Pal et al., 2007; Ercan et al., 2011; Aminedi et al., 2013). Furthermore, *in vitro* mammalian cells' studies have reported distinct ROS generation patterns by different-types of TiO_2 nano-wires [10](Park et al., 2013), differences in cytotoxicity between various crystalline-structure TiO_2NPs [11](Gerloff et al., 2012) and variations in the intracellular accumulation of different crystal-phase food-grade TiO_2 [12](Dorier et al., 2015). It has also been well documented that the crystalline phase and the primary NP diameter alters the biological impact (e.g. bio-distribution, toxico-kinetics, etc.) of TiO_2NPs *in vivo* [13-15](Grassian et al., 2007; Gui et al., 2011; Zhao et al., 2013).

Considering oral exposure as one of the principal entry routes to the human body, the lack of conclusive studies reporting the impact of newly engineered TiO_2NPs and how they behave across the gastrointestinal tract is eye-catching. Accordingly, our study aims to evaluate the bio-interactions, bio-distribution, and toxicokinetics of TiO_2NPs in the intestinal barrier by assessing the biological effects of three differently shaped TiO_2NPs (nano-sphere, nano-rods and nano-wires). For this purpose, we used an *in vitro* model comprised of Caco-2/HT29 co-cultures. After 21 days, the co-culture acquires a barrier structure that faithfully mimics the human small intestine epithelium at both the morphological and functional level [16,17](Antunes et al., 2013; Lozoya-Agullo et al., 2017). Derived from a human colon adenocarcinoma, Caco-2 cells, as enterocyte-like cells, are able to express microvilli, tight junctions (TJ) and present paracellular, transcellular, active and transcytotic transport [18](Artursson et al., 2001). Differentiated Caco-2 cells also express all of the major integral membrane enzymes in charge of nutrient hydrolysis, uptake, storage and absorption [19,20](Levy et al., 1995; Shen et al., 2008). In parallel, HT29 cells, known as goblet cells and also derived from a human colon adenocarcinoma, are characterized by their ability to produce and secrete mucus [21](Lesuffleur et al., 1990).

We have shown that, when seeding at a ratio of 90% Caco-2 to 10% HT29 and culturing for three weeks, this *in vitro* model reaches good integrity levels (<300 Ω/cm^2) and is covered by a dense mucus layer, working as a barrier with two distinct scenarios, the lumen and the mucosa [22](Garcia-Rodriguez et al., 2018). According to this, the main aim of the present study was to determine whether this structure could be compromised by the exposure to TiO_2NPs. Moreover, we aimed to assess if the potential adverse effects are shape- and structure-dependent by comparing the most commercialized TiO_2NPs, namely nano-spheres (anatase-structure), nano-rods (rutile-structure) and nano-wires (TiO_2-structure). For this purpose, we analyzed the barrier's integrity and permeability after 24 and 48 h of TiO_2NPs' exposure, monitored the NPs' location and crossing through the barrier by using laser confocal microscopy and assessed the barrier functionality by gene expression. In addition, genotoxic and oxidative DNA damage were also evaluated by using the comet assay.

3.2.3. MATERIAL AND METHODS

Nanomaterial dispersion and characterization

Three different shapes of titanium dioxide nanoparticles (TiO_2NPs), pure anatase crystal-structure nano-spheres of TiO_2 (<25 nm, TiO_2NPs-S), pure rutile crystal-structure nano-rods of TiO_2 (<100 nm, TiO_2NPs-R), and nano-wires of TiO_2 (<10 nm of diameter and 100 µm of length, TiO_2NPs-W) were purchased from Sigma Chemical Co. (St. Louis, MO). To disperse them, TiO_2NPs were pre-wetted in 0.5% absolute ethanol and suspended in 0.05% filtered bovine serum albumin (BSA) dissolved in autoclaved MilliQ water. TiO_2NPs were sonicated in their dispersion medium for 16 min at 10% of amplitude obtaining a dispersed stock of 2.56 mg/mL, according to the Nanogenotox protocol (Nanogenotox, 2011). A complete characterization of the three TiO_2NPs was carried out to see their behaviour in the cell culture medium used. First, transmission electron microscopy (TEM) was used to determine the dried nanoparticle's size and morphology on a JEOL JEM-1400 instrument (Jeol LTD, Tokyo, Japan). For this purpose, grids covered with Holey carbon film were immersed carefully in each NPs stock (2.56 mg/mL) and left to dry. Then, TEM images of random fields of view were processed with Image J software to measure and calculate the diameter of 200 NPs. Moreover, the hydrodynamic size and ζ-potential of the three TiO_2NPs diluted in DMEM cell culture medium (12.5, 50, 100 and 350 µg/mL) were evaluated at 0, 24 and 48 h after sonication by dynamic light scattering (DLS) and laser Doppler

velocimetry (LDV) methodologies in a Malvern ZetasizerNano-ZS zen3600 device (Malvern, UK).

Cell culture and the *in vitro* co-culture model

The human colorectal adenocarcinoma cell line Caco-2 was kindly provided by Dr Isabella Angelis, from Istituto Superiore di Sanità (ISS, Italia). HT29, another human cell line derived from a colorectal adenocarcinoma, was purchased from American Type Culture Collection (ATCC, Manassas VA 20108 USA). Both cell lines were maintained in Dulbecco's modified Eagle's High Glucose medium without pyruvate (DMEM w/o pruvate, Life Technologies NY) supplemented with 10% fetal bovine serum (FBS), 1% non-essential amino acids (NEAA) (PAA Laboratories GmbH, Pasching, Austria) and 2.5 mg/mL plasmocin (Invivo Gen, San Diego, CA). Cells were placed in a humidified atmosphere of 5% CO_2 and 95% air at 37 ºC. Routinely, Caco-2 and HT29 cell lines were subcultured once a week with 1% trypsin-EDTA (PAA Laboratories GmbH, Pasching, Austria) at $7.5x10^5$ cells/flask and $4x10^5$ cells/flask, respectively, in 75 cm^2 flask.

The *in vitro* co-culture model was seeded in 12-well culture plates using a Polyetylene Terephthalate Transwell® (PET) with 1 µm pore size and an area of 1.12 cm^2 (Millipore®) (Merck KGaA, Darmstadt, Germany) as a support chamber, to differentiate the apical side from the basolateral side. Briefly, $1.7x10^5$ Caco-2 and HT29 cells clones were mixed and seeded on the apical side of the transwell in a ratio of 90:10, respectively. Finally, Caco-2/HT29 co-cultures were left to differentiate during 21 days and cell culture medium was changed every two days.

Viability studies

To choose the range of sub-toxic doses to be used in our studies, an initial toxicity study was carried out. Cell viability was determined by the Beckman counter method with a ZTM Series coulter-counter (Beckman Coulter Inc., CA). 21 days-old Caco-2/HT-29 co-cultures were exposed for 24 and 48 h to different concentrations of TiO_2NPs-S, -R and –W, ranging from 0 to 350 µg/mL. After exposure to the given NPs, barriers were washed three times with 0.5 mL of PBS (1%) and incubated 4 min at 37 ºC with 0.25 mL of trypsin-EDTA 1%, to detach and individualize the cells. Finally, cells were diluted in ISOTON solution (1/100) and counted with the Beckman Cell Counter. Viability values for each concentration were calculated by averaging three independent viability experiments, each containing three replicates per sample (n=9).

Evaluation of the barrier's integrity in the *in vitro* co-culture model

To monitor the formation of the differentiated barrier and its integrity, its trans-epithelial electrical resistance (TEER) was measured weekly with an epithelial Voltmeter (Millicell-ERS volt/ohm meter). TEER was measured 7, 14 and 21 days after seeding Caco-2/HT29 in PET transwells. Caco-2/HT29 co-cultures with TEER values higher than 300 Ω/cm^2 were used for further experiments. TEER values were also measured after TiO_2NPs-S, TiO_2NPs-R, and TiO_2NPs-W exposure for 24 and 48 h. Briefly, after NPs exposure, the apical and basolateral chambers of the barriers were washed three times with PBS (1%) to remove the NPs as much as possible and fresh DMEM cell culture medium was placed again in the transwells. Each sample was measured three times in different parts of the insert before and after NPs exposure. TEER values for each concentration were calculated by averaging three independent experiments. TEER values were calculated according to the formula TEER = [Ω (cell inserts) - Ω (cell-free inserts)] x 1.12 cm^2.

Paracellular transport through the co-culture barrier

To support the integrity studies of the Caco-2/HT29 barrier, the paracellular passage of Lucifer yellow (LY) was analysed. Briefly, after 24 and 48 h of exposure to the different TiO_2NPs, barriers were washed three times with transport buffer (HBSS; Ca^{2+}, Mg^{2+}, +10 mM HEPES, pH 7.4). The inserts were transferred to a new 12-well plate with 1.5 mL of HBSS in the basolateral compartment. LY diluted in HBSS was added to the apical compartment at a final concentration of 0.4 mg/mL and plates were then placed in a 37 ºC incubator for 2 h. One hundred µL of each basal compartment were transferred in triplicates to a black 96-well plate. LY leakage through the barrier was measured in a prompt fluorimeter (Victor III, Perkin Elmet) plate reader using a 405-535 nm excitation-emission spectrum.

TiO_2NPs localization across the Caco-2/HT29 barrier

Laser Confocal Microscopy has demonstrated to be a useful method for localizing metallic NPs inside cells (Vila et al., 2017a). This method was used to visualize and locate the three different TiO_2NPs through the co-cultured barrier. For this purpose, Caco-2/HT29 barriers were exposed to 150 µg/mL of TiO_2NPs-S, -R and -W for 24 and 48 h. After the exposure time, barriers were stained *in situ* with *Hoechst 33351* and *WGA Alexa Fluor™*, diluted in DMEM cell culture medium at concentrations of 1/500 and 1/100, respectively, during 15 min. Images were obtained by using a confocal laser

scanning microscope Leica TC2 SP5. The three types of TiO_2NPs were visualized thanks to their own reflective capability and manually masked with green colour, in contrast with the blue colour of the cells' nucleus and the red colour or the extracellular membrane and the mucus layer. Confocal images were processed with the software Huygens Essential 4.4.0p6 (Scientific Volume Imaging, Netherlands), and Imaris 7.2.1 (Bitplane, AG).

TiO_2NPs transport across the Caco-2/HT29 co-culture barrier

To detect the TiO_2NPs crossing through the Caco-2/HT29 barriers, laser confocal microscopy was also used. To discern if TiO_2NPs' transport was shape-, concentration- or time-dependent, co-culture barriers were exposed to different concentrations (12.5, 50, 100, and 350 µg/mL) of TiO_2NPs-S, -R and -W for 24 and 48 h. After the NPs' exposure, the cell culture medium (1.5 mL) in the basolateral compartment was collected. To eliminate the inorganic material aggregates and crystallized proteins, samples were treated with proteinase K (100 µg/mL) during 30 min at 37 ºC. Next, samples were centrifuged in a speed vacuum at 37 ºC for 2 h to concentrate the NPs present in the medium. Finally, 10 µL of each sample were placed in slides, covered with a cover-slip, and the NPs were observed under the confocal microscopy. Several images were taken from random fields of each sample. Confocal images were processed with Huygens Essential 4.4.0p6 (Scientific Volume Imaging, Netherlands) and Imaris 7.2.1 (Bitplane, AG) softwares, where the percentage of the reflective area of each sample was calculated. Semi-quantitative values were obtained from three different experiments.

RNA extraction and gene expression by real-time qPCR

Total RNA from Caco-2/HT29 co-culture barriers exposed to 0, 50 and 150 µg/mL of TiO_2NPs-S, -R and –W, for 24 and 48 h, was extracted using TRIzol® Reagent (Invitrogen, USA) following the manufacturer's instructions. RNase-free DNase I (DNA-free TM kit; Ambion, UK) was used to discard residual DNA contamination. The first-strand cDNA synthesis kit (Roche, Basel, Switzerland) was used to obtain cDNA by from 100 ng of total RNA. The resulting cDNA was subjected to real-time PCR analysis on a LightCycler-480 to evaluate the relative expression of the brush border enzymes sucrase-isomaltase (SI: forward 5'-TGGTGGCACTGTTATCCGAC-3' and reverse 5'-GACCACCACGGACATGTAGG-3'), alkaline phosphatase (ALPI: forward 5'-GTCCATCCTGTACGGCAATG-3' and reverse 5'-ACATGCGCTACGAAGCTCTG-3'),

and solute carrier family 15 (SLC15A1: forward 5'-CTTCGATGCTGTGCTGTACC-3' and reverse 5'-GGCCAAGTGTCACCATCTCT-3'). Gene expression of tight junctions components such as claudin 2 (CLDN2: forward 5'-TACTCACCACTGGTGCCTGA-3' and reverse 5'-GAGAGCTCCTTGTGGCAAGA-3'), zonula occludens (ZO-1: forward 5'-GAGAGGTGTTCCGTGTTGTG-3' and reverse 5'-GCTGCGAAGACCTCTGAATC-3'), and occludin (OCLN: forward 5'-ACAGACTACACAACTGGCGG-3' and reverse 5'-GCAGCAGCCATGTACTCTTC-3'). The expression of β-actin (forward 5'-GCATGGAGTCCTGTGGCATC-3' and reverse 5'-CCACACGGAGTACTTGCGCT- 3') was used as the housekeeping control. Each 20 µL of reaction volume contained 5 µL cDNA, 10 µL of 2x LightCycler 480 SYBR Green I Mater (Roche, Germany), 3 µL of distilled H_2O and 1 µL of each primer pairs at a final concentration of 10 µM. The cycling parameters were the following: an initial step of 95 ºC for 5 min, then 45 cycles of 95 ºC for 10 s, 62 ºC for 15 s and 72 ºC for 25 s. Cycle time (Ct) values were calculated with the LightCycler 480 software package and then normalized with β-Actin Ct values.

Genotoxic and oxidative DNA damage quantification

The potential induction of genotoxic and oxidative DNA damage in Caco-2/HT29 co-culture barriers was assessed by the alkaline comet assay after 24 and 48 h of exposure to TiO_2NPs-S, -R, and W treatments. The concentration-range was 0, 12.5, 50, 150, and 350 µg/mL for all the TiO_2-shapes. The addition of Formamidopyrimidine-DNA glycosylase (FPG enzyme) was used to measure oxidatively-damaged DNA bases. Briefly, once treated, barriers were washed twice with PBS, trypsinized (1% trypsin), and centrifuged at 1000 rpm for 8 min. The pellet was then resuspended in PBS to a concentration of 700 cells/µL and placed in ice at 4 ºC, to avoid DNA repair. 25 µL of cells' suspension was mixed with 0.75% of LMP agarose at 37 ºC and dropped (7 µL/drop and 3 drops/sample) on Gelbond (GB) films. Cells on GB were lysed in lysis buffer at 4 ºC and pH 10 overnight. The next morning, GB were washed twice (1 x 5 min, and 1 x 50 min) in enzyme buffer at 4 ºC and pH 8.0, followed by a 30 min incubation with the enzyme buffer at 37 ºC. One GB was incubated with enzyme buffer and FPG enzyme (1/10.000), and the other in enzyme buffer without FPG. GB were incubated with electrophoresis buffer (alkaline buffer) for 35 min followed by the electrophoresis step for 20 min at 20 V and 300 mA at 4 ºC. Finally, GB were rinsed twice in cold PBS for 5 min, in distilled water for 1 min, fixed in absolute ethanol for at least 2 h, air-dried overnight at room temperature, and stained with SYBR Gold for 20 min. Each GB film was cut into two similar-sized parts to fit in an acrylic slide (52.5 x 75

x3 mm). A coverslip of 52.5 x 75 mm was placed on top of the drops, effectively sealing the samples. GB were observed using an epifluorescent Olympus BX50 and damage was quantified measuring the percentage of DNA in tail by using the Komet 5.5 Image analysis software. One hundred randomly-selected comet images were analyzed per sample. 30 min treatments of 5 mM of potassium bromate ($KBrO_3$) and 2.5 mM of methylmethanesulfonate (MMS) were used as positive control of oxidative and genotoxic damage, respectively.

Statistical analysis

All measurements were made in triplicates, at least for 2 separate experiments. Results are expressed as mean ± standard error. One-way ANOVA with Tukey's post-test, unpaired and paired Student's *t*-test or two-way ANOVA were used to compare differences between means. Data were analyzed with GraphPad Prism version 5.00 for Windows (GraphPad Software, San Diego California USA, www.graphpad.com). Differences between means were considered significant at $P<0.05$.

3.2.4. RESULTS

Nanoparticles characterization

Our TEM images demonstrate that the sizes of primary TiO_2NPs-S, TiO_2NPs-R and TiO_2NPs-W ranged from 70-80, 40-70 and 8-14 nm, respectively (Fig 1; A.1, A.2 and A.3), which are similar to the sizes given by the manufacturer. In spite of the dry form sizes of the NPs, the hydrodynamic diameter measured with the DLS technique gives higher values for the three TiO_2NPs, reaching mean diameters above 200 nm in most cases (Fig. 1E). These differences between primary and hydrodynamic size suggest that TiO_2NPs aggregate in the cell culture medium. No significant changes were seen in size distribution for -S or -R forms in cell culture medium (DMEM) along the incubation time. However, a slight size reduction in -W was observed after 48 h. As differences between TiO_2NPs structures and shapes were observed, we also aimed to study the hydrodynamic size distribution according to the used concentrations (Supplementary data; Fig. S1). Interestingly, different behaviours among TiO_2NPs were observed: -S presented a tendency to aggregate that was clearly concentration-dependent, as higher concentrations correlated with bigger NPs. On the contrary, no concentration nor time-dependent correlation was observed for TiO_2NPs-R. Regarding -W size distribution, only the lowest concentration (12.5 μg/mL) decreased its

aggregation over time, while the higher concentrations presented similar sizes distributions. PDI values were higher in -S (0.472, 0.581 and 0.544) and in -W (0.596, 0.565 and 0.629) than in -R (0.202, 0.211 and 0.216), suggesting that -R have greater monodisperse size distribution than the others.

No changes in PDI values were detected over time for any TiO_2NPs. The stability of the colloidal system was measured by LDV, indicating the TiO_2NPs surface charge when dispersed in cell culture medium. Our results evince little stability in all TiO_2NPs solutions since the ζ-potential values barely reach the ± 30 mV (Fig. 1E).

Cytotoxic effects of the Caco-2/HT29 co-culture barrier exposed to TiO_2NPs.

To determine the cytotoxic effects of TiO_2NPs-S, -R and -W and to know whether their shape and titanium-based structure play a role in cell viability, we exposed the 21-days co-cultures to concentrations ranging from 12.5 to 350 µg/mL for 24 and 48 h since ingested TiO_2NPs have low absorption in rats (Cho et al., 2013), and human ingestion has shown to be daily (Weir et al., 2012). As Figure 2 indicates, non-detrimental cytotoxic damage was detected after 24 h of -S, -R, and -W exposures, as all the registered viability values were above the 80%. Nevertheless, when checking cell viability after 48 h of exposure, a drastic decrease in cell viability was observed for in all three TiO_2NPs-shapes exposures starting at 12.5 µg/mL, although these effects weren't concentration-dependent. Interestingly, the concentration of 150 µg/mL seems to be the most toxic since it caused the highest mortality in all the TiO_2NPs tested at 48 h. In spite of the observed toxicities, we can conclude that the shape can be associated with adverse effects as cytotoxicity.

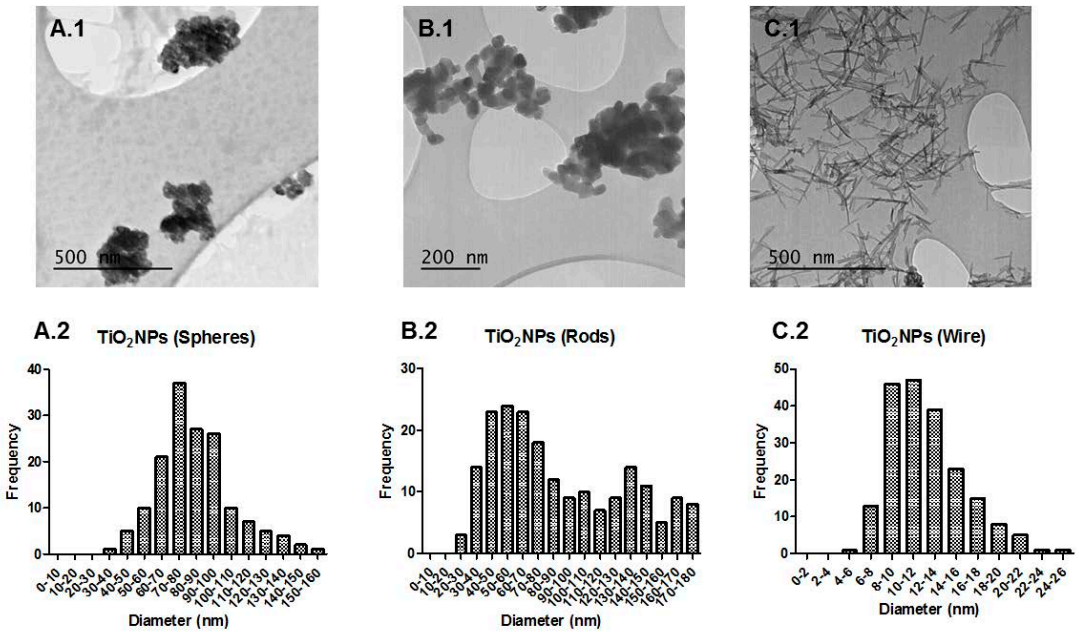

		DLS		LDV	
Nanoparticle Type	Time (hours)	Z-Average d. (nm)	PdI	Zeta Potential ζ (mV)	Electrophoretic mobility (µm·cm/V·s)
TiO_2NPs-S	0	291.2±50.69	0.472±0.052	-11.6±2.09	-0.905±0.163
	24	254.3±15.58	0.581±0.055	-12.3±3.27	-0.961±0.255
	48	281.4±6.176	0.544±0.065	-14.2±1.25	-1.117±0.096
TiO_2NPs-R	0	232.3±3.983	0.202±0.021	-11.5±0.902	-0.898±0.071
	24	241.7±6.309	0.211±0.0211	-12.3±1.65	-0.966±0.129
	48	238.4±4.013	0.216±0.011	-11.2±3.48	-0.879±0.273
TiO_2NPs-W	0	220.7±8.752	0.596±0.119	-13.4±3.28	-1.05±0.258
	24	198.3±4.518	0.565±0.035	-12.6±0.85	-0.983±0.064
	48	179.8±5.129	0.629±0.203	-9.43±1.54	-0.740±0.123

Figure 1. TiO_2NPs characterization. TEM images of TiO_2NPs-S (A.1), TiO_2NPs-R (B.1), and TiO_2NPs-W (C.1) in their dry form. Size distribution of TiO_2NPs-S (A.2), TiO_2NPs-R (B.2), and TiO_2NPs-W (C.2) of 200 randomly-selected nanoparticles. (E) Dynamic light scattering (DLS) and laser Doppler velocimetry (LDV) measurements of 50 µg/mL TiO_2NPs over the exposure time (0, 24, and 48 h). Data are represented as mean ± SD.

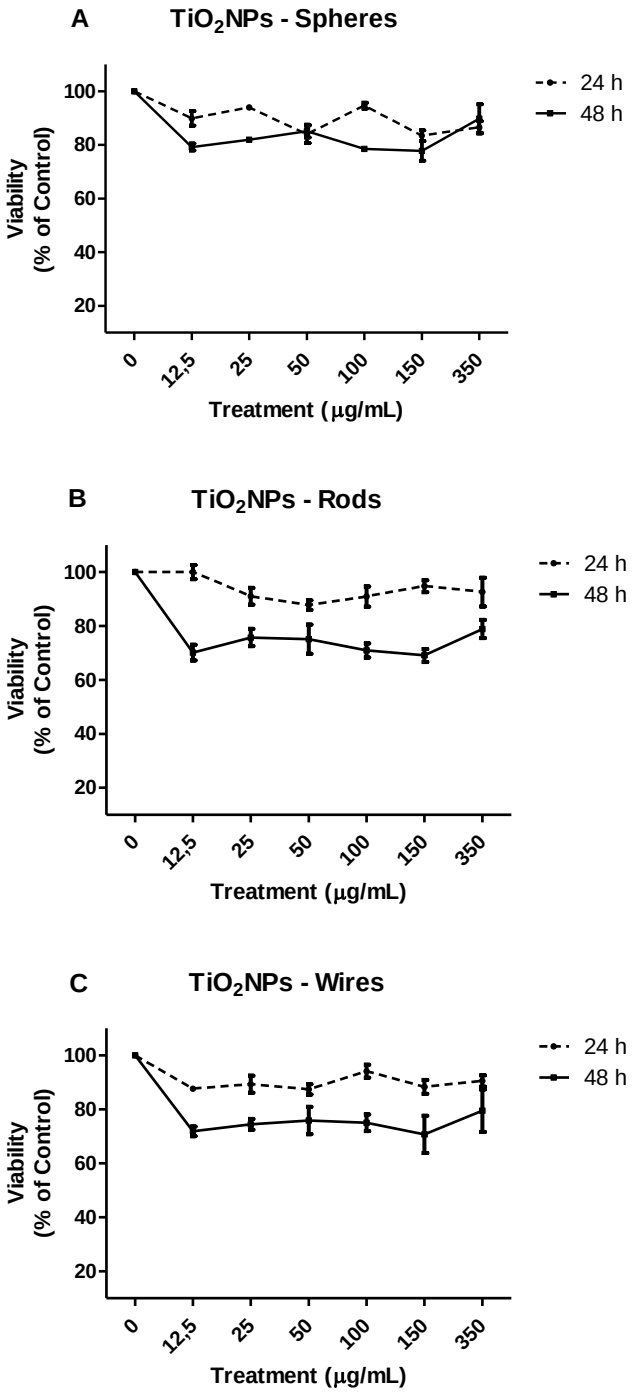

Figure 2. Cell viability (% of control) of Caco-2/HT29 co-culture barrier treated with 0-350 µg/mL of TiO_2NPs-S (A), TiO_2NPs-R (B), and TiO_2NPs-W (C) for 24 or 48 h. Results were analyzed according to the one-way ANOVA with Tukey's post-test and are represented as mean ± SEM.

Evaluation of the barrier's integrity after TiO2NPs' exposure

The main functions of an epithelial barrier are to confer stability, protection, and the desired permeability in each tissue and/or organ. TJ play an important role in these functions, forming belt-like and apical-most adhesive junctional complexes around mammalian cells (Groschwitz and Hogan, 2009). Thus, we can evaluate the functional integrity of the barrier measuring the TEER and, consequently, the stability of our Caco-2/HT29 co-culture model. In addition, we can determine whether TiO_2NPs disrupt the barrier by either disrupting the TJ or by being cytotoxic. As Figure 3 depicts, TEER values were measured pre- and post-exposure with TiO_2NPs to see any damaging effect on the barrier's integrity. As observed in previous experiments (data not shown), basal TEER values for our Caco-2/HT29 co-culture barrier surpass the 300 Ω/cm^2. No significant reduction was seen in the integrity of the barrier when exposed to TiO_2NPs-S for 24 h (Fig. 3A). However, significant differences (P<0.05) between TEER values were observed by exposing the barriers to 150 μg/mL of both TiO_2NPs-W (Fig. 3C), and TiO_2NPs-R (Fig. 3E). Moreover, rod-shaped NPs were also able to decrease the membrane's stability at 350 μg/mL (P<0.001). When the exposure time was extended to 48 h, statistically significant adverse effects on the barrier's integrity were detected for all TiO_2NPs shapes at different NPs concentrations (Fig. 3B, 3D and 3F), although no concentration-dependent effect was observed.

A reduction in the barrier's integrity and stability may cause increased permeability to a wide range of endogenous and exogenous particles and/or substances. Thus, we initially focused our integrity studies on analyzing the possible variations of paracellular transport, measuring the pass of LY across the barrier after TiO_2NPs exposure. The results obtained agree with the TEER variations observed previously. As we can see in Figure 4, no increases in the ratio of basolateral LY were observed when the barrier was exposed for 24 h to TiO_2NPs-S. However, the highest concentrations of TiO_2NPs-R, and –W significantly incremented LY's passage (Fig. 4A). Also, 48 h exposures to all the three TiO_2NPs induced significant increases in basolateral LY concentrations when compared to the control. Summarizing, our results show that all TiO2NPs disrupt the cell membrane's integrity and permeability by increasing its paracellular transport. Interestingly, exposure to TiO2NPs-W was the most harmful, modifying stability parameters in most experimental conditions.

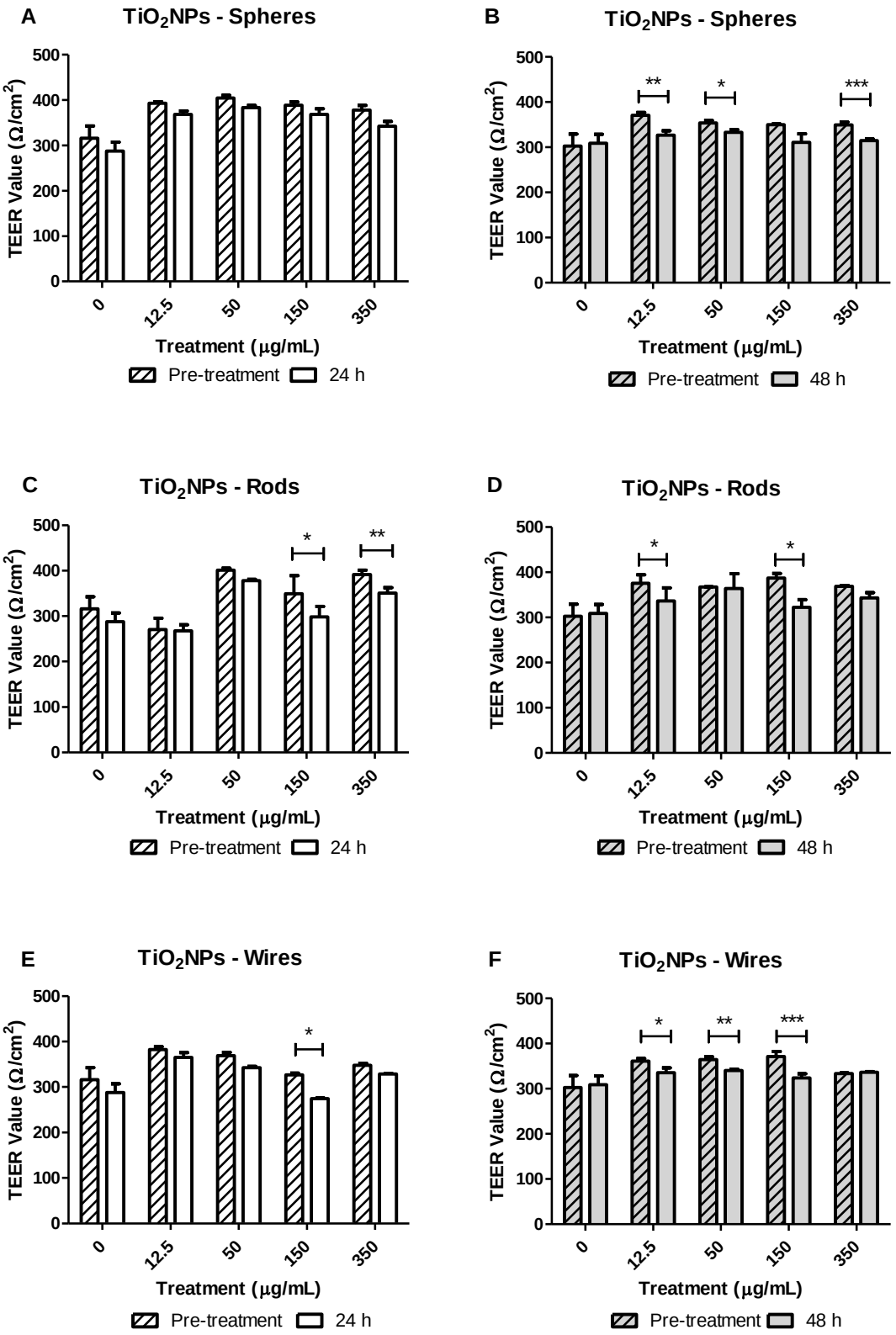

Figure 3. TEER measurements of Caco-2/HT29 co-culture barriers before and after 24 and 48 h of exposure to TiO_2NPs-S (A and B), TiO_2NPs-R (C and D), and TiO_2NPs-W (E and F). Results were analyzed with a paired Student's *t*-test and represented as mean ± SEM. **P*<0.05, ***P*<0.01, ****P*<0.001.

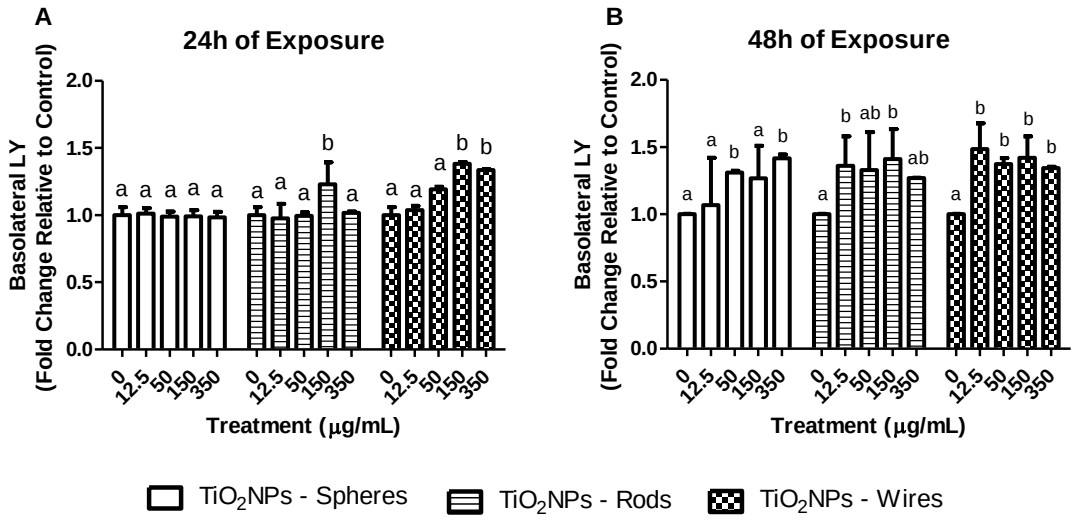

Figure 4. Percentage of LY found in the basolateral chamber of the transwell. The paracellular transport of LY was measured after treating the Caco-2/HT29 co-culture barriers with TiO_2NPs-S, TiO_2NPs-R, and TiO_2NPs-W for 24 (A) or 48 h (B). Results represented as mean ± SEM. Bars that do not share any letter are significantly different according to the one-way ANOVA with Tukey's post-test (P<0.05).

Assessing detrimental effects of TiO_2NPs exposure by gene expression

To support our integrity and permeability results and to evaluate the barrier status, changes in gene expression of several markers associated with different intestinal barrier functions were analysed. To this aim, the Caco-2/HT29 co-culture was exposed to 50 and 150 µg/mL of TiO_2NPs-S, -R, and –W, for 24 and 48 h. We analysed changes in genes related to nutrient uptake and digestion, as well as in TJ genes responsible for sealing intercellular spaces, thus conferring the barrier function. This set of genes, their encoded proteins and their functions are summarized in Table 1.

Interestingly, we observed a significant and consistent down-regulation of *ALPI* in all exposure conditions and for all the TiO_2NPs shapes tested (Fig. 5A). Contrarily, significant increases in *SI* expression were detected after 24 and 48 h of TiO_2NPs-R, and -W exposure, while -S exposure was able to upregulate this gene's expression only after 48 h (Fig. 5C). *SLC15A1* gene expression also increased significantly, but only when the barrier was exposed to 50 µg/mL TiO_2NPs-R for 48 h (Fig. 5E). Summarizing, the expression of different dietary routes could be affected distinctly depending on the TiO_2NPs structure, dose and time, either by enhancement or reduction.

Regarding the gene expression changes of the main integral membrane proteins located at the TJ (*OCLN*, *CLDN2* and *ZO-1*), results were more homogeneous. Generally, the exposure to TiO_2NPs-S did not significantly modify the gene expression of *ZO1* at any time nor concentration. Conversely, *ZO-1* was significantly downregulated when the barrier was exposed to 50 and 150 μg/mL of TiO_2NPs-R for 24 h, while 150 μg/mL TiO_2NPs-W exposure upregulated *ZO-1* expression after 24 h (Fig. 5B). *OCLN* was upregulated after 24 h of exposure to TiO_2NPs-S and also to TiO_2NPs-R, and –W, both after 24 and 48 h (Fig. 5D). Finally, *CLDN2* was significantly upregulated in all experimental conditions after exposing the barrier to TiO_2NPs-S. However, only exposure to TiO_2NPs-R and -W for 48 h upregulated *CLDN2* expression (Fig. 5F). Taken together, this data suggest that the NPs' shape could interact distinctly with the junctional complex modulating different responses.

Caco-2/HT29 barrier uptake of TiO_2NPs

Confocal microscopy was used to qualitatively localize TiO_2NPs in our barrier model, specifically in each of its components (i.e. mucus shed, cell cytoplasm, cell nuclei, apical and basal areas, etc.). As metallic NPs have the capability to reflect polarized light, their detection results easier by confocal microscope than by electron microscopy. Furthermore, we aimed to study whether the NPs' structure and shape could influence uptake and/or translocation, and check potential bio-interactions and bio-dynamics over the exposure time. Briefly, the status of Caco-2/HT29 co-culture barriers was analyzed after 24 h and 48 h exposures to 150 μg/mL of TiO_2NPs-S, TiO_2NPs-R, and TiO_2NPs-W. Figure 6 shows confocal images corresponding to transversal cuts of the barrier, where it is possible to distinguish the cell nucleus in blue, the TiO_2NPs in green, and the mucus secretions and cell membranes in red, indistinctively. As portrayed, after 24 h of exposure most of the TiO_2NPs-S and TiO_2NPs-R remained sedimented and/or attached to the apical side of the barrier, where the microvilli and mucus shed form an extracellular environment suitable for the NPs immobilization (Fig. 6; A and C). Although not in a quantitatively, we can appreciate that the trapped NPs in the apical side are more aggregated/agglomerated than those located deeper in the barrier (white circles). Interestingly, the amount of TiO_2NPs-S detected in the apical part of the barrier was clearly reduced after 48 h of NPs exposure, while the amount of TiO_2NPs-R was similar at both time points. As images E and F from Figure 6 show, after 24 and 48 h of exposures to 150 μg/mL of TiO_2NPs-W the barrier looked more damaged and compromised at a structural level when compared to the other TiO_2NPs exposures. Also, the amount of internalized TiO_2NPs-W, at both time points, was markedly lower.

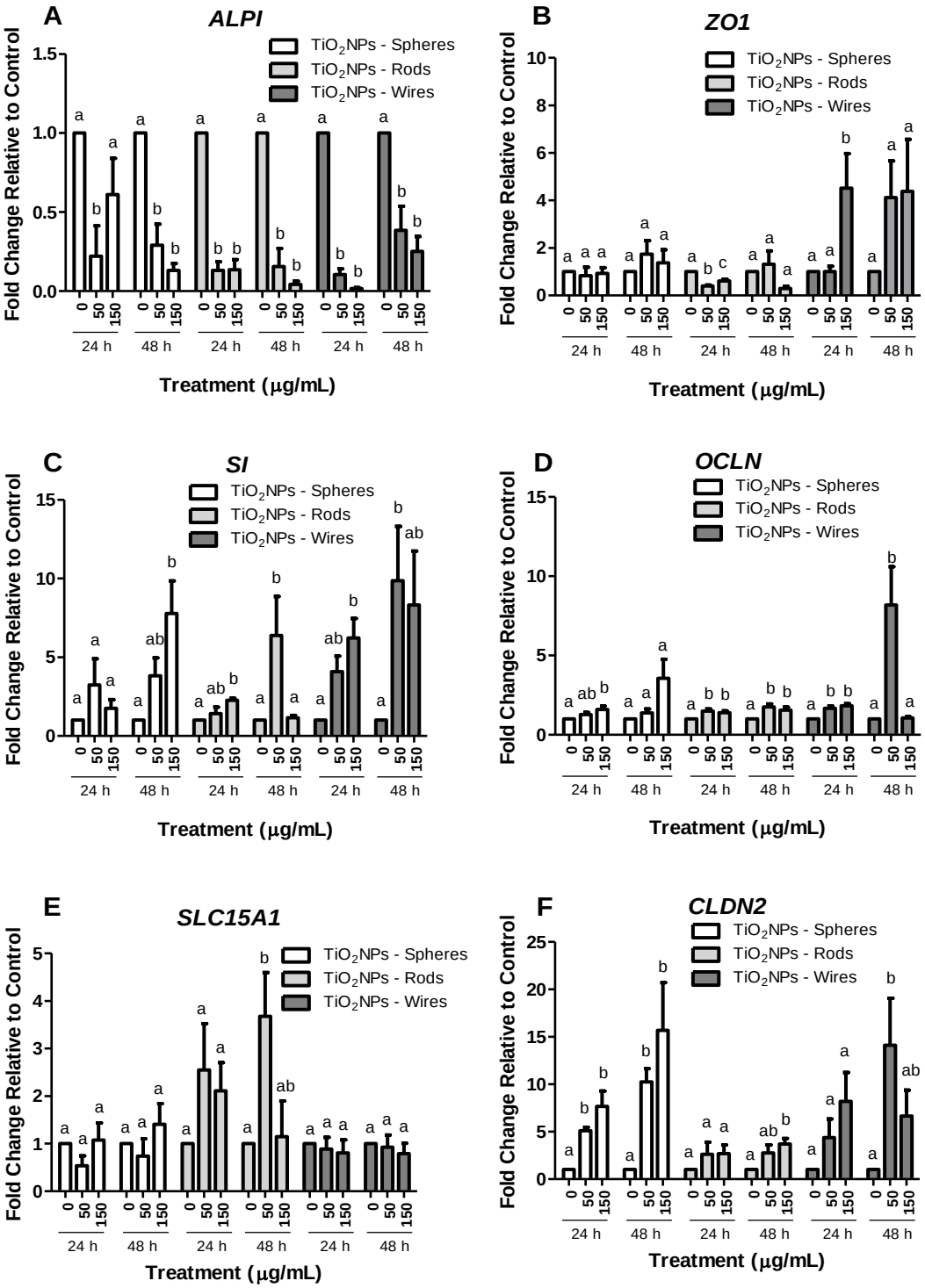

Figure 5. Gene expression of Caco-2/HT29 molecular markers in response to 24 or 48 h of TiO_2NPs-S, TiO_2NPs-R, and TiO_2NPs-W exposure. Results represented as mean ± SEM. Bars that do not share any letter are significantly different according to the one-way ANOVA with Tukey's post-test (P<0.05).

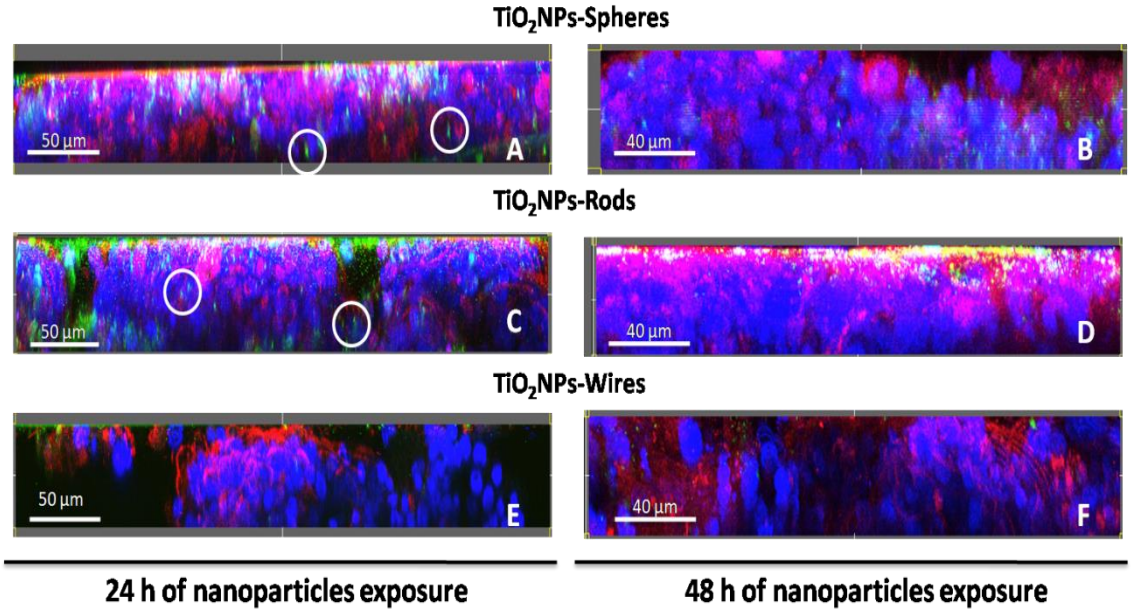

Figure 6. Confocal microscope z-scans of Caco-2/HT29 co-culture barriers after TiO_2NPs-S (A and B), TiO_2NPs-R (C and D), and TiO_2NPs-W (E and F) exposures lasting for 24 h (A, C and E), or 48 h (B, D and F). Cell nuclei (blue) were stained with Hoechst and cell membrane and mucus (red) with WGA. NPs were visualized by reflection and marked with a green mask. Images were processed with the Imaris 7.2.1 software.

Using the confocal technique, we were able to elucidate the exact location of TiO_2NPs in the co-cultured cells, although the identification of each cell type was not possible. As white arrows indicate (Figure 7), TiO_2NPs-S (A), -R (C), and -W (E) were detected in the cell cytoplasm after 24 h of exposure, and in most cases, they reached the cell nucleus. When evaluating the three-dimensional images from samples exposed to the three different TiO_2NPs shapes for 48 h, lower amounts of TiO_2NPs-S were still immobilized in the apical part of the membrane (white circle), and fewer NPs were detected inside the cells (white arrows) (Fig. 7.B). Similar results were obtained when the barriers were exposed to TiO_2NPs-R (Fig. 7D), and TiO_2NPs-W (Supplementary data; Fig. S3) for 48 h. As previously observed, fewer cell junctions and cohesion were found when checking in detail the co-cultures exposed to TiO_2NPs-W for both 24 (Fig. 7E) and 48 h (Fig. 7F). Moreover, TiO_2NPs-W were clearly detected at different levels of the barrier width (white arrow).

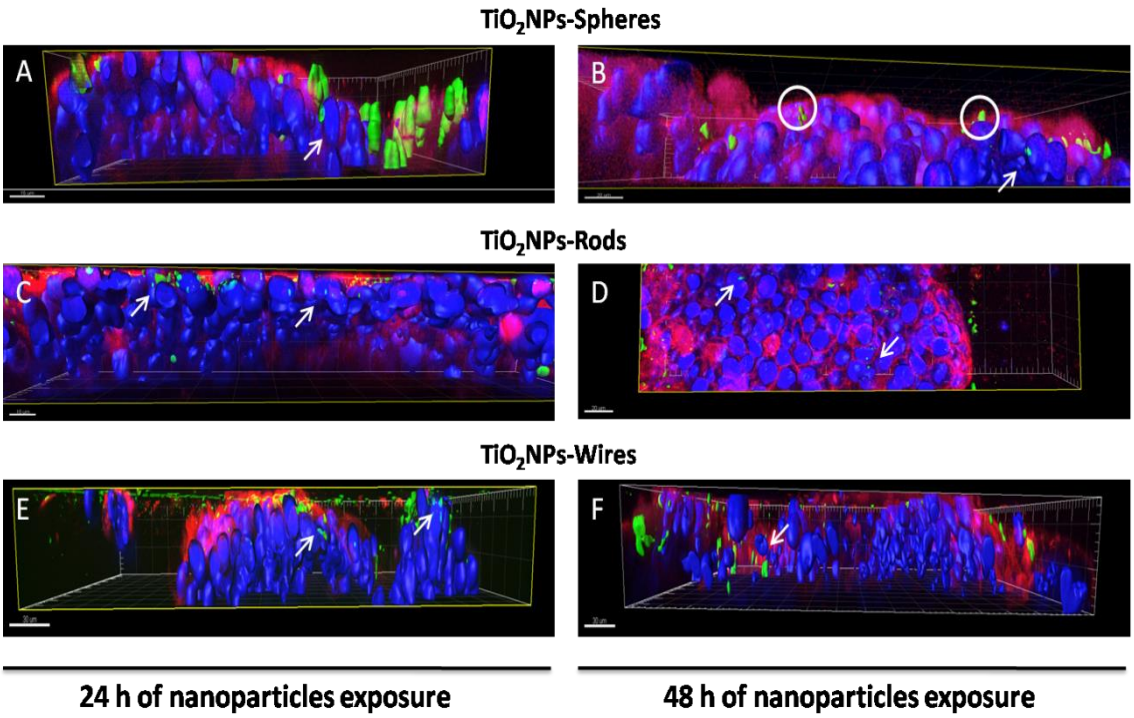

Figure 7. Three-dimensional confocal images of the Caco-2/HT29 co-culture barriers *z*-scans from Figure 6. Images were taken after exposures of 24 or 48 h to TiO_2NPs-S (A and B), TiO_2NPs-R (C and D), and TiO_2NPs-W (E and F). Cell nuclei (blue) were stained with Hoechst, and mucus (red) was stained with WGA. NPs were visualized by reflection and marked with a green mask. White arrows indicate NPs in the cell cytoplasm and NPs-nucleus interactions. Images were processed with the Imaris 7.2.1 software.

Nanoparticles translocation through the Caco-2/HT29 barrier

As the capability of the three TiO_2NPs to penetrate the Caco-2/HT29 co-culture barrier was detected, we aimed to find and quantify any amount of translocated TiO_2NPs by analysing the basolateral medium of the barrier model. Our previous experience working with Caco-2 monolayers demonstrates that confocal microscopy is one of the best techniques to localize metallic NPs in the basolateral media. Thereby, after 24 or 48 h of TiO_2NPs-S, -R, and -W exposure, we collected the entire basolateral medium (1.5 mL), treated it with proteinase *K,* and concentrated the sample by evaporating the cell medium using a speed vacuum. After that, each sample was analyzed under the confocal microscope, where several pictures were taken in random fields of a slide (Supplementary Data; Fig. S2). Semi-quantitative data was obtained by measuring the percentage of the area reflected by the different TiO_2NPs. As Figure 8 shows, the transport of TiO_2NPs-S through the barrier was not concentration-dependent. However, the amount of NPs found in the basolateral chamber 48 h after exposure (~5% of the

area) was almost two times higher than at 24 h (~2% of the area). On the other hand, the TiO_2NPs-R transport was clearly concentration- and time-dependent. Finally, although TiO_2NP-W in the basal growth medium also increased with the exposure time, nano-wires behave differently than the rods, as its transport decreased when the exposure concentration increased.

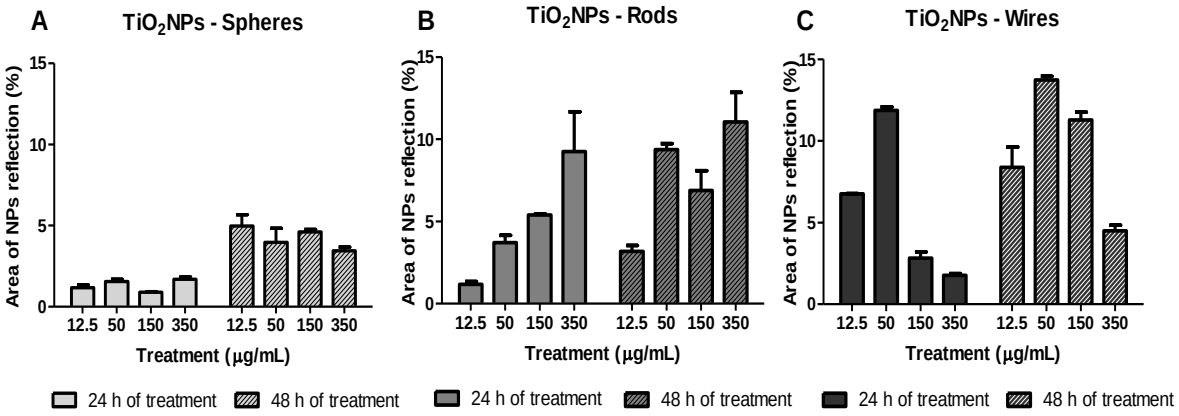

Figure 8. Percentage of the TiO_2NPs-reflective area of the basolateral chamber of the transwell. The transport of TiO_2NPs-Spheres (A), TiO_2NPs-Rods (B), and TiO_2NPs-Wires (C) across the Caco-2/HT29 co-culture barrier was calculated using Laser Confocal microscopy and by measuring the reflected light of randomly selected slide fields. Data are represented as mean ± SEM.

Genotoxic and oxidative damage. Comet Assay

The comet assay was used to analyze the consequences of the TiO_2NPs-cell nucleus interaction previously observed by confocal microscopy. Moreover, we also aimed to elucidate if this response was concentration and/or time-dependent. As depicted in Figure 9, 24 h of TiO_2NPs-S, TiO_2NPs-R, and TiO_2NPs-W exposure significantly increased the general genotoxic damage in our barrier model (Fig. 9A). Nevertheless, after 48 h of TiO_2NPs exposure, only those barriers exposed to TiO_2NPs-R sustained a non-concentration dependent genotoxic damage (Fig. 9B). Methyl methanesulphonate (MMS), a well-known genotoxic compound used as positive control, clearly induced general genotoxic damage to the co-cultured cells (Fig. 8A and 8B).

The potential ability to induce oxidative damage was also detected performing the alkaline version of the comet assay, where oxidatively-damaged DNA bases (e.g. 8-oxodG and FAPydG) were detected using the formamidopyrimidine glycosylase enzyme (FPG), thereby increasing the number of DNA breaks. The difference in the

percentage of DNA in tail between cells treated with FPG and those left untreated gave us a measure of the amount of oxidative DNA damage (Collins et al., 1995; Karlsson, 2010). In this case, no significant increase in oxidative DNA damage was detected after 24 h of TiO_2NPs-S, -R and -W exposure, or after exposures lasting for 48 h. As a positive control we used the well-known oxidant agent, potassium bromate ($KBrO_3$), which increased a 60% the oxidative DNA damage at the Caco-2/HT29 barrier.

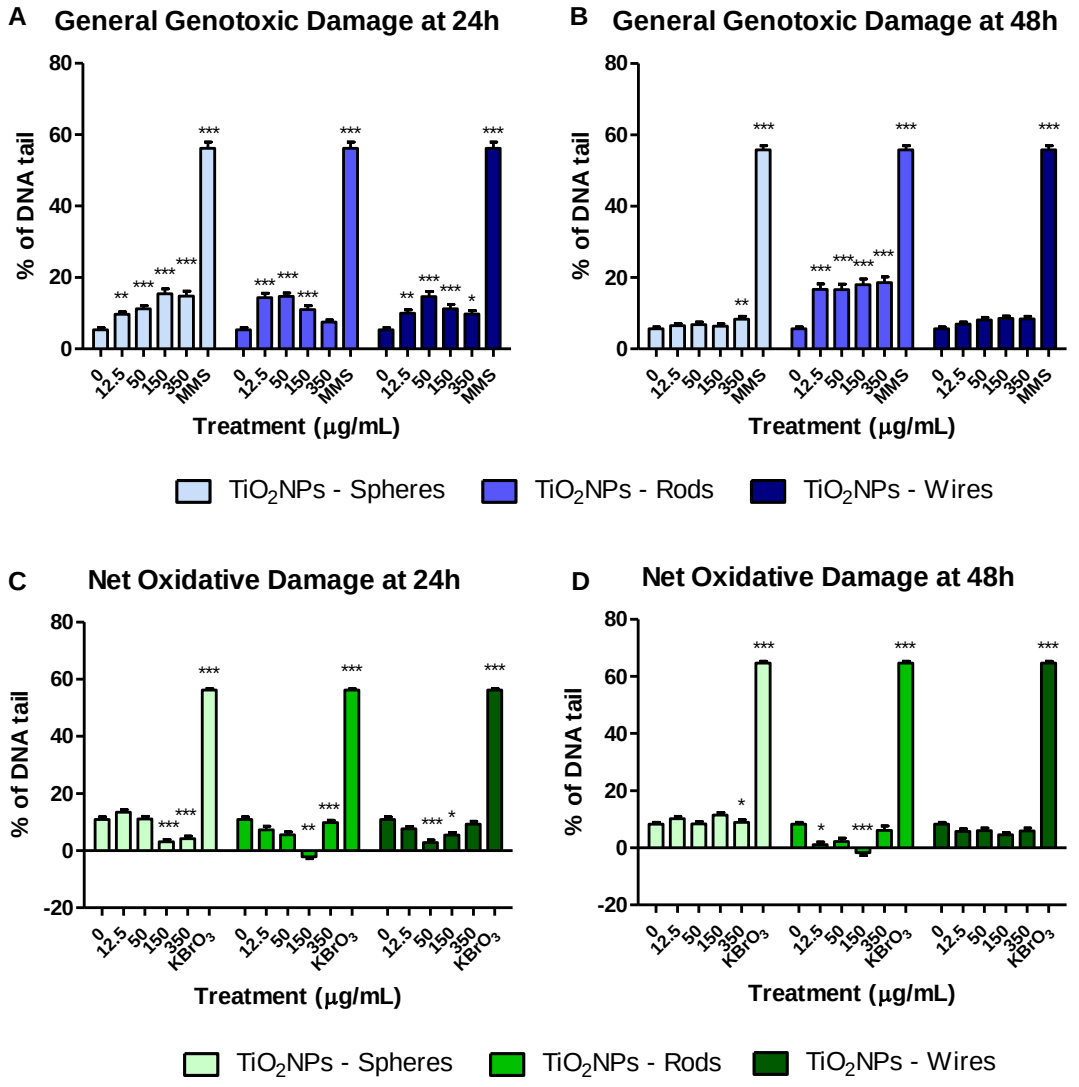

Figure 9. DNA damage studies using the Comet assay complemented with the FPG enzyme. Genotoxic damage observed after 24 (A) or 48 (B) h of exposure to TiO_2NPs (-S, -R and -W). Mean oxidative damage observed after 24 (C), and 48 (D) h of exposure to TiO_2NPs (-S, -R and -W). (*) denotes significant differences according to the one-way ANOVA with Tukey's post-test (*P<0.05, **P<0.01, ***P<0.001). Results are represented as mean ± SEM.

3.2.5. DISCUSSION

The International Agency for Research on Cancer (IARC) performed the last reevaluation on the potential cancer risk of TiO_2 in 2010 (IARC, 2010). According to the collected information, TiO_2 was classified as a potential human carcinogen in group 2B, because there was enough evidence that inhalation of nano-TiO_2 may cause lung cancer. Although IARC considered the risk associated with oral exposure, inconclusive outcomes were obtained due to the lack of standardized procedures for nano-TiO_2 risk assessment, as pointed out by Jacobs et al. (2010). Under this framework, we aimed to investigate the potential hazard of three different shapes and crystal structures of TiO_2NPs using a complex *in vitro* model of intestinal barrier constituted by Caco-2 and HT29 cells co-cultures.

A preliminary characterization of the selected TiO_2NPs showed larger hydrodynamic diameter values their primary sizes. This would agree with other studies showing the general tendency of NPs, and of TiO_2NPs in particular, to form agglomerates in cell culture media (Prasad et al., 2013; Vranic et al., 2017). Interestingly, our results showed that crystallinity and morphology are not influential factors in determining the stability of TiO_2NPs suspensions, which agrees with previously reported data (Liu et al., 2010). Although most of the studies barely take into account the potential role of incubation time when characterizing NPs, we strongly believe that this should be a prerequisite to understanding the NPs biopersistence and their multiple potential biological effects. Accordingly, we took this parameter into consideration but we did not detect relevant variations in the hydrodynamic size for TiO_2NPs-S or TiO_2NPs-R over the incubation time (0, 24, and 48 h). Nevertheless, a slight reduction in the hydrodynamic size for TiO_2NPs-W was observed, which would indicate the lack of time-dependent aggregation. The agglomeration status of NPs can influence the potential toxicity by changing their uptake and/or the way they interact with cells. In fact, changes in this parameter are considered as one of the main reasons for the contrasting data reported in different studies (Prasad et al., 2013; Raza et al., 2016).

Even though exposure to TiO_2NPs occurs chronically in humans, most of the *in vitro* studies testing potential biological effects are performed evaluating effects over a short exposure time (e.g. after 4, 6 or 24 h). These short exposure times don't reflect the observed *in vivo* NPs effects (Warheit et al., 2009). To increase the fidelity of *in vitro* models, elongating the exposure time and minimizing the exposure concentration could be a useful approach, however, the increase of the exposure times (6, 24 and 48 h) didn't cause variations in the observed effects on Caco-2 monolayers (Dorier et al.,

2017). Going one step further, we have been able to detect a significant reduction in cell viability after 48 h for all TiO_2NPs-shaped exposures using our Caco-2/HT29 co-culture model, which points out the relevance of exposure time. Nonetheless, our results are in contradiction with those observed in Caco-2/HT29-MTX co-cultures, where no cytotoxic effects were observed after similar exposure conditions (Brun et al., 2014; Dorier et al., 2017). As previously stated, the agglomeration status after 48 h of TiO_2NPs suspended in serum-containing cell culture medium was smaller for TiO_2NPs-R and TiO_2NPs-W and similar for TiO_2NPs-S in our case. This could be a potential factor explaining the increased cytotoxicity over the exposure times. In addition, our model, using the HT29 clone, and the proportion 90% of Caco-2 and 10% of HT29, has demonstrated a proper mucus secretion spreading through the surface barrier, forming a thick mucus layer and conferring a good barrier protection and integrity (Garcia-Rodriguez et al., 2018). Since Brun et al. (2014) and Dorier et al. (2017) used a different HT29 cell clone, and their co-cultures were composed by 70% of Caco-2 and 30% HT29-MTX, these factors would explain the observed differences and, at the same time, would reinforce the usefulness of our model.

To characterize the effects of the interaction of the three TiO_2NPs shapes with the barrier, we assessed its functionality and permeability by TEER and LY paracellular crossing. Although TiO_2NPs-S did not disrupt the integrity of our model after 24 h exposures, small but significant effects were observed for TiO_2NPs-R and –W at this time point, pointing out the relevance of the NPs' shape when analyzing its effects. The extension of the exposure time enhanced the damaging effects observed at 24h, as the three different shapes of TiO_2NPs affect the barrier's integrity after exposures lasting for 48 h. Interestingly, the observed adverse effects on the barrier's integrity depend on the shape of the TiO_2NPs used as well: TiO_2NPs-W causes the most adverse effects, while TiO_2NPs-S is the least hazardous. Moreover, the observed upregulation in genes encoding different TJ components (*ZO*-1, *OCLN,* and *CLDN2*) indicates the presence of active repair by inducing the novo expression of junctional proteins (Brun et al., 2014), confirming the cell junctions' and the barrier's integrity impairment.

After NPs are ingested, they can interact with a number of biologically significant tissues and structures, as the enterocytes' brush border (microvilli). In fact, it has already been observed that the adsorption of NPs results in the disruption of the brush border's structure (Zhang et al., 2010; Faust et al., 2014a), where approximately 42% of microvilli were lost after the exposure to food-grade TiO_2 (Faust et al., 2014b). In our case, we have found that exposures to different TiO_2NPs' shapes also altered significantly the Caco-2/HT29 brush border membrane and enzymatic function, as the

expression of *ALPI* was readily and radically downregulated after exposure to all of the TiO_2NPs. It must be noted that a recent study analyzing ALPI's enzymatic activity in Caco-2/HT29-MTX co-cultures observed an increased activity after acute and chronic TiO_2NPs exposures (Guo et al., 2017). These discrepancies between post-transcriptional and post-translational regulations lead us to hypothesize that an enzyme over-activation of ALPI in response to TiO_2NPs might trigger the block of its gene transcription to mRNA. It would be interesting in a future to check the protein levels in comparison to its activity. In addition, the *SI* gene expression was upregulated after most of the exposures conditions analyzed, suggesting an active response to carbohydrates starvation caused by the TiO_2NPs exposure. Finally, the upregulation of *SLC15A1* gene expression was detected after TiO_2NPs-R exposure, but not after TiO_2NPs-S and TiO_2NPs-W. This would agree with what was observed in Caco-2 monolayers exposed to rutile TiO_2NPs for 48 h (Dorier et al., 2015). Overall, TiO_2NPs exposure affects the barrier's integrity, but each brush border enzyme may follow different strategies to stabilize its correct function, independently of the concentration exposure and NP shape.

The disruption of the barrier integrity can potentially affect cellular uptake and translocation throughout the barrier of the TiO_2NPs NPs, making the evaluation of these parameters necessary to evaluate the risk of exposures. A wide number of mammalian cell type models internalize TiO_2NPs, including differentiated Caco-2 cells (Faust et al., 2014a; Song et al., 2015). Interestingly, the capability of differentiated Caco-2 cells to internalize TiO_2NPs depends on their structure, as more rutil- than anatase-structured TiO_2NPs were observed in differentiated Caco-2 (Brun et al., 2014; Dorier et al., 2015). When the Caco-2/HT29 co-cultures are established, technical difficulties to follow and locate the NPs position inside individualized Caco-2 or HT29 cells appear. To elucidate the TiO_2NPs distribution in our *in vitro* model of the intestinal barrier, we used laser scanning confocal microscopy. With this methodological approach, we detected that (i) numerous TiO_2NPs-S and -R agglomerates remain deposited and entrapped in the apical part of the barrier, where the mucus shed and microvilli are located; while the smaller agglomerates could penetrate the barrier deeper; (ii) TiO_2NPs-R were more confined between mucus and microvilli than TiO_2NPs-S and TiO_2NPs-W; (iii) differences in bio-persistence between NPs shapes were clearly seen through the time exposure; (iv) TiO_2NPs-W apparently impaired the barrier structure readily after 24 h of NPs treatment; (v) the three shapes of TiO_2NPs were able to cross the mucus shed, enter into the cell's cytoplasm and, finally, get in contact with the cell nucleus; (vi) more TiO_2NPs-R/cell nucleus interaction events were

seen when compared to TiO_2NPs-S and –W at the same concentration; and (vii) TiO_2NPs-W presented more paracellular transport through the barrier than the other shapes. Taken together, we demonstrate the usefulness of our methodological approach, as well as the differential uptake depending on the NPs' shape. In fact, Chen et al. (2010) already demonstrated that spherical TiO_2NPs and nanorods could be more readily internalized in HeLa cells than filamentous ones. In spite of the obtained images, a limitation of the technique is that it does not differentiate the NPs internalization rate on each cell type used in the model (absorptive or goblet cells). However, both cell types in monocultures have demonstrated to internalize TiO_2NPs (Song et al., 2015; Schneider et al., 2017).

TiO_2NPs are absorbed in the gastrointestinal tract, delivered to the bloodstream and distributed to different organs (Zhao et al., 2013). According to this, translocation through our barrier model must be demonstrated. Using confocal microscopy, we detected the presence of the three different shapes of TiO_2NPs in the basolateral chamber, indicating the ability of TiO_2NPs to pass through the *in vitro* intestinal barrier, independently of their shape. A relationship between TiO_2NPs' shape-translocation capacity was observed with an increasing concentration-dependent translocation for TiO_2NPs-R and the opposite for TiO_2NPs-W. Moreover, constant translocation was seen for all TiO_2NPs shapes, as the amount of NPs was higher at 48 than at 24 h. This lead us to think that the physicochemical characteristics of each TiO_2NPs shape can influence their translocation rate. Results from Brun et al. (2014) only found TiO_2NPs translocation in a Caco-2/Raji-B model, but not in the Caco-2/HT29-MTX one, suggesting that TiO_2NPs pass only through transcellular transport through M cells. However, we provided enough evidence that TiO_2NPs-S, -R and -W can alter the barrier's integrity and paracellular transport permeability to translocate to the serosa of the intestinal tract. Moreover, we also observed a clear TiO_2NPs-S and -R internalization, probably by both cell types, also indicating a putative transcellular transport.

Among the potentially adverse health effects of TiO_2NPs internalization, many authors point out genotoxicity on target cells. However, previous *in vitro* and *in vivo* studies evaluating the genotoxicity of TiO_2NPs present conflicting results (Martirosyan et al., 2014). The review of Chen et al. (2014) states that *in vitro* models generated more positive results than the *in vivo* ones, and assays detecting DNA and chromosome damage produced more positive outcomes than those measuring gene mutation. Strong evidence indicates that the genotoxicity of TiO_2NPs is specifically mediated through the generation of oxidative stress (Chen et al., 2014). ROS

production might lead to the formation of oxidative DNA damage, primarily 8-oxo-dG adducts, which are considered mutagenic lesions (Carriere et al., 2017). Hence, the accumulation of these lesions could trigger the cell transformation upon chronic exposures (Vila et al., 2017).

The morphological status of Caco-2 cells can play an important role in genetic damage prevention, as most studies on undifferentiated cells respond to NPs exposure (Gerloff et al., 2012; Zijno et al., 2015; Proquin et al., 2017), opposite to what is observed in differentiated cells (Dorier et al., 2015). This was also indirectly measured by the induction of ROS, observed only in undifferentiated Caco-2 cells (Song et al., 2015). This different behaviour can be explained by the higher uptake of observed in undifferentiated cells when compared to differentiated cells structured as a monolayer, something that has been demonstrated for nanoceria (Vila et al., 2018). In our model, none of the tested TiO_2NPs shapes was able to induce oxidative DNA damage at any of the tested conditions. This would agree with recently reported data in a Caco-2/HT29-MTX model under acute or chronic exposures (Dorier et al., 2017). In spite of this, we were able to detect DNA strand breaks in TiO_2NPs-exposed cells. These DNA breaks could result from the direct interaction of TiO_2NPs with the nucleus detected in our confocal images. General DNA strand breaks were detected readily after 24 h in all TiO_2NPs shapes exposures. Interestingly, the genotoxic damage persisted after 48 h of TiO_2-R treatment, which were the more bio-persistent TiO_2NPs in our intestinal barrier model. As previously mentioned, both Caco-2 and HT29 cell types may present different cell uptake rates and, consequently, different DNA damage. Unfortunately, we were not able to distinguish the most damaged cell type in the pool of Caco-2/HT29 cells, as the techniques used do not permit the identification of a particular cell type. The separation of both populations after the barrier's exposure to NPs by cell sorting methodologies could bring light to this issue.

3.2.6. CONCLUSIONS

The results of this study demonstrate that the three different shapes of TiO_2NPs behave distinctly when dispersed in DMEM cell culture medium. This can affect their agglomeration status and, as a consequence, their toxic effects. The observed toxic effects aggravated by increasing the time of exposure, as a slight but significant reduction in cell viability was seen after 48 h. We have shown that all three NPs were able to cross the mucus layer, the cell barrier model, and reach the basolateral compartment. Both TiO_2 nano-spheres and nano-rods were uptaken easier and faster

than nano-wires, using transcellular transport to cross the barrier model. However, more adverse effects were seen after exposing the barrier to TiO2NPs-W, as the nano-wires clearly impaired and compromised the Caco-2/HT29 barrier's integrity and permeability, using the paracellular transport to cross the barrier. Interactions between the three NPs and the cell nuclei were seen by confocal microscopy, and the consequences were reflected in a significant increase in DNA damage levels. However, we cannot discern if each cell type, Caco-2 and HT29, is equally sensitive to the adverse effects of selected NPs. Further improvements in the model and it's analysis would be useful to solve some unanswered questions regarding the different sensitivities of the cell components of this model.

Acknowledgements

A. Garcia-Rodriguez and L. Vila were funded by postgraduate fellowships from the Universitat Autònoma de Barcelona and the Generalitat de Catalunya, respectively.

Funding

This investigation has been partially supported by the Ministry of Economy and Competition (SAF2015-63519-R), and the EC FP7 NANoREG (Grant Agreement NMP4-LA-2013-310584).

Declaration of interest

The authors report no conflict of interest. The authors alone are responsible for the content and writing of the paper.

3.2.7. REFERENCES

Aminedi R, Wadhwa G, Das N, Pal B. Shape-dependent bactericidal activity of TiO2 for the killing of Gram-negative bacteria *Agrobacterium tumefaciens* under UV torch irradiation. Environ Sci Pollut Res. 2013. 20:6521-6530.

Antunes F, Andrade F, Araújo F, Ferreira D, Sarmento B. Establishment of a triple **co**-culture in vitro cell models to study intestinal absorption of peptide drugs. Eur J Pharm Biopharm. 2013 83(3):427-35

Artursson P, Palm K, Luthman K. Caco-2 monolayers in experimental and theoretical predictions of drug transport. Adv Drug Deliv. Rev. 2001. 46:27-43.

Brun E, Barreau F, Veronesi G, Fayard B, Sorieul S, Chanéac C, Carapito C, Rabilloud T, Mabondzo A, Herlin-Boime N, Carrière M. Titanium dioxide nanoparticle impact and translocation through ex vivo, in vivo and in vitro gut epithelia. Part Fibre Toxicol. 2014 11:13.

Carriere M, Sauvaigo S, Douki T, Ravanat JL. Impact of nanoparticles on DNA repair processes: current knowledge and working hypotheses. Mutagenesis. 2017. 32(1):203-213.

Chen J, Zhou H, Santulli AC, Wong SS. Evaluating cytotoxicity and cellular uptake from the presence of variously processed TiO2 nanostructured morphologies. Chem Res Toxicol. 2010. 23(5):871-9.

Chen T, Yan J, Li Y. Genotoxicity of titanium dioxide nanoparticles. J Food Drug Anal. 2014 22(1):95-104.

Cho WS, Kang BC, Lee JK, Jeong J, Che JH, Seok SH. Comparative absorption, distribution, and excretion of titanium dioxide and zinc oxide nanoparticles after repeated oral administration. Part Fibre Toxicol. 2013. 26;10:9.

Code of Federal Regulations (CFR). Title 21, updated April 1, 2016. https://www.accessdata.fda.gov/scripts/cdrh/cfdocs/cfcfr/CFRSearch.cfm.

Collins AR, Ma AG, Duthie SJ. The kinetics of repair of oxidative DNA damage (strand breaks and oxidised pyrimidines) in human cells. Mutat Res. 1995. 336(1):69-77.

Dorier M, Brun E, Veronesi G, Barreau F, Pernet-Gallay K, Desvergne C, Rabilloud T, Carapito C, Herlin-Boime N, Carrière M. Impact of anatase and rutile titanium dioxide nanoparticles on uptake carriers and efflux pumps in Caco-2 gut epithelial cells. Nanoscale. 2015; 7(16):7352-60.

Dorier M, Béal D, Marie-Desvergne C, Dubosson M, Barreau F, Houdeau E, Herlin-Boime N, Carriere M Continuous in vitro exposure of intestinal epithelial cells to E171 food additive causes oxidative stress, inducing oxidation of DNA bases but no endoplasmic reticulum stress. Nanotoxicology. 2017 11(6):751-761.

European Food Safety Authority (EFSA). Re-evaluation of titanium dioxide (E171) as a food additive. (2016). http://www.efsa.europa.eu/en/efsajournal/pub/4545

Ercan B, Taylor E, Alpaslan E, Webster T. Diameter of titanium nanotubes influences anti-bacterial efficacy. Nanotechnology. 2011. 22:5102–12.

Faust JJ, Masserano BM, Mielke AH, Abraham A, Capco DG. Engineered nanoparticles induced brush border disruption in a human model of the intestinal epithelium. Adv Exp Med Biol. 2014a. 811:55-72.

Faust JJ, Doudrick K, Yang Y, Westerhoff P, Capco DG. Food grade titanium dioxide disrupts intestinal brush border microvilli in vitro independent of sedimentation. Cell Biol Toxicol. 2014b. 30(3):169-88.

García-Rodríguez, A, Vila L, Cortés C, Hernández A, Marcos R. Exploring the usefulness of the complex *in vitro* intestinal epithelial model Caco-2/HT29/Raji-B in nanotoxicology. Food Chem Toxicol, 2018

Gerloff K, Fenoglio I, Carella E, Kolling J, Albrecht C, Boots AW, Förster I, Schins RP. Distinctive toxicity of TiO2 rutile/anatase mixed phase nanoparticles on Caco-2 cells. Chem Res Toxicol. 2012. 25(3):646-55.

Gui S, Zhang Z, Zheng L, Cui Y, Liu X, Li N, Sang X, Sun Q, Gao G, Cheng Z, Cheng J, Wang L, Tang M, Hong F. Molecular mechanism of kidney injury of mice caused by exposure to titanium dioxide nanoparticles. J Hazard Mater. 2011. 195:365-70.

Guo, Z., Martucci, N.J., Moreno-Olivas, F., Tako, E., Mahler, G.J., 2017 Titanium dioxide nanoparticle ingestion alters nutrient absorption in an *in vitro* model of the small intestine. NanoImpact 5, 70-82.

Grassian V, O'Shaughnessy P, Adamcakova-Dodd A, Pettibone J, Thorne P. Inhalation Exposure Study of Titanium Dioxide Nanoparticles with a Primary Particle Size of 2 to 5 nm. Environ Health Perspect. 2007. 115(3): 397–402.

Groschwitz KR, Hogan SP. Intestinal barrier function: molecular regulation and disease pathogenesis. J Allergy Clin Immunol. 2009. 124(1):3-20; quiz 21-2.

Horie M, Sugino S, Kato H, Tabei Y, Nakamura A, Yoshida Y. Does photocatalytic activity of TiO2 nanoparticles correspond to photo-cytotoxicity? Cellular uptake of TiO2 nanoparticles is important in their photo-cytotoxicity. Toxicol Mech Methods. 2016. 26(4):284-94.

IARC: Carbon Black, Titanium Dioxide, and Talc. 2010. In: IARC Monographs on the Evaluation of Carcinogenic Risks to Humans. World Health Organization, Vol. 93 Lyon, France: IARC

Karlsson HL. The comet assay in nanotoxicology research. Anal Bioanal Chem. 2010. 398(2):651-66.

Lesuffleur T, Barbat A, Dussaulx E, Zweibaum A. Growth adaptation to methotrexate of HT-29 human colon carcinoma cells is associated with their ability to differentiate into columnar absorptive and mucus-secreting cells. Cancer Res. 1990. 50(19):6334-43.

Levy E, Mehran M, Seiman E. Caco-2 cells as a model for intestinal lipoprotein synthesis and secretion. FASEB J. 1995. 9:626-635.

Lozoya-Agullo I, Araújo F, González-Álvarez I, Merino-Sanjuán M, González-Álvarez M, Bermejo M, Sarmento B. Usefulness of Caco-2/HT29-MTX and Caco-2/HT29-MTX/Raji B Coculture Models To Predict Intestinal and Colonic Permeability Compared to Caco-2 Monoculture. Mol Pharm. 2017 14(4):1264-1270

Martirosyan A, Schneider YJ. Engineered nanomaterials in food: implications for food safety and consumer health. Int J Environ Res Public Health. 2014. 11(6):5720-50.

Nanogenotox, http://www.nanogenotox.eu/files/PDF/Deliverables/nanogenotox%20deliverable% 203_wp4%20dispersion%20protocol.pdf (2011).

Pal S, Tak Y, Song J. Does the antibacterial activity of silver nanoparticles depend on the shape of the nanoparticle? A study of the Gram-negative bacterium Escherichi coli. Appl Environ Microbiol. 2007. 73:1712–1720.

Park E, Shim H, Lee G, Kim J, Kim D. Comparison of toxicity between the different-type TiO_2 nanowires in vivo and in vitro. Arch Toxicol. 2013. 87(7):1219-30.

Prasad RY, Wallace K, Daniel KM, Tennant AH, Zucker RM, Strickland J, Dreher K, Kligerman AD, Blackman CF, Demarini DM. Effect of treatment media on the agglomeration of titanium dioxide nanoparticles: impact on genotoxicity, cellular interaction, and cell cycle. ACS Nano. 2013. 7(3):1929-42.

Proquin H, Rodríguez-Ibarra C, Moonen CG, Urrutia Ortega IM, Briedé JJ, de Kok TM, van Loveren H, Chirino YI. tanium dioxide food additive (E171) induces ROS formation and genotoxicity: contribution of micro and nano-sized fractions. Mutagenesis. 2017 32(1):139-149.

Raza G, Amjad M, Kaur I, Baalousha M, Lead J, Wen D. Stability and Aggregation Kinetics of Titania Nanomaterials under Environmentally Realistic Conditions. Environ Sci Technol. 2016 50(16):8462-72.

Schneider T, Westermann M, Glei M. In vitro uptake and toxicity studies of metal nanoparticles and metal oxide nanoparticles in human HT29 cells. Arch Toxicol. 2017. 91(11):3517-3527.

Shen H, Qin H, Guo J. Cooperation and metallothionein and zinc transporters for regulating zinc homeostasis in human intestinal Caco-2 cells. Nutr. Res. 2008. 28:406-413.

Song ZM, Chen N, Liu JH, Tang H, Deng X, Xi WS, Han K, Cao A, Liu Y, Wang H. Biological effect of food additive titanium dioxide nanoparticles on intestine: an *in vitro* study .J Appl Toxicol. 2015. 35(10):1169-78.

Vance M, Kuiken T, Vejerano E, McGinnis S, Hochella M Jr, Rejeski D, Hull M. Nanotechnology ithe real world: Redeveloping the nanomaterial consumer produ cts inventory. Beilstein J Nanotechnol. 2015. 6:1769-80.

Vila L, Marcos R, Hernández A. Long-term effects of silver nanoparticles in caco-2 cells. Nanotoxicology. 2017a. 11(6):771-780.

Vila L., A. García-Rodríguez, C. Cortés, A. Velázquez, N. Xamena, A. Sampayo-Reyes, R. Marcos, A. Hernández. Effects of cerium oxide nanoparticles on differentiated/ undiferentiated human intestinal Caco-2 cells, as *in vitro* model of intestinal barrier. *Chemico-Biological Interactions*, acceptat (2018).

Vranic S, Gosens I, Jacobsen NR, Jensen KA, Bokkers B, Kermanizadeh A, Stone V, Baeza-Squiban A, Cassee FR, Tran L, Boland S. Impact of serum as a dispersion agent for in vitro and in vivo toxicological assessments of TiO2 nanoparticles. Arch Toxicol. 2017. 91(1):353-363.

Warheit DB, Sayes CM, Reed KL. Nanoscale and fine zinc oxide particles: can in vitro assays accurately forecast lung hazards following inhalation exposures? Environ Sci Technol. 2009. 43(20):7939-45.

Weir A, Westerhoff P, Fabricius L, Hristovski K, von Goetz N. Titanium dioxide nanoparticles in food and personal care products. Environ. Sci. Technol. 2012. 46(4):2242-2250.

Zhao X, Ze Y, Gao G, Sang X, Li B, Gui S, Sheng L, Sun Q, Cheng J, Cheng Z, Hu R, Wang L, Hong F. Nanosized TiO2-induced reproductive system dysfunction and its mechanism in female mice. PLoS One. 2013. 8(4):e59378.

Zijno A, De Angelis I, De Berardis B, Andreoli C, Russo MT, Pietraforte D, Scorza G, Degan P, Ponti J, Rossi F, Barone F.Different mechanisms are involved in oxidative DNA damage and genotoxicity induction by ZnO and TiO2 nanoparticles in human colon carcinoma cells.Toxicol In Vitro. 2015 29(7):1503-12

3.2.8. SUPPLEMENTARY DATA

Figure S1.

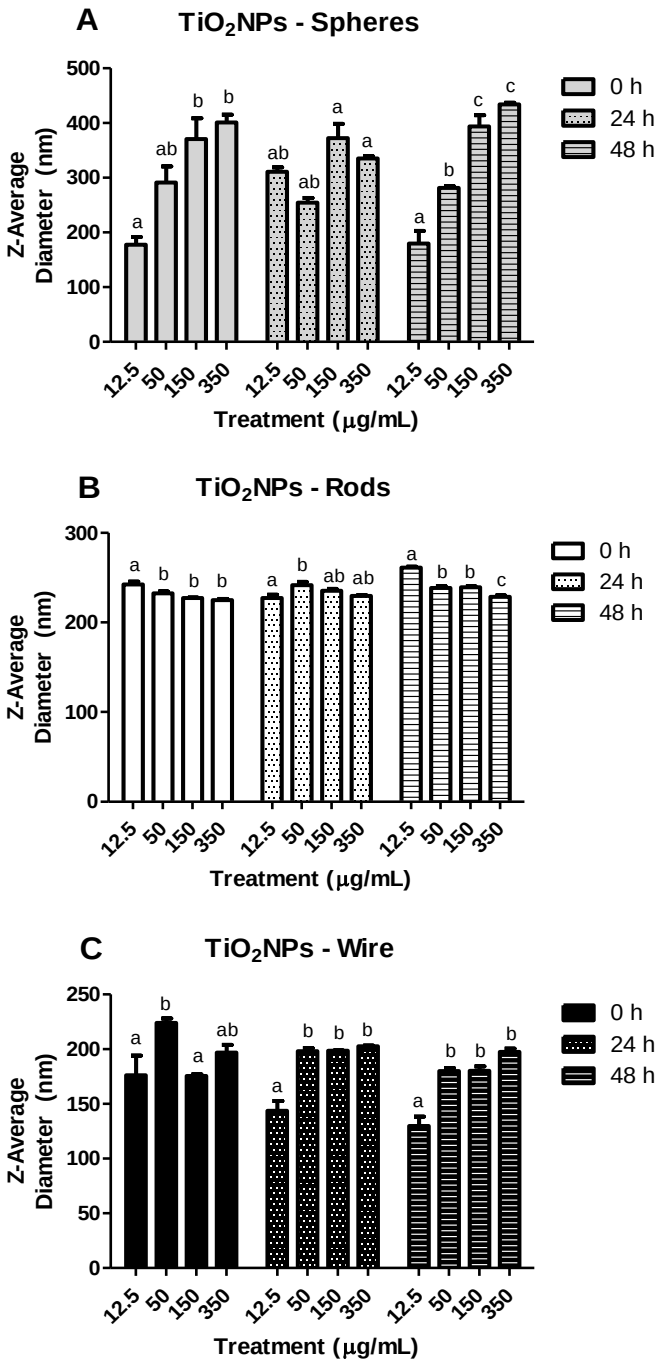

Figure S1. Dynamic light scattering characterization of the NP's over the incubation time. Hydrodynamic size for TiO2NPs-S (A), TiO2NPs-R (B), and TiO2NPs-W (C), suspended in DMEM cell culture medium at concentrations ranging from 12.5 to 350 µg/mL. Bars that do not share any letter are significantly different according to the one-way ANOVA with a Tukey's post-test (P<0.05). Data is represented as mean ± SD.

Figure S2.

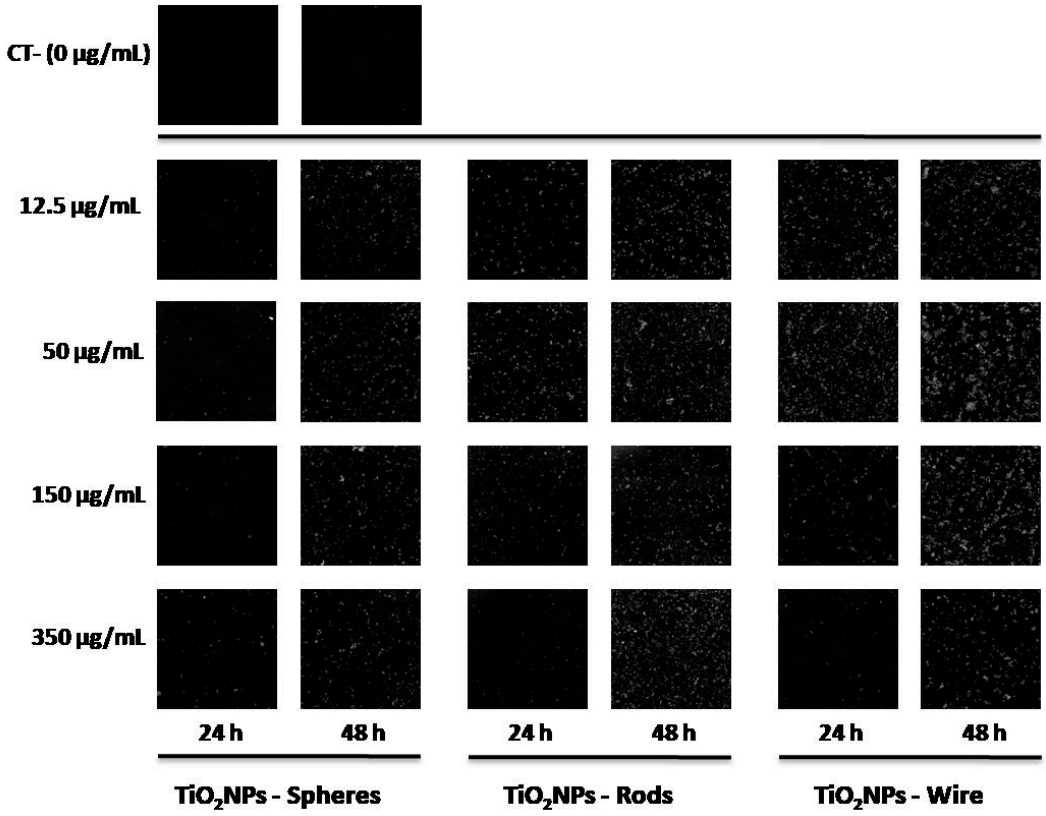

Figure S2. Confocal images of the reflected NPs found in the collected basolateral medium after exposing the Caco-2/HT29 co-culture barrier to 150 µg/mL of TiO2NPs.

Figure S3.

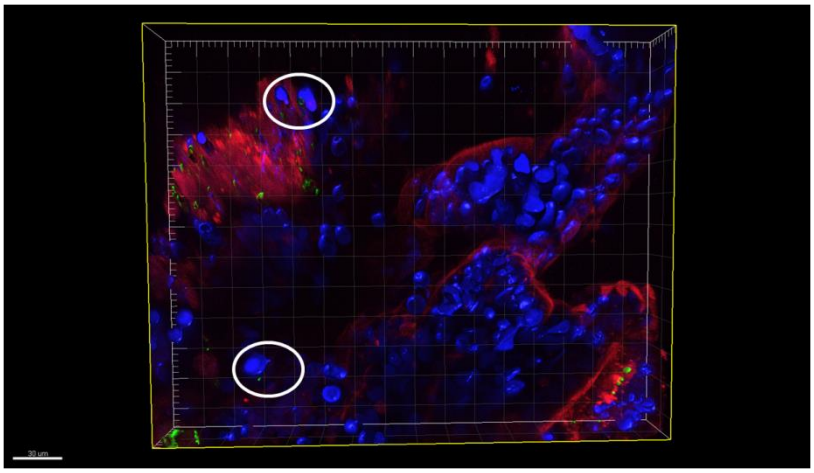

Figure S3. Three-dimensional confocal image of the Caco-2/HT29 co-culture exposed to 150 µg/mL of TiO2NPs-Wires. Cell nuclei (blue) were stained with Hoechst and mucus (red) stained with WGA. NPs were visualized by reflection and marked with a green mask. NPs-cell nucleus interactions are indicated with white arrows. Images were processed with the Imaris 7.2.1 software.

3.3. Chapter 3 (Study 3)

Dysfunctional alterations of the small intestine brush border enzymes IAP, APN and Na^+/K^+ ATPase, caused by metal oxide nanoparticles.

Paper under revision

3.3.1. SUMMARY

In accordance with the International Mention of the present Thesis, a three-month internship was done in the Biomedical Engineering Department at Binghamton University (Binghamton, New York). During this practicum, two different assays analysing the enzyme activity were developed and set-up using the Caco-2/HT29-MTX model: the aminopeptidase-N activity and the Na^+/K^+ ATPase activity assays. Furthermore, the enzyme activity of the intestinal alkaline phosphatase (IAP), aminopeptidase-N (APN) and Na^+/K^+ ATPase was measured using the aforementioned intestinal barrier *in vitro* model for the ENPs risk assessment after an acute exposure of 4 h to low, medium and high doses of SiO_2NPs and TiO_2NPs, at different physiological conditions (non-digested NPs, *in vitro* digested NPs, and digested NPs co-cultured with *Escherichia coli* and *Lactobacillus rhamnosus*). Our results pointed out that after the exposure to SiO_2NPs and TiO_2NPs, the brush border enzymatic activity of IAP and APN were significantly altered, while no differences were detected on Na^+/K^+ ATPase's activity. In some cases, *Escherichia coli* and *Lactobacillus rhamnosus* played a protective role, attenuating the effects of the NPs.

3.3.2. INTRODUCTION

Models of the gastrointestinal tract (GIT) used to evaluate the digestion and absorption of engineered nanomaterials (ENMs) released from food matrices have currently gained attention and popularity due to their advantages. The systemic *in vitro* model Caco-2/HT29-MTX has been demonstrated to be useful for its high-throughput methodology, cost-effectiveness and relatively fast experimental processes compared to *in vivo* models. Moreover, it was reported that Caco-2/HT29-MTX models present good predictability of permeability potential (Lefebvre et al., 2015; Mahler et al., 2009). However, methodologies for the assessment of the effect of digestion on nanomaterials and, as a consequence, their bioavailability in the GIT are poorly developed and require refinement and more knowledge. To date, an association has been made between GIT impairment and malfunctions (such as irritable bowel syndrome and Crohn's disease) and the occurrence of fine particulate matter. These microparticles and nanoparticles coming from food are ingested and subsequently deposited in different tissues and epithelia (Shepherd et al., 1987; Lomer et al., 2002, 2004; Butler et al., 2007). Thus, to understand the mechanism related to these pathologies, several assays for the digestion function and nutrient absorption of nanoparticles by the GIT have been developed using the systemic model Caco-2/HT29-MTX. For example, Fe,

Zn and fatty acid absorption, and alkaline phosphatase enzyme activity, among others assays, were recently reported by Guo et al. for the risk assessment of TiO_2NPs (Mahler et al., 2009; Guo et al., 2017). Guo and co-workers postulated that TiO_2NPs significantly affected Fe and Zn nutrient transport, fatty acid uptake, IAP activity and even tight junction functionality. Therefore, the development of new assays to further extend the current spectrum of methodologies in ENMs risk assessment could enhance the capacity to assess the fate and the repercussion of these NM-based products in the body, which would facilitate their safe and sustainable development in food applications. To this purpose, we sought to expand this battery of assays developing both the aminopeptidase-N (APN) and Na^+/K^+/ATP enzyme assays, which are essential enzymes for the proper GIT function.

Small intestine cells express digestive hydrolases (APN) at high levels. It has been shown that mammalian APN plays a pivotal role in many physiological processes such as pain sensation, blood pressure regulation, tumour angiogenesis and metastasis, immune cell chemotaxis, sperm motility, cell-cell adhesion, and corona-virus entry (Mina-Osorio, 2008; Chen et al., 2012). In the small intestine, APN plays an essential role in the final digestion of peptides generated from hydrolysis of proteins by gastric and pancreatic proteases (Kruse *et al.*, 1988). In addition, Na^+/K^+ ATP is an enzyme that uses the ATP hydrolysis to provide a favourable intracellular sodium ion (Na^+) gradient to promote all Na dependent co-transport processes across the membrane. Depending on the cell type, the activity of the Na^+ pump may be coupled to other crucial functions of the cell such as regulation of cell volume, nerve and muscle excitability, pH regulation, and uptake of carbohydrates, amino acids, and vitamins (Bertorello and Katz, 1993; Gal-Garber et al., 2003). Na^+/K^+ ATP is specifically located on the basolateral membrane of intestinal epithelial cells, where it plays a major role in nutrient transport in the small intestine by transferring K^+ ions into- and Na^+ ions out of the cell. Much of the intestinal nutrient transport is done by Na^+ co-transporters (Gal-Garber *et al.*, 2003; Saha *et al.*, 2015), hence, potential impairments in the activity of these enzymes could affect the absorption of many byproducts derived from the human diet and the stable cell homeostasis, leading to putative human malnutrition or GIT disorders.

The recorded effects of the toxicity of nanoparticles (NPs) upon *in vivo* oral exposure include both the effects on the exposed cells, as well as the effects on the microorganisms that populate the internal surfaces of the body and interact with the aforementioned cells. The importance of these microorganisms, collectively termed as microbiota, in the health of the host has been widely recognized (Mai and Draganov,

2009; Icaza-Chávez, 2013; D'Argenio and Salvatore, 2015; Wang et al., 2017). The intestinal microbiota comprises bacteria, fungi, viruses and archaea, which form a complex ecosystem and live in close relationship with the host. In this study, two of the most common strains of commensal intestinal bacteria, a non-pathogenic *Escherichia coli* strain and *Lactobacillus rhamnosus,* were used to further understand the role played by the intestinal microbiota on a putative NP exposure. *L. rhamnosus* is one of the most widely used probiotic strain, its positive health effects are well documented including the prevention and treatment of gastrointestinal infections and diarrhoea, the stimulation of immune responses promoted by vaccination and the prevention of certain allergic symptoms (Segers and Lebeer, 2014). Meanwhile, *E. coli* bacteria primarily live in the lower intestinal tract of mammals, where it resides as a beneficial component of the commensal microbiota. Although it is well-known that most *E. coli* are harmless and are actually an important part of a healthy human intestinal tract, specific strains of pathotypes have the potential to cause a wide spectrum of intestinal diseases (Alteri and Mobley, 2012). Thereby, the described antimicrobial properties of Ag- and ZnO-NPs (commonly used in food packaging) could further influence the interaction between the microbiota and the host leading to microbial imbalance, which may promote susceptibility to diseases (Fröhlich and Fröhlich, 2016). Williams and colleagues detected size- and dose-dependent changes in the ileal-mucosal microbial populations of rats after oral ingestion of 10, 75 and 110 nm AgNPs. Furthermore, Liu et al. postulated that the antibacterial activity of ZnONP against *E. coli* may distort and damage the bacterial cell membrane, resulting in the leakage of intracellular contents and eventually the death of the cells (Liu *et al.*, 2009; Williams *et al.*, 2015). However, little is known about the effect of the well-known food additives TiO_2- and SiO_2NPs on the intestinal microbiota niche and its repercussion on the health and function of the GIT.

Food-grade silicon dioxide (SiO_2) or amorphous silica (coded E551) and food-grade titanium dioxide (TiO_2) coded E171 have been found to contain particles in the nano-size range (Peters et al., 2012; Weir et al., 2012; Yang et al., 2016). Both NPs are currently used to enhance the taste and texture of rich foods without adding calories, preserve food colour and durability, improve handling, and carry fragrances of flavours (Dekkers et al., 2011; Jovanovi, 2014; Contado et al., 2015). In addition, TiO_2 and SiO_2 –based NMs are reported to be the most manufactured and produced NMs worldwide, ranging from 10.000 to 100.000 tons/year (Bekker et al., 2013; Piccinno et al., 2012). Thus, human GIT exposure to these NPs can occur in several ways as nano-food ingredients, additives or supplements from food packaging, and contact materials that

migrate into food can be ingested. Due to the prevalence of TiO_2NPs and SiO_2NPs, human ingestion is nearly unavoidable, which highlights the importance of studying their effects on the brush border enzymes after NPs ingestion.

The overall goal of this study is to estimate whether the physiological status of the NPs influences the NPs toxicity, as well as the presence of microbiota. To this purpose, we compared the effects of non-digested NPs (TiO_2NPs and SiO_2NPs), digested nanoparticles and digested nanoparticles co-cultured with *E. coli* or *L. rhamnosus*. The relative sensitivity of the Caco-2/HT29-MTX barrier to NPs exposure was analysed by measuring its functionality in three enzymatic activity assays: intestinal alkaline phosphatase assay, aminopeptidase-N assay and Na^+/K^+ ATPase.

3.3.3. MATERIAL AND METHODS

30 nm SiO_2NPs and 30 nm TiO_2NPs were purchased by US Research Nanomaterials, Inc. (Houston, TX). All culture flasks, plates, tubes, and pipette tips used for culturing cells were purchased from Corning (Corning, NY). All other chemicals, enzymes, and hormones were purchased from Sigma Aldrich (St. Louis, MO) unless otherwise stated. All reagents were prepared in 18 MΩ water.

Nanoparticles dose calculation and dispersion

In vitro doses of NPs were formulated to represent potential real-life exposure. Hence, the chosen concentrations of TiO_2NPs and SiO_2NPs were the same as used in previous studies, which took into account the total intestinal surface area (~2×10^6 cm^2) (DeSesso and Jacobson, 2001) and the daily intake of nano-TiO_2 (~10^{14}–10^{13} NPs/meal) (Lomer et al., 2002) and nano-SiO_2 (~35 mg/individual/day) (Lomer *et al.*, 2004; Guo *et al.*, 2017). The amount of NPs used in this study is summarized in Table 1. Regarding NPs dispersion, NP powder was weighed in a polystyrene weighing dish, and dispersed in sterile 18 MΩ water. Solutions were mixed uniformly in a sterile tube using a Thermolyne Mixer (Maxi Mix II, Type 37600) for 1 min, and then serially diluted in DMEM cell culture medium to the concentrations shown in Table 1. NPs solutions were placed in a sonicator (VWR® symphony™ Ultrasonic Cleaners, RF-48 W) for 30 min to break down NPs agglomerates.

Table 2. NPs concentration used to expose the Caco-2/HT29-MTX model.

Nanoparticles	Doses	High	Medium	Low
TiO_2NPs	mg/mL	1.4×10^{-4}	1.4×10^{-6}	1.4×10^{-8}
	Particle/mL	2.3×10^{9}	2.3×10^{7}	2.3×10^{5}
SiO_2NPs	mg/mL	2.0×10^{-3}	2.0×10^{-5}	2.0×10^{-7}
	Particle/mL	5.4×10^{10}	5.4×10^{8}	2.0×10^{6}

In vitro NPs digestion

In order to simulate more realistic conditions of NPs ingestion, both metal-based NPs were subjected to a well-established *in vitro* digestion process that contains the approximate concentrations of salts and enzymes present in the stomach and duodenum (Mahler et al., 2009). Briefly, the NPs were suspended in 20 mL of a 140 mM NaCl, 5 mM KCl, 0.05 mM CaCl solution. The pH was then adjusted to 2 using HCl and then the enzyme pepsin was added. The suspensions were placed on a rocker for 1 h at speed 7 inside an incubator at 37 ºC with 0.5% CO_2. Following, the solutions were taken out and the pH was adjusted to 5.5-6 using $NaHCO_3$. Then 5.25 mL of pancreatic and bile solution was added and the pH was then adjusted to 6.9-7. After this, the volume was adjusted to 30 mL using a 140 mM NaCl, 5 mM KCl solution and samples were referred to as “digested.”

Cell culture

The Caco-2 cell line was obtained from the American Type Culture Collection (Manassas, VA, USA) at passage 17 and used in experiments at passage 30-45. The HT29-MTX cell line was provided by Dr. Thécla Lesuffleur of INSERM U560 in Lille, France, at passage 11 and used in experiments at passage 18-33. Cells were seeded at a ratio of 75:25 Caco-2 to HT29-MTX, respectively (Mahler et al., 2009). Ninety-six-well plates (Corning) were coated with 8 $\mu g/cm^2$ rat tail type I collagen and cell monolayers were seeded at a density of 50,000 cells/cm^2. The monolayers were maintained in Dulbecco's Modified Eagle Medium (DMEM, Gibco® Thermo Fisher Scientific, Waltham, MA USA) with 10% (v/v) heat-inactivated fetal bovine serum (HI-FBS, Gibco® Thermo Fisher Scientific, Waltham, MA USA), which was changed every other day. All experiments were performed after a cell growth period of 2 weeks. Monolayers were

exposed to 100 µL of NP suspension in DMEM or in the previously described *in vitro* digestion solution at the desired concentration (high, medium and low) for 4 h before additional assays were performed.

According to previous studies (unpublished data), the Caco-2/HT29-MTX monolayer was co-exposed to NPs and bacteria as following: 5,000 colony forming units (CFU) of *E. coli* and *L. rhamnosus* (separately) were seeded to each transwell after the monolayer's differentiation period of 2 weeks. Readily, NPs were plated as previously mentioned and treatments were carried out for 4 h.

Enzymatic activity assays

i) Intestinal Alkaline Phosphatase

Co-cultures were seeded into 96 well plates and exposed to all NPs concentrations and treatments for 4 h. Following exposure, cells were rinsed twice with PBS and then 100 µL of PBS were added to each well. The plates were shut with tape and then sonicated for 5 min at room temperature using a bath sonicator. The cells were scraped from the bottom of the well by pipetting up and down. p-nitrophenyl phosphate (pNPP) solution was made by dissolving one Tris Buffer tablet and one pNPP tablet (Sigma Aldrich, St. Louis MO) in 5 mL of 18 MΩ water. IAP hydrolyzes pNPP to p-nitrophenol, which turns bright yellow based on the concentration of p-nitrophenol. 25 µL of cell lysate solution from each well was added to a new 96-well plate-reader with a multichannel micropipette. Eighty-five µL of the pNPP solution was then added to the wells and the plate was wrapped in aluminium foil and incubated at room temperature for 1 h. The absorbance was read on a plate reader at 405 nm to measure the concentration of p-nitrophenol.

ii) Aminopeptidase-N

The aminopeptidase-N *in situ* assay was adapted for Caco-2/HT29-MTX co-cultures from the study of Ferruzza and co-workers (Ferruzza et al., 2012). Briefly, co-cultures were seeded into 96 well plates and exposed to all NP concentrations and treatments for 4 h. Following exposure, cells were rinsed twice with PBS and then 50 µL of PBS were added to each well. The plates were shut with tape and then sonicated for 5 min at room temperature. The cells were scraped from the bottom of the well by pipetting up and down. An L-leucine-p-Nitroanilide (LpNA) stock solution was made by diluting LpNA (Sigma-Aldrich, Saint Lous MO) powder at 50 mg/mL in absolute ethanol. Next, a

dilution of LpNA at 2 mM was made in collection buffer (30 volumes of PBS 1x pH 7.0 and 1 volume of 10 mM Tris-HCl/150 mM NaCl pH 8.0) to be further mixed with the cell lysate. APN hydrolyzes LpNA to the coloured product p-nitroanilide, which turns bright yellow based on the concentration of p-nitroanilide. Then, 50 µL of LpNA solution at 2 mM were added to each lysate-containing well. The plate was wrapped in aluminium foil and placed in the incubator at 37 ºC for 1 h. The absorbance was read in the same culture plate at 405 nm to measure the concentration of p-nitroanilide. A standard curve was prepared with the product p-nitroanilide (Sigma-Aldrich, St. Lous MO) diluted in absolute ethanol.

iii) Na^+/K^+ ATPase

The Na^+/K^+ ATPase *in situ* assay was adapted for Caco-2/HT29-MTX co-cultures from the studies of Sarkar and El-Zein et al., where the enzymatic activity of Na^+/K^+ ATPase is determined by calculating the difference of inorganic phosphate (PO^{-3}_4) liberated in the presence and absence of its enzyme activators (Na^+, K^+ and Mg^{++}) (Sarkar, 2002; El-Zein et al., 2015). Briefly, the ninety-six-well plates were divided in to equal parts. Half of the plate was exposed to the aforementioned NPs treatments, and the other part to the same NPs treatments (Figure 1). Following the exposure, cells were rinsed twice with sterile 18 MΩ water and then 35 µL of water were added to each well. Plates were carefully shut with tape, and then sonicated for 5 min at room temperature, avoiding possible phosphates contaminants such as PBS. The cells were scraped from the bottom of the well and homogenated by pipetting up and down. Two ATP (Sighma-Aldrich, Saint Lous MO) buffers at 0.1 mM were prepared:

i) 0.1 mM of ATP diluted in sterile 18 MΩ water (buffer 1),
ii) and 0.1 mM of ATP diluted in activator buffer (19.6 mM KCl/ 121.52 mM NaCl/ 3.92 mM MgCl) (buffer 2).

Thirty µL of buffer 1 was added to half of the plate and 30 µL of buffer 2 to the other half (Figure 1). Then, plates were incubated for 45 min at 37 ºC. The reaction was stopped by adding 50 µL of Malachite Green Reagent from the Phosphate Assay Kit® (Sigma-Aldrich, St. Louis MO) to each well. Plates were covered with aluminium foil and placed at room temperature for 30 min for colour development. The absorbance was read in the same 96 culture-plate to measure the concentration of PO^{-3}_4 at 620 nm using a plate reader. The standard curve was prepared diluting the PO^{-3}_4 premix solution of the Phosphate Assay Kit® (Sigma-Aldrich, St. Louis MO). Results were

calculated as following: µM of PO^{-3}_4/mg of protein (Buffer 2) - µM of PO^{-3}_4/mg of protein (Buffer 1) = µM of PO^{-3}_4/mg of protein resulted of the ATPase activity.

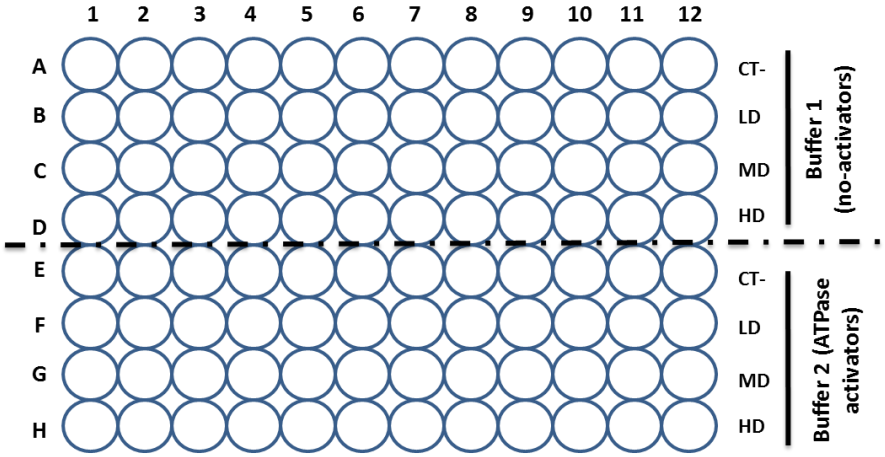

Figure 1. Experimental design of the Na^+/K^+ ATPase assay, representing the treatments carried out;(CT-) negative control, (LD) low doses, (MD) medium doses and (HD) high doses. Treatments were done in duplicates in order to mix the same treatments with both buffer 1 and buffer 2.

Statistical analysis

Four replicates were done for each treatment in at least 3 independent experiments (n=12). Results are expressed as mean ± standard error. One-way ANOVA with Tukey's post-test was performed to compare differences between means. Data were analyzed with GraphPad Prism version 5.00 for Windows (GraphPad Software, San Diego California USA, www.graphpad.com). Differences between means were considered significant at $P<0.05$.

3.3.4. RESULTS

Intestinal Alkaline Phosphatase activity

Important protective roles of IAP -including regulation of intestinal pH, absorption of lipids and detoxification of some endogenous substances, among other properties- have been recently reviewed (Lallès, 2014). Also, it has been found that IAP activity is actively modulated by numerous nutritional factors. Here, we have seen how SiO_2NPs and TiO_2NPs significantly alter the brush border's membrane enzymatic functionality. Figure 2A shows that medium and high exposures of non-digested SiO_2NPs significantly increased IAP activity. Moreover, when SiO_2NPs were previously digested *in vitro*, IAP activity was significantly increased (even more than with non-digested

SiO_2NPs) after low and medium SiO_2NPs exposure (Figure 2C). The same results were obtained in the presence of *E. coli* in the co-culture, as the medium dose (the more physiologically relevant) of SiO_2NPs increased the amount of p-nitrophenol/mg of protein, suggesting an increment of the enzymatic activity. Interestingly, when the barrier was co-cultured with the commensal microbiota *L. rhamnosus,* the the brush border alteration was attenuated and no differences in IAP activity were seen between treatments (Figure 2E).

Focusing our attention on the TiO_2NPs' effects, similar results were obtained. As Figures 2A and 2D shows, the medium dose of TiO_2NPs also altered IAP activity significantly, while digested TiO_2NPs even increased it. In this case, both *E. coli* and *L. rhamnosus* alleviated the TiO_2NPs' effects and no alterations were seen in enzymatic activity (Figure 2F).

Aminopeptidase-N activity

As previously mentioned, APN is a brush border enzyme in the small intestine in charge of the final digestion of peptides coming from the human diet. Thus, APN plays an essential role in food processing and its activity alteration can provoke an intestinal functional impairment. As Figure 3 shows, non-digested SiO_2NPs (Figure 3A) and digested SiO_2NPs (Figure 3C) are able to significantly alter APN activity after a 4 h of exposure of the Caco-2/HT29-MTX model. However, neither the presence of *E. coli* nor *L. rhamnosus* were able to attenuate the SiO_2NPs effects (Figure 3E). Regarding TiO_2NPs, no significant effects were detected after the exposure of the Caco-2/HT29-MTX model to non-digested TiO_2NPs (Figure 3B), while APN activity was significantly increased after exposure to low, medium and high doses of digested TiO_2NPs (Figure 3D). As with SiO_2NPs, this time the presence of both microbial strains was not able to stabilize APN activity, which was also significantly augmented (Figure 3F).

Na^+/K^+ ATPase activity

Measurements of Na^+/K^+ ATPase function (Figure 4) show that any of the SiO_2NPs exposures tested significantly affected the enzymatic activity compared to their respective negative controls. The same was seen after the exposure of the *in vitro* barrier to non-digested TiO_2NPs (Figure 4B). Digested TiO_2NPs (Figure 4D) and digested TiO2NPs co-cultured with *L. rhamnosus* (Figure 4F) showed no-alterations in the Na^+/K^+ ATPase activity. Only the high dose of digested Na^+/K^+

ATPase co-cultured with *E. coli* significantly down-regulated the sodium bomb enzyme activity (Figure 3F).

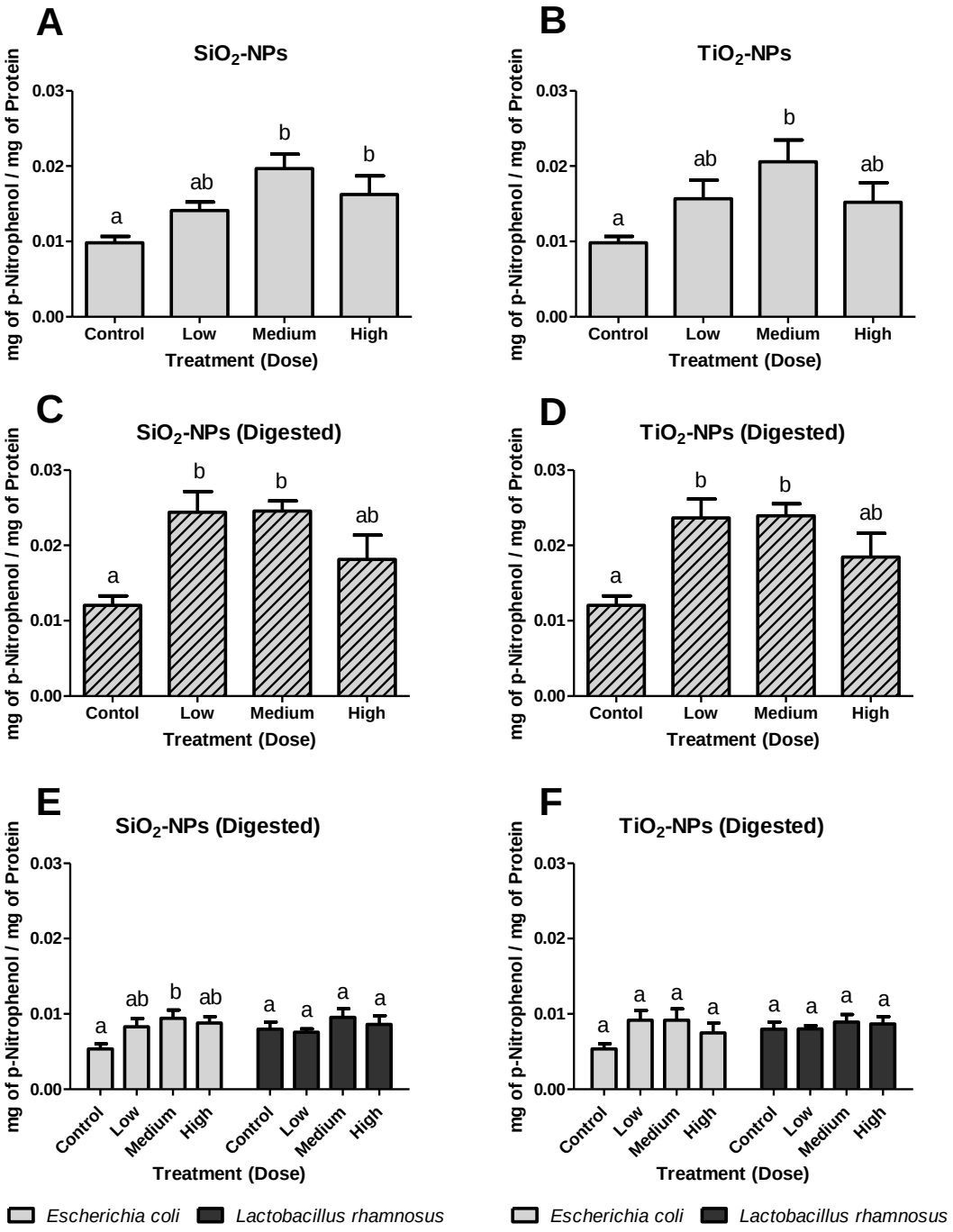

Figure 2. Intestinal alkaline phosphatase activity. (A) Non-digested SiO_2NPs, (B) non-digested TiO_2NPs, (C) *in vitro* digested SiO_2NPs, (D) *in vitro* digested TiO_2NPs. Caco-2/HT29-MTX model co-cultured with *Escherichia coli* and *Lactobacillus rhamnosus* and exposed to (E) *in vitro* digested SiO_2NPs and (F) *in vitro* digested TiO_2NPs. Bars that do not share any letter are significantly different according to the one-way ANOVA with a Tukey's post-test (P<0.05).

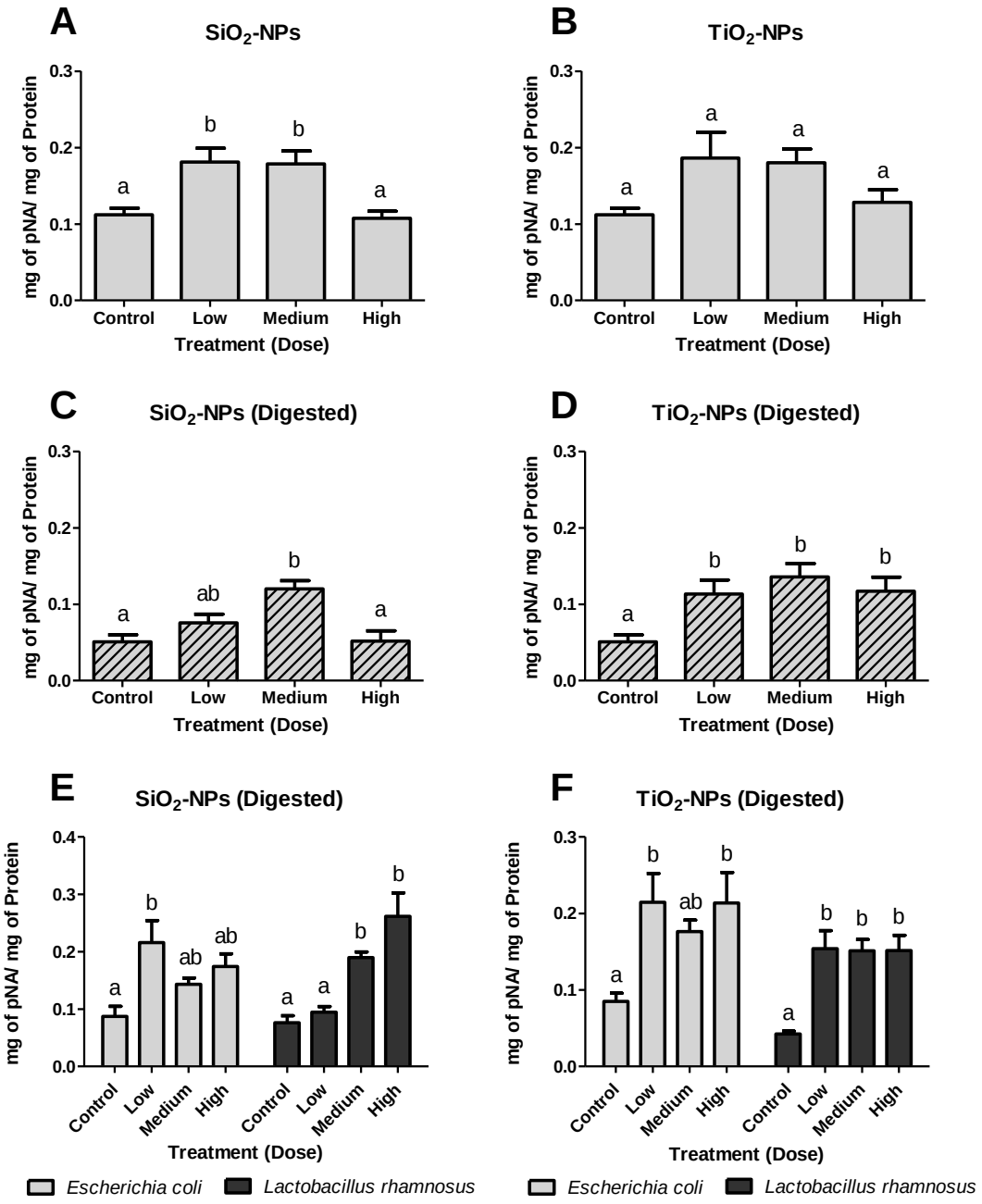

Figure 3. Aminopeptidase-N activity. (A) Non-digested SiO_2NPs, (B) non-digested TiO_2NPs, (C) *in vitro* digested SiO_2NPs, (D) *in vitro* digested TiO_2NPs. Caco-2/HT29-MTX model co-cultured with *Escherichi coli* and *Lactobacillus rhamnosus* and exposed to (E) *in vitro* digested SiO_2NPs and (F) *in vitro* digested TiO_2NPs. Bars that do not share any letter are significantly different according to a one-way ANOVA with a Tukey's post-test (P<0.05).

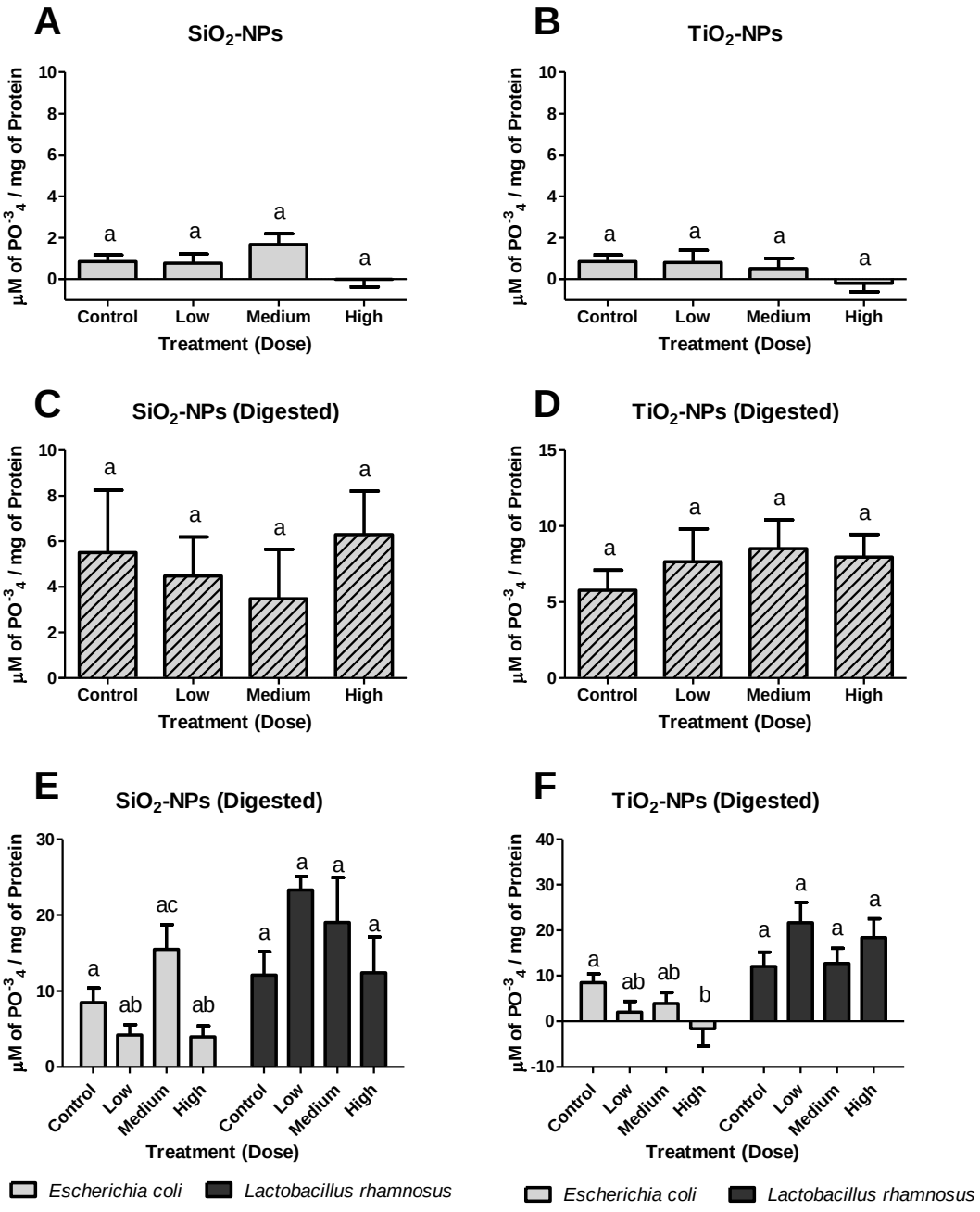

Figure 4. Na+/K+/ATPasa activity. (A) Non-digested SiO_2NPs, (B) non-digested TiO_2NPs, (C) *in vitro* digested SiO_2NPs, (D) *in vitro* digested TiO_2NPs. Caco-2/HT29-MTX model co-cultured with *Escherichia coli* and *Lactobacillus rhamnosus* and exposed to (E) *in vitro* digested SiO_2NPs and (F) *in vitro* digested TiO_2NPs. Bars that do not share any letter are significantly different according to a one-way ANOVA with a Tukey's post-test (P<0.05).

3.3.5. DISCUSSION

As demonstrated in our previous studies, the characterization of both SiO_2NPs and TiO_2NPs suspended in DMEM-10% Hi-FBS presented a good NPs dispersion compared to NPs suspensions with DMEM, suggesting an essential role of the FBS in the NPs dispersion and stability (Vranic *et al.*, 2017). The mean NP hydrodynamic diameter of the TiO_2NPs and SiO_2NPs measured by DLS was 16-20 nm (Guo *et al.*, 2017) and 33-35 nm (Guo *et al.*, 2018), respectively. Since the small size of NPs corresponds to larger specific surface area, NPs have greater reactivity and are predicted to undergo hazardous biologic activities compared with larger particles (Oberdörster et al., 2005). Meanwhile, other studies have suggested that the impact of pH on particle agglomeration during the *in vitro* NPs digestion could lead to important changes on the physicochemical properties of the NPs and their toxicological effects.

The study of Li et al. (2017) showed a moderate increase in TiO_2NPs size with decreasing pH, postulating that the particles may have undergone further agglomeration or structural rearrangement under more acidic pH conditions (Li *et al.*, 2017). Moreover, Peters and co-workers explained that the loss of nano-sized silica and thereby larger silica agglomerations in the gastric stage can be either attributed to an effect of low pH combined with high electrolyte concentrations in the gastric digestion stage (Peters *et al.*, 2012).

Thus, high NPs' hydrodynamic diameter could avoid the formation of endocytic vesicles (approximately 50-150 nm of diameter) as a mechanism of cell uptake and, therefore, likely sequester both TiO_2NPs and SiO_2NPs in the apical surface of the cell monolayers (Liang *et al.*, 2010). Our ICP-MS analysis of the co-culture and basolateral medium suggested that neither SiO_2NPs nor TiO_2NPs were able to undergo translocation or cross through the Caco-2/HT29-MTX monolayers, as no NP was detected, implying a NP bio-persistence in the membrane surface of the epithelium (Guo et al., 2017; Guo et al., 2018). This could trigger a continuous mechanical friction between NPs and the cell's brush border, which could lead to severe structural injuries.

The apical brush border surface of the intestinal epithelial cells (where all the digestive enzymes are found), is formed by a complex cytoskeletal apparatus and a high ordered array of actin filaments and associated proteins (Mooseker, 1985). Several studies have reported the disruption of the normal microvilli organization after the exposure to diversely-sized NPs (e.g 26, 53, 76 and 96 nm hematite NPs) (Zhang et al., 2010; Kalive et al., 2012). Interestingly, *in vivo* chronic exposures to 30 nm AgNPs administered orally (5, 10, 15 and 20 mg/kg body weight) triggered the

epithelial cell microvilli damage as well as the impairment of the intestinal glands, and a significant decrease in the body weight of mice (Shahare et al., 2013). These authors hypothesized that loss of microvilli reduced absorptive capacity of the intestinal epithelium, hence the weight loss. Focusing on food-grade SiO_2 and TiO_2, various studies have also reported adverse effects when treating differentiated Caco-2 cells. Faust et al. (2014) indicated that ~25% of the food-grade TiO_2 are in the nano-scale and their exposure (24 h) resulted in the loss of microvilli from Caco-2 cell system due to a biological response. Moreover, doses above 10 µg/mL TiO_2NPs contributed to alterations in both microvilli organization on the apical surface of the epithelium and in the intracellular free calcium of Caco-2 cells (Koeneman *et al.*, 2010). The authors reported these epithelium impairments following a 10-day treatment. Also, Guo and colleges demonstrated how both acute (4 h) and chronic (5 days) nanoparticle exposure to realistic doses of 30 nm TiO_2NPs resulted in a decrease in absorptive cell microvilli and alterations in nutrients transporters using the Caco-2/HT29-MTX model (e.g. Fe, Zn, etc.) (Guo *et al.*, 2017). This lead us to think that the protective role of the mucus shed can be impaired due to NPs exposure. Food-grade SiO_2NPs resulted in a net loss and disorganization of brush border microvilli. Yang et al. proved that the total number of microvilli on the surface showed a 43% loss of microvilli (MV) to a value of 24±8 MV/µm^2 (MV/µm^2; mean ± SD) compared to untreated control specimens (42 ± 8 MV/µm^2) (Yang *et al.*, 2016).

The intrinsic stability and chemical properties of these engineered nanomaterials (ENMs) determine significant differences in cytotoxicity and antimicrobial activities. Analysis of published data of metallic and metal oxide NPs suggests that oxygen is often a prerequisite for the generation of reactive oxygen species (ROS) for AgNPs and nano zero valent iron (NZVI), while illumination is necessary for TiO_2NPs and ZnONPs photo-activation to trigger ROS generation (Anas et al., 2008; Yang et al., 2013; De J. Wang and Fan 2014; Matteis et al., 2016) . Therefore, the vehicle or medium whereby NPs are dissolved and transported are also important and need to be addressed to further understand the fate of NPs. In this study, we demonstrate that both types of food-grade NPs, TiO_2 and SiO_2, are able to cause alterations in the brush border IAP and APN activity, both in DMEM-10%Hi-FBS and after *in vitro* digestion. These results are in agreement with those form Guo et al. (2017). Nonetheless, the Na^+/K^+ ATPase activity was neither altered nor decreased after exposure to both TiO_2NPs and SiO_2NPs at any physiological condition (non- digested NPs, digested NPs and digested NPs co-cultured with commensal microbiota). This could be explained by the fact that the Na^+/K^+ ATPase enzyme is localized at the

basolateral membrane of intestinal epithelial cells (Saha *et al.*, 2015), which would complicate their interaction with those NPs retained in the apical part of the Caco-2/HT29-MTX. Down-regulation of Na^+/K^+ ATPase activity has been postulated to alter the absorption *via* Na-solute co-transporters in human inflammatory bowel disease (IBD) (Wisel and Rajendren, 1997). Thus, any potential ability of ingested NPs to impair tight junctions and reach the basolateral compartment of the cells could have detrimental effects on the proper intestinal function.

The effects registered on the toxicity of nanoparticles (NPs) upon *in vivo* oral exposure intrinsically include the protective action of the microorganisms that populate the internal surfaces of the body. The intestinal tract contains a huge niche for the co-existence of fungi, virus and bacteria with commensal purposes (Wang et al., 2017). Recently, numerous studies have shown that intestinal microbiota are very important for the modulation of human health and disease (Schulz et al., 2014; Chassaing et al., 2015). It has been shown that in the steady state, commensal microorganisms have a symbiotic relationship with the host and possess critical and distinct functions, including immunomodulation, protection, nutrition, and metabolism (Marchesi *et al.*, 2016; Schirmer *et al.*, 2016). It has been reported that the imbalance of intestinal flora could be induced by various environmental factors, such as environmental contaminants, particulate matter and antibiotics (Kish *et al.*, 2013; Lu *et al.*, 2014; Williams *et al.*, 2015). Chen et al. (2017) explored the possible impacts of orally administrated TiO_2NPs, SiO_2NPs and AgNPs on gut microbiota composition and colitis induction in mice. After a chronic exposure of 7 days to TiO_2NPs and SiO_2NPs doses similar to human dietary intake, no overall toxicity was recorded for both NPs other than increased pro-inflammatory cytokine levels (IL-1β, IL-6 and TNF-α) in the colon of mice that ingested SiO_2NPs. Also, they pointed out that no disturbance of the gut microbiota was found in mice that ingested TiO_2NPs, while those that ingested SiO_2NPs increased microbial species richness and diversity within the intestinal tract, in particular of the genus *Lactobacillus* (Chen et al., 2017). Similar results have been recently obtained by Dudefoi et al. and Waller et al. as no major effect on human gut microbiota was documented when testing different sources of food-grade TiO_2NPs (Dudefoi et al., 2017; Waller et al., 2017). On the other hand, acute oral exposure following medical oral application of AgNPs, were able to induce colitis-like symptoms, disrupt microvilli and tight junctions, up-regulate pro-inflammatory cytokines, and reduce the probiotic bacteria *Lactobacillus,* among other pathological effects, in mice (Chen et al., 2017). In agreement with that, our co-culturing of Caco-2/HT29-MTX monolayer with both commensal strains did not alleviate the effects of the acute exposure to realistic

concentrations of SiO_2NPs, with the exception of IAP activity, which was attenuated in the presence of the probiotic *L. rhamnosus*. Thereby, our results lead us to hypothesize that the probiotic *L. rhamnosus* plays a more protective role than the endogenous intestine commensal, *E. coli*. However, it seems that this protective role is only partial, as *L. rhamnosus* only mitigated the adverse effects of both TiO_2NPs and SiO_2NPs over the IAP activity but not over APN activity. Supplemental toxicity assays on both bacterial strains exposed to both NPs conditions (digested and non-digested) are currently being developed for the proper analysis of the results. Moreover, given the likelihood of human oral uptake of food-grade containing nano-sized particles, further experiments of chronic NPs exposures are needed to comprehend the actual effects on the real GIT environment.

3.3.6. CONCLUSIONS

In this study, we used *in vitro* models to explore the possible impact of oral exposure of TiO_2NPs and SiO_2NPs on the intestinal epithelium at a dose relevant to human dietary intake and relative to the intestinal surface area (~2×10^6 cm^2). Our data showed that both TiO_2NPs and SiO_2NPs, under different physiological conditions -NPs suspended in DMEM-10%Hi-FBS and NPs previously *in vitro* digested-, were able to alter IAP and APN enzymatic activity, but not the activity of Na^+/K^+ ATPase. The study highlights the importance of the gut microbiota, which are closely associated with the biological responses following oral exposure to NPs. The probiotic bacteria *L. rhamnosus* seems to play an essential role in attenuating the adverse NPs' effects. Nonetheless, the impact of oral exposure of NPs on humans needs to be further investigated and the physiological status of such NPs needs deeper characterization. This study also emphaticizes the usefulness of the systemic model, Caco-2/HT2-MTX, as a high throughput assay and as a multi-parametric tool.

3.3.7. REFERENCES

Alteri CJ, Mobley HL. (2012). *Escherichia coli* physiology and metabolism dictates to diverse host microenvironments. *Current Opinion in Microbiology*, *15*, 3-9.

Anas A, Akita H, Harashima H, Itoh T, Ishikawa M, Biju V. (2008). Photosensitized breakage and damage of DNA by CdSe-ZnS Quantum Dots. *Journal of Physical Chemistry*, *112*, 10005-10011.

Bekker C, Brouwer DH, Tielemans E, Pronk A. (2013). Industrial production and

professional application of manufactured nanomaterials-enabled end products in Dutch industries: Potential for exposure. *The Annals of Occupational Hygiene*, *57*, 314-327.

Bertorello AM, Katz AI. (1993). Short-term regulation of renal Na-K-ATPase activity: physiological relevance and cellular mechanisms. *American Journal of Physiology-Renal Physiology*, *265*, F743–F755.

Butler M, Boyle JJ, Powell JJ, Playford RJ, Ghosh S. (2007). Dietary microparticles implicated in Crohn's disease can impair macrophage phagocytic activity and act as adjuvants in the presence of bacterial stimuli. *Inflammation Research*, *56*, 353-361.

Chassaing B, Koren O, Goodrich JK, Poole AC, Srinivasan S, Ley RE, Gewirtz AT. (2015). Dietary emulsifiers impact the mouse gut microbiota promoting colitis and metabolic syndrome. *Nature*, *519*, 92-96.

Chen H, Zhao R, Wang B, Cai C, Zheng L, Wang, H., Feng, W. (2017). The effects of orally administered Ag, TiO_2 and SiO_2 nanoparticles on gut microbiota composition and colitis induction in mice. *NanoImpact*, *8*, 80-88.

Chen L, Lin Y-L, Peng G, Li F. (2012). Structural basis for multifunctional roles of mammalian aminopeptidase N. *Proceedings of the National Academy of Sciences*, *109*, 17966-17971.

Contado C, Mejia J, Lozano O, Piret J.P, Dumortier E, Toussaint O, Lucas S. (2015). Physicochemical and toxicological evaluation of silica nanoparticles suitable for food and consumer products collected by following the EC recommendation. *Analytical and Bioanalytical Chemistry*, *408*, 271-286.

D'Argenio V, Salvatore F. (2015). The role of the gut microbiome in the healthy adult status. *Clinica Chimica Acta*, *451*, 97-102.

De Matteis V, Cascione M, Brunetti V, Toma CC, Rinaldi R. (2016). Toxicity assessment of anatase and rutile titanium dioxide nanoparticles: The role of degradation in different pH conditions and light exposure. *Toxicology in Vitro*, *37*, 201-210.

Dekkers S, Krystek P, Peters RJB, Lankveld DPK, Bokkers BGH, Van Hoeven-Arentzen PH, Oomen AG. (2011). Presence and risks of nanosilica in food products. *Nanotoxicology*, *5*, 393-405.

DeSesso JM, Jacobson CF. (2001). Anatomical and physiological parameters affecting gastrointestinal absorption in humans and rats. *Food and Chemical Toxicology*, *39*, 209-228.

Dudefoi W, Moniz K, Allen-Vercoe E, Ropers M-H, Walker VK. (2017). Impact of food grade and nano-TiO_2 particles on a human intestinal community. *Food and Chemical Toxicology*, *106*, 242-249.

El-Zein O, Usta J, El Moussawi L, Kreydiyyeh SI. (2015). Leptin inhibits the Na+/K+ ATPase in Caco-2 cells via PKC and p38MAPK. *Cellular Signalling*, *27*, 416-423.

Ferruzza S, Rossi C, Scarino ML, Sambuy Y. (2012). A protocol for in situ enzyme assays to assess the differentiation of human intestinal Caco-2 cells. *Toxicology in Vitro*, *26*, 1247-1251.

Fröhlich EE, Fröhlich E. (2016). Cytotoxicity of nanoparticles contained in food on intestinal cells and the gut microbiota. *International Journal of Molecular Sciences*. *17*, 509.

Gal-Garber O, Mabjeesh S, Sklan D, Uni Z. (2003). Nutrient transport in the small intestine: Na+, K+-ATPase expression and activity in the small intestine of the chicken as influenced by dietary sodium. *Poultry Science*, *82*, 1127-1133.

Guo Z, Martucci NJ, Moreno-Olivas F, Tako E, Mahler GJ. (2017). Titanium dioxide nanoparticle ingestion alters nutrient absorption in an in vitro model of the small intestine. *NanoImpact*, *5*, 70-82.

Guo Z, Martucci N, Liu Y, Yoo E, Tako E, Mahler G. (2018). Silicon dioxide nanoparticle exposure affects small intestine function in an in vitro model. *Nanotoxicology*, Unpublished.

Icaza-Chávez ME. (2013). Gut microbiota in health and disease. *Revista de Gastroenterología de México (English Edition)*, *78*, 240-248.

Jovanovi B. (2014). Critical review of public health regulations of titanium dioxide, a human food additive. *Integrated environmental assessment and management, 11*, 10-20.

Kalive M, Zhang W, Chen Y, Capco DG. (2012). Human intestinal epithelial cells exhibit a cellular response indicating a potential toxicity upon exposure to hematite nanoparticles. *Cell Biology and Toxicology*, *28*, 343-368.

Kish L, Hotte N, Kaplan GG, Vincent R, Tso R, Gänzle M, Madsen KL. (2013). Environmental particulate matter induces murine intestinal inflammatory

responses and alters the gut microbiome. *PlosOne*, *8*, e62220.

Koeneman BA, Zhang Y, Westerhoff P, Chen Y, Crittenden JC, Capco DG. (2010). Toxicity and cellular responses of intestinal cells exposed to titanium dioxide. *Cell Biology and Toxicology*, *26*, 225-238.

Kruse TA, Bolund L, Grzeschik KH, Ropers HH, Olsen J, Sjöström H, Norén O. (1988). Assignment of the human aminopeptidase N (peptidase E) gene to chromosome 15q13-qter. *FEBS Letters*, *239*, 305-308.

Lallès J-P. (2014). Intestinal alkaline phosphatase: novel functions and protective effects. *Nutrition Reviews*, *72*, 82-94.

Lefebvre DE, Venema K, Gombau L, Valerio LG, Raju J, Bondy GS., Stone V. (2015). Utility of models of the gastrointestinal tract for assessment of the digestion and absorption of engineered nanomaterials released from food matrices. *Nanotoxicology*, *9*, 523-542.

Li Q, Li T, Liu C, DeLoid G, Pyrgiotakis G, Demokritou P, McClements DJ. (2017). Potential impact of inorganic nanoparticles on macronutrient digestion: titanium dioxide nanoparticles slightly reduce lipid digestion under simulated gastrointestinal conditions. *Nanotoxicology*, *5390*, 1-15.

Liang M, Lin I-C, Whittaker MR, Minchin RF, Monteiro MJ, Toth I. (2010). Cellular uptake of densely packed polymer coatings on gold nanoparticles. *ACS Nano*, *4*, 403-413.

Liu Y, He L, Mustapha A, Li H, Hu ZQ, Lin M. (2009). Antibacterial activities of zinc oxide nanoparticles against *Escherichia coli* O157:H7. *Journal of Applied Microbiology*, *107*, 1193-1201.

Lomer MCE, Hutchinson C, Volkert S, Greenfield SM, Catterall A, Thompson RPH, Powell JJ. (2004). Dietary sources of inorganic microparticles and their intake in healthy subjects and patients with Crohn's disease. *The British Journal of Nutrition*, *92*, 947-955.

Lomer MCE, Thompson RPH, Powell JJ. (2002). Fine and ultrafine particles of the diet : influence on the mucosal immune response and association with Crohn ' s disease. *Proceedings of the Nutrition Society*, *61*, 123-130.

Lu K, Abo RP, Schlieper KA, Graffam ME, Levine S, Wishnok JS, Fox JG. (2014). Arsenic exposure perturbs the gut microbiome and its metabolic profile in mice: An integrated metagenomics and metabolomics analysis. *Environmental Health Perspectives*, *122*, 284-291.

Mahler GJ, Shuler ML, Glahn RP. (2009). Characterization of Caco-2 and HT29-MTX cocultures in an *in vitro* digestion/cell culture model used to predict iron bioavailability. *Journal of Nutritional Biochemistry*, *20*, 494-502.

Mai V, Draganov PV. (2009). Recent advances and remaining gaps in our knowledge of associations between gut microbiota and human health. *World Journal of Gastroenterology*, *15*, 81-85.

Marchesi JR, Adams DH, Fava F, Hermes GDA, Hirschfield GM, Hold G, Hart A. (2016). The gut microbiota and host health: A new clinical frontier. *Gut*, *65*, 330-339.

Mina-Osorio P. (2008). The moonlighting enzyme CD13: old and new functions to target. *Trends in Molecular Medicine*, *14*, 361-371.

Mooseker MS. (1985). Organization, chemistry, and assembly of the cytoskeletal apparatus of the intestinal brush border. *Annual Review of Cell Biology*, *1*, 209-241.

Oberdörster G, Oberdörster E, Oberdörster J. (2005). Nanotoxicology : an emerging discipline evolving from studies of ultrafine particles. *Env. Health* Persective, *113 (7)*, 823-839.

Peters R, Kramer E, Oomen AG, Herrera Rivera ZE, Oegema G, Tromp PC, Bouwmeester, H. (2012). Presence of nano-sized silica during in vitro digestion of foods containing silica as a food additive. *ACS Nano*, *6*, 2441-2451.

Piccinno F, Gottschalk F, Seeger S, Nowack B. (2012). Industrial production quantities and uses of ten engineered nanomaterials in Europe and the world. *Journal of Nanoparticle Research*, *14*, 1109-1120.

Saha P, Manoharan P, Arthur S, Sundaram S, Kekuda R, Sundaram U. (2015). Molecular mechanism of regulation of villus cell Na-K-ATPase in the chronically inflamed mammalian small intestine. *Biochimica et Biophysica Acta - Biomembranes*, *1848*, 702-711.

Sarkar PK. (2002). A quick assay for Na + -K + -ATPase specific activity. *Zeitschrift Fur Naturforschung*, *57*, 562-564.

Schirmer M, Smeekens SP, Vlamakis H, Jaeger M, Oosting M, Franzosa EA, Xavier RJ. (2016). Linking the human gut microbiome to inflammatory cytokine production capacity. *Cell*, *167*, 1125-1136.e8.

Schulz MD, Atay Ç, Heringer J, Romrig FK, Schwitalla S, Aydin B, Arkan MC. (2014). High-fat-diet-mediated dysbiosis promotes intestinal carcinogenesis

independently of obesity. *Nature*, *514*, 508-512.

Segers ME, Lebeer S. (2014). Towards a better understanding of Lactobacillus rhamnosus GG - host interactions. *Microbial Cell Factories*, *13* (Suppl 1), S7.

Shahare B, Yashpal M, Singh G. (2013). Toxic effects of repeated oral exposure of silver nanoparticles on small intestine mucosa of mice. *Toxicology Mechanisms and Methods*, *23*, 161-167.

Shepherd NA, Crocker PR, Smith AP, Levison DA. (1987). Exogenous pigment in Peyer's patches. *Human Pathology*, *18*, 50-54.

Vranic S, Gosens I, Raun N, Keld J, Bokkers B, Kermanizadeh A, Baeza A. (2017). Impact of serum as a dispersion agent for *in vitro* and *in vivo* toxicological assessments of TiO 2 nanoparticles. *Archives of Toxicology, 91,* 353-363.

Waller T, Chen C, Walker S. (2017). Food and Industrial grade titanium dioxide impacts gut microbiota. *Environmental Engineering Science*, *34*, 537-550.

Wang B, Yao M, Lv L, Ling Z, Li L. (2017). The human microbiota in health and disease. *Engineering*, *3*, 71-82.

Wang J, Fan Y. (2014). Lung injury induced by TiO_2 nanoparticles depends on their structural features: Size, shape, crystal phases, and surface coating. *International Journal of Molecular Sciences*, *15*, 22258-22278.

Weir A, Westerhoff P, Fabricius L, Hristovski K, von Goetz N. (2012). Titanium dioxide nanoparticles in food and personal care products. *Environmental Science & Technology*, *46*, 2242-2250.

Williams K, Milner J, Boudreau MD, Gokulan K, Cerniglia CE, Khare S. (2015). Effects of subchronic exposure of silver nanoparticles on intestinal microbiota and gut-associated immune responses in the ileum of Sprague-Dawley rats. *Nanotoxicology*, *9*, 279-289.

Wisel S, Rajendren VM. (1997). Mechanism of inhibition of Na 2 -glucose cotransport in the chronically inflamed rabbit ileum. *American Journal of Physiology, 273*, 913-919.

Yang Y, Faust JJ, Schoepf J, Hristovski K, Capco DG, Herckes P, Westerhoff P. (2016). Survey of food-grade silica dioxide nanomaterial occurrence, characterization, human gut impacts and fate across its lifecycle. *Science of The Total Environment*, *565*, 902-912.

Yang Y, Zhang C, Hu Z. (2013). Impact of metallic and metal oxide nanoparticles on

wastewater treatment and anaerobic digestion. *Environmental Science: Processes Impacts*, *15*, 39-48.

Zhang W, Kalive M, Capco DG, Chen Y. (2010). Adsorption of hematite nanoparticles onto Caco-2 cells and the cellular impairments: effect of particle size. *Nanotechnology*, *21*, 355103.

4. DISCUSSION

4. DISCUSSION

Nanotechnology approaches currently allow the development of engineered nanomaterials (ENMs) which present promising new applications for the food industry such as the enhancement of texture, color, flavor, nutrient stability and food packaging safety, among others (Sozer and Kokini, 2009). Big efforts are currently done for the identification, validation and standardization of scientific methodologies to assess the potential human uptake and, therefore, to determine the absorbed doses of ENMs that come from human dietary sources (Bouwmeester et al., 2009). The current risk assessment of nanoparticles (NPs) and chemicals exposures has mainly relied on animal *in vivo* studies (EFSA, 2011). However, these *in vivo* studies only provide general information on the NPs distribution in a whole organism and do not fully simulate the physiology of humans (Basketter et al., 2012; Hartung et al., 2013). In addition to other reasons, including that the use of animals is ethically debatable and costly, the vast quantity and variety of ENPs make it impossible to test all of them by *in vivo* studies. Facing this reality, several efforts are conducted to develop suitable *in vitro* models to assess ENPs potential risk (Braakhuis et al., 2015). The interest on non-animal models of epithelial has increased in various scientific fields, including scientists from academia, product developers in industry, regulatory authorities, and society in general (e.g. animal advocacy parties). However, there is no international consensus and guidance in the use of an specific digestion and absorption *in vitro* models of the gastrointestinal tract (GIT) to date, which leads to the generation of a wide disparity of data (Hartung et al., 2013). Moreover, there is a critical need for extrapolation of the *in vitro* to *in vivo* studies in the structure and modeling kinetics, as the "*dose paradigm."* This has been proposed as the main issue to be solved in the 21st Century Toxicology (Gordon et al., 2015).

As it has already been explained in the three studies included in the Results section, in this Thesis we have investigated the benefits and usefulness of three similar *in vitro* models (namely Caco-2/HT29, Caco-2/HT29-MTX, and Caco-2/HT29/Raji-B barriers) that mimicry the human GIT. Specifically, we generated useful methodological data to improve the use of these systemic models in the assessment of digestion and absorption of ENMs. These models have been tested by analyzing the effect of ENMs highly used in the food industry such as nano-sized titanium dioxide (TiO_2NPs) and nano-sized silica dioxide (SiO_2NPs). It should be noted that this is the first time we have faced the complexity of these experimental designs, since our laboratory only had experience with the simple Caco-2 monoculture.

4.1. Characterizing the 3-dimensional co-culture Caco-2/HT29/Raji-B

One of the principal purposes of extrapolating *in vivo* to *in vitro* conditions is to mimic the native structure as much as possible. This includes the components and the applicability of the organic or systemic model that is going to be set up in the laboratory. In our case, and as mentioned in Study 1 (Chapter 1), monolayers of differentiated Caco-2 cells (the most used model to date) does not simulate a small intestine environment reliably, as a fine balance of endogenous and exogenous factors in the intestine is provided by the variety of cells forming the mucosa niche. Because of this, the rate of paracellular transport is more limited in the monoculture than in the human intestine and the strength conferred by the junctional complexes is higher than in the human small intestine. Consequently, the total transport values for many molecules through Caco-2 monolayers are only similar to what occurs in specific parts of the GIT, such as human colon and rectum (Rubas et al., 1996; Chen et al., 2010). The small intestine epithelium is organized into numerous units of crypts and villi, where the villi project into the lumen to maximize nutrient uptake, breakdown and absorption. The epithelial cell layer includes four major cell types; *i)* absorptive enterocytes, *ii)* goblet cells, responsible for mucus secretion, *iii)* enteroendocrine cells, secreting important hormones, and *iv)* Paneth cells, secreting antimicrobial peptides. In addition, and in minor quantity (<5%), the characteristic microfold cells (M cells) are found in the epithelium overlaying the organized lymphoid tissue called Payer's patches in the small intestine (Verhoeckx et al., 2015). Trying to encompass all these features in an *in vitro* model, diverse authors have investigated and recently described the systemic Caco-2/HT29/Raji-B model as a more complex intestinal epithelial barrier than the simpler Caco-2 monolayer (Schimpel et al., 2014; Lozoya-Agullo et al., 2017).

Interestingly, recent studies have tested the impact of polystyrene NPs on iron absorption and insulin transport in this model, showing a good correlation with *in vivo* and *ex vivo* data, respectively (Mahler et al., 2012; Antunes et al., 2013). Moreover, Schimpel et al. obtained a proper correlation data on 50 and 200 nm polystyrene NPs permeability compared with data from *ex vivo* permeability through porcine intestinal mucosa (Schimpel et al., 2014). Furthermore, these authors pointed out that NPs uptake was strongly impacted by the mucus layer, indicating that NPs size, as well as the presence of M-like cells, plays an important role in intestinal permeability. Due to those facts, the intestinal epithelial model Caco-2/HT29/Raji-B, has been proposed as a reliable tool for the study of NPs transport and bio-kinetics. Nevertheless, due to the novelty of the model, it still presents aspects that need to be improved. The first aspect would be the HT29 cell clone to be selected to

work with: the original HT29 or the adapted HT29-MTX? Although derived from another colorectal adenocarcinoma, HT29 cells have been described to be significantly different from Caco-2. After a differentiation process, they have the capability to secrete mucus at a relative high level (Huet et al. 1987; Maoret et al. 1989). HT29-MTX, on the other hand, originated from a stepwise adaptation of exponentially-grown HT29 cells exposed to increasing concentrations of methotrexate (MTX) (up to 10^{-5} mol), which resulted in their transformation into mucus-secreting differentiated cells (Lesuffleur et al., 1990). In this Thesis, the original HT29 cells were chosen to work with in the studies 1 and 2 as a more realistic human epithelial cell model rather than HT29-MTX, as they were originally isolated from a primary tumor of a Caucasian 44 year old female but still secrete similar amount of mucus as HT29-MTX.

Other aspect to take into account is the Caco-2/HT29 cell culture ratio, as enterocyte and goblet cells are present in different percentages in the small intestine (Verhoeckx et al., 2015). In this way, Forstner et al. reported that the amount of mucus-producing goblet cells ranges from 10% in the small intestine to 24% in the distal colon (Forstner et al. 1982). Different authors have proposed the use of different ratio such as 70:30, 75:25 (Caco-2/HT29) (Mahler et al., 2012; Schimpel et al., 2014), or 90:10 (Antunes et al., 2013; Lozoya-Agullo et al., 2017). Our integrity (TEER) and permeability (paracellular LY) values obtained in Study 1 indicated that the 90:10 ratio was the best cell percentage that closely mimics the small intestine maintaining a proper barrier structure (McCracken et al., 2016). Consequently, we used this ratio in further experiments. Higher percentages of HT29 cells clearly disturbed the co-culture's organization and the monolayer's structure, reducing its integrity and increasing the paracellular permeability to unrealistic values. It is known that after 21 days of the co-culture differentiation, HT29 cells don't form junctional complexes between them or with their neighboring Caco-2 cells. This would facilitate the paracellular permeability of the NPs tested, which would be far from the reality of a small intestine. Additionally, although Caco-2 stop their cell proliferation when they are confluent, HT29 cells don't. Thereby, as seen in previous studies in our laboratory (unpublished data), higher percentages of HT29 cells tend to grow in an uncontrolled manner and lose the initial ratio of cells. Additionally, the histochemical staining with *Alcian Blue* dye for qualitative mucus detection indicated that the amount of mucus and its surface scattering as an additional layer was very similar among the different cell ratios tested (e.g. 90:10, 80:20 and 70:30). These preliminary results led us to propose the use Caco-2/HT29 co-cultures in a 90:10 ratio.

In accordance to our goal of establishing a more realistic barrier structure, we promoted the differentiation of Caco-2 cells into M-like cells. It has been widely

demonstrated that M cells found in the Peyer's Patches of the small intestine play an important role in the immune system and have the capacity to transport particulate matter by endocytosis, such as bacteria, viruses, nanoparticles, and microparticles (des Rieux et al., 2007; Lai and D'Souza, 2008; Antunes et al., 2013). Due to these functions, M cells have begun to be investigated by many researchers as an important target for drug delivery and guided vaccination, as well as for being an important entry portal of those foodborne ENMs (Gullberg et al., 2006; Braakhuis et al., 2015). As previously mentioned, Caco-2 cells co-cultured with Raji-B lymphocytes have the ability to acquire an M-like cell phenotype *in vitro*, losing their brush border organization, their microvilli, and the typical digestive function from enterocytes (Kerneis et al. 1996). Accordingly, the main challenge of many authors has been to target the specific surface receptors that appear after the *in vitro* rearrangement of the M-like cell membrane by using these receptors' ligands, lectins, and specific antibodies (Gabor et al., 2004; Pereira et al., 2014). Although we have been able to detect the induction of M-like cells in our co-culture model by electronic microscopy (TEM), discrepancies have appeared when analyzing molecular markers previously described as specific for M-like cells. In fact, only *GP2* and *TLR4* gene expression was upregulated after co-culturing Caco-2 cells with Raji-B lymphocytes, while no changes were detected for *LGALS9, PAFR* and *Spi-B* genes. This means that further experiments of protein expression and regulation levels are required to monitor their behavior. Moreover, we discarded the use of the lectin WGA, proposed by diverse authors as a putative M cell ligand (Schimpel, Teubl, Absenger, Meindl, Fröhlich, *et al.*, 2014). This is because our confocal images clearly demonstrated that WGA displayed a strong reaction binding to mucin residues.

Due to the low rate of M-like cell induction *in vitro* (<5%) (Giannasca et al., 1999), to the high extension and surface area (1.12 cm^2) of our epithelial barrier and to the complexity of the model composed by three different cell types, the likelihood of localizing M-like cells by TEM is very poor. We also discarded the use of the TEM analysis for uptake studies because this microscope technique is time-consuming due to the biological sample processing procedure and our set of ENMs samples was very large. In addition, our previous experience working with Caco-2 monolayers to detect NP uptake demonstrated that TEM was not a useful tool, due to the fact that the high cytoplasmic granulation of Caco-2 cells complicates the NPs visualization (Vila et al., 2017). For this purpose, we developed a confocal microscopy protocol where metal and metal oxide NPs can be readily and easily detected *in situ* due to their capacity to refract polarized light. Briefly, exposing the epithelial barrier to an *in situ* combination of fluorochromes such as *CellMask*™ and

Hoechst or WGA and Hoechst during 15 min, we could individuate the cell membrane from the nucleus, and the mucus shed from the cell nucleus, respectively. Another advantage conferred by confocal microscopy is that NPs (e.g. TiO_2NPs and SiO_2NPs) can be detected at low and high resolution. This allowed us to have a general view of the NPs distribution over the barrier's surface and across the barrier width. However, the M-like cells detection was still unachievable as there is no specific fluorochrome marker for M-like cells identification currently in the market. Thereby, for the ENMs risk assessment we decided to start with a simpler intestinal epithelial model, Caco-2/HT29, as more studies are needed to develop an easy and effective methodology for the detection of M-like cells and their role in ENMs' translocation.

4.2. Detrimental effects of TiO_2NPs on the systemic model Caco-2/HT29

The use of nano-particulated TiO_2 in several food matrices of daily-consumed products has been prevalent for years (Weir et al., 2012). Because of that, investigations on the putative adverse effects of TiO_2NPs on the GIT have exponentially increased. Although TiO_2 was described as a biological inherent compound (Diebold, 2003), it has been demonstrated that the different physico-chemical properties of ENPs drive adverse effects in biological systems (Gatoo et al., 2014). Nevertheless, epidemiological and occupational studies of the adverse health effects induced by nano-sized TiO_2 alone are lacking. Furthermore, most studies on workers exposed to TiO_2 were not designed to investigate the relationship between the size of TiO_2 particles and cancer risk, which represents an important question when assessing the potential occupational carcinogenicity of nano- sized TiO_2 (Shi et al., 2013; EFSA, 2016).

Nanotoxicology is oriented to gather and evaluate data obtained from *in vitro* and *in vivo* studies, in order to increase our knowledge regarding the use of nanomaterials and develop strategies to protect living organisms. An overview of the currently-available carcinogenicity data on TiO_2NPs from experimental animal studies raises serious questions about their health and environmental safety (Shi et al., 2013; Jovanovi, 2014). Carcinogenicity studies in animals indicate that TiO_2NPs can produce tumors through inhalation or intratracheal instillation exposures, being more carcinogenic, on an equal mass basis, than fine particles of TiO_2. Thus, TiO_2NPs have been evaluated by the World Health Organization (WHO) and the International Agency for Research on Cancer (IARC) as "possibly carcinogenic for human beings" (Group 2B) (IARC, 2010).

The properties of ENPs can be modified by a functionalization processes in order to change or reduce the toxicity of the chemical materials used for their production. In addition to their physico-chemical properties, the interaction between NPs and the cell culture medium or biological fluids is another crucial parameter to take into consideration in toxicology studies (Oberdörster et al., 2005; Jiang et al., 2009). In our second study (Chapter 2), we characterized three different shapes of TiO_2NPs measuring their hydrodynamic size (DLS) and suspension stability (LDV), taking into consideration their shape (<25 nm nano-spheres, <100 nm nano-rods and <10 nm nano-wires), the dispersion medium (DMEM+10%FBS), different concentrations used (12.5, 50, 150 and 350 µg/mL), and the incubation time (0, 24 and 48 h). Results indicate that in cell culture media containing FBS, all three TiO_2NPs tend to agglomerate, as their hydrodynamic sizes were higher than 150 nm in all the concentrations tested during the entire time course. Moreover, when characterizing NPs in suspension, electric charge measurements between the surfaces of the TiO_2NPs and the dispersants are significant and useful data to take into account. The value of a potential existing between both surfaces is expressed in terms of ζ-potential, which reflects the stability of the colloidal system. A solution is normally considered stable when the ζ-potential is higher than + 30 mV or lower than – 30 mV (Hanaor et al., 2012). The observed agglomerations are in accordance with the low ζ-potential values measured by LDV, ranging from -10 to -13 mV. As previously seen, primary TiO_2NPs powder in biological medium absorbs biological components such as proteins and amino acids, resulting in NP agglomeration even after an exhaustive sonication (Grassian et al., 2007). Our results agree with many other studies that analyzed TiO_2NPs suspensions using different dispersants such as water, DMEM, DMEM+FBS, or even *in vitro* digested TiO_2NPs (Dorier et al., 2015; Guo et al., 2017; Li et al., 2017). Consequently, the agglomeration status could influence the potential toxicity by changing the uptake, crossing, and bio-persistence throughout the intestinal epithelial barrier. It has been postulated that a high hydrodynamic diameter could avoid the formation of endocytic vesicles (approximately 50-150 nm of diameter) as a mechanism of cell uptake and, therefore, likely sequester TiO_2NPs to the apical surface of the cell monolayers (Liang et al., 2010; Guo et al., 2017).

4.2.1. Morphological and functional barrier impairments

Oral uptake of TiO_2NPs by consumers has continuously increased in the past years up to a daily intentional or unintentional human uptake (Rompelberg et al., 2016). *In vivo* studies with rats already concluded that orally-administrated TiO_2NPs (by food or

gavage administration) were able to penetrate the epithelial barrier of the small intestine (Onishchenko et al., 2012; Geraets et al., 2014). However, studies on TiO_2NPs translocation/distribution to various organs (e.g. liver, kidney, spleen, heart, brain, GIT) are very limited (Cho et al., 2013; MacNicoll et al., 2015). The likelihood of chronic accumulation of such NPs through different tissue barriers and in secondary-target organs raises questions about their mechanism of action. Our previous studies using the Caco-2 monolayer model (unpublished data) concluded that exposures to <100 nm TiO_2NPs up to 200 µg/mL do not affect the function of the barrier in terms of membrane stability and tight junctions (TJ) integrity. This confirmed the strength of the model seen by several authors (Faust et al., 2014; Janer et al., 2014; Song et al., 2015) which, as aforementioned, does not completely mimic the physiologic conditions of the human small intestinal epithelium. However, exposing the more reliable intestinal *in vitro* model (Caco-2/HT29) to different shapes of TiO_2NPs, gave significantly different results when compared to those from Caco-2 monolayers. Our second study indicated that high concentrations of nano-rods (TiO_2NPs-R) and nano-wires (TiO_2NPs-W), but not of nano-spheres (TiO_2NPs-S), were able to readily compromise the barrier's integrity after 24 h of exposure. Moreover, these effects were enhanced with time, as TEER values significantly decreased and the paracellular passage of LY significantly increased after 48 h. This is in agreement with the *in vivo* and *ex vivo* data, but not with the *in vitro* data from the study of Brun and co-workers from 2014, which detected an increment of the paracellular permeability after 2 and 6 h of TiO_2NPs exposure (Brun et al., 2014). Interestingly, as our results indicate, the detrimental effects over the integrity and permeability of the barrier were shape-dependent: TiO_2NPs-W provoked more adverse effects, followed by TiO_2NPs-R and TiO_2NPs-S, respectively. Moreover, upregulation of genes encoding different TJ components (*ZO-1*, *OCLN* and *CLDN2*) were detected after exposing the barrier to the three TiO_2NPs shapes, confirming that cell junctions are impaired and are actively repaired by inducing the novo expression of junctional proteins, as postulated (Brun et al., 2014). Taking these results together with the cell viability data, we concluded that nano-wires of TiO_2NPs could trigger major adverse effects because of their nano-shape, as observed in carbonanotubes (CNT) (Clark et al., 2012). One theory is that TiO_2NPs-W are unable to penetrate the cell, but its filamentous shape can reach the cell-cell interspace, impairing the junction complexes. Although no internalization occurs, cell detachment can induce the loss of cells in the barrier. Due to their potential properties and new applications (e.g. semiconductor photocatalytic, treatment of water, as a photoactive material in nanocrystalline solar cells, and medicine), TiO_2NPs-W are gaining interest in the marketplace. However, little is known about their bio-interactions and toxicity, and only

few studies have started to consider them. In agreement with our results, Tilton and colleagues showed low levels of toxicity when they exposed Caco-2/HT29-MTX cells to nano-belts of TiO_2 at 1 h (Tilton et al., 2014). Moreover, short-term ingestion of nano-fibers of TiO_2 (TNDF) in an *in vivo* study with Sprague Dawley rats produced marginal inflammatory effects indicative of toxicity (Gato et al., 2017).

The quantification of NP uptake by different organs and their cells has always raised high interest, as it is essential data for toxicological studies. The intracellular quantification of NPs has been analyzed in a cell suspension of a pellet typically containing 10^6 cells by ICP-MS (Hsiao et al., 2016). Nevertheless, this method yielded an average value that does not allow conclusions of the particles' distribution among cells or within a single cell. For this reason, a method based on laser ablation (LA-ICP-MS) was developed in order to localize and quantify metallic NPs in a single cell (Drescher et al., 2012). Despite the attractiveness of the proposal, this assay needs to be specifically tuned for each specific cell culture conditions. Many other methods have been proposed in order to detect NPs internalization in a qualitative manner. Transmission electron microscopy (TEM), time-of-flight secondary ion mass spectrometry (ToF-SIMS), and confocal Raman microspectroscopy (CRM) are methods already used allowing the simultaneous visualization of NPs and their biological environment at a sub-cellular level (Nemmar et al., 2007; Monteiro-Riviere et al., 2011; Collins et al., 2016). Nevertheless, TEM and ToF-SIMS methods are relatively costly and time-consuming, and so might not be useful as high throughput techniques for NPs screening. In contrast, CRM is an economical and relatively fast technique which provides 3D chemical composition images, but the spatial resolution and sensitivity of the assay are limited compared to the other techniques. Among the conventional image techniques such as TEM and SEM, flow cytometry methodology was developed to measure NPs uptake using side scatter. In addition, it has been described as a high throughput screening method (HTS) as it can measure 5,000 cells in seconds (Collins et al., 2016). It was postulated that an increasing cellular complexity is directly correlated with an increased NPs cell uptake. However, analytical limitations have been also pointed out at the time of data interpretation. If uptake is measured using side scatter, external NPs attached to the cell membrane cannot be distinguished; also, increased cellular density may be due to apoptosis. Therefore, additional imaging methods must be used for validation. Our previous experience in detecting NPs internalization and transcytosis in the Caco-2 monolayer suggested that; *i)* the detection limit of the ICP-MS technique is a limiting factor when working with realistic doses of NPs related to the real human consumption; *ii)* TEM was not a useful

technique, as low doses were also difficult to localize in an extensive cell surface and very granulated Caco-2 cell cytoplasm; and *iii)* TEM complemented with energy dispersive X-ray (TEM-EDX) were only useful detecting some metallic NPs such as TiO_2, as other's cells components and devices used may show false positives (Vila et al., 2017). Trying to solve these methodological difficulties and the analytical ambiguity, we used the confocal microscopy technique, already automated and set up in the first study. Although it is a semi-quantitative technique and it did not confer exhaustive NPs' size and shape information, we were able to easily detect the specific NPs location and the crossing capacity of all three TiO_2NPs types in the second study. As the three TiO_2NPs shapes have similar refractive indexes, the analysis of our confocal images lead to the following conclusions: *i)* big TiO_2NPs-S and TiO_2NPs-R agglomerates remain deposited and entrapped in the apical part of the barrier, where the mucus shed and microvilli are facing, while the smaller agglomerates can penetrate deeper in the barrier; *ii)* TiO_2NPs-R remained mostly confined between mucus and microvilli, even more than TiO_2NPs-S and TiO_2NPs-W after 48 h of treatment, showing differences in the bio-persistence capabilities of the NPs shapes; *iii)* the confocal images reinforce our TEER and LY results, as TiO_2NPs-W apparently impaired the barrier's structure after 24 h of NPs treatment; *iv*) TiO_2NPs-W were detected mainly between cells, which lead us to hypothesize that the main crossing route of filamentous TiO_2NPs is paracellular; *v)* the three shapes of TiO_2NPs were able to cross the mucus shed, enter the cell cytoplasm and finally reach the cell nucleus; *vi)* more TiO_2NPs-R/cell nucleus interaction events were seen than when exposing the barrier with TiO_2NPs-S and TiO_2NPs-W. Thus, these results agree with those from Chen et al., who already demonstrated that spherical TiO_2NPs and nano-rods of TiO_2 could be more readily internalized than filamentous TiO_2NPs into HeLa cells after 24 h (Chen et al., 2010). As already mentioned, nano-shapes with high aspect ratio (e.g. nano-wires, nano-belts and nano-filaments) determine the high mechanic reactivity of NPs, which enables the insoluble TiO_2NPs to agglomerate, affecting cellular uptake and causing epithelium injury. In spite of this, an analytical limitation was found during the image processing. First, the inability to distinguish between cell-types because of the fluorochrome used (WGA), which clearly stained the mucus spread along the barrier surfaces and both cells membranes similarly. Dealing with this, one easy and economically feasible solution would be to find another unshared/unique cell marker to specifically identify one cell type (e.g. antibodies against ZO-1, villin, etc). This second fluorochrome should have a different emission/absorption spectra than WGA, in order to avoid an image/color overlapping. Nevertheless, taking into consideration the published literature, diverse studies have postulated that both cell types (differentiated Caco-2

and HT29) actively internalize ENMs, at least spheres of TiO_2NPs (Song et al., 2015; Schneider, Westermann and Glei, 2017). However, other authors remarked that TiO_2NPs agglomerations entrapped in cytoplasmic vesicles were found mostly in cells lacking microvilli, pointing out a higher capability of HT29 cells to internalize NPs than the differentiated Caco-2 (Hansen et al., 2009; Brun et al., 2014).

Toxicokinetics describe the rate at which a substance enters the body through different exposures routes and its fate after entering the body. The level or concentration of TiO_2NPs in the body depends on the rate or kinetic of absorption, distribution, metabolism, and excretion of TiO_2NPs. Here, the analysis of the basolateral medium was also performed by confocal microscopy after both 24 and 48 h exposures to assess TiO_2NPs cross through the barrier. Our images detected the presence of all three different TiO_2NPs in the basolateral chamber. This indicates the ability of the TiO_2NPs to first cross the mucus shed, and secondly the *in vitro* intestinal barrier, independently of shape. As the previous confocal images showed the tendency of nano-spheres and nano-rods to be internalized, we hypothesize that TiO_2NPs-S and TiO_2NPs-R are more likely to cross intracellularly, while the translocation of TiO_2NPs-W is mainly paracellular. A semi-quantification of the TiO_2NPs amount was also carried out, demonstrating an increasing concentration-dependent translocation for TiO_2NPs-R, while showing a decreasing translocation for TiO_2NPs-W. No tendency was observed for TiO_2NPs-S. Moreover, a continuous translocation was seen for all TiO_2NPs shapes, since the amount of NPs was higher at 48 h than at 24 h.

Given the accumulation of the bigger TiO_2NPs agglomerates on the apical part of the barrier, the digestive function of the enterocytes was evaluated by analyzing the gene expression of *ALPI*, *SI* and *SLC15A1*. Despite the mucus shed, a potential impairment of the brush border can happen through direct contact with TiO_2NPs. As previously demonstrated, TiO_2NPs are able to reduce the number of microvilli from a Caco-2 monolayer (Faust et al., 2014a; Faust et al., 2014b). In this thesis, high differences in the modulation of the gene expression were found after exposing the *in vitro* barrier to the three TiO_2NPs. Any specific observed gene expression pattern change was neither related to the NPs shape nor to the time exposure. While the *ALPI* expression was completely downregulated after all treatments, *SI* was upregulated after almost all treatments. However, upregulation of *SLC15A1* was only significantly different after the exposure to TiO2NPs-R. Nevertheless, changes in the expression patterns of the aforementioned brush border enzymes would entail lipid and carbohydrate starvation or over-processing among other nutrient byproducts, leading to a malfunction of the small intestine and/or potential bowel disease. At this point, it has

to be pointed out that post-confluent Caco-2 cells display a remarkable heterogeneity in their differentiated characteristics, which was particularly demonstrated in the case of SI. Immunofluorescence staining with monoclonal and polyclonal antibodies has consistently revealed the presence of strongly positive and negative neighboring cells even in cultures kept for several weeks (Beaulieu and Quaroni, 1991). Also the transitory mosaic patterns of specific intestinal markers have been described as the lack of coordination between the differentiation process and genes related with proliferation (Vachon and Beaulieu, 1992; Vachon et al., 1996). This could explain variabilities between samples affecting the final general result.

4.2.2. Genotoxicity studies

Some studies have associated exposures to TiO_2NPs with potentially toxic effects. However, *in vitro* and *in vivo* investigations addressed to evaluate the genotoxicity of TiO_2NPs report contradictory results, as the employed doses were significantly different and, sometimes, too high (Martirosyan et al., 2014).

The physicochemical characteristics of NPs allow them, in most of the cases, to catalyze reactive oxygen production (ROS) and do oxidative damage to biomolecules, with potential pathological consequences (Oberdörster et al., 2005; Aillon et al., 2010; Collins et al., 2016). As TiO_2 is a material of low solubility, its genotoxic potential would be expected to be principally triggered by ROS production which, in turn, trigger indirect genotoxic effects (Donaldson et al., 2010). Evidence indicates that the genotoxicity of TiO_2NPs is specifically mediated by the generation of oxidative stress in cells. It should be remembered that the mechanisms involved in inflammatory effects included ROS production as a hallmark in TiO_2NP toxicity (Chen et al., 2013; Shi et al., 2013; Wang and Fan, 2014). Hence, ROS production might lead to the formation of primarily 8-oxo-dG (oxidative DNA damage), which can be easily detected by the comet assay when complemented with the FPG enzyme. These are considered mutagenic lesions, since 8-oxo-dG can pair with adenine and cytosine with equal efficiency (Carriere et al., 2017). The accumulation of these lesions could trigger cell transformation upon chronic exposure, as demonstrated by exposing undifferentiated Caco-2 cells to low doses of AgNPs for up to 4 weeks (Vila et al., 2017). As for cytotoxicity, previous studies demonstrated that the morphological status of Caco-2 plays an important role in genetic damage prevention. For example, Song et al. remarked that the ROS generation was significantly increased only after exposure of undifferentiated Caco-2 cells to TiO_2NPs, but not after treating differentiated Caco-2

monolayers (Song et al., 2015). Similarly, Schneider and colleagues used the HT29 cell line to evaluate the biological effects of metal and metal oxide NPs, and reported the ability of TiO_2NPs to produce oxidative stress (Schneider et al., 2017). Additionally, while different studies described the capacity of TiO_2NPs to cause genotoxic damage in undifferentiated Caco-2 cells, (Gerloff et al., 2012; Zijno et al., 2015; Proquin et al., 2017), Dorier et al. concluded that neither anatase TiO_2NPs nor rutil TiO_2NPs induced DNA strand breaks on differentiated Caco-2 monolayers (Dorier et al., 2015). Finally, factors such as size, structure, and agglomeration of TiO_2NPs could also play a pivotal role on the ROS generation (Toyooka et al., 2012).

In the second study, we also investigated the induction of oxidative DNA strand breaks by performing the alkaline comet assay combined with the use of FPG enzyme. Our results were in agreement with those mentioned before, as no type of TiO_2NPs was detected to induce oxidative DNA damage neither at 24 nor at 48 h on the systemic Caco-2/HT29 model. This might lead us to think that the Caco-2/HT29 co-culture model could modulate the ROS formation before triggering any oxidative DNA damage, for example, by activating or regulating the enzyme activity or the gene expression of those genes encoding antioxidant enzymes such as catalase (*CAT*), super oxide dismutase (*SOD*), and glutathione reductase (*GSR*). Further studies should be done in order to monitor the modulation or the activity of these anti- or pro-oxidant enzymes to back up this theory. In contrast, recent studies have detected that, after chronic exposures to TiO_2NPs, the intracellular ROS formation increased significantly in a dose-dependent manner using a similar (Caco-2/HT29-MTX) model (Dorier et al., 2017; Guo et al., 2017). Although they also did not find significant oxidative DNA damage neither in acute nor in chronic exposures, Guo et al. related the induction of ROS generation with a significant increment in intestinal permeability. They postulate that the reduction in TEER values is likely related to ROS formation, as cellular oxidative stress has been shown to activate redox-responsive signaling that disrupt TJ proteins (Chen et al., 2008). Oxidative stress causes inflammation in the gastrointestinal epithelial cells by producing pro-inflammatory cytokines such as IL-8 and TNF-α (Katayama et al., 2006), which is a major mediator of inflammation that activates NF-Kβ (Micheau and Tschopp, 2003). The pro-inflammatory mechanism induced by TNF-α can increase intestinal epithelial TJ permeability and contribute to intestinal inflammation, as seen in Crohn's disease (Ye et al., 2006).

Interestingly, another theory concerning the potential toxicity of TiO_2NPs has gained attention over the years. It was reported that, if experiments were performed under dark conditions, ROS accumulation would decrease, suggesting that TiO_2NPs generate

intracellular ROS via photocatalysis (Jugan et al., 2012). In fact, titanium dioxide is a known photocatalyst and its photocatalytic degradation cycle is shown in Figure 18. Briefly, when titanium dioxide absorbs UV light (step 1) a chain of events, possibly leading to the production of radicals (step 2b), is initiated. These radicals can attack the surroundings of the pigment and cause a breakdown of the organic medium resulting in a ductil loss of gloss or darkening (step 3). When colorants, pigments or dyestuffs are involved, the colour can also be affected (step 3) (van Driel et al., 2016). Moreover, the ratio between recombination (step 2a) and radical formation (step 2b) determines a large part of the photocatalytic activity of titanium dioxide powder. This ratio is affected by a number of the titanium dioxide characteristics, one of them being its crystal structure. In general, literature shows that anatase has the highest photocatalytic activity of the two titanium polymorphs (Sclafani and Herrmann, 1996; Kim et al., 2014). *In vitro* studies indicate that the crystalline structure nano-anatase, produces more ROS and is more cytotoxic than the nano-rutile one; but only after UV irradiation or under sunlight conditions (Sayes et al., 2006; De Matteis et al., 2016). Moreover, it is well-known that photoactivated TiO_2NPs can generate highly reactive hydroxyl radicals ($^{\bullet}OH$) in aerated aqueous solutions, and superoxide radical anions ($O_2^{\bullet-}$) in non-aqueous media (Dodd and Jha, 2011). In addition, *in vivo* studies also have argued that photoactivation of TiO_2NPs under natural levels of sunlight is sufficient to affect the output of lethal concentration 50 (LC_{50}) and effective concentration 50 (EC_{50}) values in standard toxicology tests (Ma et al., 2012a, 2012b).

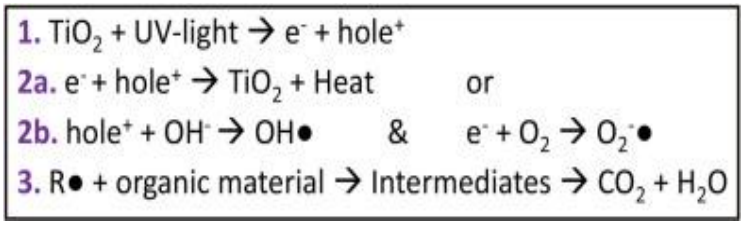

Figure 18. Photocatalytic degradation cycle of TiO_2 (Source: van Driel et al., 2016)

The DNA damaging potential of photo-activated P25 TiO_2NPs was specifically studied using the comet assay. Significant differences between non-photoactivated and photoactivated NPs were seen, suggesting that commercial P25 TiO_2NPs do not have an inherent capacity to oxidatively damage DNA bases in the absence of light. Petersen and co-workers showed that DNA samples incubated in the dark for 24 h with TiO_2NPs (0.5-50 µg/mL) do not lead to the formation of base lesions. However, when

the same DNA was exposed to either visible light from 400 to 800 nm (energy dose of ~14.5 kJ/m^2) for 24 h, or UVA light at 370 nm for 30 min (energy dose of ~10 kJ/m^2), there was a significant formation of lesions at the 50 µg/mL dose and at the 5 and 50 µg/mL doses, respectively (Petersen et al., 2014). Thus, photoactivation appears to be an important mechanism of increasing cytotoxicity of TiO_2NPs. However, the majority of studies investigating TiO_2NPs toxicity did not take photoactivation into account and performed test either in dark conditions or under indoor commercial artificial lighting that did not simulate natural solar irradiation (Jovanović, 2015). In our case, although the comet assays experiments, as well as the exposure times, were always performed under dark conditions no matter what the substance was, while other culture procedures were done in the bench and under artificial laboratory lights. However, many other *in vitro* studies using the comet assay have shown that non-photoactivated TiO_2NPs can also induce significant levels of single strand breaks. Thus, the inherent capacity of TiO_2NPs to induce oxidative damage to DNA without photoactivation is unclear. More importantly, the capacity of using the comet assay to characterize and accurately measure the purported DNA damage from TiO_2NPs has also been seriously questioned as a result of false-positive outcomes (Rajapakse et al., 2013).

In agreement with our aforementioned confocal images that showed an active cell uptake and a clear TiO_2NPs/cell nucleus interaction, general DNA strand breaks were thereby readily detected after 24 h of TiO_2NPs-S, TiO_2NPs-R and TiO_2NPs-W exposure. Interestingly, genotoxic damage was persistent after 48 h of TiO_2-R treatment, which were the most bio-persistent TiO_2NPs over the intestinal epithelium model. Again, results did not clarify if both cell types modulated the damage equally or not. Both, Caco-2 and HT29 cell types may present different cell uptake rates, and thus, different adverse toxic effects, so more efforts should be done in order to elucidate that. One solution that is currently being carried out in our laboratory is to set up a “cell sorting” protocol in order to separate both cell populations. From a separation perspective, cell sorting is an indispensable technology, as heterogeneous cell suspensions can be purified into fractions containing a single cell type based upon virtually unlimited combinations of user-defined parameters. Moreover, beyond its exceptionally accurate and analytical nature, sorting has been demonstrated to be non-destructive to the cells processed, with little to no effect on cell viability or function (Ibrahim and van den Engh, 2007). Briefly, once the *in vitro* barrier has been exposed to the desired compound, the barrier is homogenized by individualizing the cells in a cell suspension. Then, the two cell types are marked by using specific cell markers (e.g. an antibody anti-ZO-1, anti-mucus components, or anti-brush border proteins

such as DPP4 and VIL1) (Mariadason et al., 2002). After that, both cell populations can be separated using a flow cytometer and recovered to further analyze them separately. In addition to the use of cell markers, other parameters such as cell size and cell scattering can be used to divide the mixed cell population. However exposure of each cell line using separated monocultures does not closely represent the physiology of the small intestine, because differentiated Caco-2 cells will not be covered by the protective mucus layer and the HT29 cells will present a different growth aspect and culture ratio.

According to recent studies, the DNA-damaging potential of NPs' is very controversial because, at least *in vitro*, both positive and negative genotoxic results are reported for the same NP. An interesting review indicated that the *in vitro* studies evaluating the genotoxicity of TiO_2NPs reported more positive results than the *in vivo* studies. Also, it concluded that assays for DNA and chromosome damage have produced more positive outcomes than those measuring gene mutations (Chen et al., 2013). This would indicate the presence of undetected confounding factors affecting genotoxicity. Therefore, further investigations using different genotoxic approaches are needed to elucidate the exact molecular mechanisms of TiO_2NPs toxicity. For example, the commonly used *in vitro* micronucleus-formation assay (MN) is a likely choice among a battery of genotoxic assays for rapid and effective screening of NPs' gentoxic potential using high throughput methodologies. The use of flow cytometry, based on the work of Nüsse and Kramer, is currently a useful tool in nanotoxicology, however, the conventional cytokinesis-bock micronucleus assay (CBMN cyt) cannot be used in our situation, since differentiated Caco-2 cells stop dividing when forming the barrier, and micronucleus formation requires cell division (Nüsse and Kramer, 1984; Thomas and Fenech, 2011). As an alternative, other studies have been proposed, like those using C-terminal phosphorylated histone protein (γH2AX) as a potential biomarker of DNA double-strand breaks (DSB) (Collins et al., 2016).

4.3. TiO_2NPs and SiO_2NPs may alter the digestive activity of the small intestine

Regarding the third study, two different assays were developed and set-up for the first time using the Caco-2/HT29-MTX model, in order to assess the activity of diverse brush border enzymes. Concretely, the aminopeptidase-N (APN) and the Na^+/K^+ ATPase activity assays were adapted and enhanced from previous works (Ferruzza et al., 2012; El-Zein et al., 2015). In view of the large number of ENMs currently in use, high throughput screening (HTS) techniques are clearly needed and, consequently,

efforts must be put into that task (Nel et al., 2013; Collins et al., 2016). To this aim, we worked with 96 well culture plates, where cells were seeded at a density of 50,000 cells/cm^2 and maintained during 2 weeks until the monolayer formation (Mahler et al., 2009). Moreover, the intestinal alkaline phosphatase assay was also adapted to 96 well culture plates and used for further experiments. Thus, the use of 96 well culture plates and the fact that the assays were performed by colorimetry permitted us to test up to four different ENMs, at different concentrations and using different physiological conditions at the same time and in a few minutes.

Using the systemic *in vitro* model Caco-2/HT29-MTX for the ENPs risk assessment, the enzyme activities of IAP, APN and Na^+/K^+ ATPase were measured after an acute exposure of 4 h to low, medium and high doses (specified in Study 3) of SiO_2NPs and TiO_2NPs suspended in DMEM-10%Hi-FBS cell culture medium. Although previous studies indicated that neither TiO_2NPs nor SiO_2NPs were able to produce cytotoxicity over the *in vitro* barrier (Guo et al., 2017, 2018), our results demonstrated that both types of food-grade NPs were able to cause alterations in IAP and APN activity. Interestingly, Na^+/K^+ ATPase activity was neither altered nor decreased after both TiO_2NPs and SiO_2NPs exposures. These negative findings could be explained by the fact that the Na^+/K^+ ATPase enzyme is localized in the basolateral membrane of the intestinal epithelial cells (Saha et al., 2015), which would complicate its interaction with those NPs retained in the apical part of the intestinal epithelium. Down-regulation of Na^+/K^+ ATPase activity has been postulated to alter the absorption *via* Na-solute co-transporters in human inflammatory bowel disease (IBD) (Wisel and Rajendren, 1997).

In the gastrointestinal tract, there is a modulation of the pH values that change along the various sections of the system. The stomach is characterized by an acidic environment with an early-stage pH range of 1.2-2.0. When the bolus is formed, however, the pH reaches values of 5.0, followed by slow re-acidification. Finally, digestion and absorption processes are carried out by the small intestine at the duodenum, which has a typical pH value between 6.0 and 7.0 (Matteis, 2017). Thus, the circulation of NPs into and across the GIT can promote physico-chemical changes in the NPs' structure and behavior. Just as food, NPs may further degradate at a low pH in the digestive fluid. These phenomena and ion release were observed in gastric fluids after AgNPs treatment (Axson et al., 2015). However, other studies suggested that oscillations in the pH showed a moderate increase in TiO_2NPs and SiO_2NPs size, postulating that the particles may have undergone further agglomeration or structural rearrangement in the gastric digestion stage under more acidic pH conditions combined with high electrolyte concentrations (Peters et al., 2012; Li et al., 2017). In

order to simulate this digestion process, both NPs were previously digested *in vitro* following a stepwise digestion method described elsewhere (Mahler et al., 2009). Thus, when the *in vitro* barrier was exposed to the digested NPs, IAP and APN activities were even more significantly altered, while no changes were found for the Na^+/K^+ ATPase activity. This reinforces the hypothesis that bigger NPs agglomerations entrapped in the apical part of the membrane can produce more general adverse effects to the brush border functions and to its enzymes activities in particular.

The registered effects of the toxicity of NPs upon *in vivo* oral exposure intrinsically include the protective action of the microorganisms that populate the internal surfaces of the body. Recently, numerous studies have shown that intestinal microbiota are very important in the modulation of human health and disease (Schulz et al., 2014; Chassaing et al., 2015). Principally, it has been shown the importance of commensal microorganisms, which present a symbiotic relationship with the host and have critical and distinct roles for the proper functioning of intestines (Marchesi et al., 2016; Schirmer et al., 2016). The imbalance of intestinal flora could be induced by various environmental factors, such as environmental contaminants, particulate matter and antibiotics (Kish et al., 2013; Lu et al., 2014; Williams et al., 2015). In the case of the food grade TiO_2- and SiO_2NPs, it has been reported that after an *in vivo* chronic exposure of 7 days to both NPs, no overall toxicity was observed (Chen et al., 2017). However, there was increased pro-inflammatory cytokine levels (IL-1β, IL-6 and TNF-α) in the colon of mice ingesting SiO_2NPs. Also, no disturbance of the gut microbiota was found in mice that ingested TiO_2NPs, while those ingesting SiO_2NPs increased microbial species richness and diversity within the intestinal tract and, in particular, of the genus *Lactobacillus* (Chen et al., 2017). Similar results were obtained by other authors, as no major effect on human gut microbiota was documented when testing different sources of food-grade TiO_2NPs (Dudefoi et al., 2017; Waller et al., 2017). In our study, we investigated the potential of two well-known commensal strains of bacteria to mitigate the effects of digested TiO_2NPs and SiO_2NPs over the Caco-2/HT29-MTX monolayer. As pointed out in the third study, *Lactobacillus rhamnosus* attenuated the effects of both NPs on IAP activity. However, neither *Escherichia coli* nor *L. rhamnosus* could reduce the adverse effect of both NPs over APN activity. Curiously, when co-culturing the *in vitro* model with *E. coli*, the activity of Na^+/K^+ ATPase was compromised. Thereby, our results lead us to hypothesize that the probiotic *L. rhamnosus* plays a protective role in our *in vitro* model against ENMs. However, it seems that this protective role is only partial, as *L. rhamnosus* only mitigated the adverse effects of both TiO_2NPs and SiO_2NPs over the IAP activity, but not over APN activity. Toxicity assays on both bacterial strains exposed to both NPs,

digested and non-digested, are needed and currently being developed for the proper analysis and comprehension of these results. Moreover, given the likelihood of human oral uptake of food-grade containing nano-sized particles, further experiments on chronic NPs exposures are needed to understand the actual effects on a real GIT environment. Our results constitute the first data dealing with the effect of ENMs over diverse brush border enzyme's activity using the Caco-2/HT29-MTX, since no literature data was found to compare it with. Moreover, the efforts carried out to set up an *in vitro* intestinal model which tries to physiologically mimic as much as possible the real conditions of an small intestine by co-culturing human cells with commensal microbiota and simulating a digestion process should also be emphasized.

Finally, the increased interest that is generating the use of *in vitro* cell lines and their combinations for the toxico-kinetic analysis of ENMs due, among other reasons, their potential for high throughput screening should be highlighted. The use of human-derived cell lines gives good reproducibility of the models systems (Caco-2/HT29, Caco-2/HT29-MTX and Caco-2/HT29/Raji-B) and there are several reports establishing good correlations between these models and human *in vivo* studies (Mahler et al., 2009; Chen et al., 2010; Mahler et al., 2012; Araújo and Sarmento, 2013). However, due to the vast quantities of newly designed ENMs and their huge physico-chemical differences, further evaluations and comparisons to *ex vivo* tissue and animal studies, followed by standardization of these novel models will help to clarify their applicability and accuracy for the prediction of particle uptake rate in humans (Lefebvre et al., 2015). In this context, it must be remembered that the two cell lines used are easily available and easy to cultivate and, for these reasons, the model is quite easy to use and is efficient for screening purposes. A conclusion for our studies is that the ratio between the two cell types is crucial for the formation of a homogeneous mucin layer, which is of great importance for modeling the *in vivo* situation. Moreover, these models have been described to present many of the transporters/carriers found in normal human intestinal epithelium by the two cell lines. In spite of that, and due to the described mosaicism, it is recommended that, in the case of transport studies, the expression of the anlayzed molecules should be previously checked. Moreover, the 3D distribution conferred by the polyethylene terephthalate (PET) inserts, which separate both environments (the lumen part from the lamina propria), lead to multiple experimental-parameters combinations. For example, by adding microbiota in the apical part and co-culturing with the epithelial barrier, the study of the role of a specific commensal or pathogen on the barrier functionality will be possible. Also, with the addition of cells from the immune system in the basolateral chamber such as lymphocytes, macrophages or dendritic cells, we could

investigate their role in the protection against potential pathogenic phenomena.

As always, several limitations and possible solutions arise. Despite of the advantages of using immortalized cells, extrapolation of data generated with these cell lines to *in vivo* conditions is often difficult, since cells originated from tumours and may therefore not be representative of the real physiological environment. Also, simple cell culture systems using established cell lines do not take into account factors such as age and sex, or the lack of systemic circulation pathways such as the enterohepatic secretion of absorbed materials back into the GIT lumen. Other aspects lacking in the *in vitro* models are GIT lumen characteristics such as digestion by-products or the specific peristaltic GIT movements (Lefebvre et al., 2015). However, emerging approaches to account for different genotypes could possibly be developed, such as the use of induced pluripotent stem cells (Gracz et al., 2013). In addition, the InLiveTox project (http://www.inlivetox.eu/) has developed a multi-tissue fluidic model that allows flow above and below a Caco-2 monolayer, with the basolateral flow linked to endothelial and hepatocyte culture. More physiologically relevant culture fluids can be used and added to the model in order to reflect the fasted and fed states (Patel et al., 2006).

Overall, several categories of *in vitro* models are used for the assessment of conventional food and drug chemicals and, when standardized, they may have the potential to show good *in vitro* to *in vivo* correlations. According to this, there is a need to further adapt and standardize the available models and their corresponding analytical methods to allow quantification of the digestive fate of engineered NMs, including uptake across the gastrointestinal barrier.

5.CONCLUSIONS

5. CONCLUSIONS

In agreement with the objectives of the present Thesis, which mainly aimed to assess the effects and behavior of three differently-shaped TiO_2NPs over the systemic *in vitro* Caco-2/HT29 model, the obtained results lead us to the following conclusions:

1. The first objective was achieved, as the *in vitro* Caco-2/HT29/Raji-B barrier was well-established at a seeding ratio of 90% Caco-2 and 10% HT29. This co-culture condition presented a well-organized cell distribution, a good barrier integrity and an homogeneous mucus layer scattering.

2. Although the *in vitro* Caco-2/HT29/Raji-B barrier was well-established, M cells' detection was difficult and could hinder the ENMs risk assessment results interpretation. Consequently, Caco-2/HT29 co-cultures were used for further experiments instead of Caco-2/HT29/Raji-B.

3. Regarding the third objective, exposing the *in* vitro Caco-2/HT29 model to all the selected TiO_2NPs shapes determined significant impairments in the barrier in a time- and shape-dependent manner. Interestingly, the effects were not concentration-dependent. The specific conclusions of this objective were:
    a. All the tested shapes of TiO_2NPs were able to impair the barrier's integrity and increase the barrier's permeability after 48 h of exposure.
    b. The three TiO_2NPs were able to translocate through the barrier, though the shape was important for the modality of translocation: spheres and rods were more likely to cross the barrier using an intracellular path, while wires crossed the barrier paracellularly.
    c. All the different shapes of TiO_2NPs were internalized readily after 24 h. The internalization was found to be size and shape-dependent, as the smaller agglomerations of nano-spheres and nano-rods were highly detected inside the cells than nano-wires.
    d. None of the three different shapes of TiO_2NPs produced oxidative DNA damage, however, general DNA damage was readily seen after 24 h of exposure to the three shapes of TiO_2NPs. Only the nano-rods were able to sustain the DNA damage after exposures lasting for 48 h.
    e. All TiO_2NPs induced significant changes in the gene expression of *ALPI*, *SI* and *SLC15A1*, suggesting a dysfunction in the nutrients digestion activity after being exposed to TiO_2NPs. The NPs also induced the upregulation of *ZO-1*, *OCLN* and *CLDN2* transcription, components of the junctional

complex, suggesting the active TJ repair in response to the barrier's stability loss.

4. Regarding the studies carried out during the three-month internship at Binghamton University and the respective planned objectives, we concluded that:

   a. We were able to successfully set up two fast and reliable data for the APN and Na^+/K^+ ATPase activity analysis using colorimetric-based assays in 96-well cell culture plates.

   b. IAP and APN, but not Na^+/K^+ ATPase activity, were significantly altered after exposing the systemic model Caco-2/HT29-MTX to both TiO_2NPs and SiO_2NPs NPs at the three different physiological conditions (non-digested NPs, *in vitro* digested NPs and *in vitro* digested co-cultured with *Escherichia coli* and *Lactobacillus rhamnosus*).

6. REFERENCES

6. REFERENCES

Abreu, M. T. (2010). Toll-like receptor signalling in the intestinal epithelium: How bacterial recognition shapes intestinal function. *Nature Reviews Immunology*, *10*(2), 131–143.

Aillon, K. L., Xie, Y., El-Gendy, N., Berkland, C. J., & Forrest, L. M. (2010). Effects of nanomaterial physicochemical properties on in vivo toxicity. *Advanced Drug Delivety Review*, *61*(6), 457–466.

Aitken, R. J., Creely, K. S., & Tran, C. L. (2004). Nanoparticles : an occupational hygiene review prepared by the institute of occupational medicine nanoparticles : An occupational hygiene review. *Health and Safety Executive*, 1–113.

Amenta, V., Aschberger, K., Arena, M., Bouwmeester, H., Botelho Moniz, F., Brandhoff, P., Peters, R. J. (2015). Regulatory aspects of nanotechnology in the agri/feed/food sector in EU and non-EU countries. *Regulatory Toxicology and Pharmacology*, *73*(1), 463–476.

Antunes, F., Andrade, F., Araújo, F., Ferreira, D., & Sarmento, B. (2013). Establishment of a triple co-culture in vitro cell models to study intestinal absorption of peptide drugs. *European Journal of Pharmaceutics and Biopharmaceutics*, *83*(3), 427–435.

Araújo, F., & Sarmento, B. (2013). Towards the characterization of an in vitro triple co-culture intestine cell model for permeability studies. *International Journal of Pharmaceutics*, *458*(1), 128–134.

Armstrong, A. R., Armstrong, G., Canales, J., & Bruce, P. G. (2004). TiO2-B Nanowires. *Angewandte Chemie*, *116*(17), 2336–2338.

Arts, J. H. E., Hadi, M., Keene, A. M., Kreiling, R., Lyon, D., Maier, M., Landsiedel, R. (2014). A critical appraisal of existing concepts for the grouping of nanomaterials. *Regulatory Toxicology and Pharmacology*, *70*(2), 492–506.

Artursson, P. (1991). Cell cultures as models for drug absorption across the intestinal mucosa. *Critical Reviews in Therapeutic Drug Carrier Systems*, *8*(4), 305–30.

Artursson, P., Palm, K., & Luthman, K. (2001). Caco-2 monolayers in experimental and theoretical predictions of drug transport. *Advanced Drug Delivery Reviews*, *46*(1–

3), 27–43.

Axson, J. L., Stark, D. I., Bondy, A. L., Capracotta, S. S., Maynard, A. D., Philbert, M. A., Ault, A. P. (2015). Rapid kinetics of size and pH-dependent dissolution and aggregation of silver nanoparticles in simulated gastric fluid. *The Journal of Physical Chemistry C*, *119*(35), 20632–20641.

Basketter, D. A., Clewell, H., Kimber, I., Rossi, A., Blaauboer, B., Burrier, R., Hartung, T. (2012). A roadmap for the development of alternative (non-animal) methods for systemic toxicity testing. *Altex*, *29*(1), 3–91.

Beaulieu, J. F., & Quaroni, A. (1991). Clonal analysis of sucrase-isomaltase expression in the human colon adenocarcinoma Caco-2 cells. *Biochemical Journal*, *280*, 599–608.

Behrens, I., Stenberg, P., Artursson, P., & Kissel, T. (2001). Transport of lipophilic drug molecules in a new mucus-secreting cell culture model based on HT29-MTX cells. *Pharmaceutical Research*, *18*(8), 1138–1145.

Bekker, C., Brouwer, D. H., Tielemans, E., & Pronk, A. (2013). Industrial production and professional application of manufactured nanomaterials-enabled end products in dutch industries: potential for exposure. *The Annals of Occupational Hygiene*, *57*(3), 314–327.

Bennat, C., & Müller-Goymann, C. (2000). Skin penetration and stabilization of formulations containing microfine titanium dioxide as physical UV filter. *International Journal of Cosmetic Science*, *22*, 271–283.

Bhatia, S. (2016). Nanoparticles types, classification, characterization, fabrication methods. *Natural Polymer Drug Delivery Systems,* Chapter 2, 33–93.

Björk, M. T., Thelander, C., Hansen, A. E., Jensen, L. E., Larsson, M. W., Wallenberg, L. R., & Samuelson, L. (2004). Few-electron quantum dots in nanowires. *Nano Letters*, *4*(9), 1621–1625.

Bouwmeester, H., Dekkers, S., Noordam, M. Y., Hagens, W. I., Bulder, A. S., de Heer, C., Sips, A. J. A. M. (2009). Review of health safety aspects of nanotechnologies in food production. *Regulatory Toxicology and Pharmacology*, *53*(1), 52–62.

Bouwmeester, H., Zande, M. Van Der, & Jepson, M. A. (2017). Effects of food-borne nanomaterials on gastrointestinal tissues and microbiota. *WIREs Nanomedicine*

and Nanobiotechnology, *10*, 1–12.

Braakhuis, H. M., Kloet, S. K., Kezic, S., Kuper, F., Park, M. V. D. Z., Bellmann, S., Bouwmeester, H. (2015). Progress and future of in vitro models to study translocation of nanoparticles. *Archives of Toxicology*, *89*, 1469–1495.

Brouwer, D. (2010). Exposure to manufactured nanoparticles in different workplaces. *Toxicology*, *269*(2), 120–127.

Brun, E., Barreau, F., Veronesi, G., Fayard, B., Sorieul, S., Chanéac, C., Carrière, M. (2014). Titanium dioxide nanoparticle impact and translocation through ex vivo, in vivo and in vitro gut epithelia. *Particle and Fibre Toxicology*, *11*.

Buzea, C., Blandino, I. I. P., & Robbie, K. (2007). Nanomaterials and nanoparticles : Sources and toxicity. *Biointerphases, 2*(4), 1–103.

Carriere, M., Sauvaigo, S., Douki, T., & Ravanat, J.-L. (2017). Impact of nanoparticles on DNA repair processes: current knowledge and working hypotheses. *Mutagenesis*, *32*(1), 203–213.

Charitidis, C. A., Georgiou, P., Koklioti, M. A., Trompeta, A., & Markakis, V. (2014). Manufacturing nanomaterials: from research to industry. *Manufacturing Review*, *1*, 1–11.

Chassaing, B., Koren, O., Goodrich, J. K., Poole, A. C., Srinivasan, S., Ley, R. E., & Gewirtz, A. T. (2015). Dietary emulsifiers impact the mouse gut microbiota promoting colitis and metabolic syndrome. *Nature*, *519*, 92–96.

Chaudhry, M. Q., Boxall, A. B. A., Aitken, R. J., & Hull, M. (2006). Manufacture and use of nanomaterials : current status in the UK and global trends. *Occupacional Medicine*, *56*, 300–306.

Chen, H., Zhao, R., Wang, B., Cai, C., Zheng, L., Wang, H., Feng, W. (2017). The effects of orally administered Ag, TiO2 and SiO2 nanoparticles on gut microbiota composition and colitis induction in mice. *NanoImpact*, *8*(July), 80–88.

Chen, J., Zhou, H., Santulli, A. C., & Wong, S. S. (2010). Evaluating Cytotoxicity and Cellular Uptake from the Presence of Variously Processed TiO2 Nanostructured Morphologies. *Chemical Research in Toxicology*, *23*(5), 871–879.

Chen, L., Yokel, R. A., Hennig, B., & Toborek, M. (2008). Manufactured aluminum oxide nanoparticles decrease expression of tight junction proteins in brain

vasculature. *Journal of Neuroimmune Pharmacology : The Official Journal of the Society on NeuroImmune Pharmacology*, *3*(4), 286–295.

Chen, T., Yan, J., & Li, Y. (2014). Genotoxicity of titanium dioxide nanoparticles. *Journal of Food and Drug Analysis*, 22(1), 95-104.

Chen, X.-X., Cheng, B., Yang, Y.-X., Cao, A., Liu, J.-H., Du, L.-J., Wang, H. (2013). Characterization and preliminary toxicity assay of nano-titanium dioxide additive in sugar-coated chewing gum. *Small*, *9*(9–10), 1765–1774.

Chen, X. M., Elisia, I., & Kitts, D. D. (2010). Defining conditions for the co-culture of Caco-2 and HT29-MTX cells using Taguchi design. *Journal of Pharmacological and Toxicological Methods*, *61*(3), 334–342.

Cho, W., Kang, B., Lee, J. K., Jeong, J., & Che, J. (2013). Comparative absorption , distribution, and excretion of titanium dioxide and zinc oxide nanoparticles after repeated oral administration. *Particle and Fibre Toxicology*, *10*, 1–9.

Ciappellano, S. G., Tedesco, E., Venturini, M., & Benetti, F. (2016). In vitro toxicity assessment of oral nanocarriers. *Advanced Drug Delivery Reviews*, *106*(Part B), 381–401.

Clark, K. A., O'Driscoll, C., Cooke, C. A., Smith, B. A., Wepasnick, K., Fairbrother, D. H., Bressler, J. P. (2012). Evaluation of the interactions between multiwalled carbon nanotubes and caco-2 cells. *Journal of Toxicology and Environmental Health, Part A*, *75*(1), 25–35.

Code of Federal Regulations (CFR).Title 21, updated April 1, 2016.https://www.accessdata.fda.gov/scripts/cdrh/cfdocs/cfcfr/CFRSearch.cfm.

Collins, A. R., Annangi, B., Rubio, L., Marcos, R., Dorn, M., Merker, C., Ribeiro, A. R. (2016). High throughput toxicity screening and intracellular detection of nanomaterials. *Nanomedicine and Nanobiotechnology, 9*(1), 1–30.

Corr, S. C., Gahan, C. C. G. M., & Hill, C. (2008). M-cells: origin , morphology and role in mucosal immunity and microbial pathogenesis. *FEMS Immunology and medical microbiology, 52(1)*, 2–12.

De Matteis, V., Cascione, M., Brunetti, V., Toma, C. C., & Rinaldi, R. (2016). Toxicity assessment of anatase and rutile titanium dioxide nanoparticles: The role of degradation in different pH conditions and light exposure. *Toxicology in Vitro*, *37*, 201–210.

Debia, M., Beaudry, C., Weichenthal, S., Ardif, R., & Dufresne, A. (2013). Characterization and control of occupational exposure to nanoparticles and ultrafine particles. *Institut de recherche Robert-Sauvé en santé et en securité du travail (IRSST)*. Report R-777.

Denker, B. M., & Nigam, S. K. (1998). Molecular structure and assembly of the tight junction, *The American Journal of Physiology*, 274(1 Pt 2):F 1–9.

des Rieux, A., Fievez, V., Théate, I., Mast, J., Préat, V., & Schneider, Y.-J. (2007). An improved in vitro model of human intestinal follicle-associated epithelium to study nanoparticle transport by M cells. *European Journal of Pharmaceutical Sciences*, *30*(5), 380–391.

Diebold, U. (2003). The surface science of titanium dioxide. *Surface Science Reports*, *48*(5–8), 53–229.

Dodd, N. J. F., & Jha, A. N. (2011). Photoexcitation of aqueous suspensions of titanium dioxide nanoparticles: an electron spin resonance spin trapping study of potentially oxidative reactions. *Photochemistry and Photobiology*, *87*(3), 632–640.

Donaldson, K., Poland, C. A., & Schins, R. P. F. (2010). Possible genotoxic mechanisms of nanoparticles: Criteria for improved test strategies. *Nanotoxicology*, *4*(4), 414–420.

Dorier, M., Béal, D., Marie-desvergne, C., Dubosson, M., Barreau, F., Houdeau, E., Carriere, M. (2017). Continuous in vitro exposure of intestinal epithelial cells to E171 food additive causes oxidative stress , inducing oxidation of DNA bases but no endoplasmic reticulum stress. *Nanotoxicology*, *11*(6), 751–761.

Dorier, M., Brun, E., Veronesi, G., Barreau, F., Desvergne, C., Rabilloud, T., Carrière, M. (2015). Impact of anatase and rutile titanium dioxide nanoparticles on uptake carriers and efflux pumps in Caco-2 gut epithelial cells. *Nanoscale*, *7*, 7352–7360.

Drescher, D., Giesen, C., Traub, H., Panne, U., Kneipp, J., & Jakubowski, N. (2012). Quantitative imaging of gold and silver nanoparticles in single eukaryotic cells by laser ablation ICP-MS. *Analytical Chemistry*, *84*(22), 9684–9688.

Dudefoi, W., Moniz, K., Allen-Vercoe, E., Ropers, M.-H., & Walker, V. K. (2017). Impact of food grade and nano-TiO2 particles on a human intestinal community. *Food*

and Chemical Toxicology, *106*, 242–249.

DuPont. (2007). *DuPont ™ Ti-Pure titanium dioxide - Titanium Dioxide For Coatings*. https://www.chemours.com/Titanium_Technologies/es_US/tech_info/literature/Coatings/CO_B_H_65969_Coatings_Brochure.pdf

ECO. (2009). The European Consumer Organization. hhtp://www.beuc.org/

EFSA. (2011). *Guidance on the risk assessment of the application of nanoscience and nanotechnologies in the food and feed chain*. *EFSA Journal* (Vol. 9).

EFSA. (2016). Re-evaluation of titanium dioxide (E 171) as a food additive. *EFSA Journal*, *14*(9), e04545.

El-Zein, O., Usta, J., El Moussawi, L., & Kreydiyyeh, S. I. (2015). Leptin inhibits the Na+/K+ ATPase in Caco-2 cells via PKC and p38MAPK. *Cellular Signalling*, *27*(3), 416–423.

FAO/WHO. Expert meeting on the application of nanotechnologies in he food and agriculture sectors: potential food safety implications. Meeting report http://www.fao.org/docrep/012/i1434e/i1434e00.pdf. 20102

Faust, J. J., Doudrick, K., Yang, Y., Westerhoff, P., & Capco, D. G. (2014). Food grade titanium dioxide disrupts intestinal brush border microvilli in vitro independent of sedimentation. *Cell Biology and Toxicology*, *30*, 169–188.

Faust, J. J., Masserano, B. M., Mielke, A. H., Abraham, A., & Capco, D. G. (2014). Engineered Nanoparticles Induced Brush Border Disruption in a Human Model of the Intestinal Epithelium BT - Nanomaterial: Impacts on Cell Biology and Medicine. *Advances in Experimental Medicine and Biology*, *811*, 55–72.

Ferruzza, S., Rossi, C., Scarino, M. L., & Sambuy, Y. (2012). A protocol for in situ enzyme assays to assess the differentiation of human intestinal Caco-2 cells. *Toxicology in Vitro*, *26*(8), 1247–1251.

Foldvari, M., & Bagonluri, M. (2008). Carbon nanotubes as functional excipients for nanomedicines: II. Drug delivery and biocompatibility issues. *Nanomedicine*, *4*, 183–200.

Forstner, J., Forstner, G., Gastrointestinal mucus. In physiology of the gastrointestinal tract; Johnson, L. R., Ed.; Raven Press: New York, 1994; Vol. 1994; pp 1255−83. (39).

Forstner, G., Wesley, A., & Forstner, J. (1982). Clinical Aspects of Gastrointestinal Mucus BT - Mucus in Health and Disease—II. In E. N. Chantler, J. B. Elder, & M. Elstein (Eds.), *Advances in experimental medicine and biology* (pp. 199–224). Boston, MA: Springer US.

Gabor, F., Bogner, E., Weissenboeck, A., & Wirth, M. (2004). The lectin-cell interaction and its implications to intestinal lectin-mediated drug delivery. *Advanced Drug Delivery Reviews*, *56*(4), 459–480.

Gao, X., Yang, L., Petros, J. A., Marshall, F. F., Simons, J. W., & Nie, S. (2005). In vivo molecular and cellular imaging with quantum dots. *Current Opinion in Biotechnology*, *16*(1), 63–72.

Gartia, M. R., Hsiao, A., Pokhriyal, A., Seo, S., Kulsharova, G., Cunningham, B. T., Liu, G. L. (2013). Colorimetric Plasmon Resonance Imaging Using Nano Lycurgus Cup Arrays. *Advanced Optical Materials*, *1*(1), 68–76.

Gato, W. E., Hunter, D. A., Byrd, I. C., Mays, C. A., Yau, W., & Wu, J. (2017). Assessment of the short-term toxicity of TiO2 nanofiber in Sprague Dawley rats. *Environmental Toxicology*, *32*(6), 1775–1783.

Gatoo, M. A., Naseem, S., Arfat, M. Y., Dar, A. M., Qasim, K., & Zubair, S. (2014). Physicochemical Properties of Nanomaterials : Implication in Associated Toxic Manifestations. *BioMed Research International*, *2014*(498420).

Geraets, L., Oomen, A. G., Krystek, P., Jacobsen, N. R., Wallin, H., Laurentie, M., Jong, W. H. De. (2014). Tissue distribution and elimination after oral and intravenous administration of different titanium dioxide nanoparticles in rats. *Particle and Fibre Toxicology Toxicology*, *11*(30), 1–21.

Gerloff, K., Fenoglio, I., Carella, E., Kolling, J., Albrecht, C., Boots, A. W., Schins, R. P. F. (2012). Distinctive Toxicity of TiO2 Rutile/Anatase Mixed Phase Nanoparticles on Caco-2 Cells. *Chemical Research in Toxicology*, *25*(3), 646–655.

Giannasca, P. J., Giannasca, K. T., Falk, P., Gordon, J. I., & Neutra, M. R. (1994). Regional Differences in Glycoconjugates of Intestinal M-Cells in Mice - Potential Targets for Mucosal Vaccines. *American Journal of Physiology-Gastrointestinal and Liver Physiology*, *267*(6), G1108–G1121.

Giannasca, P. J., Giannasca, K. T., Leichtner, A. M., & Neutra, M. R. (1999). Human intestinal M cells display the sialyl Lewis A antigen. *Infection and Immunity*, *67*(2),

946–53.

Golovkina, T. V, Shlomchik, M., Hannum, L., & Chervonsky, A. (1999). Organogenic Role of B Lymphocytes in Mucosal Immunity. *Science*, *286*(5446), 1965 LP-1968.

Gordon, S., DAneshian, Ma., Bouwstra, J., Caloni, F., & Leher, C. M. (2015). Non-Animal Models of Epithelial Barriers (Skin , Intestine and Lung) in Research , Industrial Applications and Regulatory Toxicology. *Altex*, *32*(4), 327–378.

Gracz, A. D., Fuller, M. K., Wang, F., Li, L., Stelzner, M., Dunn, J. C., Magness, S. T. (2013). CD24 and CD44 mark human intestinal epithelial cell populations with characteristics of active and facultative stem cells. *Stem Cells*, *31*(9), 2021–2030.

Grassian, V. H., Shaughnessy, P. T. O., Adamcakova-dodd, A., Pettibone, J. M., & Thorne, P. S. (2007). Inhalation Exposure Study of Titanium Dioxide Nanoparticles with a Primary Particle Size of 2 to 5 nm. *Environmental Health Perspectives*, *115*(3), 397–402.

Grieger, K. D., Hansen, S. F., Mortensen, N. P., Cates, S., & Kowalcyk, B. (2016). International Implications of Labeling Foods Containing Engineered Nanomaterials. *Journal of Food Protection*, *79*(5), 830–842.

Gullberg, E., Keita, Å. V, Salim, S. Y., Andersson, M., Caldwell, K. D., So, J. D., & Artursson, P. (2006). Identification of Cell Adhesion Molecules in the Human Follicle- Associated Epithelium That Improve Nanoparticle Uptake into the Peyer ' s Patches. *The Journal Pharmcology And Experimental Therpeutics*, *319*(2), 632–639.

Gullberg, E., Leonard, M., Karlsson, J., Hopkins, A. M., Brayden, D., Baird, A. W., & Artursson, P. (2000). Expression of Specific Markers and Particle Transport in a New Human Intestinal M-Cell Model. *Biochemical and Biophysical Research Communications*, *279*(3), 808–813.

Gulson B, McCall MJ, Bowman DM, Pinheiro T. A review of critical factors for assessing the dermal absorption of metal oxide nanoparticles from sunscreens applied to humans, and a research strategy to address current deficiencies. Archives of Toxicology. 2015. 89(11):1909-30.

Guo, Z., Martucci, N. J., Moreno-olivas, F., Tako, E., & Mahler, G. J. (2017). NanoImpact Titanium dioxide nanoparticle ingestion alters nutrient absorption in an in vitro model of the small intestine. *NanoImpact*, *5*, 70–82.

Guo, Z., Martucci, N., Liu, Y., Yoo, E., Tako, E., & Mahler, G. (2018). Silicon dioxide nanoparticle exposure affects small intestine function in an in vitro model. *Nanotoxicology*, Unpublished.

Guttman, J. A., & Finlay, B. B. (2009). Tight junctions as targets of infectious agents. *Biochimica et Biophysica Acta - Biomembranes*, *1788*(4), 832–841.

Halleux, C., & Schneider, Y.-J. (1991). Iron absorption by intestinal epithelial cells: 1. CaCo2 cells cultivated in serum-free medium, on polyethyleneterephthalate microporous membranes, as an in vitro model. *In Vitro Cellular & Developmental Biology - Animal*, *27*(4), 293–302.

Han, O., & Wessling-Resnick, M. (2002). Copper repletion enhances apical iron uptake and transepithelial iron transport by Caco-2 cells. *American Journal of Physiology. Gastrointestinal and Liver Physiology*, *282*(3), G527-33.

Hanaor, D. A. H., Michelazzi, M., Leonelli, C., Sorrell, C. C., Hanaor, D. A. H., Michelazzi, M., … Sorrell, C. C. (2012). The Effects of Carboxylic Acids on the Aqueous Dispersion and Electrophoretic Deposition of ZrO 2. *Journal of the European Ceramic Society*, *32*(321), 235–244.

Hansen, G. H., Rasmussen, K., Niels-Christiansen, L.-L. L., & Danielsen, E. M. (2009). Endocytic trafficking from the small intestinal brush border probed with FM dye. *American Journal of Physiology. Gastrointestinal and Liver Physiology*, *297*(4), G708–G715.

Hanus, M. J., & Harris, A. T. (2013). Nanotechnology innovations for the construction industry. *Progress in Materials Science*, *58*(7), 1056–1102.

Harhaj, N. S., & Antonetti, D. A. (2004). Regulation of tight junctions and loss of barrier function in pathophysiology. *The International Journal of Biochemistry & Cell Biology*, *36*(7), 1206–1237.

Haas KH (2013) Industrial relevant production processes for nanomaterials and nanostructures. In: Luther W ZA (ed) Safety aspects of engineered nanomaterials. Pan Standford Publishing Pte. Ltd., Singapore, pp 30–66

Hartung, T., Luechtefeld, T., Maertens, A., & Kleensang, A. (2013). Food for Thought Integrated Testing Strategies for Safety Assessments. *ALTEX*, *30*(1), 3–18.

Hauri, H.-P., Sterchi, E. E., Bienz, D., Fransen, J. A. M., & Marxer, A. (1985). Expression and intracellular transport of microvillus membrane hydrolases in

human intestinal epithelial cells. *The Journal of Cell Biology*, *101*, 838–851.

Hett, A. (2004). Nanotechnology Small matter, many unknowns. *Swiss Reinsurance Company*, 1–57.

Hidalgo, I. (1996). Cultured intestinal epithelial cell models. *Pharmaceutical Biotechnology*, *8*, 35–50.

Hilgendorf, C., Spahn-langguth, H., Regårdh, C. G., & Lipka, E. (2000). Caco-2 versus Caco-2 / HT29-MTX Co-cultured Cell Lines : Permeabilities Via Diffusion , Inside- and Outside-Directed Carrier-Mediated Transport, *89*(1), 63–75.

Hillyer, J., & M. Albrecht, R. (2001). Gastrointestinal persorption and tissue distribution of differently sized colloidal gold nanoparticles. *Journal of Pharmaceutical Sciences*, *90*(12), 1927–1936.

Hincapié, I., Caballero-Guzman, A., Hiltbrunner, D., & Nowack, B. (2015). Use of engineered nanomaterials in the construction industry with specific emphasis on paints and their flows in construction and demolition waste in Switzerland. *Waste Management*, *43*(Supplement C), 398–406.

Hoek, G., Brunekreef, B., Goldbohm, S., Fischer, P., & Brandt, P. A. Van Den. (2002). Association between mortality and indicators of traffic-related air pollution in the Netherlands : a cohort study. *The Lancet*, *360*, 1203–1209.

Hoet, P. H. ., Geys, J., Nemmar, A., & Nemery, B. (2007). Inhalation of Nanomaterials: Short Overview of the Local and Systemic Effects. *Nanotechnology - Toxicological Issues and Environmental Safety*, 77–90.

Hsiao, I.-L., Bierkandt, F. S., Reichardt, P., Luch, A., Huang, Y.-J., Jakubowski, N., … Haase, A. (2016). Quantification and visualization of cellular uptake of TiO2 and Ag nanoparticles: comparison of different ICP-MS techniques. *Journal of Nanobiotechnology*, *14*(1), 50.

Huet, C., Sahuquillo-Merino, C., Coudrier, E., & Louvard, D. (1987). Absorptive and mucus-secreting subclones isolated from a multipotent intestinal cell line (HT-29) provide new models for cell polarity and terminal differentiation. *The Journal of Cell Biology*, *105*(1), 345–357.

Hummel, T. Z., Kindermann, A., Stokkers, P. C. ., Benninga, M. A., & ten Kate, F. J. . (2014). Exogenous Pigment in Peyer Patches of Children Suspected of Having

IBD. *Journal of Pediatric Gastroenterology and Nutrition*, *58*(4), 477–480.

IARC. (2010). *Monographs on the Evaluation of Carcinogenic Risks to Humans; Carbon Black, Titanium Dioxide and Talc.* (Vol. 93).

Ibrahim, S. F., & van den Engh, G. (2007). Flow Cytometry and Cell Sorting BT - Cell Separation: Fundamentals, Analytical and Preparative Methods. In A. Kumar, I. Y. Galaev, & B. Mattiasson (Eds.) (pp. 19–39). Berlin, Heidelberg: Springer Berlin Heidelberg.

Iyono, B. H. K., & Zegami, T. A. (2015). The mucosal immune system : From dentistry to vaccine development. *Proceeding of the Japan Academy. Series B, Physical and Biological Science*, *91*(8), 423–439.

Jacobs, J. F., Poel, I. Van De, & Osseweijer, P. (2010). Sunscreens with Titanium Dioxide (TiO 2) Nano-Particles : A Societal Experiment, 103–113.

Jiang, J., Oberdörster, G., & Biswas, P. (2009). Characterization of size, surface charge, and agglomeration state of nanoparticle dispersions for toxicological studies. *Journal of Nanoparticle Research*, *11*(1), 77–89.

Johansson, M. E. V, Phillipson, M., Petersson, J., Velcich, A., Holm, L., Hansson, G. C., de Vos, W. M. (2008). The inner of the two Muc2 mucin-dependent mucus layers in colon is devoid of bacteria. *Pnas*, *105*(39), 15064–15069.

Jovanović, B. (2014). Critical Review of Public Health Regulations of Titanium Dioxide, a Human Food Additive. *Integrated Environmental Assessment and Management 11*(1), 10–20.

Jovanović, B. (2015). Review of titanium dioxide nanoparticle phototoxicity: Developing a phototoxicity ratio to correct the endpoint values of toxicity tests. *Environmental Toxicology and Chemistry*, *34*(5), 1070–1077.

Jugan, M.-L., Barillet, S., Simon-Deckers, A., Herlin-Boime, N., Sauvaigo, S., Douki, T., & Carriere, M. (2012). Titanium dioxide nanoparticles exhibit genotoxicity and impair DNA repair activity in A549 cells. *Nanotoxicology*, *6*(5), 501–513.

Kaluza, S., J.K. Balderhaar, B. Orthen, B. Honnert, E. Jankowska, P. Pietrowski, M.G. Rosell, C. Tanarro, J. Tejedor, et A. Zugasti, "Workplace exposure to nanoparticles", ed. J. Kosk-Bienko. 2009, Bilbao, Spain: European Agency for Safety and Health at Work (EU-OSHA). 89.

Kanaya, T., & Ohno, H. (2014). The Mechanisms of M-cell differentiation. *Bioscience of Microbiota, Food and Health*, *33*(3), 91–97.

Katayama, S., Xu, X., Fan, M. Z., & Mine, Y. (2006). Antioxidative stress activity of oligophosphopeptides Derived from Hen Egg Yolk Phosvitin in Caco-2 Cells. *Journal of Agricultural and Food Chemistry*, *54*(3), 773–778.

Kernéis, S., Bogdanova, A., Kraehenbuhl, J.-P., & Pringault, E. (1997). Conversion by Peyer's Patch lymphocytes of human enterocytes into M cells that transport bacteria. *Science*, *277*(5328), 949–952.

Kernéis, S., Caliot, E., Stubbe, H., Bogdanova, A., Kraehenbuhl, J.-P., & Pringault, E. (2000). Molecular studies of the intestinal mucosal barrier physiopathology using cocultures of epithelial and immune cells: a technical update. *Microbes and Infection*, *2*(9), 1119–1124.

Kim, W., Tachikawa, T., Moon, G., Majima, T., & Choi, W. (2014). Molecular-level understanding of the photocatalytic activity difference between anatase and rutile nanoparticles. *Angewandte Chemie International Edition*, *53*(51), 14036–14041.

Kipp, H., Khoursandi, S., Scharlau, D., & Kinne, R. K. H. (2003). More than apical: Distribution of SGLT1 in Caco-2 cells. *American Journal of Physiology. Cell Physiology*, *285*(4), C737-49.

Kish, L., Hotte, N., Kaplan, G. G., Vincent, R., Tso, R., Gänzle, M., … Madsen, K. L. (2013). Environmental particulate matter induces murine intestinal inflammatory responses and alters the gut microbiome. *PLOS ONE*, *8*(4), e62220.

Kreider, M. L., Cyrs, W. D., Tosiano, M. A., & Panko, J. M. (2017). Evaluation of quantitative exposure assessment method for nanomaterials in mixed dust environments : application in tire manufacturing facilities. *Annals of Occupational Hygiene*, *59*(9), 1122–1134.

Kreyling, W. G., Semmler, M., Erbe, F., Mayer, P., Takenaka, S., Schulz, H., & Ziesenis, A. (2011). Translocation fo ultrafine insoluble iridium particles from lung epithelium to extrapulmonary organs is size dependent but very low. *Journal of Toxicology and Environmental Health*, *65*, 1513–1530.

Kucharzik, T., Lügering, N., Rautenberg, K., Lügering, A., Schmidt, M. A., Stoll, R., & Domschke, W. (2000). role of M cells in intestinal barrier function. *Annals of the New York Academy of Sciences*, *915*(1), 171–183.

Kucki, M., Diener, L., Bohmer, N., Hirsch, C., Krug, H. F., Palermo, V., & Wick, P. (2017). Uptake of label-free graphene oxide by Caco-2 cells is dependent on the cell differentiation status. *Journal of Nanobiotechnology*, *15*(1), 1–18.

Kuhlbusch, T. A. J., Asbach, C., Fissan, H., Göhler, D., & Stintz, M. (2011). Nanoparticle exposure at nanotechnology workplaces : A review. *Particle and Fibre Toxicology*, *8*(1), 22.

Lademann, J., Weigmann, H.-J., Rickmeyer, C., Barthelmes, H., Schaefer, H., Mueller, G., & Sterry, W. (1999). Penetration of titanium dioxide microparticles in a sunscreen formulation into the horny layer and the follicular orifice. *Skin Pharmacology and Physiology*, *12*, 247–256.

Lai, Y. H., & D'Souza, M. J. (2008). Microparticle transport in the human intestinal M cell model. *Journal of Drug Targeting*, *16*(1), 36–42.

Laux, P., Tentschert, J., Riebeling, C., Braeuning, A., Creutzenberg, O., & Epp, A. (2017). Nanomaterials: certain aspects of application, risk assessment and risk communication. *Archives of Toxicology*, *92*(1), 121–141.

Lefebvre, D. E., Venema, K., Gombau, L., Valerio, L. G., Raju, J., Bondy, G. S., Stone, V. (2015). Utility of models of the gastrointestinal tract for assessment of the digestion and absorption of engineered nanomaterials released from food matrices. *Nanotoxicology*, *9*(4), 523–542.

Lesuffleur, I. I., Barbai, A., Dussaulx, E., & Zweibaum, A. (1990). Growth adaptation to methotrexate of HT-29 human colon carcinoma cells is associated with their ability to differentiate into columnar absorptive and mucus-secreting cells. *Cancer Research*, *50*, 6334–6343.

Lesuffleur, T., Porchet, N., Aubert, J., Swallow, D., Gum, J. R., Young, S., Zweibaum, A. (1993). Differential expression of the human mucin genes MUC1 to MUC5 in relation to growth and differentiation of different mucus-secreting HT-29 cell subpopulations. *Journal of Cell Science*, *106*, 771–783.

Levy, E., Mehran, M., & Seidman, E. (1995). Caco-2 cells as a model for intestinal lipoprotein synthesis and secretion. *The FASEB Journal*, *9*(8), 626–635.

Li, Q., Li, T., Liu, C., DeLoid, G., Pyrgiotakis, G., Demokritou, P., McClements, D. J. (2017). Potential impact of inorganic nanoparticles on macronutrient digestion: titanium dioxide nanoparticles slightly reduce lipid digestion under simulated

gastrointestinal conditions. *Nanotoxicology*, *5390*, 1–15.

Liang, M., Lin, I.-C., Whittaker, M. R., Minchin, R. F., Monteiro, M. J., & Toth, I. (2010). Cellular uptake of densely packed polymer coatings on gold nanoparticles. *ACS Nano*, *4*(1), 403–413.

Lomer, M. C. E., Thompson, R. P. H., & Powell, J. J. (2002). Fine and ultrafine particles of the diet : influence on the mucosal immune response and association with Crohn' s disease. *Proceedings of the Nutrition Society*, *61*, 123–130.

Lozoya-Agullo, I., Araújo, F., González-Álvarez, I., Merino-Sanjuán, M., González-Álvarez, M., Bermejo, M., & Sarmento, B. (2017). Usefulness of Caco-2/HT29-MTX and Caco-2/HT29-MTX/Raji B coculture models to predict intestinal and colonic permeability compared to Caco-2 monoculture. *Molecular Pharmaceutics*, *14*(4), 1264–1270.

Lu, K., Abo, R. P., Schlieper, K. A., Graffam, M. E., Levine, S., Wishnok, J. S., … Fox, J. G. (2014). Arsenic exposure perturbs the gut microbiome and its metabolic profile in mice: An integrated metagenomics and metabolomics analysis. *Environmental Health Perspectives*, *122*(3), 284–291.

Luther, W. (Ed) (2004) Industrial application of nanomaterials—chances and risks. VDI Technologiezentrum GmBH, Future Technologies Division. Düsseldorf, Germany.

Ma, H., Brennan, A., & Diamond, S. A. (2012a). Photocatalytic reactive oxygen species production and phototoxicity of titanium dioxide nanoparticles are dependent on the solar ultraviolet radiation spectrum. *Environmental Toxicology and Chemistry*, *31*(9), 2099–2107.

Ma, H., Brennan, A., & Diamond, S. A. (2012b). Phototoxicity of TiO_2 nanoparticles under solar radiation to two aquatic species: Daphnia magna and Japanese medaka. *Environmental Toxicology and Chemistry*, *31*(7), 1621–1629.

MacNicoll, A., Kelly, M., Aksoy, H., Kramer, E., Bouwmeester, H., & Chaudhry, Q. (2015). A study of the uptake and biodistribution of nano-titanium dioxide using in vitro and in vivo models of oral intake. *Journal of Nanoparticle Research*, *17*(2), 66.

Mahler, G. J., Esch, M. B., Tako, E., Southard, T. L., Archer, S. D., Glahn, R. P., & Shuler, M. L. (2012). Oral exposure to polystyrene nanoparticles affects iron absorption. *Nature Nanotechnology*, *7*(4), 264–271.

Mahler, G. J., Shuler, M. L., & Glahn, R. P. (2009). Characterization of Caco-2 and HT29-MTX cocultures in an in vitro digestion/cell culture model used to predict iron bioavailability. *Journal of Nutritional Biochemistry*, *20*(7), 494–502.

Malanowski, N., Heimer, T., Luther, W., & Werner, M. (2007). Growth market nanotechnology. An analysis of technology and innovation. *Wiley-VCH Verlag GmbH & Co*.

Maoret, J. J., Font, J., Augeron, C., Codogno, P., Bauvy, C., Aubery, M., & Laboisse, C. L. (1989). A mucus-secreting human colonic cancer cell line. Purification and partial characterization of the secreted mucins. *The Biochemical Journal*, *258*(3), 793–9.

Marchesi, J. R., Adams, D. H., Fava, F., Hermes, G. D. A., Hirschfield, G. M., Hold, G., Hart, A. (2016). The gut microbiota and host health: A new clinical frontier. *Gut*, *65*(2), 330–339.

Mariadason, J. M., Arango, D., Corner, G. A., Aran, M. J., Hotchkiss, K. A., Yang, W., & Augenlicht, L. H. (2002). A gene expression profile that defines colon cell maturation in vitro. *Cancer Research*, *62*(16), 4791–4804.

Matsukawa, R., Michikawa, T., & Ueda, K. (2014). Desert dust is a risk factor for the incidence of acute. *Circulation. Cardiovascular Quality and Outcomes*, *7*, 743–748.

Matteis, V. De. (2017). Exposure to Inorganic Nanoparticles: Routes of entry, immune response, biodistribution and in vitro/in vivo toxicity evaluation. *Toxics*, *5*(29), 1–21.

Maynard, A. D., & Michelson, E. (2005). The project on emerging nanotechnologies. The Nanotechnology Consumer Products Inventory. http://nanotechproject.org/cpi

McCracken, C., Dutta, P. K., & Waldman, W. J. (2016). Critical assessment of toxicological effects of ingested nanoparticles. *Environmental Science: Nano*, *3*(2), 256–282.

Meyer, P., & Smith, E. M. (2002). Wildland forest fire smoke : health effects and intervention evaluation, Hoopa, California, 1999. *West Journal Medicine*, *176*, 157–162.

Micheau, O., & Tschopp, J. (2003). Induction of TNF receptor i-mediated apoptosis via two sequential signaling complexes. *Cell*, *114*(2), 181–190.

Michelson, E. S. (2013). “The train has left the station”: The project on emerging nanotechnologies and the shaping of nanotechnology policy in the united states. *Review of Policy Research*, *30*(5), 464–487.

Miller, F., Asgharian, B., & Hofmann, W. (2005). Dosimetry of particles in humans: from children to adults. *In: Gardner DE (Ed) Toxicol. Lung, 4th Ed. CRC Press, Boca Raton.*, 151–194.

Monteiro-Riviere, N. A., Wiench, K., Landsiedel, R., Schulte, S., Inman, A. O., & Riviere, J. E. (2011). Safety evaluation of sunscreen formulations containing titanium dioxide and zinc oxide nanoparticles in UVB sunburned skin: An In vitro and in vivo study. *Toxicological Sciences*, *123*(1), 264–280.

Mühlfeld, C., Gehr, P., & Rothen-Rutishauser, B. (2008). Translocation and cellular entering mechanisms of nanoparticles in the respiratory tract. *Swiss Medical Weekly*, *138*, 387–391.

Nel, A., Xia, T., Mädler, L., & Li, N. (2006). Toxic potential of materials at the nanolevel. *Science*, *311*(5761), 622–627.

Nel, A., Xia, T., Meng, H., Wang, X., Lin, S., Ji, Z., & Zhang, H. (2013). Nanomaterial toxicity testing in the 21st century: use of a predictive toxicological approach and high-throughput screening. *Accounts of Chemical Research*, *46*(3), 607–21.

Nemmar, A., Al-Maskari, S., Ali, B. H., & Al-Amri, I. S. (2007). Cardiovascular and lung inflammatory effects induced by systemically administered diesel exhaust particles in rats. *American Journal of Physiology. Lung Cellular and Molecular Physiology*, *292*(3), L664–L670.

NIOSH. (2011). *Occupational exposure to titanium dioxide*. *Current Intelligence Bulletin 63*. http://www.cdc.gov/niosh/docs/2011-160/

NNI (National Nanotechnology Initiative). 2000. http://www.nano.gov/nanoech-101/what.

Nogueira, C. M., Azevedo, W. M. De, Lucia, M., Dagli, Z., Toma, S. H., Leite, Z. D. A., Lúcia, C. (2012). Titanium dioxide induced inflammation in the small intestine. *World Journal of Gastroenterology*, *18*(34), 4729–4735.

Nüsse, M., & Kramer, J. (1984). Flow cytometric analysis of micronuclei found in cells after irradiation. *Cytometry*, *5*(1), 20–25.

Oberdörster, G., Oberdörster, E., & Oberdörster, J. (2005). Review Nanotoxicology : an emerging discipline evolving from studies of ultrafine particles. *Environmental Health Perspectives*. *113*(7), 823–839.

Oberdörster, G., Sharp, Z., Atudorei, V., Elder, A., Gelein, R., Lunts, A., Cox, C. (2002). Extrapulmonary translocation of ultrafine carbon particles following whole-body inhalation exposure of rats. *Journal of Toxicology and Environmental Health. Part A*, *65*, 1531–1543.

OCDE. (2004). Test Guideline No. 428. Skin absorption: in vitro method. *OECD Guidelines for the Testing of Chemicals*, *428*, 1–8.

Ohno, H., & Hase, K. (2010). Glycoprotein 2 (GP2): grabbing the FimH bacteria into M cells for mucosal immunity. *Gut Microbes*, *1*(6), 407–410.

Onishchenko, G. E., Erokhina, M. V, Abramchuk, S. S., Shaitan, K. V, Raspopov, R. V, Smirnova, V. V, Tutelyan, V. A. (2012). Effects of titanium dioxide nanoparticles on small intestinal mucosa in rats. *Bulletin of Experimental Biology and Medicine*, *154*(2), 265–270.

P Farrell, T., & Magnuson, B. (2017). Absorption, distribution and excretion of four forms of titanium dioxide pigment in the rat. *Journal of Food Science*, *82*(8), 1985–1993.

Paris, L., Tonutti, L., Vannini, C., & Bazzoni, G. (2008). Structural organization of the tight junctions. *Biochimica et Biophysica Acta (BBA) - Biomembranes*, *1778*(3), 646–659.

Patel, N., Forbes, B., Eskola, S., & Murray, J. (2006). Use of simulated intestinal fluids with caco-2 cells and rat ileum. *Drug Development and Industrial Pharmacy*, *32*(2), 151–161.

Pereira, C., Araújo, F., Granja, P. J., Santos, H. A., & Sarmento, B. (2014). Targeting membrane transporters and receptors as a mean to optimize orally delivered biotechnological based drugs through nanoparticle delivery systems. *Current Pharmaceutical Biotechnology*, *15*, 650–658.

Peters, R., Kramer, E., Oomen, A. G., Herrera Rivera, Z. E., Oegema, G., Tromp, P. C., Bouwmeester, H. (2012). Presence of nano-sized silica during in vitro digestion of foods containing silica as a food additive. *ACS Nano*, *6*(3), 2441–2451.

Petersen, E. J., Reipa, V., Watson, S. S., Stanley, D. L., Rabb, S. A., & Nelson, B. C. (2014). DNA damaging potential of photoactivated P25 titanium dioxide nanoparticles. *Chemical Research in Toxicology*, *27*(10), 1877–1884.

Piccinno, F., Gottschalk, F., Seeger, S., & Nowack, B. (2012). Industrial production quantities and uses of ten engineered nanomaterials in Europe and the world. *Journal of Nanoparticle Research*, *14*, 1109–1120.

Pielage, J. F., Cichon, C., Greune, L., Hirashima, M., Kucharzik, T., & Schmidt, M. A. (2007). Reversible differentiation of Caco-2 cells reveals galectin-9 as a surface marker molecule for human follicle-associated epithelia and M cell-like cells. *The International Journal of Biochemistry & Cell Biology*, *39*(10), 1886–1901.

Pinilla, S., Machín, A., Park, S.-H., Arango, J. C., Nicolosi, V., Márquez -Linares, F., & Morant, C. (2017). TiO_2-Based nanomaterials for the production of hydrogen and the development of lithium-ion batteries. *The Journal of Physical Chemistry B*, 122(2), 972-983.

Pinto, M., Robine, S., & Appay, M. D. (1983). Enterocyte-like differentiation and polarization of the human colon carcinoma cell line Caco-2 in culture. *Biology of the Cell*, *47*, 323–330.

Proquin, H., Rodríguez-Ibarra, C., Moonen, C. G. J., Urrutia Ortega, I. M., Briedé, J. J., de Kok, T. M., … Chirino, Y. I. (2017). Titanium dioxide food additive (E171) induces ROS formation and genotoxicity: contribution of micro and nano-sized fractions. *Mutagenesis*, *32*(1), 139–149.

Rajapakse, K., Drobne, D., Kastelec, D., & Marinsek-Logar, R. (2013). Experimental evidence of false-positive Comet test results due to TiO_2 particle – assay interactions. *Nanotoxicology*, *7*(5), 1043–1051.

Roberts, C. L., Keita, Å. V., Duncan, S. H., O'Kennedy, N., Söderholm, J. D., Rhodes, J. M., & Campbell, B. J. (2010). Translocation of Crohn's disease *Escherichia coli* across M-cells: Contrasting effects of soluble plant fibres and emulsifiers. *Gut*, *59*(10), 1331–1339.

Roduner, E. (2006). Size matters: why nanomaterials are different. *Chemical Society Reviews*, *35*, 583–592.

Rompelberg, C., Heringa, M. B., Donkersgoed, G. Van, Drijvers, J., Roos, A., Westenbrink, S., Agnes, G. (2016). Oral intake of added titanium dioxide and its nanofraction from food products, food supplements and toothpaste by the Dutch population. *Nanotoxicology*, *10*(10), 1404–1414.

Rubas, W., Cromwell, M. E. M., Shahrokh, Z., Villagran, J., Nguyen, T.-N., Wellton, M., Mrsny, R. J. (1996). Flux Measurements across Caco-2 monolayers may predict transport in human large intestinal tissue. *Journal of Pharmaceutical Sciences*, *85*(2), 165–169.

Ruiz, P. A., Morón, B., Becker, H. M., Lang, S., Atrott, K., Spalinger, M. R., Rogler, G. (2016). Titanium dioxide nanoparticles exacerbate DSS-induced colitis: role of the NLRP3 in fl ammasome. *Gut*, *66*, 1216–1224.

Rundell, K. W. (2003). High levels of airborne ultrafine and fine particulate matter in indoor ice arenas. *Inhalation Toxicology*, *15*, 237–250.

Saha, P., Manoharan, P., Arthur, S., Sundaram, S., Kekuda, R., & Sundaram, U. (2015). Molecular mechanism of regulation of villus cell Na-K-ATPase in the chronically inflamed mammalian small intestine. *Biochimica et Biophysica Acta - Biomembranes*, *1848*(2), 702–711.

Sajid, M., Ilyas, M., Basheer, C., Tariq, M., Daud, M., Baig, N., & Shehzad, F. (2015). Impact of nanoparticles on human and environment : review of toxicity factors , exposures , control strategies, and future prospects. *Environmental Science and Pollution Research International*, *22*(6), 4122–4143.

Sayes, C. M., Wahi, R., Kurian, P. A., Liu, Y., West, J. L., Ausman, K. D., Colvin, V. L. (2006). Correlating nanoscale titania structure with toxicity: A cytotoxicity and inflammatory response study with human dermal fibroblasts and human lung epithelial cells. *Toxicological Sciences*, *92*(1), 174–185.

Schimpel, C., Teubl, B., Absenger, M., Meindl, C., Fro, E., Leitinger, G., Roblegg, E. (2014). Development of an advanced intestinal in vitro triple culture permeability model to study transport of nanoparticles. *Molecular Pharmaceutics*, *11*(3), 808–818.

Schimpel, C., Teubl, B., Absenger, M., Meindl, C., Fröhlich, E., Leitinger, G., Roblegg,

E. (2014). Development of an advanced intestinal in vitro triple culture permeability model to study transport of nanoparticles. *Molecular Pharmaceutics*, *11*(3), 808–818.

Schirmer, M., Smeekens, S. P., Vlamakis, H., Jaeger, M., Oosting, M., Franzosa, E. A., Xavier, R. J. (2016). Linking the human gut microbiome to inflammatory cytokine production capacity. *Cell*, *167*(4), 1125–1136.

Schneider, T., Westermann, M., & Glei, M. (2017). In vitro uptake and toxicity studies of metal nanoparticles and metal oxide nanoparticles in human HT29 cells. *Archives of Toxicology*, *91*(11), 3517–3527.

Schulte, R., Kerneis, S., Klinke, S., Bartels, H., Preger, S., Pringault, E., Munich, D.-. (2000). Translocation of *Yersinia enterocolitica* across reconstituted intestinal epithelial monolayers is triggered by *Yersinia invasin* binding to b 1 integrins apically expressed on M-like cells. *Cellular Microbiology,* 2(20), 173–185.

Schulz, M. D., Atay, Ç., Heringer, J., Romrig, F. K., Schwitalla, S., Aydin, B., Arkan, M. C. (2014). High-fat-diet-mediated dysbiosis promotes intestinal carcinogenesis independently of obesity. *Nature*, *514*, 508–512.

Sclafani, A., & Herrmann, J. M. (1996). Comparison of the photoelectronic and photocatalytic activities of various anatase and rutile forms of titania in pure liquid organic phases and in aqueous solutions. *The Journal of Physical Chemistry*, *100*(32), 13655–13661.

Shah, P., Jogani, V., Bagchi, T., & Misra, A. (2006). Role of caco-2 cell monolayers in prediction of intestinal drug absorption. *Biotechnology Progress*, *22*(1), 186–198.

Shen, H., Qin, H., & Guo, J. (2008). Cooperation of metallothionein and zinc transporters for regulating zinc homeostasis in human intestinal Caco-2 cells. *Nutrition Research*, *28*(6), 406–413.

Shepherd, N. A., Crocker, P. R., Smith, A. P., & Levison, D. A. (1987). Exogenous pigment in Peyer's patches. *Human Pathology*, *18*(1), 50–54.

Shi, H., Magaye, R., Castranova, V., & Zhao, J. (2013). Titanium dioxide nanoparticles : a review of current toxicological data. *Particle and Fiber Toxicology*, *10*(15), 1–33.

Siebers, A., & Finlay, B. B. (1996). M cells and the pathogenesis of mucosal and

systemic infections. *Trends in Microbiology*, *4*(1), 22–29.

Song, Z., Chen, N., Liu, J., Tang, H., & Deng, X. (2015). Biological effect of food additive titanium dioxide nanoparticles on intestine: an in vitro study. *Journal of Applied Toxicology*, *35*(10), 1169–1178.

Sozer, N., & Kokini, J. L. (2009). Nanotechnology and its applications in the food sector. *Trends in Biotechnology*, *27*(2), 82–89.

Stern, S. T., & Mcneil, S. E. (2008). Nanotechnology safety concerns revisited. *toxicological science, 101*(1), 4–21.

Szakal, C., Tsytsikova, L., Carlander, D., & Duncan, T. V. (2014). Measurement methods for the oral uptake of engineered nanomaterials from human dietary sources : summary and outlook. *Comprehensive Reviews in Food Science and Food Safety*, *13*, 669–678.

Tarucha, L. P. K. and D. G. A. and S. (2001). Few-electron quantum dots. *Reports on Progress in Physics*, *64*(6), 701.

Taylor, D. A. (2002). Dust in the wind. *Environmental Health Perspectives*, *110*(2), 80–87.

Teow, Y., Nair, A., Hande, P., & Valiyaveettil, S. (2011). Health impact and safety of engineered nanomaterials. *Chemical Communications (Cambridge, England)*, *47*(25), 7025–7038.

Thomas, P., & Fenech, M. (2011). Cytokinesis-block micronucleus cytome assay in lymphocytes bt - dna damage detection in situ, ex vivo, and in vivo: methods and protocols. In V. V Didenko (Ed.), *Methods in Molecular Biology* (pp. 217–234). Totowa, NJ: Humana Press.

Tilton, S. C., Karin, N. J., Tolic, A., Xie, Y., Lai, X., Hamilton, R. F., Orr, G. (2014). Three human cell types respond to multi-walled carbon nanotubes and titanium dioxide nanobelts with cell-specific transcriptomic and proteomic expression patterns. *Nanotoxicology*, *8*(5), 533–548.

Tinkle, S. S., Antonini, J. M., Rich, B. A., Roberts, J. R., Salmen, R., Depree, K., & Adkins, E. J. (2003). Skin as a route of exposure and sensitization in chronic beryllium disease. *Environmental Health Perspectives*, *111*(9), 1202–1208.

Toll, R., Jacobi, U., Richter, H., Lademann, J., & Schaefer, H. (2004). Penetration

profile of microspheres in follicular targeting of terminal hair follicles. *Journal of Investigative Dermatology*, *123*(1), 168–176.

Toyooka, T., Amano, T., & Ibuki, Y. (2012). Titanium dioxide particles phosphorylate histone H2AX independent of ROS production. *Mutation Research/Genetic Toxicology and Environmental Mutagenesis*, *742*(1–2), 84–91.

Tsuji, J. S., Maynard, A. D., Howard, P. C., James, J. T., Lam, C., Warheit, D. B., & Santamaria, A. B. (2006). Research strategies for safety evaluation of nanomaterials, part iv : risk assessment of nanoparticles. *Toxicological Science*, *89*(1), 42–50.

Tyrer, P. C., Ruth Foxwell, A., Kyd, J. M., Otczyk, D. C., & Cripps, A. W. (2007). Receptor mediated targeting of M-cells. *Vaccine*, *25*(16), 3204–3209.

Tyrer, P., Ruth Foxwell, A., Kyd, J., Harvey, M., Sizer, P., & Cripps, A. (2002). Validation and quantitation of an in vitro M-cell model. *Biochemical and Biophysical Research Communications*, *299*(3), 377–383.

Urrutia-Ortega, I. M., Garduño-Balderas, L. G., Delgado-Buenrostro, N. L., Freyre-Fonseca, V., Flores-Flores, J. O., González-Robles, A., Chirino, Y. I. (2016). Food-grade titanium dioxide exposure exacerbates tumor formation in colitis associated cancer model. *Food and Chemical Toxicology*, *93*, 20–31.

Vachon, P. H., & Beaulieu, J.-F. (1992). Transient mosaic patterns of morphological and functional differentiation in the Caco-2 cell line. *Gastroenterology*, *103*(2), 414–423.

Vachon, P. H., Perreault, N., Magny, P., & Beaulieu, J.-F. (1996). Uncoordinated, transient mosaic patterns of intestinal hydrolase expression in differentiating human enterocytes. *Journal of Cellular Physiology*, *166*(1), 198–207.

Valant, J., Drobne, D., & Novak, S. (2012). Effect of ingested titanium dioxide nanoparticles on the digestive gland cell membrane of terrestrial isopods. *Chemosphere*, *87*(1), 19–25.

Vales, G., Rubio, L., & Marcos, R. (2015). Long-term exposures to low doses of titanium dioxide nanoparticles induce cell transformation, but not genotoxic damage in BEAS-2B cells. *Nanotoxicology*, *9*(5), 568–578.

van der Meulen, B., Bremmers, H., Purnhagen, K., Gupta, N., Bouwmeester, H., & Geyer, L. L. (2014). *Governing nano foods: principles-based responsive regulation: EFFoST Critical Reviews# 3* (Vol. 3). Academic Press.

van Driel, B. A., Kooyman, P. J., van den Berg, K. J., Schmidt-Ott, A., & Dik, J. (2016). A quick assessment of the photocatalytic activity of TiO_2 pigments - From lab to conservation studio!. *Microchemical Journal*, *126*, 162–171.

Vance, M. E., Kuiken, T., Vejerano, E. P., Mcginnis, S. P., Hochella, M. F., Rejeski, D., & Hull, M. S. (2015). Nanotechnology in the real world : Redeveloping the nanomaterial consumer products inventory. *Beilstein Journal of Nanotechnology,* 6, 1769–1780.

Vemylen, J., Nemmar, A., Nemery, B., & Hoylaerts, F. (2005). Ambient air pollution and acute myocardial infarction. *Journal of Thrombosis and Haemostasis*, *3*, 1955–1961.

Verhoeckx, K., Cotter, P., López-Expósito, I., Kleiveland, C., Lea, T., Mackie, A., Requena, T., Swiatecka, D., Wichers, H. (2015). The impact of food bioactives on health: in vitro and ex vivo models. *Springer International Publishing AG. Part of Springer Nature.*

Vila, L., Marcos, R., & Hernández, A. (2017). Long-term effects of silver nanoparticles in caco-2 cells. *Nanotoxicology*, *11*(6), 771–780.

Vila Vecilla, L. (2016). *Tesis - Modelo invitro de barrera intestinal para la evaluacion del riesgo de los nanomateriales*. https://ddd.uab.cat/pub/tesis

Waller, T., Chen, C., & Walker, S. (2017). Food and industrial grade titanium dioxide impacts gut microbiota. *Environmental Engineering Science*, *34*(8), 537–550.

Walter, E., Janich, S., Roessler, B. J., Hilfinger, J. M., & Amidon, G. L. (1996). HT29-MTX/Caco-2 cocultures as an in vitro model for the intestinal epithelium: in vitro and in vivo correlation with permeability data from rats and humans. *Journal of Pharmaceutical Sciences*, *85*(10), 1070–1076.

Wang, J., & Fan, Y. (2014). Lung injury induced by TiO_2 nanoparticles depends on their structural features: Size, shape, crystal phases, and surface coating. *International Journal of Molecular Sciences*, *15*(12), 22258–22278.

Warheit, D. B., Webb, T. R., Reed, K. L., Frerichs, S., & Sayes, C. M. (2007). Pulmonary toxicity study in rats with three forms of ultrafine-TiO2 particles:

Differential responses related to surface properties. *Toxicology*, *230*(1), 90–104.

Weir, A., Westerhoff, P., Fabricius, L., Hristovski, K., & Goetz, N. Von. (2012). Titanium dioxide nanoparticles in food and personal care products. *Environmental Science and Technology,* 46(4), 2242-2250.

Wikman-Larhed, A., & Artursson, P. (1995). Co-cultures of human intestinal goblet (HT29-H) and absorptive (Caco-2) cells for studies of drug and peptide absorption. *European Journal of Pharmaceutical Sciences*, *3*(3), 171–183.

Williams, K., Milner, J., Boudreau, M. D., Gokulan, K., Cerniglia, C. E., & Khare, S. (2015). Effects of subchronic exposure of silver nanoparticles on intestinal microbiota and gut-associated immune responses in the ileum of Sprague-Dawley rats. *Nanotoxicology*, *9*(3), 279–289.

Wisel, S., & Rajendren, V. M. (1997). Mechanism of inhibition of Na+-glucose cotransport in the chronically inflamed rabbit ileum. *American Journal of Physiology*, 913–919.

Xu, Y., Wen, W., & Wu, J.-M. (2018). Titania nanowires functionalized polyester fabrics with enhanced photocatalytic and antibacterial performances. *Journal of Hazardous Materials*, *343*, 285–297.

Ye, D., Ma, I., & Ma, T. Y. (2006). Molecular mechanism of tumor necrosis factor alpha modulation of intestinal epithelial tight junction barrier. *American Journal of Physiology Gastrointestinal Liver Physiology*, *290*, 496–504.

Zijno, A., De Angelis, I., De Berardis, B., Andreoli, C., Russo, M. T., Pietraforte, D., Barone, F. (2015). Different mechanisms are involved in oxidative DNA damage and genotoxicity induction by ZnO and TiO_2 nanoparticles in human colon carcinoma cells. *Toxicology in Vitro*, *29*(7), 1503–1512.

Zimmer, A. T., Baron, P. A., & Biswas, P. (2002). The influence of operating parameters on number-weighted aerosol size distribution generated from a gas metal arc welding process. *Journal of Aerosol Science*, *33*, 519–531.

Zrazhevskiy, P., Sena, M., & Gao, X. (2010). Designing multifunctional quantum dots for bioimaging, detection, and drug delivery. *Chemical Society Reviews*, *39*(11), 4326–4354.

Zweibaum, A. Enterocytic differentiation of cultured human colon cancer cell lines: negative modulation by D-glucose. In: *Ion-gradient-coupled transport. Vol. INSERM Symposium*. 1986. p. 345-352.

Zweibaum, A., Laburthe, M., Grasset, E., & Louvard, D. (2010). Use of cultured cell lines in studies of intestinal cell differentiation and function. *Comprehensive Physiology*. John Wiley & Sons, Inc.

7. ANNEXES

Food and Chemical Toxicology 113 (2018) 162–170

Contents lists available at ScienceDirect

Food and Chemical Toxicology

journal homepage: www.elsevier.com/locate/foodchemtox

Exploring the usefulness of the complex in vitro intestinal epithelial model Caco-2/HT29/Raji-B in nanotoxicology

Alba García-Rodríguez[a], Laura Vila[a], Constanza Cortés[a], Alba Hernández[a,b,*], Ricard Marcos[a,b,**]

[a] Grup de Mutagènesi, Departament de Genètica i de Microbiologia, Facultat de Biociències, Universitat Autònoma de Barcelona, Bellaterra, Spain
[b] CIBER Epidemiología y Salud Pública, ISCIII, Madrid, Spain

ARTICLE INFO

Keywords:
In vitro epithelial barrier model
Caco-2 cells
HT29 cells
Raji-B cells
Nanomaterials

ABSTRACT

The use of in vitro barrier models is gaining relevance as an alternative to animal studies in risk assessment, pharmacokinetic, and toxicological studies in general. These models permit an easier evaluation of the under-lying mechanisms taking place at the molecular and cellular levels on the barrier site. Here, we report several methodological modifications of the three-dimensional in vitro intestinal epithelial model Caco-2/HT29/Raji-B for its successful application in the Nanotoxicology field. In addition, new insights in the study of specific molecular markers and new confocal microscope approaches have also been incorporated. Due to the multiple variables and parameters playing a part when the model's complexity is increased, we have monitored the barrier's formation and cell differentiation over time. Finally, the practical usability of the proposed model was tested by evaluating the action of the food additives titanium dioxide and silica dioxide nanoparticles (TiO_2NPs and SiO_2NPs). The NPs-associated effects were evaluated by confocal microscopy. We have demonstrated the essential role of the mucus layer in the decrease of cellular uptake, avoiding potential NPs-cell nuclei interac-tions.

1. Introduction

Because of the apparent lack of predictivity observed in animal models (Leist et al., 2014), a variety of in vitro approaches are currently used to mimic different biological targets, including epithelial barriers. Until now, the described non-animal models aiming to simulate epi-thelial barriers include the utilization of ex vivo tissues, reconstructed combined in vitro cell lines, the use of synthetic membranes, and the use of in silico modelling approaches. In all the aforementioned cases, ef-forts have pursued rapid and economic methods able to evaluate the interactions between defined compounds and the biological barriers they must cross (Gordon et al., 2015).

The interest in the development of in vitro epithelial barriers is common to various industrial fields such as pharmaceutics, cosmetics, and food industries. In addition, different research fields like toxicology and biomedical engineering also need to focus their research on the processes taking part in these entry gates. Furthermore, different in-stitutional organisms as the Center for Alternatives to Animal Testing or the European Food Safety Authority are demanding information on this direction to enforce the scientific regulatory laws towards more sus-tainable and efficient in vitro alternatives (Gordon et al., 2015).

The rapid emergence of new nanotechnology products demands to improve the existing methodologies to test the potentially harmful ef-fects of nanocompounds. Different nanoparticles (NPs) are increasingly used by the food industry in different consumer products (i.e. food packaging, food additives, colourants, antimicrobial agents, etc.) (Vance et al., 2015). In this way, the intestinal epithelium became the main entrance portal of such NPs. To evaluate their potential health effects, different in vitro intestinal barrier models have been proposed so far (Schimpel et al., 2014; Braakhuis et al., 2015; Guo et al., 2017). Among them, one of the most common examples of in vitro gut model, the intestinal Caco-2 monolayer, has been largely described and used in the past two decades. Derived from a human colorectal adenocarci-noma, Caco-2 cells have the capability to differentiate themselves forming a morphologically and functionally enterocyte-like monolayer (Pinto et al., 1983; Sambuy et al., 2005). Caco-2 monolayers disposed into inserts with distinct, differentiated apical and basolateral sides, have been widely used in the past for chemical transport and drug pharmacokinetics studies, because of its well-known correlation with human studies (Artursson et al., 2001; van Breemen and Li, 2005). Recently, the Caco-2 monolayer has also been used and adapted to test potential detrimental and bio-dynamics effects of metallic-based NPs

* Corresponding author. Grup de Mutagènesi, Departament de Genètica i de Microbiologia, Universitat Autònoma de Barcelona, Edifici Cn, Campus de Bellaterra, 08193, Cerdanyola del Vallès, Barcelona, Spain.
** Corresponding author. Grup de Mutagènesi, Departament de Genètica i de Microbiologia, Facultat de Biociències, Universitat Autònoma de Barcelona, Bellaterra, Spain. E-mail addresses: alba.hernandez@uab.es (A. Hernández), ricard.marcos@uab.es (R. Marcos).

https://doi.org/10.1016/j.fct.2018.01.042
Received 22 December 2017; Received in revised form 19 January 2018; Accepted 23 January 2018

such as titanium dioxide (TiO_2NPs), silica dioxide (SiO_2NPs) and silver (AgNPs) nanoparticles (Faust et al., 2014; Sakai-Kato et al., 2014; Imai et al., 2017).

However, there is a fine balance of endogenous and exogenous factors in the intestine, provided by the multiple types of cells existing in the mucosa niche. Accordingly, assays based on a single cell line do not properly represent the complex gut environment. Thus, improved and more complex intestinal in vitro barrier models have been proposed to accomplish a more realistic in vitro system. Different studies added the goblet cell clones HT29 or HT29-MTX to the barrier model, which are capable to secrete vacuoles full of mucin, conferring an extracellular protective shed of mucus (Mahler et al., 2009; Araújo and Sarmento, 2013; Lozoya-Agullo et al., 2017). The presence of the mucus layer led to the protection against ROS and a decrease in IL-8 release when treating the Caco-2/HT29 model with AgNPs (Georgantzopoulou et al., 2016).

A further improvement of the system was the addition of cell types to generate advanced three-dimensional co-culture models. Some stu-dies have paid special attention to the development of an in vitro fol-licle-associated epithelium (FAE), characterized by the presence of microfold cells (M cells) (Smith and Peacock, 1980). M cells are con-sidered antigen-sampling cells, acting as a gateway for antigens from the gut lumen and promoting particle transcytosis (Kucharzik et al., 2000). Thus, by adding human Raji-B lymphocytes to the basolateral chamber of the insert, Caco-2 are induced to differentiate into M-like cells (Gullberg et al., 2000; des Rieux et al., 2007). In this context, it is important to indicate that several reports suggested that NPs are cap-able to enter intestinal epithelium mainly via M-cells (Gullberg et al., 2000; des Rieux et al., 2005).

Despite the efforts put to improve the existing intestinal epithelium models that have led to the generation of a more complex and realistic bioengineered three-dimensional co-culture Caco-2/HT29/Raji-B, fur-ther efforts are required. The absence of integrated and common methodological strategies between laboratories supposes the lack of a defined model to be used when testing nanomaterials. In this context, this works aims to further adapt and standardize the three-dimensional bioengineered co-culture Caco-2/HT29/Raji-B described previously by different authors (Antunes et al., 2013; Araújo and Sarmento, 2013; Schimpel et al., 2014) for the study of nanomaterials-associated effects. We have focused our attention on enhancing cell culture conditions to improve their visualization by using confocal microscopy, and on in-corporating new molecular endpoints to determine the cells' status. In addition, the interaction of TiO_2NP and SiO_2NPs with our model was evaluated by confocal microscopy to test the model's performance.

2. Materials and methods

2.1. Cell culture and the in vitro co-culture model

Dr Isabella Angelis (Istituto Superiore di Sanità, Italy), kindly pro-vided the human colorectal adenocarcinoma cell line Caco-2. HT29, a human cell line derived from a colorectal adenocarcinoma, and Raji-B, a B-lymphocyte cell line derived from a human Burkitt's lymphoma, were both purchased from the American Type Culture Collection (ATCC, Manassas VA 20108, USA). All cell lines were maintained in Dulbecco's modified Eagle's High Glucose medium without Pyruvate (DMEM w/o Pyruvate, Life Technologies, USA) and supplemented with 10% fetal bovine serum (FBS), 1% non-essential amino acids (NEAA) (PAA Laboratories GmbH, Pasching, Austria), and 2.5 mg/mL plas-mocin (Invivo Gen, San Diego, USA). Cells were placed in a humidified atmosphere of 5% CO_2 and 95% air at 37 °C. Routinely, Caco-2 and HT29 cell lines were subcultured once a week with 1% trypsin-EDTA (PAA Laboratories GmbH, Pasching, Austria) in 75 cm^2 flasks at 7.5 × 10^5 cells/flask and 4 × 10^5 cells/flask, respectively. Raji-B cells were grown in suspension, and sub-cultured weekly by diluting the cells at 3 × 10^5 cells/mL.

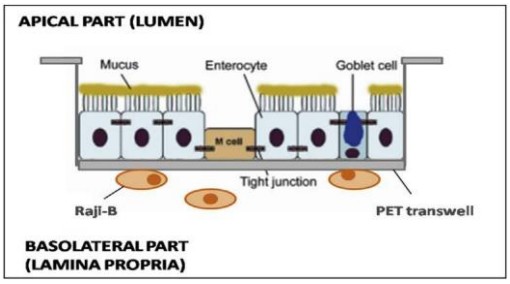

Fig. 1. Pictographical representation of a well-differentiated Caco-2/HT29/Raji-B model.

The co-cultures were grown in 12-well culture plates using 1.12 cm^2 Polyethylene Terephthalate Transwells® (PET) with a pore size of 1 or 3 μm (Millipore®) (Merck KGaA, Darmstadt, Germany) as previously validated by Araújo and Sarmento (2013). These transwells act as a support chamber to differentiate between the cells' apical and baso-lateral side, mimicking the intestinal epithelium lumen and mucosa, respectively. In Fig. 1 a scheme of the model is presented. Briefly, 1.7 × 10^5 Caco-2 and HT29 cells were mixed and seeded on the PET apical compartment, following a 90:10, 80:20, and 70:30 ratio, re-spectively. For the M-like cell induction, at day 14 of co-culture dif-ferentiation, 5 × 10^5 Raji-B cells were seeded in the basolateral com-partment. Finally, Caco-2/HT29/Raji-B co-cultures were left to differentiate until day 21, when a fully-formed functional barrier is obtained. Culture medium was changed every two days.

2.2. Integrity evaluation of the in vitro co-culture model

In order to oversee the integrity of the cell barrier, the trans-epi-thelial electrical resistance (TEER) was measured with an epithelial Voltmeter (Millicell-ERS volt/ohm meter) (Millipore®) (Merck KGaA, Darmstadt, Germany). TEER values were checked during the differ-entiation process of the Caco-2 monolayer, Caco-2/Raji-B and Caco-2/ HT29/Raji-B co-cultures at days 7, 14 and 21 after seeding the different Caco-2/HT29 ratios to establish the best proportion. TEER values were calculated according to the formula TEER = [Ω (cell inserts) - Ω (cell-free inserts)] x 1.12 cm^2. Only Caco-2/HT29/Raji-B co-cultures with TEER values higher than 250 Ω/cm^2 were used for further experiments.

2.3. Paracellular permeability of the in vitro co-culture model

To study the in vitro barrier permeability, the paracellular transport of Lucifer yellow (LY) (ThermoFisher Scientific, USA) was measured. Briefly, after 21 days of cellular differentiation and barrier formation, PET membranes were washed twice with transport buffer (HBSS Ca^{2+}, Mg^{2+}, +10 mM HEPES, pH 7.4). Then, membranes were transferred to a new 12-well plate filled with 1.5 mL of transport buffer in the baso-lateral compartment. Lucifer yellow was also diluted in transport buffer and added to the apical compartment at a final concentration of 0.4 μg/ mL. In vitro co-cultures were placed in the incubator during 2 h. Subsequently, triplicates of 100 μL of each basal compartment were transferred to a black 96-well plate to measure fluorescence leakage. A prompt fluorometry plate reader (Victor III, Perkin Elmer, USA) was used to determine the amount of LY able to cross the barrier by using 405–535 nm as an excitation-emission spectrum.

2.4. Histochemical characterization of the in vitro mucus secretion

To locate mucus secretion and visualize mucus shedding, differ-entiated HT29 and Caco-2 monocultures and Caco-2/HT29 co-cultures at 90:10, 80:20 and 70:30 ratios were cultured for 21 days in 1.12 cm^2 PET with a pore size of 3 μm. Next, PET were washed twice with PBS (1x), fixed with 3% acetic acid for 5 min, and stained with Alcian Blue (pH 2.5) (Abcam Plc., USA) for 30 min. After washing the samples with

running tap water for 1 min, the obtained cell barriers were separated from their supports and 3–5 μm cross-sections were obtained with a microtome and fixed in microscope slides. A cross-section of a rat in-testine was used as positive control of the staining assay. Sample images were obtained with an inverted light Axio Observer A1 microscope (Zeiss, Germany) complemented with an AxioCam MRm camera (Zeiss, Germany).

2.5. Morphological characterization of the M-like cell phenotype induction

To see the morphological changes associated with Caco-2 cells differentiation into M-like cells, we used transmission electron microscopy (TEM). Caco-2/HT29 co-cultures were seeded in PET with two different pore sizes (1 or 3 μm). After 14 days of co-culture, Raji-B cells were seeded in the basolateral chamber and the Caco-2/HT29/Raji-B co-culture was maintained until day 21. Then, the cell barrier was fixed in 2% (w/v) paraformaldehyde (Hatfield, PA, USA) and 2.5% (v/v) glu-taraldehyde (Merck, Darmstadt, Germany) in 0.1 M cacodylate buffer (Sigma-Aldrich, Steinheim, Germany) at pH 7.4. Cells were post-fixed with osmium, dehydrated in acetone, embedded in Epon, polymerized at 60 °C, and cut with an ultramicrotome. Finally, ultrathin barrier's cross-sections placed in copper grids were contrasted with conventional uranyl acetate and Reynolds lead citrate solution and observed using a Jeol 1400 (Jeol LTD, Tokyo, Japan) transmission electron microscope equipped with a CCD GATAN ES1000 W Erlangshen camera.

2.6. Cell type detection and barrier characterization using confocal microscopy

Laser Confocal Microscopy was used to visualize and discriminate Caco-2 cells from HT29 cells in the same co-culture while observing a three-dimensional disposition of the in vitro barrier model and its components (i.e. nucleus, mucus layer, cell membranes). In vitro co-culture barriers, Caco-2 monolayers and HT29 mono-cultures, were seeded in PET as previously stated. Briefly, in vitro cultures were stained after the differentiation period in the PET during 15 min at room tem-perature with Cellmask™, Hoechst 33342, and WGA Alexa Fluor™ fluor-ochromes diluted in DMEM culture medium at concentrations of 1/500, 1/500, and 1/100, respectively. Cellmask™ Deep Red plasma (Life Technologies, USA) was used to stain the cell membrane, having an excitation/emission spectrum of 633/785 nm. For the staining of the cell nucleus, we used Hoechst 33342 (ThermoFisher Scientific, USA) with a maximum excitation/emission of ~405/425-475 nm. Finally, the Wheat Germ Agglutinin, Alexa Fluor™ 633 Conjugate (WGA) (ThermoFisher Scientific, USA) was used to stain the mucus layer (maximum excitation/emission of ~632/647). After the incubation with the fluorochromes, samples were washed twice with culture medium and separated from the transwell supports by cutting the PET′ membrane with a scalpel. The cells' co-culture attached to the mem-brane was placed face down in a Glass Bottom Microwell Dishes (MatTek, USA) petri dish with 250 μL of culture medium to maintain cell in-tegrity and homeostasis while acquiring images. A confocal Leica TCS SP5 complemented with an HC x PLAPO Lambda blue 63x1.40 oil UV objective was used. Images were processed with Huygens essential 4.4.0p6 (Scientific Volume Imaging, Netherlands) and Imaris 7.2.1 (Bitplane, AG) software.

2.7. Gene expression studies of molecular markers from the in vitro co-culture model

The total RNA from Caco-2/HT29/Raji-B co-cultures was extracted 7, 14 and 21 days after seeding using TRIzol® Reagent (Invitrogen, USA), following the manufacturer's instructions. To remove residual DNA contamination, the samples were then treated with RNase-free DNase I (DNA-free TM kit; Ambion, UK) and, subsequently, the First-strand cDNA Synthesis Kit (Roche, Basel, Switzerland) was used to obtain cDNA by using 100 ng of total RNA. The resulting cDNA was subjected to real-time PCR analysis on a LightCycler-480 to evaluate the relative expression of different genes. We selected the brush border genes Sucrase-isomaltase (SI) and Alkaline phosphatase (ALPI). As genes of tight-junctions components, we selected Occludin (OCLN), Claudin (CLDN2), and Zona occludens (ZO1) genes. In addition, the membrane receptors Glycoprotein (GP), Galactine-9 (LGALS9), and Toll-like receptor 4 (TLR-4) genes and Mucine 1, 2 and 5 (MUC1, MUC2, MUC5) genes were also selected. The expression of β-actin was used as housekeeping control. (SI: direct 5′-TGGTGGCACTGTTATCCGAC-3′ and reverse 5′-GACCACCACGGACATGTAGG-3'; ALPI: direct 5′-GTCCATCCTGTAC GGCAATG-3′ and reverse 5′-ACATGCGCTACGAAGCTCTG-3'; CLDN2: direct 5′-TACTCACCACTGGTGCCTGA-3′ and reverse 5′-GAGAGCTCCT TGTGGCAAGA-3'; ZO-1: direct 5′-GAGAGGTGTTCCGTGTTGTG-3′ and reverse 5′-GCTGCGAAGACCTCTGAATC-3'; GP2: direct 5′-CAGTGCAG CGAGGTTATGGA-3′ and reverse 5′-ACAGGCAGTGTGGTTGGTGA-3': LGALS9: direct 5′-GATGGAGGGTACGTGGTGTG-3′ and reverse 5′-AGC CATTGACGGAGATGGTG-3'; MUC1: direct 5′-CGACGTGGAGACACAG TTCA-3′ and reverse 5′-GACAGACAGCCAAGGCAATG-3'; MUCA5C: direct 5′-GTGTGCCTGCGTCTACAACG-3′ and reverse 5′-GTGTGCCTGCG TCTACAACG-3'; SPIB: direct 5′-AGACTTACCGTTGGACAGCC-3′ and reverse 5′-AGCTTCTGGTAGGTCATGCG-3'; PTAFR: direct 5′ TAATGGC TACGTGCTGTGGG 3′ and reverse 5′ TGGCCTGAGCAGTCTTGATG 3'; TLR4: direct 5′ TGCGTGGAGGTGGTTCCTA 3′ and reverse 5′ GGGCTA AACTCTGGATGGGG 3'; β-actin: direct 5′-GCATGGAGTCCTGTGGC ATC-3′ and reverse 5′-CCACACGGAGTACTTGCGCT- 3′). Each 20 μL of reaction volume contained 5 μL cDNA, 10 μL of 2x LightCycler 480 SYBR Green I Mater (Roche, Germany), 3 μL of distilled H_2O, and 1 μL of each primer (forward and reverse) at a final concentration of 10 μM. The cycling parameters were the following: an initial step of 95 °C for 5 min, then 45 cycles of 95 °C for 10 s, 62 °C for 15 s and 72 °C for 25 s. Cycle time (Ct) values were calculated with the LightCycler 480 soft-ware package and then normalized with β-actin Ct values.

2.8. Nanoparticles exposure

Titanium dioxide (TiO_2NPs, NM100) and silica dioxide (SiO_2NPs, NM203) nanoparticles were supplied by the Joint Research Center (Ispra, Italy) in the frame of the EU project NanoReg, and were dis-persed according to the EU Nanogenotox protocol (Nanogenotox, 2011). The primary particle size of TiO_2NPs and SiO_2NPs were 110 and 24.7 nm, respectively. Briefly, 15.3 mg of TiO_2NPs and SiO_2NPs were pre-wetted in 0.5% absolute ethanol and dispersed in 0.05% bovine serum albumin (BSA) in MilliQ water. Each NP was sonicated in the dispersion medium for 16 min at 10% of amplitude to obtain a stock dispersion of 2.56 mg/mL. The NPs used were characterized in a pre-vious work (Vila et al., 2017).

After the cell differentiation process and barrier maturation, Caco-2/HT29/Raji-B co-cultures were exposed to 150 μg/mL of TiO_2NPs and 150 μg/mL of SiO_2NPs for 24 h per separate. Briefly, after 21 days of co-cultures seeding, the apical culture medium was replaced by adding 100 μg/mL of the selected NPs diluted in DMEM culture medium. Fresh culture medium without NPs was placed in the basolateral chamber of the insert. Finally, membranes were placed in the incubator at 37 °C for 24 h for further confocal microscopy analysis.

2.9. Statistical analysis

All sample treatments were measured in triplicate in at least three separate experiments. Results are expressed as mean ± standard error. One-way ANOVA with Tukey's post hoc test, unpaired Student's t-test, or two-way ANOVA were performed as convenient using GraphPad Prism version 5.00 for Windows (GraphPad Software, San Diego California USA, www.graphpad.com). Differences were considered significant at $P < 0.05$.

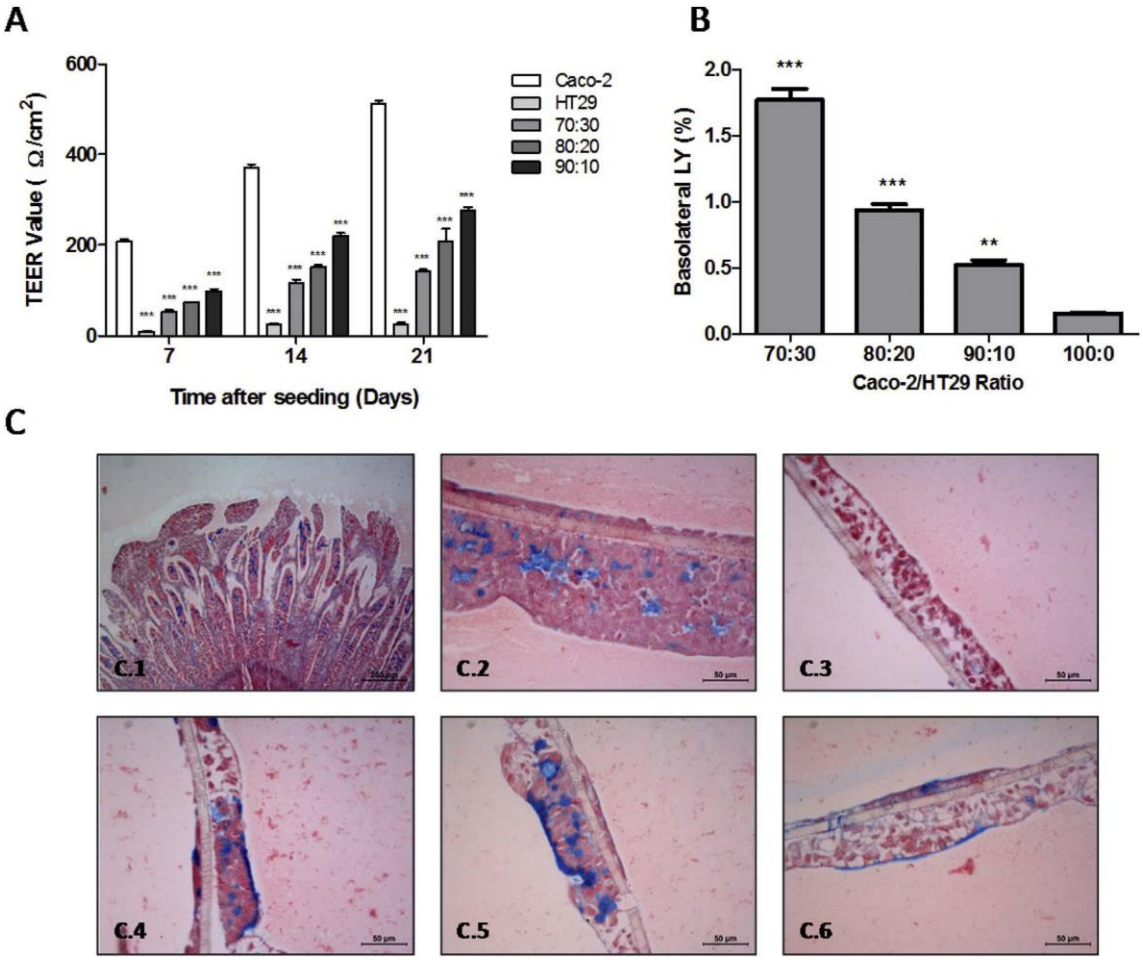

Fig. 2. Several characteristics of Caco-2/HT29 co-cultures. (A) TEER values of different co-cultures ratios compared with the Caco-2 and HT29 monocultures. (B) Amount (%) of Lucifer yellow detected in the basolateral chamber of different co-cultures ratios. (C) Transversal cuts and Alcian Blue staining of (C.1) rat intestine as a positive control, (C.2) HT29 monoculture, (C.3) Caco-2 monoculture, (C.4) Caco-2/HT29 co-culture in a ratio of 70:30, (C.5) 80:20, and (C.6) 90:10%. Results are represented as mean ± SEM. One-way ANOVA with a Tukey's post-test was performed. **P < 0.01, ***P < 0.001. (For interpretation of the references to color in this figure legend, the reader is referred to the Web version of this article.)

3. Results

3.1. Functional and morphological evaluation of the Caco-2/HT29 barrier

To increase the Caco-2 monolayer's complexity, HT29 colon adenocarcinoma cells were added to the in vitro barrier. HT29 cells, also known as goblet cells, have the capability to produce mucine secretions, forming an extracellular mucus shed. Thus, to set the best suitable Caco-2/HT29 ratio of cells, different ratios of both cell clones were studied: 70:30, 80:20, 90:10 and 100:0 of Caco-2 and HT29, respec-tively.

Firstly, the barrier integrity was evaluated by measuring the TEER throughout the differentiation time. As expected, the TEER values of all cultured ratios, except for HT29 monocultures, increased progressively during the differentiation span (Fig. 2A). At the end of the 21 days of differentiation process, TEER values reached a plateau where Caco-2 monoculture presented the highest value (513.28 ± 16 Ω/cm^2) fol-lowed by 90:10 (277.15 ± 17.55 Ω/cm^2), 80:20 (207.91 ± 69.35 Ω/ cm^2) and 70:30 (142.01 ± 10.93 Ω/cm^2), while HT29 monoculture barely showed resistance (26.28 ± 7.06 Ω/cm^2). Following the func-tional characterization of the different co-cultures, the percentage of paracellular LY transported was also calculated (Fig. 2B). The LY assay is commonly used to complement the membrane integrity studies and to address paracellular permeability studies due to the capability of this compound to cross in vitro epithelial barriers by paracellular transport. As shown in Fig. 2B, the amount of LY able to cross the co-culture barrier decreases while the ratio of Caco-2 cells in the co-culture in-creases. LY results matched well with TEER values, since Caco-2 monoculture and 90:10 co-culture, the cultures with highest TEER va-lues, present the lowest amount of paracellular LY passage. Accord-ingly, co-cultures with a ratio of 90% Caco-2 and 10% HT29 were considered as the best combination, maintaining high barrier integrity and, consequently, was used for further experiments. It should be pointed out that when 3 μm pore-sized PET were used, important cell migration from the apical to the basolateral chamber was observed. To avoid this problem, further experiments were done using 1 μm pore-size PET. This simple change avoids migration and the subsequent forma-tion of a second barrier on the basolateral side of the filter (see Supplementary Fig. S1).

In addition, the secreted and scattered mucus along the barrier model was evaluated using the Alcian Blue staining. Also, the Caco-2/ HT29 cell distribution over the PET was checked. Alcian Blue is a his-tochemical staining dye that interacts with the acidic mucosubstances and acetic mucins, allowing the qualitative visualization of the amount of mucus secreted. As observed in the images from Fig. 2C, our HT29 cell clone (C.2) grown in PET for 21 days was able to produce mucus in a physiologically-relevant amount, similar to the positive control (rat intestine) (C.2). On the other hand, Caco-2 monolayers' mucus was barely noticeable. No differences were seen in mucus se-cretion and distribution between the different co-culture ratios eval-uated. As observed in the supplied images, all Caco-2/HT29 ratios tend to form a mucus shed close to HT29-rich regions. One interesting

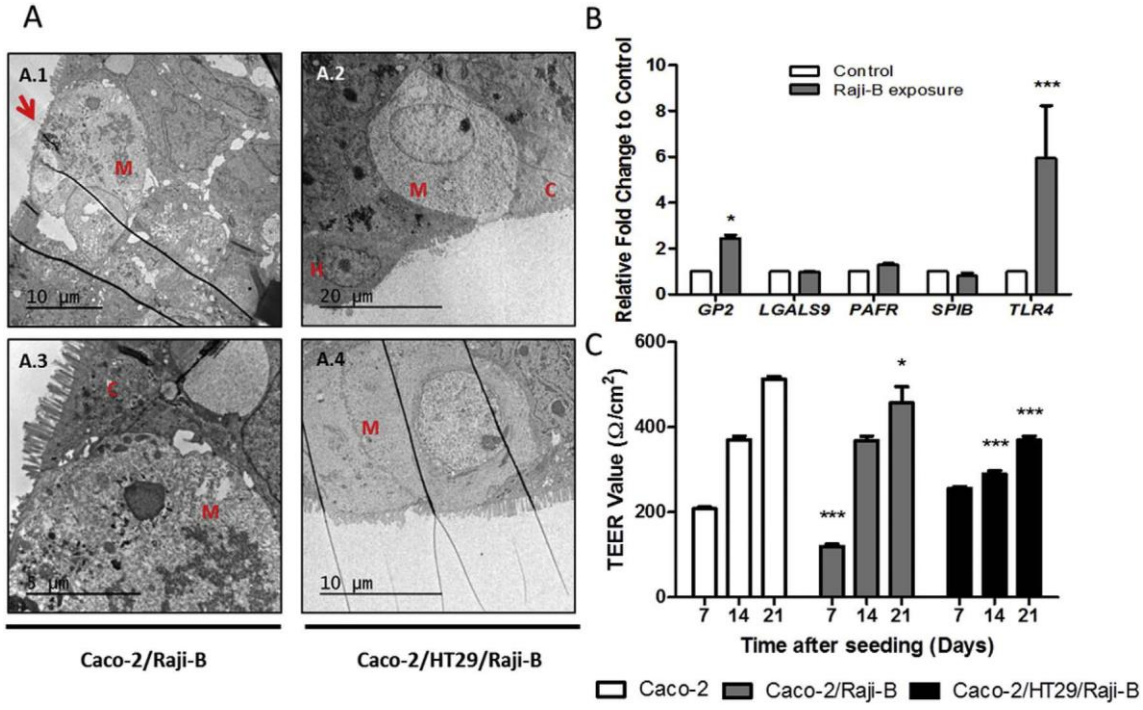

Fig. 3. Caco-2 cells conversion into M-like cells. TEM images of Caco-2 cells monocultures (A.1 and A.3), and Caco-2/HT29 co-cultures (A.2 and A.4) exposed to Raji-B cells at day 14 of culture differentiation. Images shows M cells (M), Caco-2 cells (C), and HT29 cells (H). The red arrow indicates the loss of microvilli. (B) Gene expression of Caco-2 cells in response to Raji-B exposure. Data represented as mean ± SEM, *denotes significant differences according to an unpaired Student's t-test. (C) TEER values of differentiated Caco-2, Caco-2/Raji-B and Caco-2/HT29/Raji-B co-cultures. One-way ANOVA with a Tukey's post-test was performed. *P < 0.05, **P < 0.01, and ***P < 0.001. (For interpretation of the references to color in this figure legend, the reader is referred to the Web version of this article.)

observation detected with this assay is that the well-structure/mor-phology of the barrier (Caco-2 alone) and the barrier integrity are compromised when the proportion of HT29 cells increase. Since HT29 cells do not grow in a monolayer, they tend to form small piles whose width directly affects the barrier integrity (data not shown).

3.2. Induction of M cells-like cells and their characterization

To mimic as much as possible the real conditions of an intestinal epithelium, this in vitro epithelial barrier model was further modified. After 14 days of Caco-2/HT29 co-culture, Raji-B lymphocytes were placed in the basolateral chamber of the PET. It is already known that co-culturing Caco-2 with lymphocytes induce several morphological changes, such as stumpy and short microvilli and the loss of Caco-2 brush border, indicating the generation of M-like cells. Our TEM images evidence the correct induction of an M-like phenotype in Caco-2 monolayers (Fig. 3; A.1 and A.3) and in Caco-2/HT29 co-culture bar-riers (Fig. 3; A.2 and A.4). Both cell phenotypes can be clearly dis-tinguished due to their different morphology and cell structure ar-rangement. As previously demonstrated by TEM studies, differentiated, enterocyte-like Caco-2 cells display a well-organized brush border, with tight junctions and a granulated cytoplasm that confers a dark contrast to the cells under the microscope (data not shown). Aside from the brush border rearrangement, our TEM images also show that M-like modified Caco-2 cells lose the columnar shape common on differ-entiated, enterocyte-like Caco-2 cells, and present a shinier cytoplasm due to their cytoskeleton reorganization. In addition, slight but sig-nificant differences ($P < 0.05$) were found between differentiated Caco-2 cells (413.25 ± 6.53 Ω/cm^2) and differentiated Caco-2/Raji-B (457.3 ± 37.9 Ω/cm^2) co-cultures when the TEER was measured at 21 days (Fig. 3C).

Since our work also aimed to develop new tools to characterize and detect these M cell-like cells, we also analysed several molecular mar-kers previously described as putative indicators of M-like cells. The induction of M-like cells was additionally confirmed by detecting changes in gene expression of genes involved in pathogen recognition, membrane receptors, intracellular transport or cell adhesion, among others. After one week of co-culture of differentiated Caco-2 with Raji-B lymphocytes, a significant upregulation in the expression of GP2 and TLR4 genes (1.45 ± 0.13and 4.37 ± 2.06 fold, respectively) was ob-served when compared with the control (mono-cultured differentiated Caco-2 cells) (Fig. 3B).

3.3. Gene expression: complementary verification of a well-barrier differentiation using molecular markers

Considering the high complexity of the in vitro epithelial barrier model, further efforts to monitor the system must be carried out. Thus, we checked a set of genes that could act as molecular markers as complementary data to better understand the behaviour of the Caco-2/ HT29/Raji-B barrier and its proper development over the differentia-tion process. The selected genes play essential roles in several barrier functions such as barrier integrity (ZO-1 and CLDN2), nutrient digestion and hydrolysis (ALPI and SI), protective mucus shed (MUC1 and MUC5AC), and pathogen recognition and macromolecules transcytosis (GP2 and TLR4). As Fig. 4 shows, there is a progressive increase over the differentiation span in the expression of all genes except SI, which expression decreases at day 21. At the end of the co-culture differ-entiation, most of the genes significantly increased at least 2-fold compared to the first 7 days. Interestingly, ALPI, ZO-1 and MUC1 were highly upregulated (4.78 ± 0.11, 3.32 ± 0.17, and 4.52 ± 0.27 fold, respectively). As expected, the gene expression of the M-like cells markers GP2 (6.54 ± 0.79 fold) and TLR4 (6.78 ± 1.87 fold) only increased after the second week, when the co-cultures were grown with Raji-B cells in the basolateral chamber.

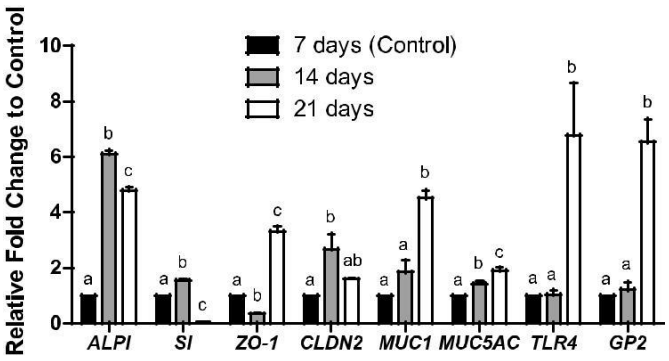

Fig. 4. Study of the correct Caco-2/HT29 barrier formation using RT-qPCR. Gene ex-pression in response to the barrier differentiation, through the culture time (7, 14 and 21 days). Data represented as mean ± SEM. One-way ANOVA with a Tukey's post-test was performed. *P < 0.05, **P < 0.01, and ***P < 0.001.

3.4. Laser scanning confocal microscope barrier characterization

To better illustrate the obtained intestinal epithelial barrier as a complete system, we analysed the Caco-2/HT29/Raji-B co-culture under the confocal microscope. Thanks to the use of different im-munostaining fluorochromes and their combinations, it was possible to identify various barrier structures and distinguish them in an in situ staining (Fig. 5). In this case, the fluorochromes used were Hoetch, CellMask (Fig. 5; A.1, A.2 and A.3) and WGA (Fig. 5; B.1, B.2 and B.3) to stain the nucleus membrane, cell membrane and the mucus secretion, respectively. Caco-2 (Figs. A.1 and B.1) and HT29 (Figs. A.2 and B.2) monocultures, and the Caco-2/HT29 (Fig. 5; A.3 and B.3) co-culture were grown in PET for 21 days and immediately stained with the aforementioned fluorochromes. Clearly, WGA tends to bind strongly to mucin residues produced by the HT29 cells, making the mucus shed easy to identify (Fig. B.2). As Fig. 5 displays, confocal images can cover a wide area of the barrier surface and, at the same time, transversal x/y-scans. In this case, we can specifically distinguish i) the apical from the basal side of the barrier (membrane polarization), ii) differences be-tween both Caco-2 and HT29 cell types (i.e distribution, conformation, etc.), iii) the mucus shed cover, and iv) in more detail, the cell mem-brane, the cell nucleus, and the cell-to-cell interaction.

3.5. NPs identification in the Caco-2/HT29/Raji-B model

Regarding the exponential growth of research studies in the nano-toxicology field, several assays must be modified and improved to make them suitable for studying the biological effects of NPs exposure. The interaction (uptake and translocation) of nanomaterials with epithelial barriers is of particular relevance in nanotoxicological screening. To detect such interactions, we exposed our Caco-2/HT29/Raji-B co-cul-ture model to TiO_2NPs and SiO_2NPs. A 24 h exposure to a concentration of 150 μg/mL of both nanomaterials [TiO_2NPs (< 100 nm) and SiO_2NPs (25 nm)] was selected. Fig. S2 and Table S1 show some characteristics of the NPs used. Laser scanning confocal microscopy was used to locate the selected metallic NPs, which are considered appropriate for this study since they refract the polarized light, allowing their localization over the co-culture barrier using the confocal microscope (Fig. 6). As the confocal images show, both NPs (green dots) are easily dis-tinguished from the rest of the co-culture barrier components. At first sight, both NPs are found homogenously spread over the surface barrier and stratified across the barrier thickness (Fig. 6; A.1 and B.1). More-over, we were also able to go further on the barrier imaging and create accurate three-dimensional images using the Imaris® software. Ac-cordingly, we were able to observe that both types of NPs were able to cross the mucus shed, the cell membrane and, finally, reach the cell nucleus (Fig. 6; A.3 and B.3). These results support the suitability of this co-culture model to study the fate of NPs when they interact with the epithelial barriers.

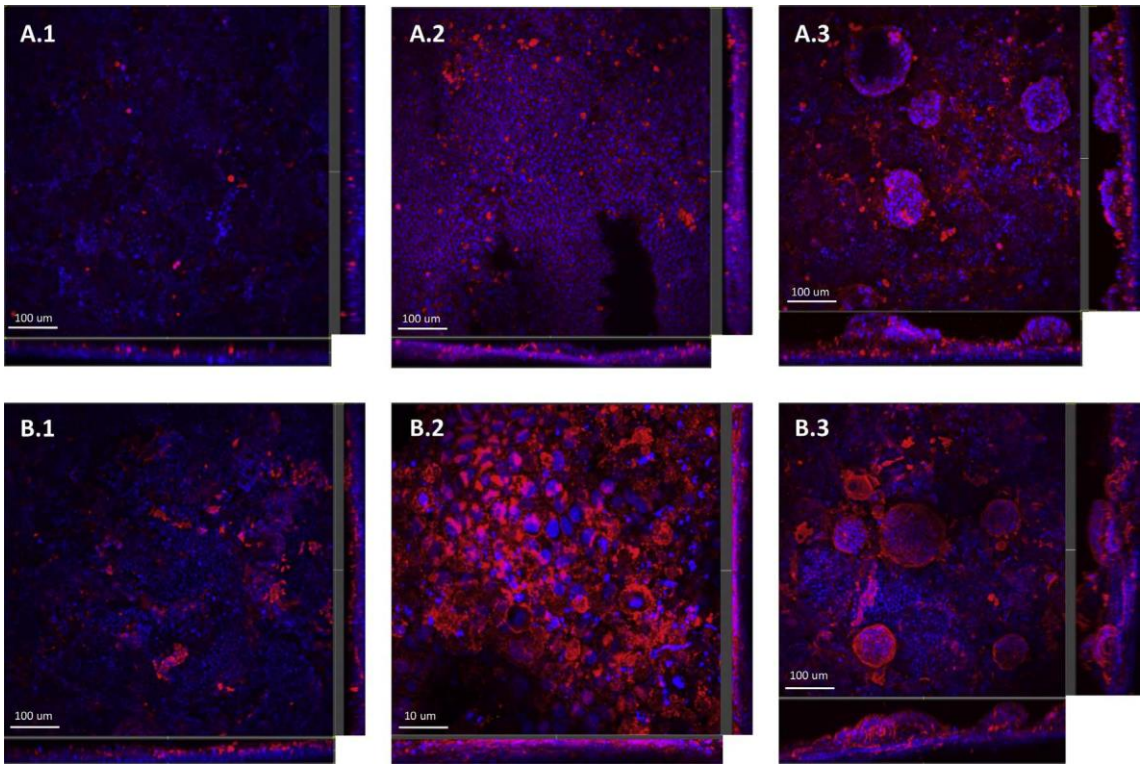

Fig. 5. Evaluation of the barrier distribution using a laser scanning confocal microscope. Confocal images of Caco-2 monolayers (A.1 and B.1); 21 days HT29 mono-culture (A.2 and B.2); and the complete co-culture Caco-2/HT29/Raji-B (A.3 and B.3). Cell nuclei were stained with Hoechst (blue), cells membrane were stained with CellMask (A.1, A.2 and A.3), and mucus shed was stained with WGA (B.1, B.2 and B.3). (For interpretation of the references to color in this figure legend, the reader is referred to the Web version of this article.)

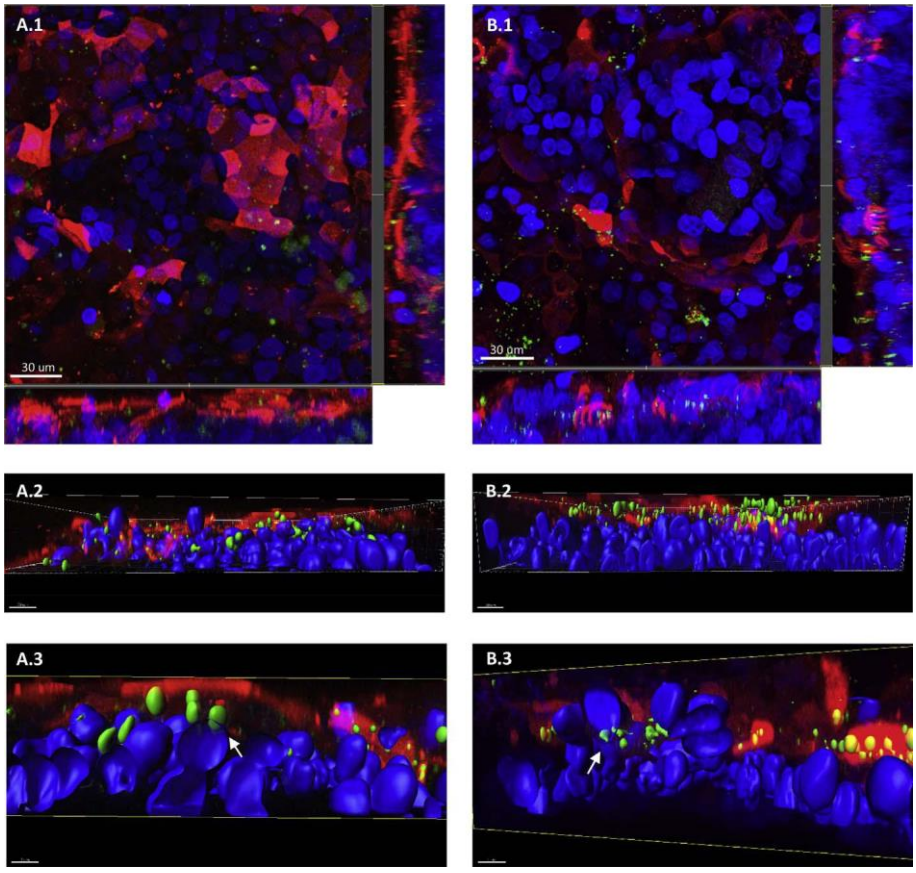

Fig. 6. Confocal microscope images of the in vitro co-culture model Caco-2/HT29/Raji-B treated with SiO_2NPs (A) and TiO_2NPs (B) at 150 μg/mL and during 24 h. Cells nuclei were stained with Hoecht (blue), mucus shed with WGA (red) and the NP refraction visualized in green. X, Y and Z-scans were done (A.1 and B.1). Three-dimensional images of the intestinal barrier model treated with SiO_2NPs (A.2 and A.3), and TiO_2NPs (B.2 and B.3). White arrows indicate the interaction between both, NPs and cell nuclei (A.3 and B.3). (For interpretation of the references to color in this figure legend, the reader is referred to the Web version of this article.)

4. Discussion

The combination of Caco-2/HT29/Raji-B cells is an already-de-scribed in vitro epithelial barrier model that tries to simulate as much as possible the real environment of the human small intestine (Antunes et al., 2013). This complex model, as well as the simpler Caco-2 monolayer model, have been proposed as predictive tools to evaluate the permeability of different drugs (Ingels et al., 2004; Lozoya-Agullo et al., 2017). In this work, we have analysed the suitability of the model, introducing different methodological changes, to evaluate the interaction of nanomaterials with the intestinal barrier. Hence, we propose the use of the HT29 cell clone instead of the commonly used HT29-MTX, since clear pictures of mucus layer are obtained using this clone. Furthermore, we suggest a new ratio Caco-2/HT29 to optimize translocation resistance. In addition, the use of a wide set of gene markers showed its appropriateness to evaluate the integrity of the model. We also demonstrated that confocal microscopy is a powerful tool to visualize many of the events taking place in these barriers. Fi-nally, we have shown the usefulness of this well-structured barrier to study its interaction with nanomaterials.

Several differences were demonstrated when comparing the com-plex Caco-2/HT29/Raji-B barrier with the Caco-2 monolayer at a functional and morphological level. Firstly, we observed a significant reduction in the TEER values, confirming previous findings by other authors (Schimpel et al., 2014; Araújo et al., 2016). This can be ex-plained by the presence of HT29 cells, which blocks the contact be-tween enterocyte-like cells and, as a consequence, the formation of tight junctions. Moreover, we confirmed these results by measuring the paracellular transport of LY through the different co-culture barriers. As expected, the amount of LY found in the basolateral chamber increased concomitantly with the amount of HT29 cells. To choose the optimal ratio of HT29 cells to have a well-established mucus shed, the Alcian Blue staining protocol was performed in transversal cuts of the co-culture. We did not find differences in the mucus extension throughout the barrier with different proportions of HT29, unlike Schimpel et al. (2014). These differences can be attributed to the used cell clones, or to the fact that they did not use transversal cuts to visualize mucus dis-tribution. Since the ratio 90:10 of Caco-2/HT29 produced the most well-established barrier, according to TEER and LY values and without significant variations in mucus shed formation, we propose this ratio as the optimal one. Interestingly, with this staining we also observed cells crossing through the 3 μm pore-size membrane and, as a consequence, a second cell layer was formed facing the basolateral chamber. This double membrane represents an extra obstacle for the NPs crossing and is far from the real scenario, therefore, further experiments were carried out using 1 μm pore-size PET (see Fig. S1). Accordingly, the use of 1 μm pore-size PET constitutes a further improvement of the method.

In the intestinal barrier, M-cells are located in the epithelia over-lying mucosa-associated lymphoid tissues, where they work as the an-tigen-sampling cells of the mucosal immune system (Clark and Jepson, 2003). According to our goal of establishing a more realistic barrier structure, we promoted the transformation of Caco-2 cells into M-cells. Although M-like cell induction could be achieved by the proximity of B-lymphocytes to Caco-2 cells, no direct contact is required since soluble factors and mediators secreted by B-lymphocytes are enough for its formation (des Rieux et al., 2005). M-cells are characterized by an ir-regular brush border, few microvilli and decreased glycocalyx. Several methodologies have been proposed to demonstrate their induction be-sides morphological analyses, including the quantification of the en-zymatic activity of proteins such as alkaline phosphatase (API) and sucrose isomaltase (SI) (Schimpel et al., 2014). Nevertheless, these molecules are not ubiquitously expressed among different species and do not present a high specificity for M-like cells, making them a con-troversial differentiation marker (Ohno and Hase, 2010). For instance, the WGA fluorochrome strongly stained the mucus layer produced by the HT29 cells, hampering M-like cell recognition in our model. To

overcome these difficulties, we evaluated the expression of a set of genes related to M-like cells functions as possible biomarkers for M-cells differentiation. The cell surface markers LGALS9, GP2, TLR4 and PAFR, and the transcription factor Spi-B were chosen because they have al-ready been described as M-like cells' biommmarkers in previous works (Wang et al., 2015; Albac et al., 2016). In our case, the gene expression of GP2 and TLR4 was significantly upregulated after the addition of Raji-B cells to the basolateral chamber. Nevertheless, no changes were detected for LGALS9, PAFR and Spi-B markers. Our results agree with those reporting the expression of TLR4 and GP2, as detected by im-muno-labelling (Tyrer et al., 2006; Albac et al., 2016). Both genes en-code integral membrane proteins, playing fundamental roles in M-cells such as membrane receptors, transcytotic machinery, signal inductors in pathogen recognition, uptake, and activators of innate immunity pathways (Hase et al., 2009; Kanaya and Ohno, 2014). According to our results, we propose the detection of expression changes in TLR4 and GP2 genes as an indicator of the functional M-cells presence in our in vitro model of the intestinal barrier.

Traditionally, TEM and SEM microscopy techniques have been the most used tools for M-like cells' detection (Schimpel et al., 2014; Araújo et al., 2016), despite the difficulty to find them due to their variable and poor rate of differentiation (Albac et al., 2016). We have been able to detect their presence in both Caco-2/Raji-B and Caco-2/HT29/Raji-B co-cultures thanks to morphological characteristics like their typically short and irregular microvilli structures, their loss of enterocyte-like shape and the cytoskeleton rearrangement. Therefore, we suggest that a simple preliminary study by gene expression of the molecular markers TLR4 and GP2, in addition to the microscope imaging, could be useful to show up the goodness of the barrier seeding, culturing, and cell differentiation processes.

The pristine in vitro Caco-2/HT29/Raji-B model must comprise the main functions of the human small intestine. One of its most important activities is the digestion and absorption of the uptaken nutrients, where several proteins and enzymes such as the intestinal alkaline phosphatase (ALPI) and sucrose isomaltase (SI), are involved (Nakano et al., 2009; Cheng et al., 2014). Additionally, the coordinated task of the tight junctions' (TJ) components (zonula occludens, occludin, claudins, etc) confers membrane integrity and stability, and the extra-cellular mucus shed grants an extra-protective layer to the barrier (Suzuki, 2013). In our model, ALPI and SI gene expression steadily increased during the first 2 weeks; however, on day 21 of their differentiation, they experiment a significant reduction. This could be ex-plained by the inclusion of Raji-B cells and the consequent formation of M-like cells, reducing the expression of brush border markers (Schimpel et al., 2014). We have also demonstrated that the gene expression of the TJ components ZO-1 and CLDN2, and the mucus produced components MUC1 and MUC5AC, are significantly increased during the barrier differentiation process but with different expression rates and plateaus. These outcomes were associated with our TEER values, Alcian Blue staining, and confocal images. Regarding the transcytotic capability of the barrier associated with the presence of M-like cells, the increase in the expression of the GP2 and TLR4 genes was only detected at the 21st day of barrier differentiation, one week after the exposure to Raji-B cells. Taken together, we propose all the aforementioned markers as indicators to demonstrate the integrity of the barrier given that the principal functions of the intestinal barrier are working properly.

Another aspect of this study to be pointed out is the usefulness of the laser scanning confocal microscopy to demonstrate the integrity of this in vitro intestinal model. We have observed a good signal when fluor-ochrome CellMasK™ was used, staining the plasma membranes of Caco-2 and HT29 cells uniformly. Likewise, the lectin-labelling fluorochrome WGA stained both cell types in a different manner. Our confocal images displayed the strong reaction of WGA to the mucin-secreting goblet cells HT29. Moreover, we were not able to distinguish any M-like cell specifically labelled by WGA, like Schimpel et al. (2014) described. Consequently, we propose the use of WGA only as a mucus shed detector. Summarizing the goodness of this microscopic approach, this technique allows the observation of the multicellular barrier con-formation and the disposition of its components, characterized by being thicker than the Caco-2 monolayer and for forming rounded protuber-ances. We hypothesize that these protuberances are mainly formed by HT29 cells, as mucus production is higher near this structures.

In the nanotoxicology field, very few studies have used the complex Caco-2/HT29 or the Caco-2/HT29/Raji-B models to quantitatively as-sess cell uptake rates and transport kinetics of nanomaterials. In fact, the few existing studies have only focused on the effects of drug de-livery nano-carriers (Antunes et al., 2013; Lopes et al., 2016). None-theless, since metallic NPs are increasingly used as food additives in many consumer products (Yang et al., 2014; Vance et al., 2015), the interest to uncover their potential interactions with the gastrointestinal tract is raising. Similarly, nano-carrier drugs should also be screened with this complex, more realistic barrier model, to better select po-tentially-interesting NPs for drug-delivery. Once our model was well established, we carried out a preliminary test to qualitatively assess its interaction with the metallic TiO_2NPs and SiO_2NPs, which are highly used as food additives. Assuming that NPs transport through an epi-thelial barrier can take place via paracellular or intracellular mechan-isms, we aimed to check this process by confocal microscopy. Using this methodology, it is possible to distinguish between cell components and NPs, since metallic NPs have the ability to refract polarized light when visualized under a scanning laser microscope. To reduce possible ag-glomerations, NPs were dispersed and characterized as done in previous works (Vila et al., 2017) (see supplementary data). Our confocal images clearly demonstrated that, after the exposure, a significant amount of NPs remained in the apical side of the membrane, detained between microvilli and by the mucus matrix. In both cases, some NPs were de-tected actively crossing the barrier, mainly by cellular uptake. Finally, we were also able to detect several NPs-cell nucleus interactions, what would imply the potential risk of inducing DNA damage.

Summarizing, in addition to the data that reinforces the general usefulness of the proposed Caco-2/HT29 model, we defend its use as a powerful tool to evaluate the gastrointestinal barrier's interaction with nanomaterials, mainly those used in the food industry. The obtained data qualitatively shows that the protective function of the barrier is working well, as NPs are mostly located in the mucus shed. However, some NPs are able to enter the cell's cytoplasm, even reaching the cells' nucleus, suggesting a potential toxic/genotoxic hazard. Accordingly, further efforts should be done in order to understand the mechanisms of NPs' internalization and its effects at both cellular and barrier level.

Funding

This investigation has been partially supported by the Ministry of Economy and Competition (SAF2015-63519-R), and the EC FP7 NANoREG (Grant Agreement NMP4-LA-2013-310584).

Declaration of interest

The authors report no conflict of interest. The authors alone are responsible for the content and writing of the paper.

Acknowledgements

A. Garcia-Rodriguez and L. Vila were funded by postgraduate fellowships from the Universitat Autònoma de Barcelona and the Generalitat de Catalunya, respectively.

Appendix A. Supplementary data

Supplementary data related to this article can be found at http://dx.doi.org/10.1016/j.fct.2018.01.042.

Transparency document

Transparency document related to this article can be found online at http://dx.doi.org/10.1016/j.fct.2018.01.042.

References

Albac, S., Schmitz, A., Lopez-Alayon, C., d'Enfert, C., Sautour, M., Ducreux, A., Labruère-Chazal, C., Laue, M., Holland, G., Bonnin, A., Dalle, F., 2016. Candida albicans is able to use M cells as a portal of entry across the intestinal barrier in vitro. Cell Microbiol. 18, 195–210.

Antunes, F., Andrade, F., Araújo, F., Ferreira, D., Sarmento, B., 2013. Establishment of a triple co-culture in vitro cell models to study intestinal absorption of peptide drugs. Eur. J. Pharm. Biopharm. 83, 427–435.

Araújo, F., Pereira, C., Costa, J., Barrias, C., Granja, P.L., Sarmento, B., 2016. In vitro M-like cells genesis through a tissue-engineered triple-culture intestinal model. J. Biomed. Mater. Res. B Appl. Biomater. 104, 782–788.

Araújo, F., Sarmento, B., 2013. Towards the characterization of an in vitro triple co-cul-ture intestine cell model for permeability studies. Int. J. Pharm 458, 128–134.

Artursson, P., Palm, K., Luthman, K., 2001. Caco-2 monolayers in experimental and theoretical predictions of drug transport. Adv. Drug Deliv. Rev. 46, 27–43.

Braakhuis, H.M., Kloet, S.K., Kezic, S., Kuper, F., Park, M.V., Bellmann, S., van der Zande, M., Le Gac, S., Krystek, P., Peters, R.J., Rietjens, I.M., Bouwmeester, H., 2015. Progress and future of in vitro models to study translocation of nanoparticles. Arch. Toxicol. 89, 1469–1495.

Cheng, M.W., Chegeni, M., Kim, K.H., Zhang, G., Benmoussa, M., Quezada-Calvillo, R., Nichols, B.L., Hamaker, B.R., 2014. Different sucrose-isomaltase response of Caco-2 cells to glucose and maltose suggests dietary maltose sensing. J. Clin. Biochem. Nutr. 54, 55–60.

Clark, M.A., Jepson, M.A., 2003. Intestinal M cells and their role in bacterial infection. Iran. J. Med. Microbiol. 293, 17–39.

des Rieux, A., Fievez, V., Théate, I., Mast, J., Préat, V., Schneider, Y.J., 2007. An improved in vitro model of human intestinal follicle-associated epithelium to study nanoparticle transport by M cells. Eur. J. Pharm. Sci. 30, 380–391.

Faust, J.J., Doudrick, K., Yang, Y., Westerhoff, P., Capco, D.G., 2014. Food grade titanium dioxide disrupts intestinal brush border microvilli in vitro independent of sedi-mentation. Cell Biol. Toxicol. 30, 169–188.

Georgantzopoulou, A., Serchi, T., Cambier, S., Leclercq, C.C., Renaut, J., Shao, J., Kruszewski, M., Lentzen, E., Grysan, P., Eswara, S., Audinot, J.N., Contal, S., Ziebel, J., Guignard, C., Hoffmann, L., Murk, A.J., Gutleb, A.C., 2016. Effects of silver na-noparticles and ions on a co-culture model for the gastrointestinal epithelium. Part. Fibre Toxicol. 13, 9.

Gordon, S., Daneshian, M., Bouwstra, J., Caloni, F., Constant, S., Davies, D.E., Dandekar, G., Guzman, C.A., Fabian, E., Haltner, E., Hartung, T., Hasiwa, N., Hayden, P., Kandarova, H., Khare, S., Krug, H.F., Kneuer, C., Leist, M., Lian, G., Marx, U., Metzger, M., Ott, K., Prieto, P., Roberts, M.S., Roggen, E.L., Tralau, T., van den Braak, C., Walles, H., Lehr, C.M., 2015. Non-animal models of epithelial barriers (skin, in-testine and lung) in research, industrial applications and regulatory toxicology. ALTEX 32, 327–778.

Gullberg, E., Leonard, M., Karlsson, J., Hopkins, A.M., Brayden, D., Baird, A.W., Artursson, P., 2000. Expression of specific markers and particle transport in a new human intestinal M-cell model. Biochem. Biophys. Res. Commun. 279, 808–813.

Guo, Z., Martucci, N.J., Moreno-Olivas, F., Tako, E., Mahler, G.J., 2017. Titanium dioxide nanoparticle ingestion alters nutrient absorption in an in vitro model of the small intestine. NanoImpact 5, 70–82.

Hase, K., Kawano, K., Nochi, T., Pontes, G.S., Fukuda, S., Ebisawa, M., Kadokura, K., Tobe, T., Fujimura, Y., Kawano, S., Yabashi, A., Waguri, S., Nakato, G., Kimura, S., Murakami, T., Iimura, M., Hamura, K., Fukuoka, S., Lowe, A.W., Itoh, K., Kiyono, H., Ohno, H., 2009. Uptake through glycoprotein 2 of FimH(+) bacteria by M cells in-itiates mucosal immune response. Nature 462, 226–230.

Imai, S., Morishita, Y., Hata, T., Kondoh, M., Yagi, K., Gao, J.Q., Nagano, K., Higashisaka, K., Yoshioka, Y., Tsutsumi, Y., 2017. Cellular internalization, transcellular transport, and cellular effects of silver nanoparticles in polarized Caco-2 cells following apical or basolateral exposure. Biochem. Biophys. Res. Commun. 484, 543–549.

Ingels, F., Beck, B., Oth, M., Augustijns, P., 2004. Effect of simulated intestinal fluid on drug permeability estimation across Caco-2 monolayers. Int J Pharm 274, 221–232.

Kanaya, T., Ohno, H., 2014. The mechanisms of M-cell differentiation. Biosci. Microbiota Food Health 33, 91–97.

Kucharzik, T., Lügering, N., Rautenberg, K., Lügering, A., Schmidt, M.A., Stoll, R., Domschke, W., 2000. Role of M cells in intestinal barrier function. Ann. NY Acad. Sci. 915, 171–183.

Leist, M., Hasiwa, N., Rovida, C., Daneshian, M., Basketter, D., Kimber, I., Clewell, H., Gocht, T., Goldberg, A., Busquet, F., Rossi, A.M., Schwarz, M., Stephens, M., Taalman, R., Knudsen, T.B., McKim, J., Harris, G., Pamies, D., Hartung, T., 2014. Consensus report on the future of animal-free systemic toxicity testing. ALTEX 31, 341–356.

Lopes, M., Shrestha, N., Correia, A., Shahbazi, M.A., Sarmento, B., Hirvonen, J., Veiga, F., Seiça, R., Ribeiro, A., Santos, H.A., 2016. Dual chitosan/albumin-coated alginate/ dextran sulfate nanoparticles for enhanced oral delivery of insulin. J. Contr. Release 232, 29–41.

Lozoya-Agullo, I., Araújo, F., González-Álvarez, I., Merino-Sanjuán, M., González-Álvarez, M., Bermejo, M., Sarmento, B., 2017. Usefulness of Caco-2/HT29-MTX and Caco-2/HT29-MTX/Raji B coculture models to predict intestinal and colonic permeability compared to Caco-2 monoculture. Mol. Pharm. 14, 1264–1270.

Mahler, G.J., Shuler, M.L., Glahn, R.P., 2009. Characterization of Caco-2 and HT29-MTX cocultures in an in vitro digestion/cell culture model used to predict iron bioavail-ability. J. Nutr. Biochem. 20, 494–502.

Nakano, T., Inoue, I., Alpers, D.H., Akiba, Y., Katayama, S., Shinozaki, R., Kaunitz, J.D., Ohshima, S., Akita, M., Takahashi, S., Koyama, I., Matsushita, M., Komoda, T., 2009. Role of lysophosphatidylcholine in brush-border intestinal alkaline phosphatase re-lease and restoration. Am. J. Physiol. Gastrointest. Liver Physiol. 297, G207–G214.

Nanogenotox, 2011. http://www.nanogenotox.eu/files/PDF/Deliverables/nanogenotox%20deliverable%203_wp4_%20dispersion%20protocol.pdf.

Ohno, H., Hase, K., 2010. Glycoprotein 2 (GP2): grabbing the FimH bacteria into M cells for mucosal immunity. Gut Microb. 1, 407–410.

Pinto, M., Robine, S., Appay, M.-D., Kedinger, M., Triadou, N., Dussaulx, E., Lacroix, B., Simon, P., Haffen, K., Fogh, J., Zweibaum, A., Assam, P.F., Robineleon, S., Simonassmann, P., Robin, S., Zwwibaum, A., 1983. Enterocyte-like differentiation and polarization of the human colon carcinoma cell line Caco-2 in culture. Biol. Cell. 47, 323–330.

Sambuy, Y., De Angelis, I., Ranaldi, G., Scarino, M.L., Stammati, A., Zucco, F., 2005. The Caco-2 cell line as a model of the intestinal barrier: influence of cell and culture-related factors on Caco-2 cell functional characteristics. Cell Biol. Toxicol. 21, 1–26.

Sakai-Kato, K., Hidaka, M., Un, K., Kawanishi, T., Okuda, H., 2014. Physicochemical properties and in vitro intestinal permeability properties and intestinal cell toxicity of silica particles, performed in simulated gastrointestinal fluids. Biochim. Biophys. Acta 1840, 1171–1180.

Schimpel, C., Teubl, B., Absenger, M., Meindl, C., Fröhlich, E., Leitinger, G., Zimmer, A., Roblegg, E., 2014. Development of an advanced intestinal in vitro triple culture permeability model to study transport of nanoparticles. Mol. Pharm. 11, 808–818.

Smith, M.W., Peacock, M.A., 1980. "M" cell distribution in follicle-associated epithelium of mouse Peyer's patch. Am. J. Anat. 159, 167–175.

Suzuki, T., 2013. Regulation of intestinal epithelial permeability by tight junctions. Cell. Mol. Life Sci. 70, 631–659.

Tyrer, P., Foxwell, A.R., Cripps, A.W., Apicella, M.A., Kyd, J.M., 2006. Microbial pattern recognition receptors mediate M-cell uptake of a gram-negative bacterium. Infect. Immun. 74, 625–631.

van Breemen, R.B., Li, Y., 2005. Caco-2 cell permeability assays to measure drug ab-sorption. Expert Opin. Drug Metab. Toxicol 1, 175–185.

Vance, M.E., Kuiken, T., Vejerano, E.P., McGinnis, S.P., Hochella Jr., M.F., Rejeski, D., Hull, M.S., 2015. Nanotechnology in the real world: redeveloping the nanomaterial consumer products inventory. Beilstein J. Nanotechnol. 6, 1769–1780.

Vila, L., Rubio, L., Annangi, B., García-Rodríguez, A., Marcos, R., Hernández, A., 2017. Frozen dispersions of nanomaterials are a useful operational procedure in nanotox-icology. Nanotoxicology 11, 31–40.

Wang, L., Luo, X., Zheng Zhou, L., Zhu, Y., Wu, X., 2015. Culture supernatants of lym-phocytes from different lymphoid tissues induce transdifferentiation of Caco2 cells into M-like cells. Xi Bao Yu Fen Zi Mian Yi Xue Za Zhi 31, 1311–1315.

Yang, Y., Doudrick, K., Bi, X., Hristovski, K., Herckes, P., Westerhoff, P., Kaegi, R., 2014. Characterization of food-grade titanium dioxide: the presence of nanosized particles. Environ. Sci. Technol. 48, 6391–6400.